INTERFACIAL BIOORTHOGONAL CHEMISTRY FOR BIOMATERIALS SYNTHESIS AND PATTERNING AND DEVELOPMENT OF CATALYTIC METHOD FOR "TURNING-ON" THE TETRAZINE LIGATION

by

Han Zhang

A dissertation submitted to the Faculty of the University of Delaware in partial fulfillment of the requirements for the degree of Doctor of Philosophy in Chemistry and Biochemistry

Spring 2017

INTERFACIAL BIOORTHOGONAL CHEMISTRY FOR BIOMATERIALS SYNTHESIS AND PATTERNING AND DEVELOPMENT OF CATALYTIC METHOD FOR "TURNING-ON" THE TETRAZINE LIGATION

by

Han Zhang

Approved: _____
Murray V. Johnston, Ph.D.
Chair of the Department of Chemistry and Biochemistry

Approved: _____
George H. Watson, Ph.D.
Dean of the College of Arts and Sciences

Approved: _____
Ann L. Ardis, Ph.D.
Senior Vice Provost for Graduate and Professional Education

I certify that I have read this dissertation and that in my opinion it meets the academic and professional standard required by the University as a dissertation for the degree of Doctor of Philosophy.

Signed: _____

Joseph Fox, Ph.D.
Professor in charge of dissertation

I certify that I have read this dissertation and that in my opinion it meets the academic and professional standard required by the University as a dissertation for the degree of Doctor of Philosophy.

Signed: _____

Mary Watson, Ph.D.
Member of dissertation committee

I certify that I have read this dissertation and that in my opinion it meets the academic and professional standard required by the University as a dissertation for the degree of Doctor of Philosophy.

Signed: _____

Joel Rosenthal, Ph.D.
Member of dissertation committee

I certify that I have read this dissertation and that in my opinion it meets the academic and professional standard required by the University as a dissertation for the degree of Doctor of Philosophy.

Signed: _____

Xinqiao Jia, Ph.D.
Member of dissertation committee

ACKNOWLEDGMENTS

First and foremost, I would like to take this opportunity to thank my research advisor Joseph Fox for accepting me into his research group and teaching me how to be a successful chemist. His continuous guidance, support, and patience over the years made graduate school a very positive experience to me.

I would also like to thank my committee member and collaborating advisor, Xinqiao Jia for giving the chance to participate in a series of interesting and rewarding projects, I will be forever indebted to her kindness and inspirations.

I am grateful to my committee members, Professors Mary Watson and Joel Rosenthal, as well as Professor Colin Thorpe, for their constructive ideas, insights and valuable suggestions towards my dissertation work.

Special thanks to my collaborators: Kevin Dicker, Dr. Shuang Liu and William Trout, none of these projects would have been possible without your hard work.

I would like to thank all the current and former lab members from both Fox and Jia lab, I'm so grateful to work with such an extraordinary group of scientists.

I also need to thank all the administrative and facility staffs for keeping everything running smoothly within the department.

Last but certainly not least, to my family, my parents, my little brother and my beautiful wife: thank you for your unconditional and unwavering love and support, you made the past years a memorable journey.

Finally, Grandma Junyuan Meng (1923-2011) and Grandpa Peilin Li (1928-2015), this dissertation is dedicated to you, we miss you dearly.

TABLE OF CONTENTS

LIST OF TABLES

LIST OF FIGURES

LIST OF SCHEMES

ABSTRACT

The bioorthogonal *trans*-cyclooctene-tetrazine ligation has emerged into a powerful tool in the field of biomedical research. The development and the versatile applications of tetrazine ligation was made possible by the advancement of *trans*-cyclooctene synthesis. Based on the previous art of photoisomerization methods in Fox group, I carried out the first practical photosynthesis of *trans*-cycloheptene derivatives that were stabilized as silver(I) complexes form, as well as the photoisomerization of silicon-containing hetero-*trans*-cycloheptene derivatives. The reactivity of both the *trans*-cycloheptene silver(I) complexes and the hetero-*trans*-cycloheptene derivatives were investigated.

Based on the rapid *trans*-cyclooctene-tetrazine ligation, first example of interfacial crosslinking will be described in Chapter 2. Bioocompatible hyaluronic acid-based hydrogel microspheres and channels were generated in a diffusion controlled fashion. These hydrogels can be covalently tagged with 3D resolution without the help of any external stimulus or triggers. An *in vitro* tumor model was achieved by 3D encapsulation and culture of LNCaP prostate cancer cells.

Also included in Chapter 2 will be a novel interfacial polymerization strategy developed for the synthesis of hybrid multiblock copolymer. Meter-long copolymer fibers were pulled out of interface of two immiscible solutions. The unique modular approach enables the facile incorporation of functional peptides into the copolymer to fine-tune its biological properties. A fibronectin-derived peptide was successfully

introduced onto the fibers during the polymerization and dramatically promoted the attachment and alignment of fibroblasts and myoepithelial-like cells.

In Chapter 3, a novel method to activate rapid bioorthogonal reactivity catalytically will be described. This was achieved by catalytic conversion of an unreactive, latent dihydrotetrazine to reaction-ready tetrazine functionality. Series of long wavelength photosensitizers were found to catalyze the oxidation of DHTz to Tz effieciently in the presence of light and air. Horseradish peroxidase (HRP) was found to catalyze the oxidation at nanomolar concentrations in absence of peroxide. These methods can provide a milder and more physiology-friendly way to "turn-on" rapid tetrazine ligation reactivity with great promise in extending to a wide range of applications in materials, cellular, and in vivo systems.

Moreover, based on the previous bioorthogonal interfacial polymerization developed from our group, DHTz functionality can be successfully incorporated onto the copolymer fibers, which can be activated postsynthetically by either light or an HRP enzyme. Conjugations with small molecule fluorophores, cell-instructive peptide sequences and fluorescent proteins were accomplished, providing a new tool for modulating the cell adhesive properties of a biomaterial.

TCO-tetrazine ligation has emerged as a multifaceted strategy in polymer and biomaterials discovery, bringing promising results and exhilarating progress. The versatile materials we developed here will prove useful and become indispensable elements in the tissue engineering toolbox.

Chapter 1

BIOORTHOGONAL CHEMISTRY AND TETRAZINE LIGATION

1.1 Brief History of Bioorthogonal Chemistry

The development of chemical reactions for studying biology at the molecular level under physiological condition is challenging due to the diverse chemical functionality that is present in any biological system. The term "bioorthogonal chemistry" was first coined by Bertozzi in 2003[1,2] to describe chemical reactions in which the reacting components can selectively couple with each other, forming a covalent linkage inside of living system without interfering with native biochemistry. Research in the area of bioorthogonal chemistry has been expanding dramatically since then,[1-4] and various kinds of ligation tools have been developed and enabled the study of biomolecules such as proteins, glycans and lipids in living systems.

One of the first examples of bioorthogonal chemistry is the Staudinger ligation (Table 1.1, Entry 2) independently developed by Bertozzi[5,6] and Raines[7] in the year 2000. This method was adapted from the classic Staudinger reduction[8] between azides and triarylphosphines. The Staudinger ligation can proceed under water-tolerant conditions to generate a stable amide bond linkage. It has shown excellent bioorthogonality and has been applied to labeling of proteins and live cells.[9-14]

However, the Staudinger ligation is not without limitation, and its broader application has been limited by its relatively slow reaction kinetics (k_2 0.003 M^{-1} s^{-1} in PBS).[15] Like most bioorthogonal reactions, the Staudinger ligation is a two-component reaction and follows second-order kinetics. The reaction rate depends on the

concentrations of both components as well as on the intrinsic second-order rate constant k_2 [M^{-1} s^{-1}] of the reaction. Slower reactions therefore have a disadvantage when the labeling targets are of low abundance. This can only be compensated by applying large excess of labeling reagents which furthermore causes the problem of solubility, toxicity and background/off target signal.

The most broadly utilized bioorthogonal reaction is the copper(I) catalyzed azide-alkyne cycloaddition (CuAAC) (Table 1.1, Entry 4). This "click" reaction features a 1,3-dipolar cycloaddition between an azide and an alkyne, which was originally reported by Michael in 1890[16] and extensively studied by Huisgen beginning in 1967[17]. The thermal cycloaddition reaction using unstrained alkynes was limited due to its slow kinetics and harsh conditions. In 2002, Meldal[18] and Sharpless[19] developed the copper(I) catalyzed version of the cycloaddition between terminal alkynes and azides under mild reaction conditions and also with dramatically increased reaction kinetics. The CuAAC reaction gained immediate application in chemical biology,[1,3] surface chemistry,[20-23] materials science.[24-26] However, the cytotoxicity of copper can be a limitation for *in vivo* studies[27-30], although recent studies have shown that non-toxic Cu-ligand complexes can be used to catalyze the 3+2 reaction in the extracellular environment.[31]

An approach to facilitate the 3+2 cycloaddition without the need for catalysis was described by Bertozzi in 2004,[32] where cyclooctynes were used to improve the reaction kinetics through release of strain energy. This reaction has been referred to as a strain-promoted azide-alkyne cycloaddition (SPAAC) (Table 1.1 Entry 5). Since the initial report, a series of cyclooctyne derivatives were developed by Bertozzi,[33,34] Boons[35] and van Delft[36,37] to enhance the reactivity.[38] Because of the excellent

biocompatibility, the SPAAC has been widely used in the applications of bioconjugation for not only live cells but also for live animals.[35,39]

Table 1.1: Representative bioorthogonal reactions and their reaction rates.[4,15,40-47]

Entry	Reaction	k_2 (M^{-1} s^{-1})
1	**Ketone/hydroxylamine condensation:** 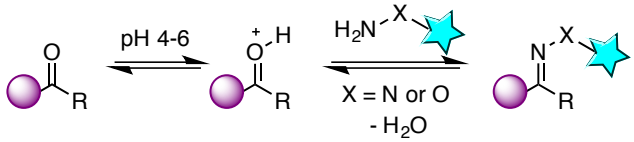	10^{-4} - 10^{-3}
2	**Staudinger ligation (traceless):** 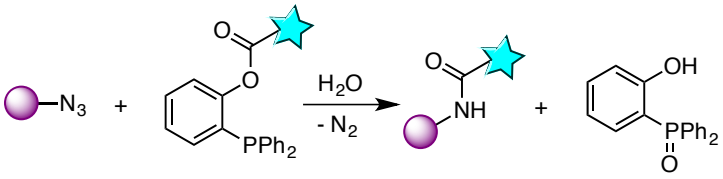	0.003 (PBS)
3	**Cyanobenzothiazole (CBT) condensation:** 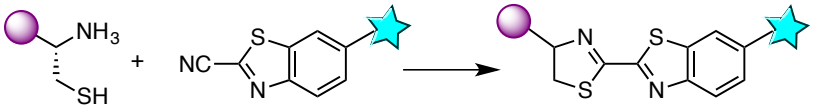	9.19 (PBS)
4	**Cu(I)-catalyzed alkyne-azide cycloaddition (CuAAC):** 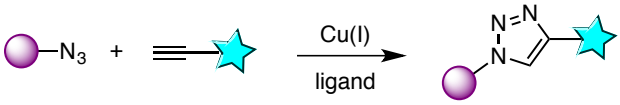	k_{obs} 10 - 200
5	**Strain-promoted alkyne-azide cycloaddition (SPAAC):** 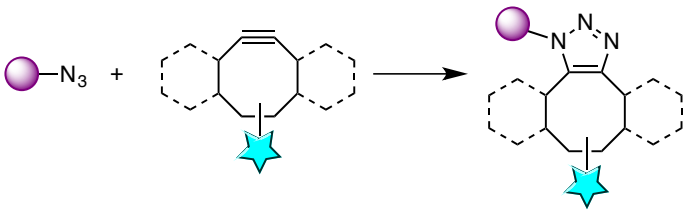	10^{-2} - 1
6	**Strain-promoted alkyne-nitrone cycloaddition (SPANC):** 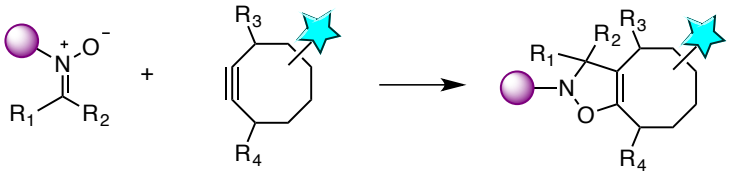	< 30

Entry	Reaction	k_2 (M^{-1} s^{-1})
7	**Photo-click cycloaddition:** 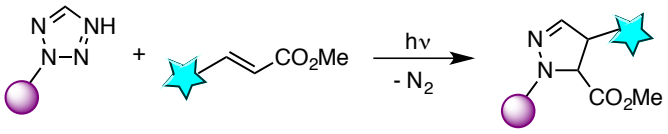	< 60
8	**Quadricyclane ligation:** 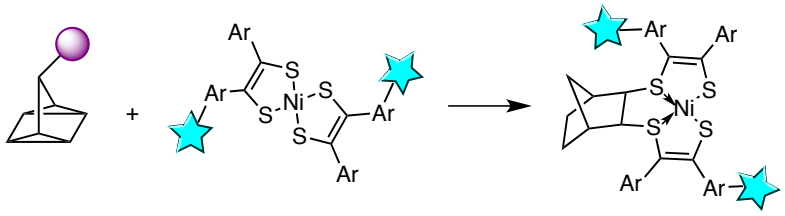	0.25 (PBS/tBuOH)

1.2 Inverse-electron-demand Diels-Alder Cycloaddition (IEDDA) and *trans*-Cyclooctene-Tetrazine Ligation

Another major class of bioorthogonal reactions (Table 1.2) that played significant roles in the past years is inverse-electron-demand Diels-Alder cycloaddition (IEDDA) between tetrazines and strained alkenes or alkynes. The reactions yield dihydropyridazines or pyridazines with nitrogen gas as the only byproduct.[48]

In 2008, the Fox group reported an inverse-electron-demand Diels-Alder cycloaddition between *trans*-cyclooctene derivatives and 1,2,4,5-diaryl-*s*-tetrazine(Table 1.2, Entry 1).[49] This methodology was inspired by an early study from Sauer,[50,51] in which he reported that compared to the *cis* isomer, *trans*-cyclooctene can react towards electron-deficient diene (tetrazine) with extraordinarily faster kinetics.

In Fox's initial report, the reaction between *trans*-cyclooctene and dipyridyl-*s*-tetrazine could proceed rapidly and quantitatively with rate up to k_2 400 M^{-1} s^{-1} k_2, 1,140 M^{-1} s^{-1}, and k_2 2,000 M^{-1} s^{-1} when carried out in THF, methanol, and 9:1

methanol/water respectively. As a proof of bioorthogonality, the reaction was run successfully in cell media and in rabbit reticulocyte lysate. In a further demonstration, a TCO functionalized thioredoxin (Trx) protein (prepared from conjugating TCO-maleimide derivative to reduced thioredoxin) was treated with dipyridyl-*s*-tetrazine and full conversion was observed in less than 5 minutes.

The tetrazine ligation showed a hydrophobic effect by exhibiting a dramatically enhanced reaction rate with increasing content of water in the solvent, a secondary rate constant as high as 24,500 M^{-1} s^{-1} was measured when the reaction was carried on in pure water.[52]

Over the following years, the Fox group further developed several additional *trans*-cyclooctene derivatives with enhanced performance. With the help of computational design, conformationally strained *cis*-fused bicyclic skeleton was introduced, bringing more strain energy to the system and lead to enhanced kinetics. Mike Taylor from the Fox group developed sTCO in 2011,[53] a *trans*-cyclooctene derivative with a cis-fused cyclopropane ring can react with dipyridyl-*s*-tetrazine in an unprecedented bimolecular rate at 3,300,000 M^{-1} s^{-1},[54] which makes it the fastest bioorthogonal reaction ever reported. In 2014, dTCO were developed by Ampofo Darko by adopting a dioxolane-fused *trans*-cyclooctene derivative which displayed elevated reactivity towards tetrazine compared to parent TCO (k_2 at 366,000 M^{-1} s^{-1} in water) and better water solubility.[54]

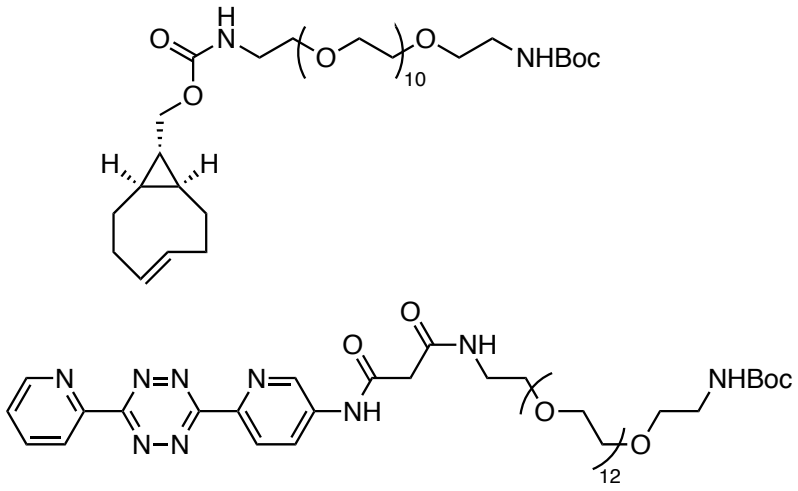

Scheme 1.1: The fastest bioorthogonal reaction pair reported to date.[54]

Although only recently developed, the TCO-tetrazine ligation has drawn a tremendous amount of attention which leads to considerable number of applications in various areas including protein labeling,[40,55] cell imaging[56], drug release,[57,58] nuclear medicine and materials sciences.[59,60]

Ting[61] demonstrated fluorescence labeling to specific proteins inside living cells via a two-step, site-specific labeling using lipoic acid ligase. Chin[52] and Mehl[62,63] reported rapid and efficient site-specific protein labeling using genetically encoded *trans*-cyclooctene or tetrazine-based unnatural amino acids (UAAs) within living cells. In an on-going collaboration with Pfizer[64], the researchers compared *trans*-cyclooctenes with a series of strained alkene and alkyne partners in evaluation of bioorthogonal reactions in live cells with clickable HaloTag® ligands in which TCO probes showed considerable advantages.

Aside from above, the tetrazine ligation has been extensively employed in the field of nuclear medicine for imaging and diagonostics.[65-67] Together with Li and

Conti, the Fox group developed a novel methods of ^{18}F PET imaging utilizing the unusual-rapid TCO-tetrazine ligation.[68-71] Most recently, a newer modification of the method was reported in which the faster sTCO was employed.[72,73]

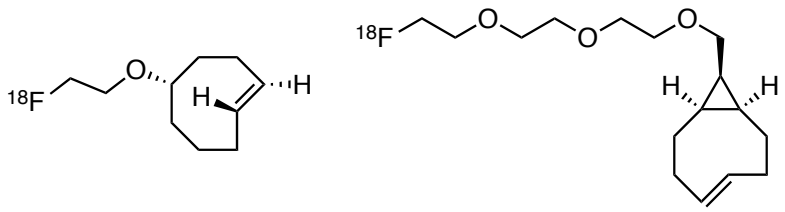

Scheme 1.2: ^{18}F-TCO[70] and ^{18}F-sTCO probes.[72,73]

Coinciding with the Fox group in the year of 2008, the Weissleder/Hilderbrand group described bioconjugation method in which norbornenes were used as dienophile to react with tetrazines.[74] Pretargeted labeling and imaging of live SKBR3 cancer cells were achieved, demonstrating the specificity of the tetrazine and norbornene conjugates in the presence of live cells and serum. This method benefits from the good shelf stability and commercial availability of norbornene derivatives. However, one limiting factor lies in the sluggish reaction kinetics compared to TCO-tetrazine ligation, the second order rate constant was measured at 2 to 9 M^{-1} s^{-1} when the reaction was carried out in fetal bovine serum (FBS).

Over the years, a good number of strained alkenes and alkynes aside from TCOs and norbornenes were developed as dienophiles to conjugate with tetrazines. Prescher[75] and Devaraj[76] independently discovered that methylcyclopropenes were amendable to reactions with tetrazines. Although these conjugations are significantly slower than TCO-tetrazine ligation, they are smaller in size. Bicyclo[6.1.0]non-4-yne

(BCN), which was originally developed by van Delft[36] for use in SPAAC, was later utilized by Wang as dienophile towards tetrazines.[77] The reaction rate of BCN-tetrazine pair (k_2 measured 44.8 M^{-1} s^{-1} in MeOH) was not comparable to TCO-tetrazine ligation, yet the relatively more straightforward synthetic route to BCN has made it popular in the field of chemical biology.

Table 1.2: Representative inverse-electron-demand Diels-Alder cycloadditions (IEDDA) and their reaction rates.[4,40,49,53,54,75-78]

Entry	Dienophile	Cycloadduct	k_2 (M^{-1} s^{-1})
1	***trans*-Cyclooctene (TCO)** 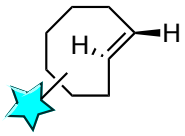	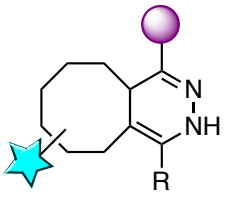	$10 - 10^5$
2	**sTCO** 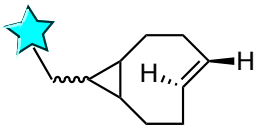	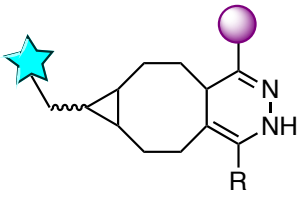	$10^5 - 10^7$
3	**Norbornene** 	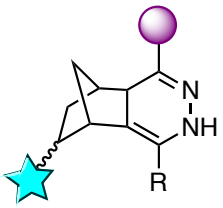	1 - 10
4	**Cyclopropene** 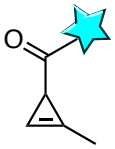	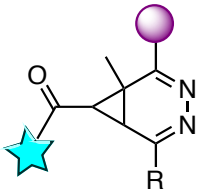	10 - 100
5	**Bicyclo[6.1.0]non-4-yne (BCN)** 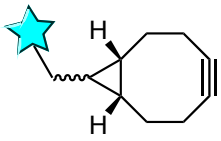	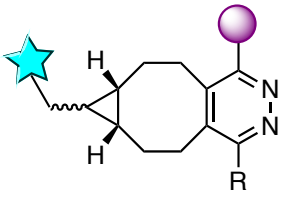	$10^2 - 10^4$

1.3 Flow Photochemical *trans*-Cyclooctene Synthesis

The development and applications of TCO-tetrazine ligation largely rely on the synthesis of *trans*-cyclooctene derivatives. The first synthesis of parent *trans*-

cyclooctene was reported in 1950 by when Ziegler and Wilms. Mixture of *cis*-cyclooctene and *trans*-cyclooctene were prepared through Hoffman elimination of trimethylcyclooctyl ammonium iodide (Scheme 1.3).[79] In 1953, Cope and co-workers reported isolation of pure *trans*-cyclooctene by extraction with 20% aqueous silver nitrate (Scheme 1.3).[80] *trans*-Cyclooctene forms a water-soluble complex with silver nitrate while the *cis*-isomer is retained in the organic phase. Pure *trans*-cyclooctene was recovered by treating the complex with ammonium hydroxide.

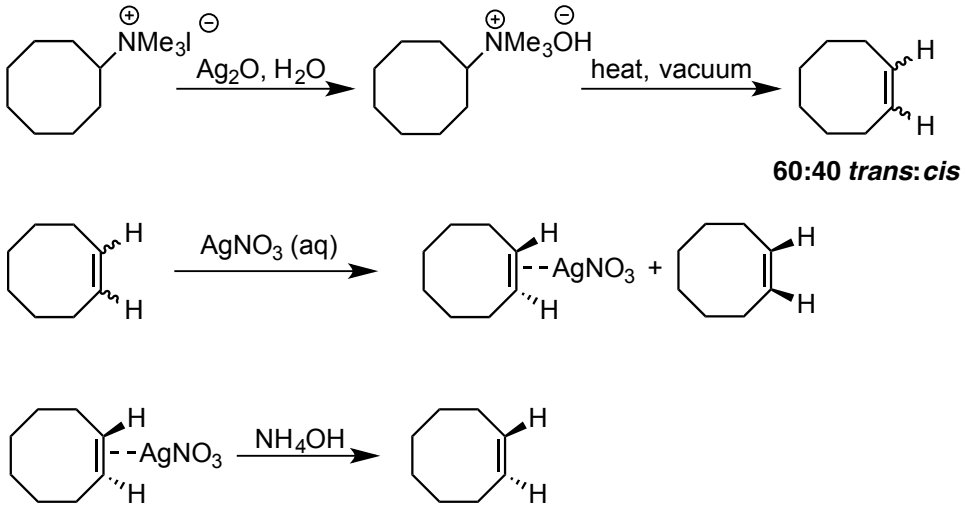

Scheme 1.3: Ziegler[79] and Cope's[80,81] approaches of parent *trans*-cyclooctene.

A number of methods for the synthesis of parent *trans*-cyclooctene have been reported,[82-84] yet the methods of preparing functionalized *trans*-cyclooctene derivatives are limited.[85-88] There are a few approaches reported over the years but most of them require multiple steps and often involve harsh conditions. An attractive alternative approach is to utilize alkene isomerization to directly elaborate *trans*-

cyclooctene derivatives from the corresponding *cis*-isomers. The photoisomerization of *cis*-cyclooctene to *trans*-cyclooctene was first reported by Swenton[89] in 1969 and was extensively studied by Inoue in the past decades. In 1977, Inoue reported the direct *cis*-*trans* photoisomerization of cyclooctene using 185 nm UV irradiation which could produce *trans*-cyclooctene in gram scale at yield of 26%.[90] In the following years, Inoue continued his study of cyclooctene photoisomerization and extensively investigated the singlet sensitization using aromatic esters. A series of articles were published towards the evaluation of reaction conditions such as solvent,[91,92] temperature,[91,93-95] pressure,[96] as well as enantioselective photoisomerization with help of chiral photosensitizers.[91,93-102] These studies have greatly expanded the scope and understanding of the photoisomerization. However, the photochemical synthesis of functionalized *trans*-cyclooctene derivatives was still limited by low *trans*/*cis* ratio under preparative conditions.

In 2008, Royzen and Fox devised a closed-loop flow photochemical reactor that enables efficient preparation of *trans*-cyclooctene and derivatives in the scale of grams with excellent yields.[103] This design exploits Le Chatelier's principle by introducing silver (I) nitrate as a *trans*-cyclooctene scavenger, by removing *trans*-isomer from the system, the equilibrium between *trans* and *cis*-isomers can be perturbed to favor the *trans*-isomer.

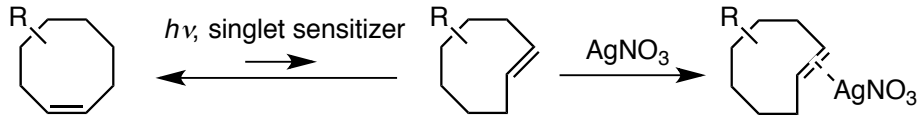

Scheme 1.4: Coordination of silver nitrate drives the unfavorable *trans*/*cis* equilibrium by forming a stable *trans*-cyclooctene silver complex.

Shown in Figure 1.1 is an illustration of the flow photoisomerization apparatus. A solution containing the *cis*-cycloalkene substrate and a photosensitizer (in this case methyl benzoate) solution was irradiated at 254 nm in a Rayonet® photoreactor and the solution was continuously cycled through a column packed with $AgNO_3$ adsorbed onto silica gel. The *trans*-isomer is trapped on the silica gel in form of a silver(I) complex while the *cis*-isomer can flow back to the photoreactor. The process is constantly repeated until the starting material is depleted. The *trans*-cyclooctene product can easily be liberated by treating the silver complex with ammonium hydroxide.

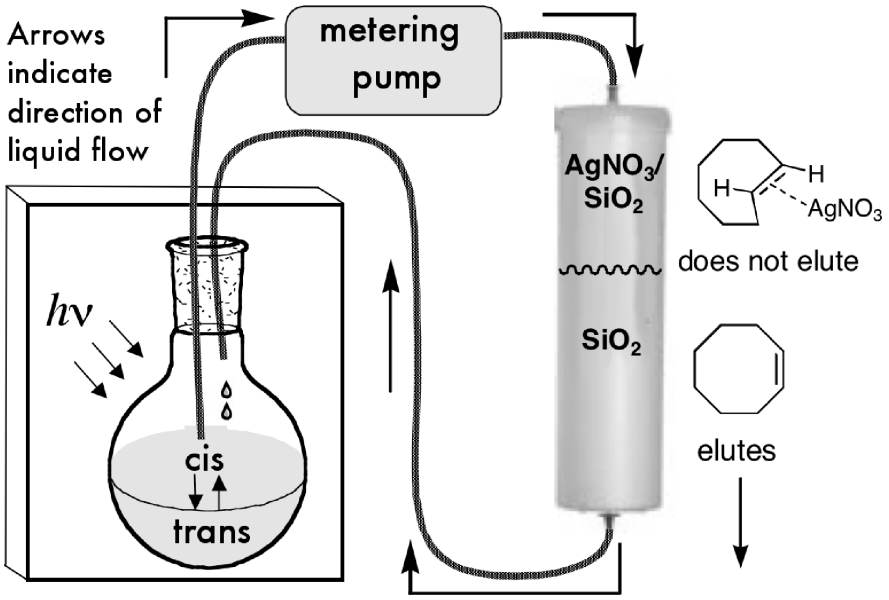

Figure 1.1: Illustration of Royzen and Fox's closed-loop flow photochemical reactor.[103]

Royzen and Fox's approach was the first practical example of preparative scale, direct synthesis of functionalized *trans*-cyclooctene derivatives from *cis*-cyclooctene precursors. A series of *trans*-cyclooctene derivatives were prepared successfully on gram scale and satisfactory yield (Table 1.3).

Table 1.3: Representative substrates synthesized using the closed-loop flow photochemical reactor.[103]

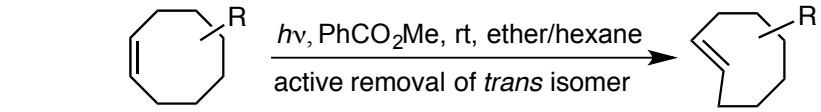

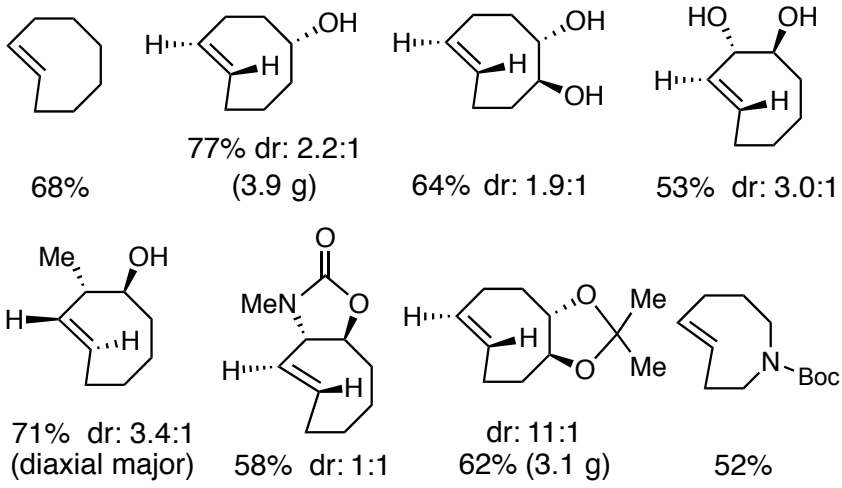

1.4 Flow-enabled Photosynthesis of *trans*-Cycloheptene (TCH) and hetero-*trans*-Cycloheptene Derivatives

trans-Cycloheptene possesses a high strain energy of 25 kcal/mol[104] and a severely twisted alkene bond with dihedral angle of 116.3° (compared to 139° that of *trans*-Cyclooctene)[105] which makes it highly reactive and thermally unstable. At room temperature, *trans*-cycloheptene rapidly isomerizes back to *cis*-cycloheptene with a half-life as short as 45 seconds[106] at r.t. Even at –10 C°, the isomerization of *trans*-cycloheptene is still quite fast (half-life 23 minutes).[106] Due to the very limited stability, there has been very little investigation into the chemistry of *trans*-cycloheptene compared to its eight-member ring homolog, *trans*-cyclooctene.

1.4.1 Previous Arts of *trans*-Cycloheptene Synthesis

The trapping of *trans*-cycloheptene was first reported by Corey in 1965.[107] In this study, *trans*-1,2-cycloheptenethionocarbonate was treated with $P(OMe)_3$ generating the unstable parent *trans*-cycloheptene which was trapped *in situ* with diphenylisobenzofuran, forming a *trans*-cycloadduct (Scheme 1.5).

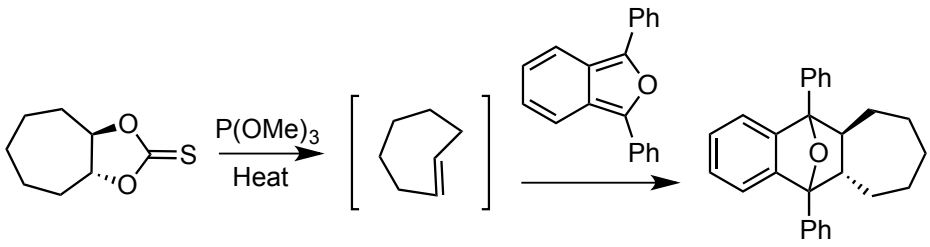

Scheme 1.5: Corey's trapping of parent *trans*-Cycloheptene.[107]

As mentioned before, Inoue have made tremendous efforts on developing methods for medium-size cycloalkane photoisomerization, which includes the direct photochemical synthesis of *trans*-cycloheptene.[104,106,108] In 1981, Inoue and co-workers reported preparation of *trans*-cycloheptene at –78 °C by a singlet-sensitized photoisomerization of the *cis*-isomer.[104] The *trans*-cycloheptene was subsequently trapped by acidic methanol to give methoxycycloheptene in 15% yield.

Similar to *trans*-cyclooctenes, *trans*-cycloheptenes serve as excellent ligands for transition metals and it has been demonstrated in several studies that the *trans*-cycloheptene metal complexes are isolable. Jendralla reported that the preparation of $AgClO_4$ and AgOTf complexes of 3-methoxy-*trans*-cycloheptene and 6-methoxy-(*Z*),4(*E*)-cycloheptadiene and the $AgClO_4 \cdot$3-methoxy-*trans*-cycloheptene complex are

able to reversibly dissociate and react with a number of dienes to give 4+2 cycloadducts (Scheme 1.6).[109-111]

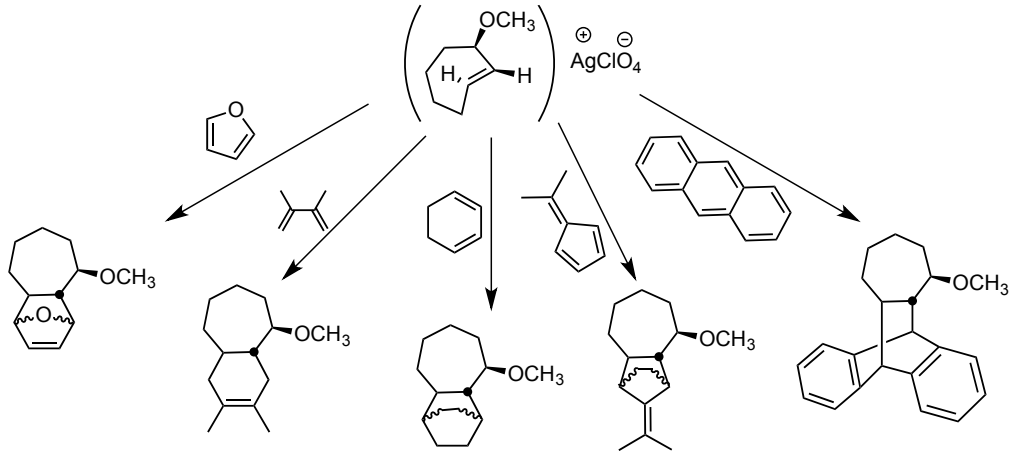

Scheme 1.6: Jendralla's study towards 3-methoxy-*trans*-cycloheptene silver complex.[109]

By incorporating silicon into the *trans*-cycloheptene backbone, it is possible to partially relieve the high strain energy and distorted alkene bond of *trans*-cycloheptene because of the longer C-Si bonds. Several room temperature-stable silicon-containing *trans*-cycloheptene derivatives have been synthesized. In 1991, Ando[112] reported preparation of *trans*-l,2-Dipheny1-4,4,5,5,6,6-hexamethyl-4,5,6-trisila-cycloheptene from photoisomerization of its *cis*-isomer. In 1999, enantiomerically pure (*E*)-1,1,3,3,6,6-hexamethyl-1-sila-4-cycloheptene was synthesized, resolved and characterized crystallographically by Krebs.[113] Recent studies by Woerpel demonstrated application of heteroatom-containing *trans*-oxasilacycloheptene derivatives in synthesis.[114-117]

1.4.2 Modification of the Flow Photochemistry Apparatus

I sought to adapt the current well-developed method of synthesizing *trans*-cyclooctenes[103] into the synthesis of *trans*-cycloheptenes. Due to the thermal lability of *trans*-cycloheptenes and the previous arts in which it was demonstrated that *trans*-cycloheptenes complexes are isolable, I planned to isolate and store *trans*-cycloheptenes in form of silver(I) complexes, in this way the products can maintain their reactivity as *trans*-isomer and can stay intact from undesired isomerization.

Due to the thermal lability of carbocyclic *trans*-cycloheptenes, it was necessary to alter our reactor design (Figure 1.2). In the modified configuration, the reservoir containing starting substrates and sensitizers were moved out of the photowell and put in a temperature controlled chilling bath (–50 °C). The photoisomerization was carried out in a coil of optically transparent FEP (fluorinated ethylene propylene) tubing[118] which provides higher surface area and minimal volume (approx. 30 mL for a tubing coil of 8 m length) compared to quartz flask. The use of FEP tubing also minimized the time lag (typical flow rate was set to 100 mL/min) between photoisomerization and product scavenging on silver nitrate impregnated silica gel. I sought to learn if the apparatus could serve to minimize undesired isomerization and degradation of the *trans*-cycloheptene product before it could be captured as a Ag(I) complex.

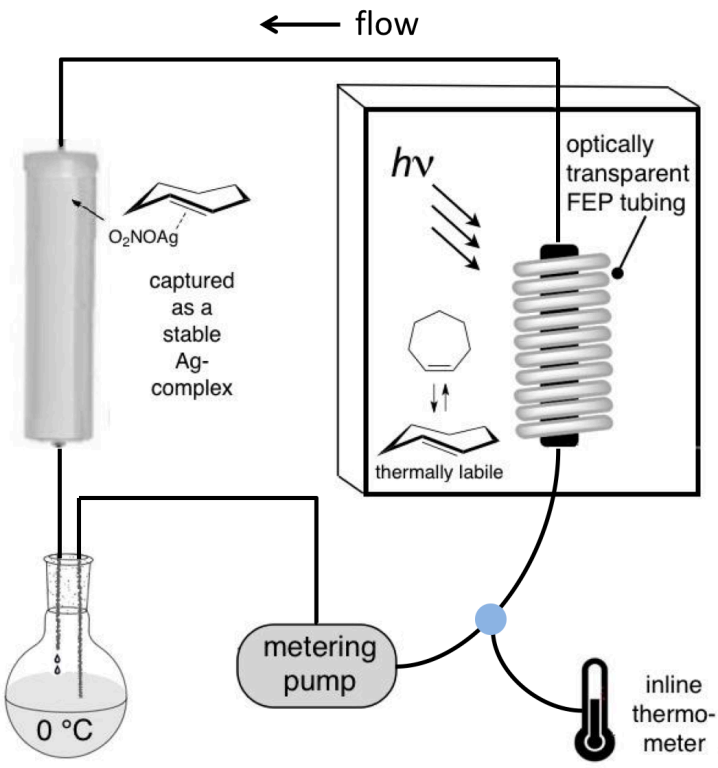

Figure 1.2: Illustration of modified flow photochemical reactor apparatus for *trans*-cycloheptene synthesis.

1.4.3 Photosynthesis and Reactivity of *trans*-Cycloheptene (TCH) and hetero-*trans*-Cycloheptene Derivatives

With the newly modified flow photoreactor in hand, I moved on to test out the photoisomerization of *cis*-cycloheptene and hetero-*cis*-cycloheptene substrates. Reaction conditions such as solution concentration, solvent polarity, temperature, flow rate, tubing volume size were carefully evaluated.

According to an earlier mechanistic study,[119] the isomerization from *trans*-cycloheptene to its *cis*-isomer proceeds via an "interrupted dimerization" mechanism, where an initially formed 1,4-biradical changes geometry rapidly and cleaves to produce two *cis*-cycloheptene molecules. According to this theory, the concentration

of reaction solution mixture could play significant role in the reaction efficiency. Thus, I chose to run the reaction at relatively diluted concentration (approx. 10 mM) to prevent possible dimerization.

Solvent-wise, mixture consisted of various ratios of diethyl ether and hexanes were used according to the inherent polarity of *cis*-cycloheptene substrates. Solvent with proper polarity was chosen to ensure successful turnover of unreacted *cis*-cycloheptene while not too polar to flush the *cis*-cycloheptene silver(I) complex and silver nitrate off the column. A Neslab CB 80 was used to regulate an ethanol bath to –50 °C, and the inline temperature of the reaction mixture before entering photowell was measured to be 0 °C and the inline temperature after exiting the photowell but before entering the silver nitrate impregnated silica column was measured to be 20 °C. In each photoisomerization, approx. 5 mmol *cis*-cycloheptene substrate was used with coil of FEP tubing with a 30 mL capacity. The flow rate was set to 100 mL/min which made the time delay between irradiation and trapping on $AgNO_3$/silica to be 20 seconds.

With the above parameters determined, I carried out photoisomerization of commercial available parent *cis*-cycloheptene. The *cis* substrates were consumed in 6 hours, based on GC analysis. Different solvents (MeOH/DCM, ethanol and acetonitrile) were tested to extract the silver(I) complex out of silica column and ethanol showed best performance. The resulting *trans*-cycloheptene silver(I) complex was stored in –18 °C freezer without isomerization. While the Ag(I) complex could be isolated as a solid, it was contaminated by excess $AgNO_3$, which lead to an overestimation of the yield when the solid was directly weighed. Thus, the yield was

determined by ^{1}H NMR analysis, and measured to be 53% by ^{1}H NMR using mesitylene as internal standard.

Besides parent *cis*-cycloheptene, I also carried out the syntheses and photoisomerizations of substrates (4*Z*)-cyclohept-4-en-1-ylmethanol and (*Z*)-*Si, Si*-diphenyl-5-silacycloheptene to afford silver complexes (4*E*)-Cyclohept-4-en-1-ylmethanol•$AgNO_3$ and (*E*)-Si, Si-diphenyl-5-silacycloheptene•$AgNO_3$ with yields of 60% and 66%, respectively.

Graduate student Yinzhi Fang extensively participated in this project and developed numbers of hetero-*cis*-cycloheptene substrates and carried out photoisomerizations on them (substrates **1-4** to **1-7** in Table 1.4). A summary of successful photochemical *trans*-cycloheptene and hetero-*trans*-cycloheptene syntheses is illustrated in Table 1.4.

Table 1.4: Summary of Successful Photochemical *trans*-Cycloheptene and hetero-*trans*-Cycloheptene Substrates. Compounds **1-1** – **1-3** were prepared by me. Compounds **1-4** – **1-7** were prepared by Yinzhi Fang.

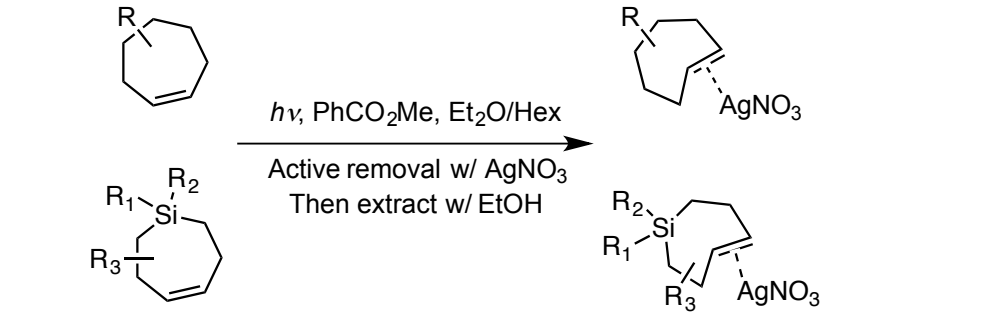

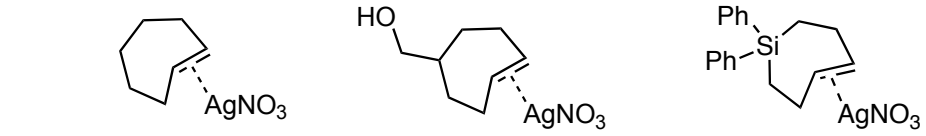

1-1 53%

1-2 64%

1-3 53%

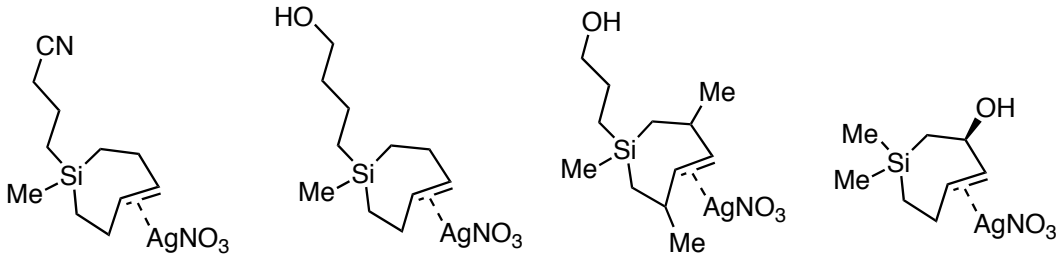

1-4 77%

1-5 72%

1-6 64%

1-7 62%
dr: 1.1:1

I furthermore performed a series of reactivity experiments (Table 1.5) on *trans*-cycloheptene·$AgNO_3$ (**1-1**) to produce dihydroxylation product (**1-10**) and cycloaddition products (**1-8**; **1-9**). The reactions proceeded smoothly in ethanol solution without prior removal of coordinated $AgNO_3$.

Table 1.6: Reactivity Scope of *trans*-Cycloheptene·$AgNO_3$ (**1-1**)

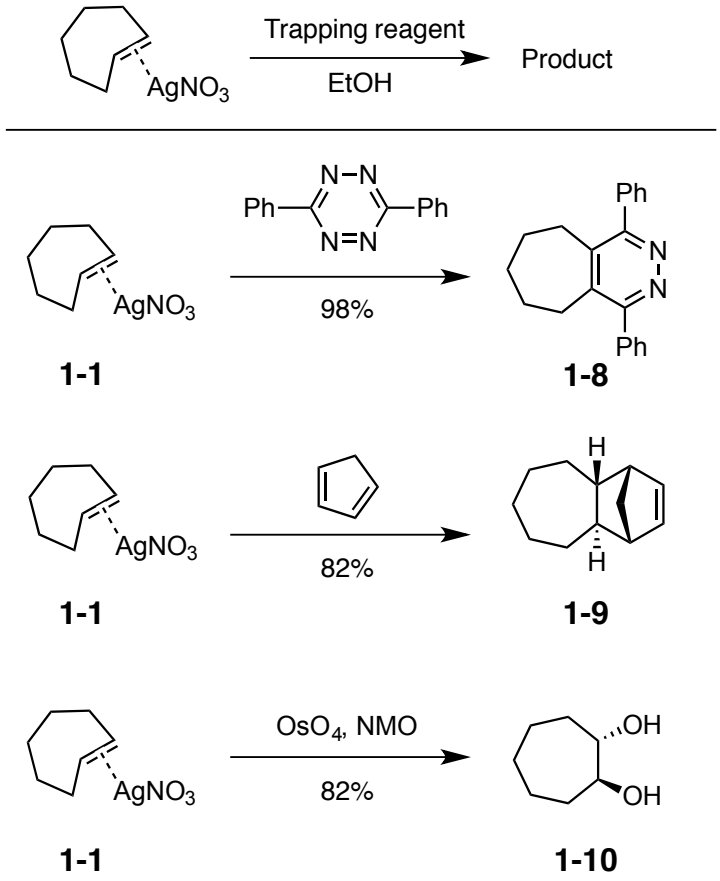

Because of the incorporation of silicon atom, the hetero-*trans*-cycloheptenes exhibit better stability compared to the carbon-cyclic *trans*-cycloheptenes and have good stability in solution. Thus the reactivity experiments were carried out in solution after desalting of the $AgNO_3$ (Table 1.6). Fleming-Tamao oxidation with cycloadduct (5a*S*,6*R*,9*S*,9a*S*)-3,3-diphenyl-2,3,4,5,5a,6,9,9a-octahydro-1H-6,9-methanobenzo[*d*]silepine (**1-13**) provided the corresponding ring-opening product 2,2'-((1*R*,2*S*,3*S*,4*S*)-bicyclo[2.2.1]hept-5-ene-2,3-diyl)bis(ethan-1-ol) (**1-16**)

Table 1.7: Reactivity Scope of (*E*)-Si, Si-diphenyl-5-silacycloheptene (**1-11**). Compounds **1-13** and **1-16** were prepared by me. Compounds **1-12**, **1-14** and **1-15** were prepared by Yinzhi Fang.

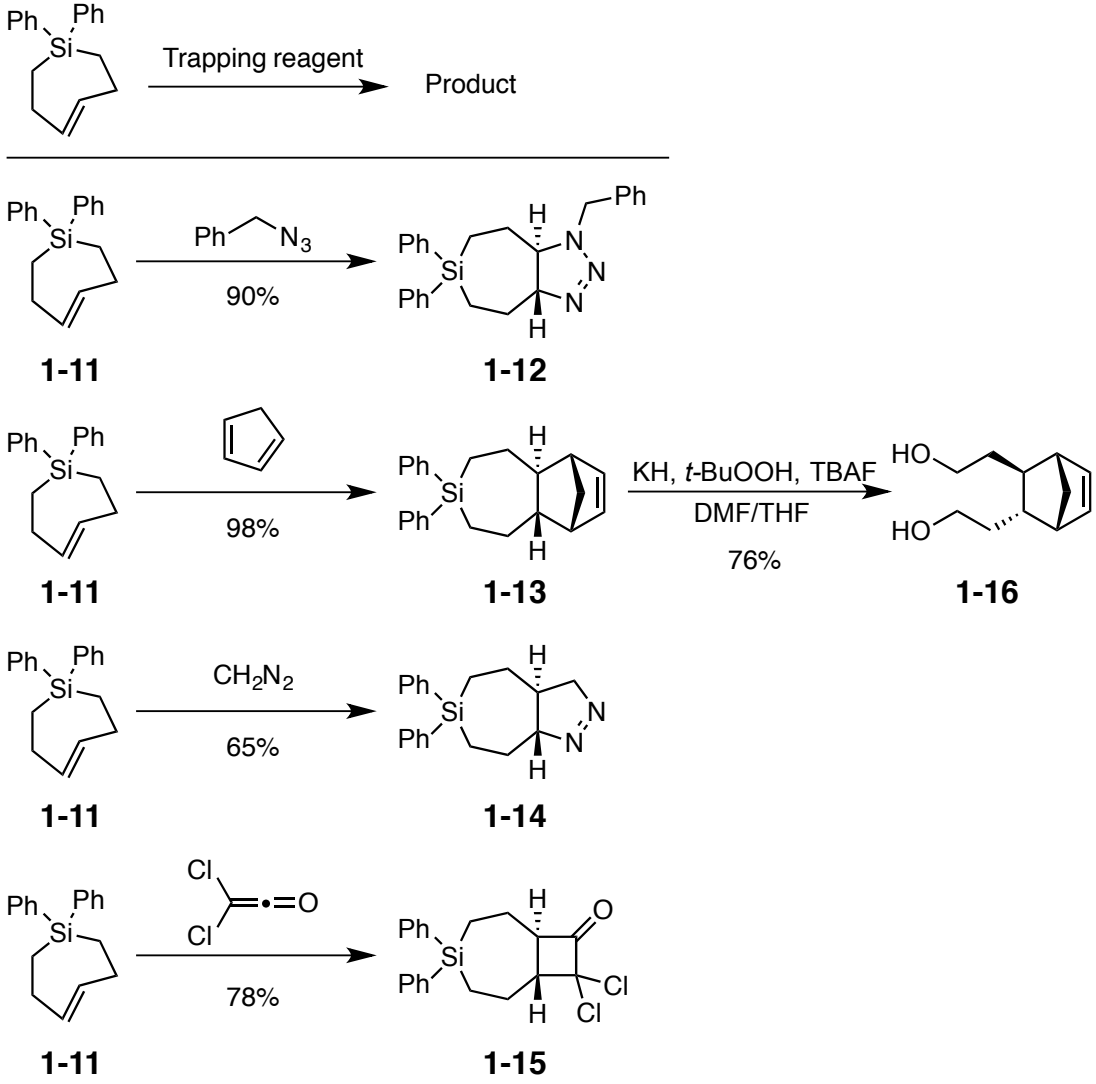

1.5 Conclusions

The bioorthogonal *trans*-cyclooctene-tetrazine ligation has emerged into a powerful tool in the field of biomedical research. The development and the versatile applications of tetrazine ligation was made possible by the advancement of *trans*-cyclooctene synthesis. Based on the previous art of photoisomerization methods in

Fox group, I carried out the first practical photosynthesis of *trans*-cycloheptene derivatives that were stabilized as silver(I) complexes form, as well as the photoisomerization of silicon-containing hetero-*trans*-cycloheptene derivatives. The reactivity of both the *trans*-cycloheptene silver(I) complexes and the hetero-*trans*-cycloheptene derivatives were investigated.

1.6 Experimental Procedures

General Considerations

2-(but-3-en-1-yl) hex-5-enoic acid[120] and silver nitrate impregnated silica gel[103] were prepared by known procedures. THF was purified by distillation from Na/benzophenone. All other solvents and reagents were purchased from commercial sources without additional purification. All reactions were carried out in glassware that was flame-dried under vacuum and cooled under nitrogen. Flash Chromatography was performed using normal phase Silicycle silica gel (40-63D, 60Å). An APT pulse sequence was used for ^{13}C NMR spectra, where methylene and quaternary carbons appear 'up' (u), and methine and methyl carbons appear 'down' (dn).

2-(but-3-en-1-yl)hex-5-en-1-ol (1-17)

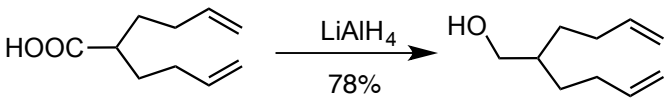

1-16 **1-17**

A dry two-neck round-bottom flask equipped with a reflux condenser was sequentially charged with anhydrous THF (5.30 mL) and $LiAlH_4$ (271 mg, 7.14 mmol).

The mixture was chilled by an ice bath, and a solution of 2-(but-3-en-1-yl) hex-5-enoic acid[120] (**1-16**, 600 mg, 3.57 mmol) in anhydrous THF (5.30 mL) was added dropwise with a syringe. The reaction mixture was then heated to reflux overnight. The reaction mixture was then allowed to cool to room temperature and then to ice bath temperature, and 20 mL of 15% NaOH solution was added dropwise. The resulting mixture was filtered and the filter cake was washed with ethyl acetate (20 mL). The aqueous phase was extracted with ethyl acetate (3 × 20 mL). The resulting solution was dried with Na_2SO_4, filtered and concentrated on the rotary evaporator. Purification by column chromatography with a gradient of 5% ethyl acetate in hexanes yielded 2-(but-3-en-1-yl)hex-5-en-1-ol (**1-17**, 431 mg, 2.80 mmol, 78%) as a clear oil. ^{1}H NMR (600 MHz, $CDCl_3$) δ: 5.82 (ddt, *J* = 16.9, 10.2, 6.6 Hz, 2H), 5.04-5.01 (m, 2H), 4.97-4.95 (m, 2H), 3.58 (d, *J* = 5.3 Hz, 2H), 2.09 (dt, *J* = 14.4, 7.2 Hz, 2H), 1.57-1.53 (m, 1H), 1.50-1.44 (m, 2H), 1.43-1.37 (m, 2H), 1.35 (s, 1H); ^{13}C NMR (100MHz, $CDCl_3$) δ:139.0 (CH), 114.6 (CH_2), 65.3 (CH_2), 39.5 (CH), 31.2 (CH_2), 30.2 (CH_2); HRMS (CI) *m/z*: $[M+H]^+$ calcd. for $C_{10}H_{19}O^+$, 155.1436 found 155.1420.

(4*Z*)-Cyclohept-4-en-1-ylmethanol (1-18)

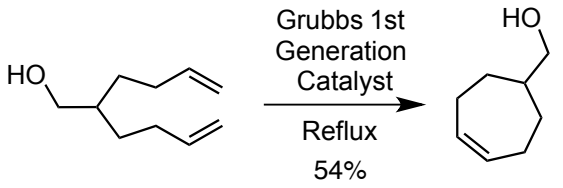

1-17 **1-18**

A 2 L round-bottom flask equipped with a reflux condenser was charged with 1 L of dichloromethane, followed by addition of 2-(but-3-en-1-yl)hex-5-en-1-ol (1.00

g, 6.49 mmol, 1.00 equv). The solution was heated to reflux by an oil bath at 47 °C. Grubbs 1st generation catalyst (267 mg, 0.324 mmol, 0.05 equiv) was added. The reaction mixture was allowed to reflux for 3 hours. The solvent was removed with a rotary evaporator. Purification by column chromatography with 8% ethyl acetate in hexanes yielded 430 mg (3.41 mmol, 54%) of the title compound (**1-18**) as a green oil. ^{1}H NMR (600 MHz, $CDCl_3$) δ: 5.79-5.72 (m, 2H), 3.42 (d, *J* = 6.5 Hz, 2H), 2.29-2.17 (m, 3H), 2.07-2.00 (m, 2H), 1.80-1.75 (m, 2H), 1.72-1.64 (m, 1H), 1.15-1.06 (m, 2H); ^{13}C NMR (100MHz, $CDCl_3$) δ: 132.1 (CH), 68.2 (CH_2), 44.9 (CH), 29.6 (CH_2), 26.9 (CH_2); HRMS (CI) *m/z*: $[M+H]^+$ calcd. for $C_8H_{15}O^+$, 127.1123 found 127.1105.

Di(but-3-en-1-yl)diphenylsilane (1-19)

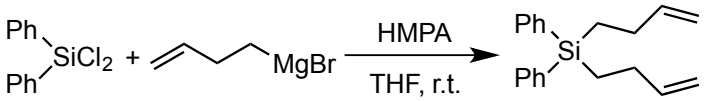

1-19

A dry round-bottomed flask was charged with Mg (2.85 g, 119 mmol, 3.50 equiv) and dry THF (200 mL) under nitrogen atmosphere. 4-Bromo-l-butene (12.3 ml, 121 mmol, 3.56 equiv) was introduced to the flask dropwise via syringe. The reaction mixture was allowed to stir at room temperature. After the formation of the Grignard reagent was judged complete, HMPA (29.6 ml, 170 mmol, 5.00 equiv, dried over molecular sieve) was added, followed by dichlorodiphenylsilane (7.15 ml, 34.0 mmol, 1.00 equiv). The reaction mixture was stirred at room temperature overnight. After reaction, THF was removed via rotary evaporation. Saturated aq. NH_4Cl (100 mL) and ethyl acetate (100 mL) were added and the aqueous layer was extracted three times

with ethyl acetate. The organics were combined, dried with anhydrous $MgSO_4$, filtered, and concentrated via rotary evaporation. Purification by flash column chromatography (hexane) afforded the title compound as colorless oil (**1-19**, 7.03 g, 24.0 mmol, 71%). ^{1}H NMR (400 MHz, $CDCl_3$) δ: 7.54-7.49 (m, 4H), 7.43-7.33 (m, 6H), 5.95-5.83 (m, 2H), 5.03-4.82 (m, 4H), 2.15-2.06 (m, 4H), 1.25-1.17 (m, 4H); ^{13}C NMR (100MHz, $CDCl_3$) δ: 141.4 (CH), 135.8 (C), 135.0 (CH), 129.4 (CH), 128.0 (CH), 113.1 (CH_2), 27.9 (CH_2), 11.8 (CH_2); HRMS (LIFDI-TOF) *m/z*: $[M]^+$ calculated for $C_{20}H_{24}Si^+$ 292.1642; Found 292.1659.

(*Z*)-Si,-Si-diphenyl-5-sila-cycloheptene (1-20)

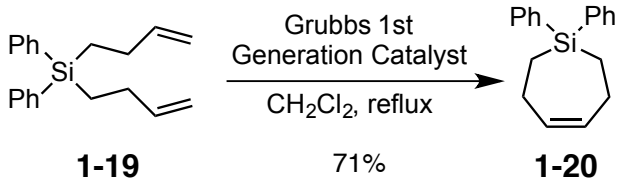

1-19 71% **1-20**

Di(but-3-en-1-yl)diphenylsilane (7.03 g, 24.0 mmol, 1.00 equiv) was dissolved in dry CH_2Cl_2 (120 mL). Grubbs 1st generation catalyst (594 mg, 0.722 mmol, 0.030 equiv) was added as a solution in CH_2Cl_2 (1.7 L) and the mixture was refluxed under nitrogen for 1 hour. The mixture was cooled to room temperature, and the reaction mixture was concentrated via rotary evaporation. Purification by flash column chromatography (hexane, R_f=0.6) afforded the title compound (**1-20**, 4.50 g, 71% yield) as colorless solid, mp 59 °C. ^{1}H NMR (400 MHz, $CDCl_3$) δ: 7.56-7.50 (m, 4H), 7.41-7.32 (m, 6H), 5.90-5.82 (m, 2H), 2.40-2.30 (m, 4H), 1.29-1.22 (m, 4H); ^{13}C NMR (100MHz, $CDCl_3$) δ: 137.2 (CH), 134.7 (C), 132.7 (CH), 129.3 (CH), 128.0

(CH), 21.1 (CH_2), 11.4 (CH_2); HRMS (LIFDI-TOF) *m/z*: $[M]^+$ calculated for $C_{18}H_{20}Si^+$ 264.1329; Found 264.1338.

***trans*-Cycloheptene•$AgNO_3$ (1-1)**

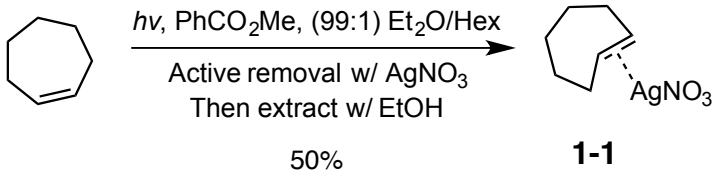

50% **1-1**

The *cis*-cycloheptene (500 mg, 5.20 mmol, 1.00 equiv.) and methyl benzoate (1.43 g, 10.4 mmol, 2.0 equiv) were dissolved in 500 mL of solvent (2% diethyl ether/hexane) in a round bottom flask. The round bottom flask was immersed in a cooling bath (NESLAB CB 80 with a CRYOTROL controller, bath temperature was set to –50 °C) and connected via PTFE tubing successively to an FMI "Q" pump, a three-way tee that was equipped with a thermometer probe, a coil of FEP tubing (total length: 8m; ID: 1/16 inch; OD 1/8 inch) and a 25g Biotage® SNAP cartridge as illustrated in **Figure 1.2**. The FEP tubing coil was placed in a Rayonet® RPR-100 reactor with eight 254 nm bulbs. The bottom of the SNAP cartridge was packed with dry silica gel (6 cm), and the top of the column was packed with silver nitrate impregnated silica (10 wt% of $AgNO_3$, 11.5 g, 1.30 equiv). The column was flushed with 200 mL of the reaction solvent. The pump was turned on and the rate of circulation was adjusted to approx. 100 mL per minute. The temperature at the three-way tee was maintained at 0 ˚C. The lamp was then turned on, and photoisomerization of the stirring mixture was carried out for 6 hours. Afterwards, the sensitizer was flushed from the column with 300 mL of 10% ether in hexanes. The column was then

dried by a stream of compressed air, and then flushed with ethanol. The ethanol solution was concentrated via rotary evaporation, affording dark brown viscous oil consisting of *trans*-cycloheptene•$AgNO_3$ complex (**1-1**) (2.60 mmol by NMR analysis, 50% yield) and free $AgNO_3$. ^{1}H NMR (400 MHz, CD_3OD) δ: 5.57-5.54 (m, 2H), 2.55-2.50 (m, 2H), 2.28-2.19 (m, 2H), 1.75-1.56 (m, 6H); ^{13}C NMR (100MHz, CD_3OD) δ: 120.2 (CH), 32.3 (CH_2), 25.5 (CH_2); HRMS (CI-TOF) *m/z*: $[M\text{-}AgNO_3]^+$ calcd. for $C_7H_{13}^+$ 97.1017, found 97.1021.

(4*E*)-Cyclohept-4-en-1-ylmethanol •$AgNO_3$ (1-2)

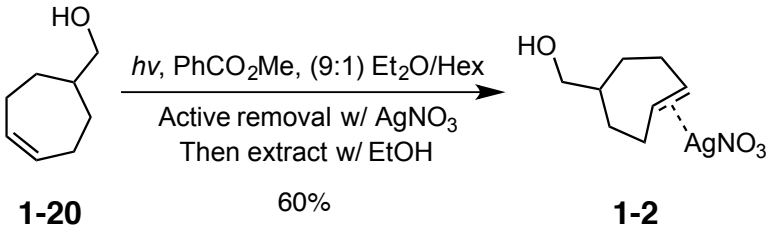

The (4*Z*)-Cyclohept-4-en-1-ylmethanol (**1-20**, 100 mg, 0.79 mmol, 1.00 equiv.) and methyl benzoate (216 mg, 1.59 mmol, 2.0 equiv) were dissolved in 100 mL of solvent (70% diethyl ether/hexane) in a round bottom flask. The round bottom flask was immersed in a cooling bath (NESLAB CB 80 with a CRYOTROL controller, bath temperature was set to –40 °C) and connected via PTFE tubing successively to an FMI "Q" pump, a three-way tee that was equipped with a thermometer probe, a coil of FEP tubing (total length: 2m; ID: 1/16 inch; OD 1/8 inch) and a 10g Biotage® SNAP cartridge as illustrated in Figure **1.2**. The FEP tubing coil was placed in a Rayonet® RPR-100 reactor. The bottom of the column was packed with dry silica gel (4.60 cm), and the top of the SNAP cartridge was packed with silver nitrate impregnated silica

(10 wt% of $AgNO_3$, 2.70 g, 2.00 equiv). The column was flushed with 200 mL of the reaction solvent. The pump was turned on and the rate of circulation was adjusted to approx. 100 mL per minute. The temperature at the three-way tee was maintained at 0 ˚C. The lamp was then turned on, and photoisomerization of the stirring mixture was carried out for 2 hours. Afterwards, the sensitizer was flushed from the column with 100 mL of 10% ether in hexanes. The column was then dried by a stream of compressed air, and then flushed with 100 ml ethanol. The ethanol solution was concentrated via rotary evaporation, affording dark brown viscous oil consisting of (4*E*)-Cyclohept-4-en-1-ylmethanol •$AgNO_3$ complex (**1-2**, 0.474 mmol by NMR analysis, 60% yield) and free $AgNO_3$. ^{1}H NMR (400 MHz, CD_3OD) δ: 5.67 (ddd, *J* = 17.5, 9.9, 5.7 Hz, 1H), 5.39 (ddd, *J* = 17.6, 10.8, 2.6 Hz, 1H), 3.38-3.27 (m, 2H), 2.85-2.80 (m, 1H), 2.52-2.36 (m, 2H), 2.30-2.20 (m, 1H), 2.08-2.03 (m, 1H), 2.01-1.96 (m, 1H), 1.70-1.61 (m, 1H), 1.31-1.21 (m, 1H), 1.14-1.03 (m, 1H); ^{13}C NMR (100MHz, CD_3OD) δ: 121.7 (CH), 118.8 (CH), 68.9 (CH_2), 41.1 (CH), 37.3 (CH_2), 36.4 (CH_2), 35.4 (CH_2), 26.9 (CH_2); HRMS (CI-TOF) *m/z*: $[M\text{-}OH\text{-}AgNO_3]^+$ calcd. for $C_8H_{13}^+$ 109.1017, found 109.1021.

(*E*)-*Si*, *Si*-diphenyl-5-silacycloheptene•$AgNO_3$ (1-3)

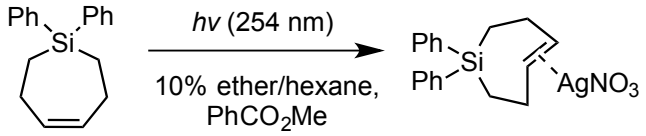

1-20 **1-3**

(*Z*)-*Si, Si*-diphenyl-5-silacycloheptene (**1-20**, 100 mg, 0.378 mmol, 1.00 equiv) and methyl benzoate (285 mg, 1.89 mmol, 5.0 equiv) were placed in a quartz flask and

dissolved in 100 mL of 1:24 Et_2O: hexanes that had been degassed through three freeze/pump/thaw cycles. Dodecane (64.4 mg, 0.378 mmol, 1.00 equiv) was added to the flask to allow for GC monitoring. Following the procedure of Royzen, the flask was configured with a 10 g Biotage® SNAP cartridge and an FMI "Q" pump. The quartz flask was placed in a Rayonet® RPR-100 reactor with eight 254 nm bulbs. The bottom of the Biotage column was packed with dry silica gel, and the top of the SNAP cartridge was packed with silver nitrate impregnated silica (10 wt% of $AgNO_3$, 1.29 g, 2.00 equiv.). The SNAP cartridge was flushed with 100 mL of the reaction solvent. The pump was turned on and the rate of circulation was adjusted to approx. 100 mL per minute. The solution in the quartz flask was then irradiated (254 nm) under continuous flow conditions (100 mL/min) for 3 hours with N_2 sparging, at which point GC analysis indicated that the reaction was complete. The SNAP cartridge was flushed with 100 mL of 1:9 Et_2O/hexanes and then dried with compressed air. The SNAP cartridge was then flushed with 100 mL of EtOH to afford an ethanol solution of (*E*)-*Si*, *Si*-diphenyl-5-silacycloheptene•$AgNO_3$. The ethanol solution was concentrated via rotary evaporation, affording dark brown viscous oil consisting of *trans*-cycloheptene•$AgNO_3$ complex (**1-3**, 0.190 mmol by NMR analysis, 50% yield) and free $AgNO_3$. ^{1}H NMR (400 MHz, CD_3OD) δ: 7.48-7.46 (m, 4H), 7.37-7.34 (m, 6H), 5.57-5.55 (m, 2H), 2.68-2.61 (m, 2H), 2.45-2.36 (m, 2H), 1.67 (ddd, J = 14.7, 8.5, 4.5 Hz, 2H), 1.52-1.45 (m, 2H); ^{13}C NMR (100MHz, CD_3OD) δ: 137.9 (C), 135.2 (CH), 130.2 (CH), 129.1 (CH), 120.2 (CH), 28.6 (CH_2), 17.9 (CH_2); HRMS (CI-TOF) *m/z*: $[M+H-AgNO_3]^+$ calcd. for $C_{18}H_{21}Si^+$ 265.1413, found 265.1424.

1,4-Diphenyl-6,7,8,9-tetrahydro-5H-cyclohepta[*d*]pyridazine (1-8)

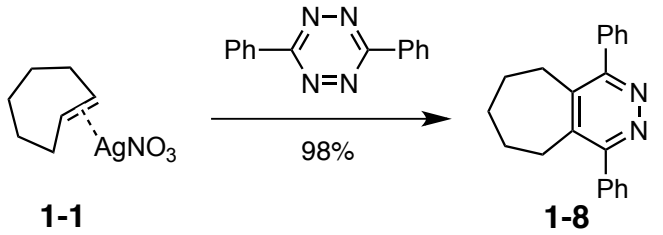

1-1 **1-8**

3,6-diphenyl-s-tetrazine (234 mg, 1.00 mmol) in 10 mL dichloromethane was added to an ethanolic solution of *trans*-cycloheptene•$AgNO_3$ (**1-1**, 0.833 mmol, in 60.0 mL EtOH) with stirring at room temperature. Nitrogen evolved immediately upon mixing and a black precipitate was formed. After stirring for 30 minutes, the reaction mixture was filtered and the filtrate was concentrated down onto silica gel using a rotary evaporator and loaded onto a flash column. Column chromatography using a gradient (0-50%) of ethyl acetate in hexanes followed by 5% methanol in dichloromethane as eluents afforded the title product (**1-8**, 246 mg, 0.820 mmol, 98%) as a white solid, mp 120 °C (decomposition). ^{1}H NMR (600 MHz, $CDCl_3$, δ): 7.48-7.42 (m, 10H), 2.83-2.78 (m, 4H), 1.93-1.86 (m, 2H), 1.72-1.62 (m, 4H). ^{13}C NMR (100 MHz, $CDCl_3$) δ: 161.5 (u, 2C), 145.8 (u, 2C), 137.0 (u, 2C), 130.0 (d, 2C), 129.4 (d, 2C), 128.4 (d, 2C), 31.9 (u, 2C), 31.2(u, 1C), 25.8 (u, 2C); HRMS (LIFDI-TOF) *m/z*: $[M]^+$ for $C_{21}H_2N_2^+$, 300.1621 found 300.1605.

***rel*-(1*R*,4*S*,4a*R*,9a*R*)-4,4a,5,6,7,8,9,9a-Octahydro-1*H*-1,4-methanobenzo[7]annulene (1-9)**

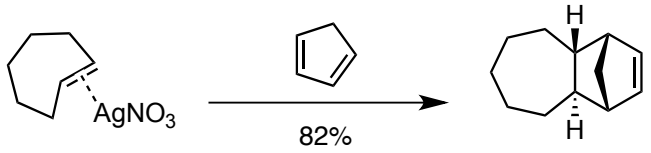

1-1 **1-9**

Freshly cracked cyclopentadiene (412 mg, 6.24 mmol) was added to a 12.5 mM ethanol solution that contains *trans*-cycloheptene silver (I) nitrate complex (**1-1**, 50.0 mL, 0.624 mmol). The mixture was allowed to stir at room temperature overnight. The reaction mixture was then filtered and concentrated down using rotary evaporator. Purification by column chromatography using hexane afforded title product (**1-9**, 83.0 mg, 0.512 mmol, 82%) as a clear oil. ^{1}H NMR (400 MHz, $CDCl_3$, δ): 6.23 (dd, *J*=5.8, 3.0 Hz, 1H), 5.90 (dd, *J*=5.7, 2.9 Hz, 1H), 2.61 (m, 1H), 2.34 (m, 1H), 1.85-1.40 (m, 10H), 1.40-1.33 (m, 1H), 1.30-1.17 (m, 1H), 1.00-0.92 (m, 1H), 0.83-0.72 (m, 1H). ^{13}C NMR ($CDCl_3$, 100 MHz, δ): 139.1 (d, 1C), 131.7 (d, 1C), 47.5 (d, 1C), 47.3 (u, 1C), 47.2 (d, 1C), 45.3 (d, 1C), 44.9 (d, 1C), 32.8 (u, 1C), 30.8 (u, 1C), 29.5 (u, 1C), 29.3 (u, 1C), 25.1 (u, 1C); HRMS (LIFDI-TOF) *m/z*: $[M]^+$ calcd. for $C_{12}H_{18}^+$, 163.1403 found 162.1404.

***rel*-(1*R*,2*R*)-Cycloheptane-1,2-diol (1-10)**

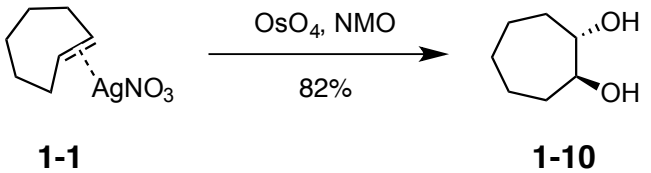

1-1 **1-10**

N-Methylmorpholine *N*-oxide monohydrate (115 mg, 0.852 mmol) and 4 wt% OsO_4 in aqueous solution (125 μL, 20.5 μmol) were sequentially added to an ethanolic solution of *trans*-cycloheptene•$AgNO_3$ (**1-1**, 50.0 mL of a 13.1 mM solution in EtOH,

0.654 mmol) The resulting mixture was allowed to stir for 2 hours at room temperature. The mixture was diluted with saturated $NaHSO_3$ aqueous solution (50 mL) and filtered, and filtrate was extracted with ethyl acetate (8 × 25.0 mL), and the organics were combined, dried over $MgSO_4$ and concentrated by rotary evaporation. Purification by column chromatography with a gradient (0-5%) of methanol in dichloromethane afforded the title compound (**1-10**, 70.0 mg, 0.538 mmol, 82%) as a pale yellow solid, mp 53-54 °C. ^{1}H NMR (600 MHz, $CDCl_3$, δ): 3.45-3.40 (m, 2H), 2.61 (br s, 2H), 1.90-1.85 (m, 2H), 1.70-1.62 (m, 2H), 1.55-1.42 (m, 6H). ^{13}C NMR (100 MHz, $CDCl_3$) δ: 78.1 (d, 2C), 32.5 (u, 2C), 26.5 (u, 1C), 22.2 (d, 2C); HRMS (LIFDI-TOF) *m/z*: $[M]^+$ calcd. for $C_7H_{14}O_2^+$, 130.0988 found 130.0975.

(5aR,9aR)-3,3-diphenyl-2,3,4,5,5a,6,9,9a-octahydro-1H-6,9-methanobenzo[d]silepine (1-13)

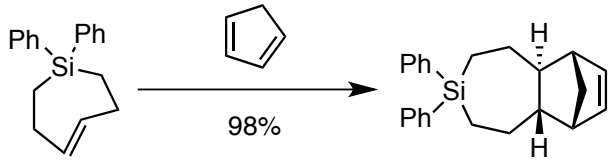

1-11 **1-13**

(*E*)-*Si*, *Si*-Diphenyl-5-silacycloheptene•$AgNO_3$ (**1-11**, 0.305 mmol, 1.0 equiv) was suspended in diethyl ether (2 mL) and ammonium hydroxide (2 mL). The aqueous layer was extracted with 2×2ml diethyl ether. The organics were combined dried with anhydrous Na_2SO_4 and filtered. Then freshly cracked cyclopentadiene (205 mg, 3.05 mmol, 10.0 equiv) was added to this ether solution of (*E*)-*Si*, *Si*-Diphenyl-5-silacycloheptene. The mixture was allowed to stir at room temperature for 1 hour. After reaction, the ether solution was concentrated via rotary evaporation, the residue

was purified by flash column chromatography (1% Diethyl ether/hexane) to afford the title compound (**1-13**, 99.6 mg, 99% yield) as a colorless oil. ^{1}H NMR (400 MHz, $CDCl_3$) δ: 7.50-7.48 (m, 2H), 7.46-7.43 (m, 2H), 7.36-7.29 (m, 6H), 6.11 (dd, *J* = 5.6, 3.0 Hz, 1H), 5.94 (dd, *J* = 5.6, 2.8 Hz, 1H), 2.58 (s, 1H), 2.35 (s, 1H), 2.06-1.99 (m, 1H), 1.94-1.86 (m, 1H), 1.61-1.56 (m, 1H), 1.53-1.44 (m, 2H), 1.43-1.36 (m, 1H), 1.34-1.22 (m, 4H), 1.12-1.02 (m, 1H), 0.98-0.93 (m, 1H); ^{13}C NMR (100MHz, $CDCl_3$) δ: 138.2 (C), 138.12 (C), 138.05 (CH), 134.2 (CH), 133.2 (CH), 129.04 (CH), 128.98 (CH), 128.03 (CH), 127.97 (CH), 49.3 (CH), 47.98 (CH), 47.93 (CH), 46.89 (CH_2) , 46.8 (CH), 30.4 (CH_2), 28.2 (CH_2), 12.9 (CH_2), 12.4 (CH_2); HRMS (LIFDI-TOF) *m/z*: $[M]^+$ calculated for $C_{23}H_{26}Si^+$ 330.1798, found 330.1798.

***rel*-2,2'-((1*R*,2*S*,3*S*,4*S*)-bicyclo[2.2.1]hept-5-ene-2,3-diyl)bis(ethan-1-ol) (1-16)**

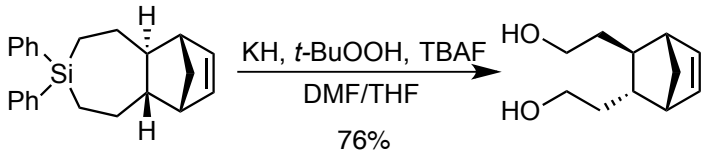

1-13 **1-16**

Potassium hydride (494 mg, 6.18 mmol, purchased as a suspension in mineral oil and rinsed with hexane prior to use) was suspended in DMF (3 mL), and the flask cooled by an ice bath (0 °C). *tert*-Butyl hydroperoxide (1.13 mL, 5.5 M in decane, 6.2 mmol) was added dropwise. The mixture was allowed to warm to room temperature. *rel*-(5a*S*,6*R*,9*S*,9a*S*)-3,3-diphenyl-2,3,4,5,5a,6,9,9a-octahydro-1*H*-6,9-methanobenzo[*d*]silepine (**1-13**, 170 mg, 0.515 mmol) in anhydrous DMF (4 mL) was added to the mixture dropwise. After 10 min, *n*-Bu_4NF solution (1.0 M in THF, 2.10 mL, 2.10 mmol) was added. The reaction was heated at 70 °C overnight. After the

mixture was cooled to room temperature, excessive amount of sodium thiosulfate pentahydrate (3.00 g, 12.1 mmol) was added. After stirring for 30 min, the resulting mixture was filtered and solvent was removed by rotary evaporator. The solid residue was dissolved by dichloromethane and the resulting solution was filtered, and concentrated by rotary evaporation. Purification by column chromatography with a gradient (30%-100%) of ethyl acetate in hexanes yielded title compound (**1-16**, 71.4 mg, 0.396 mmol, 76%) as a white solid, mp 61-63 °C. ^{1}H NMR (600 MHz, $CDCl_3$, δ): 6.18 (dd, *J*=5.8, 3.1 Hz, 1H), 5.99 (dd, *J*=5.8, 2.9 Hz, 1H), 3.80-2.60 (m, 4H), 2.73 (s, 1H), 2.49 (s, 1H), 1.92 (brs, 2H), 1.76-1.62 (m, 3H), 1.49-1.36 (m, 4H), 1.06-1.02 (m, 1H). ^{13}C NMR ($CDCl_3$, 100 MHz, δ): 137.8 (d, 1C), 133.8 (d, 1C), 62.31 (u, 1C), 63.28 (u, 1C), 47.4 (d, 1C), 46.5 (u, 1C), 45.9 (d, 1C), 43.5 (d, 1C), 42.4 (d, 1C), 39.3 (u, 1C), 37.8 (u, 1C); HRMS (LIFDI-TOF) *m/z*: $[M]^+$ calculated for $C_{11}H_{18}O_2^+$ 182.1301, found 182.1286.

REFERENCES

(1) Sletten, E. M.; Bertozzi, C. R. From Mechanism to Mouse: A Tale of Two Bioorthogonal Reactions. *Acc. Chem. Res.* **2011**, *44*, 666-676.

(2) Sletten, E. M.; Bertozzi, C. R. Bioorthogonal Chemistry: Fishing for Selectivity in a Sea of Functionality. *Angew. Chem. Int. Ed.* **2009**, *48*, 6974-6998.

(3) McKay, C. S.; Finn, M. G. Click chemistry in complex mixtures: bioorthogonal bioconjugation. *Chem. Biol.* **2014**, *21*, 1075-1101.

(4) Patterson, D. M.; Nazarova, L. A.; Prescher, J. A. Finding the right (bioorthogonal) chemistry. *ACS Chem. Biol.* **2014**, *9*, 592-605.

(5) Saxon, E.; Bertozzi, C. R. Cell Surface Engineering by a Modified Staudinger Reaction. *Science* **2000**, *287*, 2007.

(6) Saxon, E.; Armstrong, J. I.; Bertozzi, C. R. A "Traceless" Staudinger Ligation for the Chemoselective Synthesis of Amide Bonds. *Org. Lett.* **2000**, *2*, 2141-2143.

(7) Nilsson, B. L.; Kiessling, L. L.; Raines, R. T. Staudinger Ligation: A Peptide from a Thioester and Azide. *Org. Lett.* **2000**, *2*, 1939-1941.

(8) Staudinger, H.; Meyer, J. Über neue organische Phosphorverbindungen III. Phosphinmethylenderivate und Phosphinimine. *Helv. Chim. Acta* **1919**, *2*, 635-646.

(9) Prescher, J. A.; Dube, D. H.; Bertozzi, C. R. Chemical remodelling of cell surfaces in living animals. *Nature* **2004**, *430*, 873-877.

(10) Schilling, C. I.; Jung, N.; Biskup, M.; Schepers, U.; Brase, S. Bioconjugation viaazide-Staudinger ligation: an overview. *Chem. Soc. Rev.* **2011**, *40*, 4840-4871.

(11) Hang, H. C.; Geutjes, E.-J.; Grotenbreg, G.; Pollington, A. M.; Bijlmakers, M. J.; Ploegh, H. L. Chemical Probes for the Rapid Detection of Fatty-Acylated Proteins in Mammalian Cells. *J. Am. Chem. Soc.* **2007**, *129*, 2744-2745.

(12) Neves, A. A.; Stöckmann, H.; Harmston, R. R.; Pryor, H. J.; Alam, I. S.; Ireland-Zecchini, H.; Lewis, D. Y.; Lyons, S. K.; Leeper, F. J.; Brindle, K. M. Imaging sialylated tumor cell glycans in vivo. *FASEB J.* **2011**, *25*, 2528-2537.

(13) Kiick, K. L.; Saxon, E.; Tirrell, D. A.; Bertozzi, C. R. Incorporation of azides into recombinant proteins for chemoselective modification by the Staudinger ligation. *Proc. Natl. Acad. Sci. USA* **2002**, *99*, 19-24.

(14) Ovaa, H.; van Swieten, P. F.; Kessler, B. M.; Leeuwenburgh, M. A.; Fiebiger, E.; van den Nieuwendijk, A. M. C. H.; Galardy, P. J.; van der Marel, G. A.; Ploegh, H. L.; Overkleeft, H. S. Chemistry in Living Cells: Detection of Active

Proteasomes by a Two-Step Labeling Strategy. *Angew. Chem. Int. Ed.* **2003**, *42*, 3626-3629.

(15) Lin, F. L.; Hoyt, H. M.; van Halbeek, H.; Bergman, R. G.; Bertozzi, C. R. Mechanistic Investigation of the Staudinger Ligation. *J. Am. Chem. Soc.* **2005**, *127*, 2686-2695.

(16) Michael, A. Ueber die Einwirkung von Diazobenzolimid auf Acetylendicarbonsäuremethylester. *J. Prakt. Chem.* **1893**, *48*, 94-95.

(17) Huisgen, R. 1,3-Dipolar Cycloadditions. Past and Future. *Angew. Chem. Int. Ed.* **1963**, *2*, 565-598.

(18) Tornøe, C. W.; Christensen, C.; Meldal, M. Peptidotriazoles on Solid Phase: [1,2,3]-Triazoles by Regiospecific Copper(I)-Catalyzed 1,3-Dipolar Cycloadditions of Terminal Alkynes to Azides. *J. Org. Chem.* **2002**, *67*, 3057-3064.

(19) Rostovtsev, V. V.; Green, L. G.; Fokin, V. V.; Sharpless, K. B. A Stepwise Huisgen Cycloaddition Process: Copper(I)-Catalyzed Regioselective "Ligation" of Azides and Terminal Alkynes. *Angew. Chem. Int. Ed.* **2002**, *41*, 2596-2599.

(20) Gouget-Laemmel, A. C.; Yang, J.; Lodhi, M. A.; Siriwardena, A.; Aureau, D.; Boukherroub, R.; Chazalviel, J. N.; Ozanam, F.; Szunerits, S. Functionalization of Azide-Terminated Silicon Surfaces with Glycans Using Click Chemistry: XPS and FTIR Study. *J. Phys. Chem. C.* **2013**, *117*, 368-375.

(21) London, G.; Chen, K.-Y.; Carroll, G. T.; Feringa, B. L. Towards Dynamic Control of Wettability by Using Functionalized Altitudinal Molecular Motors on Solid Surfaces. *Chem. Eur. J.* **2013**, *19*, 10690-10697.

(22) Lallana, E.; Riguera, R.; Fernandez-Megia, E. Reliable and Efficient Procedures for the Conjugation of Biomolecules through Huisgen Azide–Alkyne Cycloadditions. *Angew. Chem. Int. Ed.* **2011**, *50*, 8794-8804.

(23) Meldal, M.; Tornøe, C. W. Cu-Catalyzed Azide−Alkyne Cycloaddition. *Chem. Rev.* **2008**, *108*, 2952-3015.

(24) Lutz, J.-F.; Zarafshani, Z. Efficient construction of therapeutics, bioconjugates, biomaterials and bioactive surfaces using azide–alkyne "click" chemistry. *Adv. Drug Del. Rev.* **2008**, *60*, 958-970.

(25) Moses, J. E.; Moorhouse, A. D. The growing applications of click chemistry. *Chem. Soc. Rev.* **2007**, *36*, 1249-1262.

(26) Arseneault, M.; Wafer, C.; Morin, J.-F. Recent Advances in Click Chemistry Applied to Dendrimer Synthesis. *Molecules* **2015**, *20*.

(27) Kalia, J.; Raines, R. T. Advances in Bioconjugation. *Curr. Org. Chem.* **2010**, *14*, 138-147.

(28) Wolbers, F.; ter Braak, P.; Le Gac, S.; Luttge, R.; Andersson, H.; Vermes, I.; van den Berg, A. Viability study of HL60 cells in contact with commonly used microchip materials. *Electrophoresis* **2006**, *27*, 5073-5080.

(29) Hong, V.; Steinmetz, N. F.; Manchester, M.; Finn, M. G. Labeling Live Cells by Copper-Catalyzed Alkyne−Azide Click Chemistry. *Bioconjugate Chem.* **2010**, *21*, 1912-1916.

(30) Agard, N. J.; Baskin, J. M.; Prescher, J. A.; Lo, A.; Bertozzi, C. R. A Comparative Study of Bioorthogonal Reactions with Azides. *ACS Chem. Biol.* **2006**, *1*, 644-648.

(31) Kennedy, D. C.; McKay, C. S.; Legault, M. C. B.; Danielson, D. C.; Blake, J. A.; Pegoraro, A. F.; Stolow, A.; Mester, Z.; Pezacki, J. P. Cellular Consequences of Copper Complexes Used To Catalyze Bioorthogonal Click Reactions. *J. Am. Chem. Soc.* **2011**, *133*, 17993-18001.

(32) Agard, N. J.; Prescher, J. A.; Bertozzi, C. R. A Strain-Promoted [3 + 2] Azide−Alkyne Cycloaddition for Covalent Modification of Biomolecules in Living Systems. *J. Am. Chem. Soc.* **2004**, *126*, 15046-15047.

(33) Codelli, J. A.; Baskin, J. M.; Agard, N. J.; Bertozzi, C. R. Second-Generation Difluorinated Cyclooctynes for Copper-Free Click Chemistry. *J. Am. Chem. Soc.* **2008**, *130*, 11486-11493.

(34) Gordon, C. G.; Mackey, J. L.; Jewett, J. C.; Sletten, E. M.; Houk, K. N.; Bertozzi, C. R. Reactivity of Biarylazacyclooctynones in Copper-Free Click Chemistry. *J. Am. Chem. Soc.* **2012**, *134*, 9199-9208.

(35) Ning, X.; Guo, J.; Wolfert, M. A.; Boons, G.-J. Visualizing Metabolically Labeled Glycoconjugates of Living Cells by Copper-Free and Fast Huisgen Cycloadditions. *Angew. Chem. Int. Ed.* **2008**, *47*, 2253-2255.

(36) Dommerholt, J.; Schmidt, S.; Temming, R.; Hendriks, L. J.; Rutjes, F. P.; van Hest, J. C.; Lefeber, D. J.; Friedl, P.; van Delft, F. L. Readily accessible bicyclononynes for bioorthogonal labeling and three-dimensional imaging of living cells. *Angew. Chem. Int. Ed.* **2010**, *49*, 9422-9425.

(37) Debets, M. F.; van Berkel, S. S.; Schoffelen, S.; Rutjes, F. P. J. T.; van Hest, J. C. M.; van Delft, F. L. Aza-dibenzocyclooctynes for fast and efficient enzyme PEGylation via copper-free (3+2) cycloaddition. *Chem. Commun.* **2010**, *46*, 97-99.

(38) Debets, M. F.; van Berkel, S. S.; Dommerholt, J.; Dirks, A. J.; Rutjes, F. P. J. T.; van Delft, F. L. Bioconjugation with Strained Alkenes and Alkynes. *Acc. Chem. Res.* **2011**, *44*, 805-815.

(39) Baskin, J. M.; Prescher, J. A.; Laughlin, S. T.; Agard, N. J.; Chang, P. V.; Miller, I. A.; Lo, A.; Codelli, J. A.; Bertozzi, C. R. Copper-free click chemistry for dynamic in vivo imaging. *Proc. Natl. Acad. Sci. USA* **2007**, *104*, 16793-16797.

(40) Lang, K.; Chin, J. W. Bioorthogonal reactions for labeling proteins. *ACS Chem. Biol.* **2014**, *9*, 16-20.

(41) Rideout, D. Self-assembling cytotoxins. *Science* **1986**, *233*, 561.

(42) Nguyen, D. P.; Elliott, T.; Holt, M.; Muir, T. W.; Chin, J. W. Genetically Encoded 1,2-Aminothiols Facilitate Rapid and Site-Specific Protein Labeling via a Bio-orthogonal Cyanobenzothiazole Condensation. *J. Am. Chem. Soc.* **2011**, *133*, 11418-11421.

(43) Presolski, S. I.; Hong, V.; Cho, S.-H.; Finn, M. G. Tailored Ligand Acceleration of the Cu-Catalyzed Azide−Alkyne Cycloaddition Reaction: Practical and Mechanistic Implications. *J. Am. Chem. Soc.* **2010**, *132*, 14570-14576.

(44) Jewett, J. C.; Sletten, E. M.; Bertozzi, C. R. Rapid Cu-Free Click Chemistry with Readily Synthesized Biarylazacyclooctynones. *J. Am. Chem. Soc.* **2010**, *132*, 3688-3690.

(45) Ning, X.; Temming, R. P.; Dommerholt, J.; Guo, J.; Ania, D. B.; Debets, M. F.; Wolfert, M. A.; Boons, G.-J.; van Delft, F. L. Protein Modification by Strain-Promoted Alkyne–Nitrone Cycloaddition. *Angew. Chem. Int. Ed.* **2010**, *49*, 3065-3068.

(46) Yu, Z.; Pan, Y.; Wang, Z.; Wang, J.; Lin, Q. Genetically Encoded Cyclopropene Directs Rapid, Photoclick-Chemistry-Mediated Protein Labeling in Mammalian Cells. *Angew. Chem. Int. Ed.* **2012**, *51*, 10600-10604.

(47) Sletten, E. M.; Bertozzi, C. R. A Bioorthogonal Quadricyclane Ligation. *J. Am. Chem. Soc.* **2011**, *133*, 17570-17573.

(48) Boger, D. L. Diels-Alder reactions of heterocyclic aza dienes. Scope and applications. *Chem. Rev.* **1986**, *86*, 781-793.

(49) Blackman, M. L.; Royzen, M.; Fox, J. M. Tetrazine Ligation: Fast Bioconjugation Based on Inverse-Electron-Demand Diels−Alder Reactivity. *J. Am. Chem. Soc.* **2008**, *130*, 13518-13519.

(50) Thalhammer, F.; Wallfahrer, U.; Sauer, J. Reaktivität einfacher offenkettiger und cyclischer dienophile bei Diels-Alder-reaktionen mit inversem elektronenbedarf. *Tetrahedron Lett.* **1990**, *31*, 6851-6854.

(51) Sauer, J.; Heldmann, D. K.; Hetzenegger, J.; Krauthan, J.; Sichert, H.; Schuster, J. 1,2,4,5-Tetrazine: Synthesis and Reactivity in [4+2] Cycloadditions. *Eur. J. Org. Chem.* **1998**, *1998*, 2885-2896.

(52) Lang, K.; Davis, L.; Wallace, S.; Mahesh, M.; Cox, D. J.; Blackman, M. L.; Fox, J. M.; Chin, J. W. Genetic Encoding of Bicyclononynes and trans-Cyclooctenes for Site-Specific Protein Labeling in Vitro and in Live Mammalian Cells via Rapid Fluorogenic Diels–Alder Reactions. *J. Am. Chem. Soc.* **2012**, *134*, 10317-10320.

(53) Taylor, M. T.; Blackman, M. L.; Dmitrenko, O.; Fox, J. M. Design and synthesis of highly reactive dienophiles for the tetrazine-trans-cyclooctene ligation. *J. Am. Chem. Soc.* **2011**, *133*, 9646-9649.

(54) Darko, A.; Wallace, S.; Dmitrenko, O.; Machovina, M. M.; Mehl, R. A.; Chin, J. W.; Fox, J. M. Conformationally Strained trans-Cyclooctene with Improved Stability and Excellent Reactivity in Tetrazine Ligation. *Chem. Sci.* **2014**, *5*, 3770-3776.

(55) Lang, K.; Chin, J. W. Cellular Incorporation of Unnatural Amino Acids and Bioorthogonal Labeling of Proteins. *Chem. Rev.* **2014**, *114*, 4764-4806.

(56) Devaraj, N. K.; Hilderbrand, S.; Upadhyay, R.; Mazitschek, R.; Weissleder, R. Bioorthogonal Turn-On Probes for Imaging Small Molecules inside Living Cells. *Angew. Chem. Int. Ed.* **2010**, *49*, 2869-2872.

(57) Versteegen, R. M.; Rossin, R.; ten Hoeve, W.; Janssen, H. M.; Robillard, M. S. Click to Release: Instantaneous Doxorubicin Elimination upon Tetrazine Ligation. *Angew. Chem. Int. Ed.* **2013**, *52*, 14112-14116.

(58) Rossin, R.; van Duijnhoven, S. M. J.; ten Hoeve, W.; Janssen, H. M.; Kleijn, L. H. J.; Hoeben, F. J. M.; Versteegen, R. M.; Robillard, M. S. Triggered Drug Release from an Antibody–Drug Conjugate Using Fast "Click-to-Release" Chemistry in Mice. *Bioconjugate Chem.* **2016**, *27*, 1697-1706.

(59) Liu, S.; Zhang, H.; Remy, R. A.; Deng, F.; Mackay, M. E.; Fox, J. M.; Jia, X. Meter-long multiblock copolymer microfibers via interfacial bioorthogonal polymerization. *Adv. Mater.* **2015**, *27*, 2783-2790.

(60) Zhang, H.; Dicker, K. T.; Xu, X.; Jia, X.; Fox, J. M. Interfacial Bioorthogonal Cross-Linking. *ACS Macro Lett* **2014**, *3*, 727-731.

(61) Liu, D. S.; Tangpeerachaikul, A.; Selvaraj, R.; Taylor, M. T.; Fox, J. M.; Ting, A. Y. Diels–Alder Cycloaddition for Fluorophore Targeting to Specific Proteins inside Living Cells. *J. Am. Chem. Soc.* **2012**, *134*, 792-795.

(62) Blizzard, R. J.; Backus, D. R.; Brown, W.; Bazewicz, C. G.; Li, Y.; Mehl, R. A. Ideal Bioorthogonal Reactions Using A Site-Specifically Encoded Tetrazine Amino Acid. *J. Am. Chem. Soc.* **2015**, *137*, 10044-10047.

(63) Seitchik, J. L.; Peeler, J. C.; Taylor, M. T.; Blackman, M. L.; Rhoads, T. W.; Cooley, R. B.; Refakis, C.; Fox, J. M.; Mehl, R. A. Genetically Encoded Tetrazine Amino Acid Directs Rapid Site-Specific in Vivo Bioorthogonal Ligation with trans-Cyclooctenes. *J. Am. Chem. Soc.* **2012**, *134*, 2898-2901.

(64) Murrey, H. E.; Judkins, J. C.; am Ende, C. W.; Ballard, T. E.; Fang, Y.; Riccardi, K.; Di, L.; Guilmette, E. R.; Schwartz, J. W.; Fox, J. M.; Johnson, D. S. Systematic Evaluation of Bioorthogonal Reactions in Live Cells with Clickable HaloTag Ligands: Implications for Intracellular Imaging. *J. Am. Chem. Soc.* **2015**, *137*, 11461-11475.

(65) Keliher, E. J.; Reiner, T.; Turetsky, A.; Hilderbrand, S. A.; Weissleder, R. High-Yielding, Two-Step 18F Labeling Strategy for 18F-PARP1 Inhibitors. *ChemMedChem* **2011**, *6*, 424-427.

(66) Zeng, D.; Zeglis, B. M.; Lewis, J. S.; Anderson, C. J. The Growing Impact of Bioorthogonal Click Chemistry on the Development of Radiopharmaceuticals. *J. Nucl. Med.* **2013**, *54*, 829-832.

(67) Meyer, J.-P.; Adumeau, P.; Lewis, J. S.; Zeglis, B. M. Click Chemistry and Radiochemistry: The First 10 Years. *Bioconjugate Chem.* **2016**, *27*, 2791-2807.

(68) Li, Z.; Cai, H.; Hassink, M.; Blackman, M. L.; Brown, R. C. D.; Conti, P. S.; Fox, J. M. Tetrazine-trans-cyclooctene ligation for the rapid construction of 18F labeled probes. *Chem. Commun.* **2010**, *46*, 8043-8045.

(69) Selvaraj, R.; Giglio, B.; Liu, S.; Wang, H.; Wang, M.; Yuan, H.; Chintala, S. R.; Yap, L.-P.; Conti, P. S.; Fox, J. M.; Li, Z. Improved Metabolic Stability for 18F PET Probes Rapidly Constructed via Tetrazine trans-Cyclooctene Ligation. *Bioconjugate Chem.* **2015**, *26*, 435-442.

(70) Selvaraj, R.; Liu, S.; Hassink, M.; Huang, C.-w.; Yap, L.-p.; Park, R.; Fox, J. M.; Li, Z.; Conti, P. S. Tetrazine-trans-cyclooctene ligation for the rapid construction of integrin αvβ3 targeted PET tracer based on a cyclic RGD peptide. *Bioorg. Med. Chem. Lett.* **2011**, *21*, 5011-5014.

(71) Wu, Z.; Liu, S.; Hassink, M.; Nair, I.; Park, R.; Li, L.; Todorov, I.; Fox, J. M.; Li, Z.; Shively, J. E.; Conti, P. S.; Kandeel, F. Development and Evaluation of 18F-TTCO-Cys40-Exendin-4: A PET Probe for Imaging Transplanted Islets. *J. Nucl. Med.* **2013**, *54*, 244-251.

(72) Wang, M.; Svatunek, D.; Rohlfing, K.; Liu, Y.; Wang, H.; Giglio, B.; Yuan, H.; Wu, Z.; Li, Z.; Fox, J. Conformationally Strained trans-Cyclooctene (sTCO) Enables the Rapid Construction of (18)F-PET Probes via Tetrazine Ligation. *Theranostics* **2016**, *6*, 887-895.

(73) Wang, M.; Svatunek, D.; Rohlfing, K.; Liu, Y.; Wang, H.; Giglio, B.; Yuan, H.; Wu, Z.; Fox, J.; Li, z. Tetrazine s-TCO ligation: A simple approach to improve probe's blood circulation? *J. Nucl. Med.* **2016**, *57*, 1090-1090.

(74) Devaraj, N. K.; Weissleder, R.; Hilderbrand, S. A. Tetrazine-Based Cycloadditions: Application to Pretargeted Live Cell Imaging. *Bioconjugate Chem.* **2008**, *19*, 2297-2299.

(75) Patterson, D. M.; Nazarova, L. A.; Xie, B.; Kamber, D. N.; Prescher, J. A. Functionalized cyclopropenes as bioorthogonal chemical reporters. *J. Am. Chem. Soc.* **2012**, *134*, 18638-18643.

(76) Yang, J.; Šečkutė, J.; Cole, C. M.; Devaraj, N. K. Live-Cell Imaging of Cyclopropene Tags with Fluorogenic Tetrazine Cycloadditions. *Angew. Chem. Int. Ed.* **2012**, *51*, 7476-7479.

(77) Chen, W.; Wang, D.; Dai, C.; Hamelberg, D.; Wang, B. Clicking 1,2,4,5-tetrazine and cyclooctynes with tunable reaction rates. *Chem. Commun. (Camb.)* **2012**, *48*, 1736-1738.

(78) Lang, K.; Davis, L.; Torres-Kolbus, J.; Chou, C.; Deiters, A.; Chin, J. W. Genetically encoded norbornene directs site-specific cellular protein labelling via a rapid bioorthogonal reaction. *Nat. Chem.* **2012**, *4*, 298-304.

(79) Ziegler, K.; Wilms, H. Uber vielgliedrige Ringsysteme XIII: Ungesättigte Kohlenwasserstoff-8-Ringe. *Justus Liebigs Ann. Chem.* **1950**, *567*, 1-43.

(80) Cope, A. C.; Pike, R. A.; Spencer, C. F. Cyclic Polyolefins. XXVII. cis- and trans-Cycloöctene from N,N-Dimethylcycloöctylamine1. *J. Am. Chem. Soc.* **1953**, *75*, 3212-3215.

(81) Cope, A. C.; Bach, R. D. trans-CYCLOOCTENE. *Org. Synth.* **1969**, *49*, 39.

(82) Corey, E. J.; Shulman, J. I. The direct synthesis of optically active trans-cyclooctene. Optically active trans-bicyclo[6.1.0]nonane. *Tetrahedron Lett.* **1968**, *9*, 3655-3658.

(83) Hines, J. N.; Peagram, M. J.; Thomas, E. J.; Whitham, G. H. Some reactions of benzaldehyde acetals with alkyl-lithium reagents; a stereospecific olefin synthesis from 1,2-diols. *J. Chem. Soc., Perkin Trans. 1* **1973**, 2332-2337.

(84) Vedejs, E.; Fuchs, P. L. Olefin inversion by the phosphorus betaine method. *J. Am. Chem. Soc.* **1971**, *93*, 4070-4072.

(85) Reese, C. B.; Shaw, A. Silver-perchlorate-promoted ring expansion of halocarbene adducts of cyclic olefins. A facile synthesis of trans-cyclooctene and trans-cyclononene derivatives. *J. Am. Chem. Soc.* **1970**, *92*, 2566-2568.

(86) Braddock, D. C.; Cansell, G.; Hermitage, S. A.; White, A. J. P. An asymmetric synthesis of enantiopure chair and twist trans-cyclooctene isomers. *Tetrahedron: Asymmetry* **2004**, *15*, 3123-3129.

(87) Whitham, G. H.; Wright, M. trans-Cycloalkenes. Part II. Application of the dioxolan olefin synthesis to the stereospecific formation of trans-cyclo-octene derivatives. (1SR,2RS)-trans-Cyclo-oct-2-en-1-ol. *Journal of the Chemical Society C: Organic* **1971**, 886-891.

(88) Shea, K. J.; Kim, J. S. Influence of strain on chemical reactivity. Relative reactivity of torsionally strained double bonds in 1,3-dipolar cycloadditions. *J. Am. Chem. Soc.* **1992**, *114*, 4846-4855.

(89) Swenton, J. S. Photoisomerization of cis-cyclooctene to trans-cyclooctene. *J. Org. Chem.* **1969**, *34*, 3217-3218.

(90) Inoue, Y.; Takamuku, S.; Sakurai, H. Direct cis-trans Photoisomerization of Cyclooctene. A Convenient Method for Preparing trans-Cyclooctene. *Synthesis* **1977**, *2*.

(91) Inoue, Y.; Ikeda, H.; Kaneda, M.; Sumimura, T.; Everitt, S. R. L.; Wada, T. Entropy-Controlled Asymmetric Photochemistry: Switching of Product Chirality by Solvent. *J. Am. Chem. Soc.* **2000**, *122*, 406-407.

(92) Inoue, Y.; Takamuku, S.; Kunitomi, Y.; Sakurai, H. Singlet photosensitization of simple alkenes. Part 1. cis-trans-Photoisomerization of cyclo-octene sensitized by aromatic esters. *Journal of the Chemical Society, Perkin Transactions 2* **1980**, 1672-1677.

(93) Inoue, Y.; Yokoyama, T.; Yamasaki, N.; Tai, A. An optical yield that increases with temperature in a photochemically induced enantiomeric isomerization. *Nature* **1989**, *341*, 225-226.

(94) Inoue, Y.; Yokoyama, T.; Yamasaki, N.; Tai, A. Temperature switching of product chirality upon photosensitized enantiodifferentiating cis-trans isomerization of cyclooctene. *J. Am. Chem. Soc.* **1989**, *111*, 6480-6482.

(95) Fukuhara, G.; Mori, T.; Wada, T.; Inoue, Y. Entropy-Controlled Supramolecular Photochirogenesis: Enantiodifferentiating Z−E Photoisomerization of Cyclooctene Included and Sensitized by Permethylated 6-O-Modified β-Cyclodextrins. *J. Org. Chem.* **2006**, *71*, 8233-8243.

(96) Inoue, Y.; Matsushima, E.; Wada, T. Pressure and Temperature Control of Product Chirality in Asymmetric Photochemistry. Enantiodifferentiating Photoisomerization of Cyclooctene Sensitized by Chiral Benzenepolycarboxylates. *J. Am. Chem. Soc.* **1998**, *120*, 10687-10696.

(97) Inoue, Y. Asymmetric photochemical reactions in solution. *Chem. Rev.* **1992**, *92*, 741-770.

(98) Inoue, Y.; Yamasaki, N.; Yokoyama, T.; Tai, A. Enantiodifferentiating Z-E photoisomerization of cyclooctene sensitized by chiral polyalkyl benzenepolycarboxylates. *J. Org. Chem.* **1992**, *57*, 1332-1345.

(99) Inoue, Y.; Yamasaki, N.; Yokoyama, T.; Tai, A. Highly enantiodifferentiating photoisomerization of cyclooctene by congested and/or triplex-forming chiral sensitizers. *J. Org. Chem.* **1993**, *58*, 1011-1018.

(100) Tsuneishi, H.; Hakushi, T.; Inoue, Y. Singlet-versus triplet-sensitized enantiodifferentiating photoisomerization of cyclooctene: remarkable effects of spin multiplicity upon optical yield. *Journal of the Chemical Society, Perkin Transactions 2* **1996**, 1601-1605.

(101) Lu, R.; Yang, C.; Cao, Y.; Tong, L.; Jiao, W.; Wada, T.; Wang, Z.; Mori, T.; Inoue, Y. Enantiodifferentiating Photoisomerization of Cyclooctene Included and Sensitized by Aroyl-β-cyclodextrins: A Critical Enantioselectivity Control by Substituents. *J. Org. Chem.* **2008**, *73*, 7695-7701.

(102) Maeda, R.; Wada, T.; Mori, T.; Kono, S.; Kanomata, N.; Inoue, Y. Planar-to-Planar Chirality Transfer in the Excited State. Enantiodifferentiating Photoisomerization of Cyclooctenes Sensitized by Planar-Chiral Paracyclophane. *J. Am. Chem. Soc.* **2011**, *133*, 10379-10381.

(103) Royzen, M.; Yap, G. P. A.; Fox, J. M. A Photochemical Synthesis of Functionalized trans-Cyclooctenes Driven by Metal Complexation. *J. Am. Chem. Soc.* **2008**, *130*, 3760-3761.

(104) Inoue, Y.; Ueoka, T.; Kuroda, T.; Hakushi, T. trans-Cycloheptene. Photochemical generation and thermal trans-cis isomerization. *J. Chem. Soc., Chem. Commun.* **1981**, 1031-1033.

(105) Bach, R. D. Ring Strain Energy in the Cyclooctyl System. The Effect of Strain Energy on [3 + 2] Cycloaddition Reactions with Azides. *J. Am. Chem. Soc.* **2009**, *131*, 5233-5243.

(106) Inoue, Y.; Ueoka, T.; Kuroda, T.; Hakushi, T. Singlet photosensitization of simple alkenes. Part 4. cis-trans Photoisomerization of cycloheptene sensitized by aromatic esters. Some aspects of the chemistry of trans-cycloheptene. *Journal of the Chemical Society, Perkin Transactions 2* **1983**, 983-988.

(107) Corey, E. J.; Carey, F. A.; Winter, R. A. E. Stereospecific Syntheses of Olefins from 1,2-Thionocarbonates and 1,2-Trithiocarbonates. trans-Cycloheptene. *J. Am. Chem. Soc.* **1965**, *87*, 934-935.

(108) Hoffmann, R.; Inoue, Y. Trapped Optically Active (E)-Cycloheptene Generated by Enantiodifferentiating Z−E Photoisomerization of Cycloheptene Sensitized by Chiral Aromatic Esters. *J. Am. Chem. Soc.* **1999**, *121*, 10702-10710.

(109) Jendralla, H. Cycloadditions with Silver Ion-Stabilized (2RS,3RS)-3-Methoxy-trans-Cycloheptene. *Angew. Chem. Int. Ed.* **1980**, *19*, 1032-1033.

(110) Jendralla, H.; Spur, B. Cycloaddition reaction of silver ion stabilized 6-methoxycyclohepta-1-cis, 4-trans-diene. *J. Chem. Soc., Chem. Commun.* **1984**, 887-888.

(111) Jendralla, H. (5RS,6RS)-6-Methoxy-1(Z),4(E)-cycloheptadien. Erzeugung, Nachweis und Folgereaktionen. *Chem. Ber.* **1980**, *113*, 3557-3569.

(112) Shimizu, T.; Shimizu, K.; Ando, W. Synthesis, structure, and stabilities of trans-1,2-diphenyl-4,4,5,5,6,6-hexamethyl-4,5,6-trisilacycloheptene. *J. Am. Chem. Soc.* **1991**, *113*, 354-355.

(113) Krebs, A. W.; Thölke, B.; Pforr, K.-I.; König *, W. A.; Scharwächter, K.; Grimme *, S.; Vögtle *, F.; Sobanski, A.; Schramm, J.; Hormes *, J. Synthesis of enantiomerically pure (E)-1,1,3,3,6,6-hexamethyl-1-sila-4-cycloheptene and its absolute configuration. *Tetrahedron: Asymmetry* **1999**, *10*, 3483-3492.

(114) Greene, M. A.; Prevost, M.; Tolopilo, J.; Woerpel, K. A. Diastereoselective synthesis of seven-membered-ring trans-alkenes from dienes and aldehydes by silylene transfer. *J. Am. Chem. Soc.* **2012**, *134*, 12482-12484.

(115) Hurlocker, B.; Hu, C.; Woerpel, K. A. Structure and reactivity of an isolable seven-membered-ring trans-alkene. *Angew. Chem. Int. Ed.* **2015**, *54*, 4295-4298.

(116) Santucci, J.; Sanzone, J. R.; Woerpel, K. A. [4+2] Cycloadditions of Seven-Membered-Ring trans-Alkenes: Decreasing Reactivity with Increasing Substitution of the Seven-Membered Ring. *Eur. J. Org. Chem.* **2016**, *2016*, 2933-2943.

(117) Sanzone, J. R.; Woerpel, K. A. High Reactivity of Strained Seven-Membered-Ring trans-Alkenes. *Angew. Chem. Int. Ed.* **2016**, *55*, 790-793.

(118) Hook, B. D. A.; Dohle, W.; Hirst, P. R.; Pickworth, M.; Berry, M. B.; Booker-Milburn, K. I. A Practical Flow Reactor for Continuous Organic Photochemistry. *J. Org. Chem.* **2005**, *70*, 7558-7564.

(119) Squillacote, M. E.; DeFellipis, J.; Shu, Q. How Stable Is trans-Cycloheptene? *J. Am. Chem. Soc.* **2005**, *127*, 15983-15988.

(120) Matsuo, J.-i.; Sasaki, S.; Hoshikawa, T.; Ishibashi, H. Intramolecular formal [4+2] cycloaddition of 3-ethoxycyclobutanones and alkenes. *Chem. Commun.* **2010**, *46*, 934-936.

Chapter 2

BIOORTHOGONAL TETRAZINE LIGATION IN BIOMATERIALS DISCOVERY

Work described here has already been published (Zhang, H.; Dicker, K. T.; Xu, X.; Jia, X.; Fox, J. M., Interfacial Bioorthogonal Cross-Linking. *ACS Macro Lett* **2014,** *3* (8), 727-731. Liu, S.; Zhang, H.; Remy, R. A.; Deng, F.; Mackay, M. E.; Fox, J. M.; Jia, X., Meter-long Multiblock Copolymer Microfibers Via Interfacial Bioorthogonal Polymerization. *Adv Mater* **2015,** *27* (17), 2783-90.). It is reprinted in this chapter with permissions of *ACS Macro Letters* (Copyright 2014 American Chemical Society) and *Advanced Materials* (Copyright 2015 John Wiley & Sons, Inc.).

2.1 Introduction: Click Chemistry in Polymer Synthesis and Material Science

The high selectivity and versatility of "click-type" chemistry has greatly facilitated the syntheses and functionalization of polymers, and over the past decades several kinds of click reactions have had huge impact on polymer and materials science.[1-8]

Ever since first introduced by Sharpless[9] and Meldal,[10] the copper(I) mediated alkyne-azide cycloaddition (CuAAC), researchers have been using this powerful tool to construct a wide range of diverse materials including terminal and pendant functional polymers, block copolymers, and polymers with complex (star, brush, dendritic, etc.) architectures, as well as crosslinked gels and networks. Matyjaszewski reported the syntheses of block copolymers from CuAAC[11] where an acetylene azido terminated polystyrene itself polymerized in a step-growth polymerization (Scheme

2.1a), forming a triazole-containing polymer with significant amount (17%) of cyclized byproduct. In the same paper, he demonstrated the polymerization between a *bis*-azido-monomer and propargyl ether (Scheme 2.1b) to give polymer with a reduced amount (7%) of cyclized byproduct.

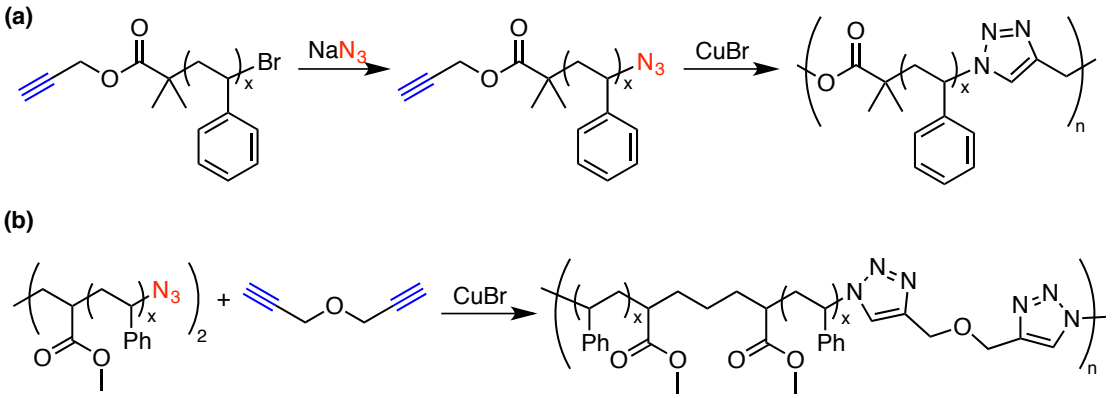

Scheme 2.1: Step growth polymerization of ATRP-derived polymers where (a) the azide and alkyne in the same molecule and (b) the azides and alkynes in separate molecules.[11]

This methodology has also been applied to provide poly(ethylene glycol) (PEG) hydrogel networks by reacting tetraethylene glycol containing four azide groups with PEG diacetylene in an aqueous environment (Scheme 2.2).[12] The crosslinking was very efficient with as high as 99.8% of the functional groups consumed based on fluorescence spectroscopy analysis. However, the study also showed the resulting polytriazole coordinate to copper which made the copper residue a significant issue to the biocompatible applications.

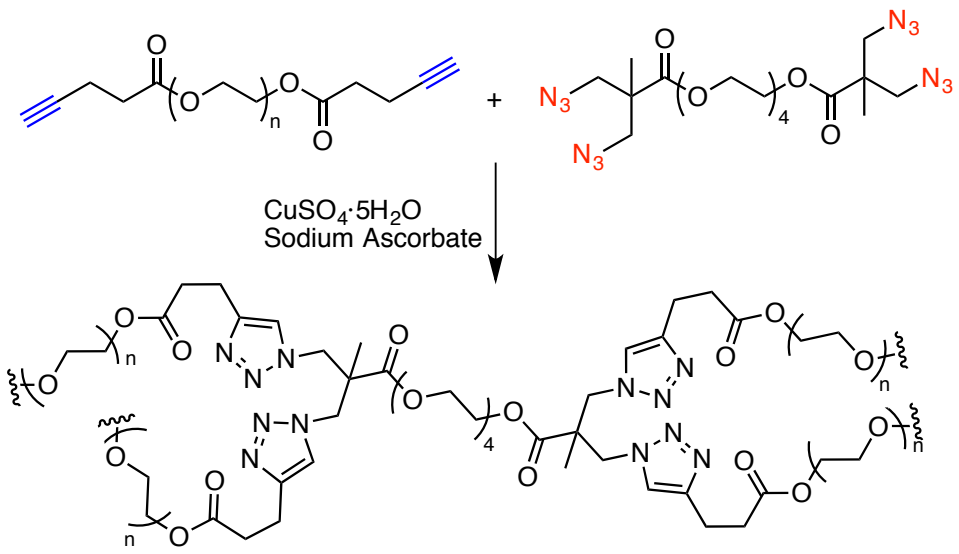

Scheme 2.2: Crosslinked PEG hydrogel formed by aqueous CuAAC reaction.[12]

Instead of creating step-growth linear polymer and crosslinked networks, it is more common to introduce terminal or pendant clickable functionalities to the polymer. "Clickable" terminal functionality can be accomplished by using functional initiators/transfer agents (Scheme 2.3),[13] or by post-polymerization modification of end groups(Scheme 2.4).[14] On the other hand, "clickable" pendant functionality on the side-chain of the polymer can be introduced by adopting functional monomers (Scheme 2.5),[15] or post-polymerization transformation of backbone functionality (Scheme 2.6).[16]

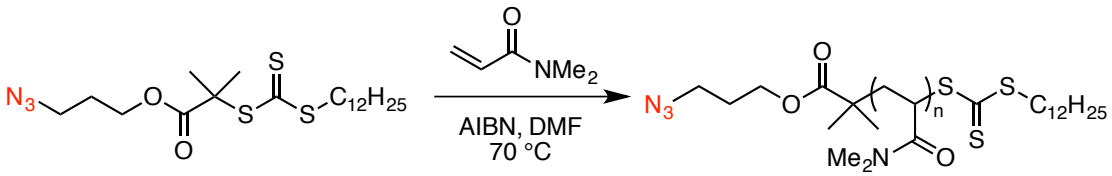

Scheme 2.3: RAFT polymerization with azido-functionalized chain transfer agent.[13]

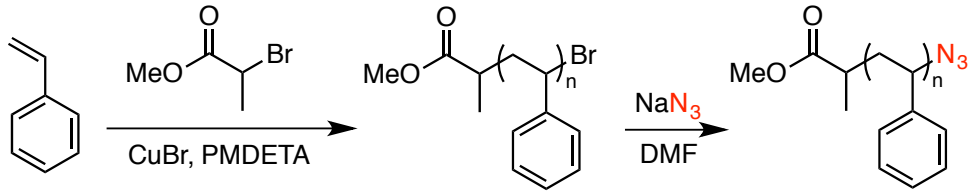

Scheme 2.4: Polystyrene (PS) with bromine terminal converted to PS-N_3.[14]

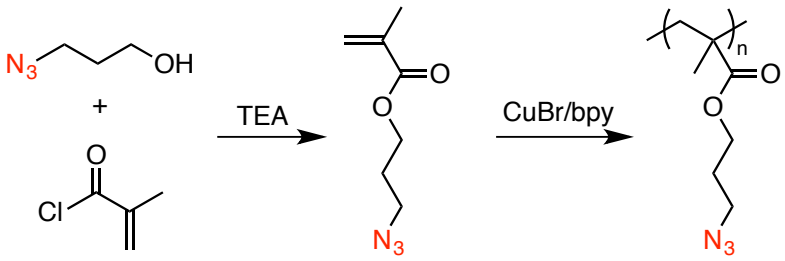

Scheme 2.5: Synthesis of poly(3-azidopropyl methacrylate) with pendent azide functionality from azide-containing monomer.[15]

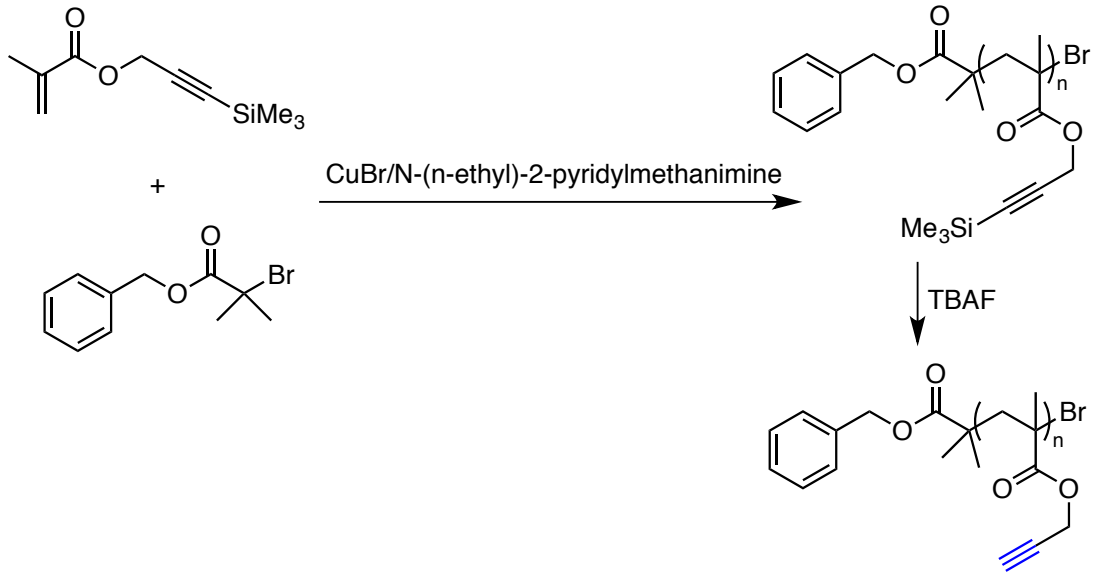

Scheme 2.6: ATRP of methylacrylate monomer containing trimethylsilyl-protected alkyne and post-polimerization deprotection.[16]

2.2 Norbornene-Tetrazine Ligation and Applications in Biomaterials

The recently developed inverse-electron-demand Diels-Alder (IEDDA) reactions have been widely used in live-cell/animal labeling, drug delivery and pre-targeted PET imaging.[17-21] The advantageous properties of this class of bioorthogonal reactions also lead to many excited applications in biomaterials discovery including designing of nanoparticles, biocompatible hydrogel formation and the creation and fabrication of cell culture scaffolds.[22-25] Among the many applications, most were achieved with help of norbornene-tetrazine ligation developed by Weissleder and Hilderbrand in 2008.

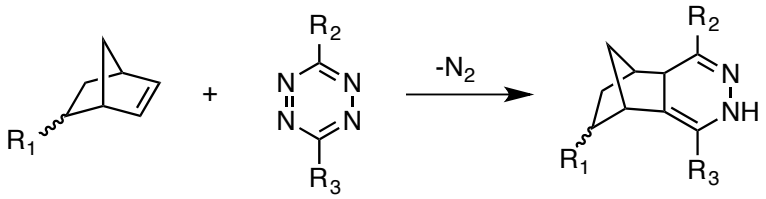

Scheme 2.7: Norbornene-tetrazine ligation.

In 2014, O'Reilly and coworkers reported nanoparticle formation from single polymer "chain collapse".[23] By treating a polymer containing pendant norbornene functionality with a *bis*-tetrazine crosslinker, the single polymer chain collapsed resulting in nanoparticles by norbornene-tetrazine ligation. The nanoparticle formation proceeded without needs for catalyst or extra reagent, but the heating was required.

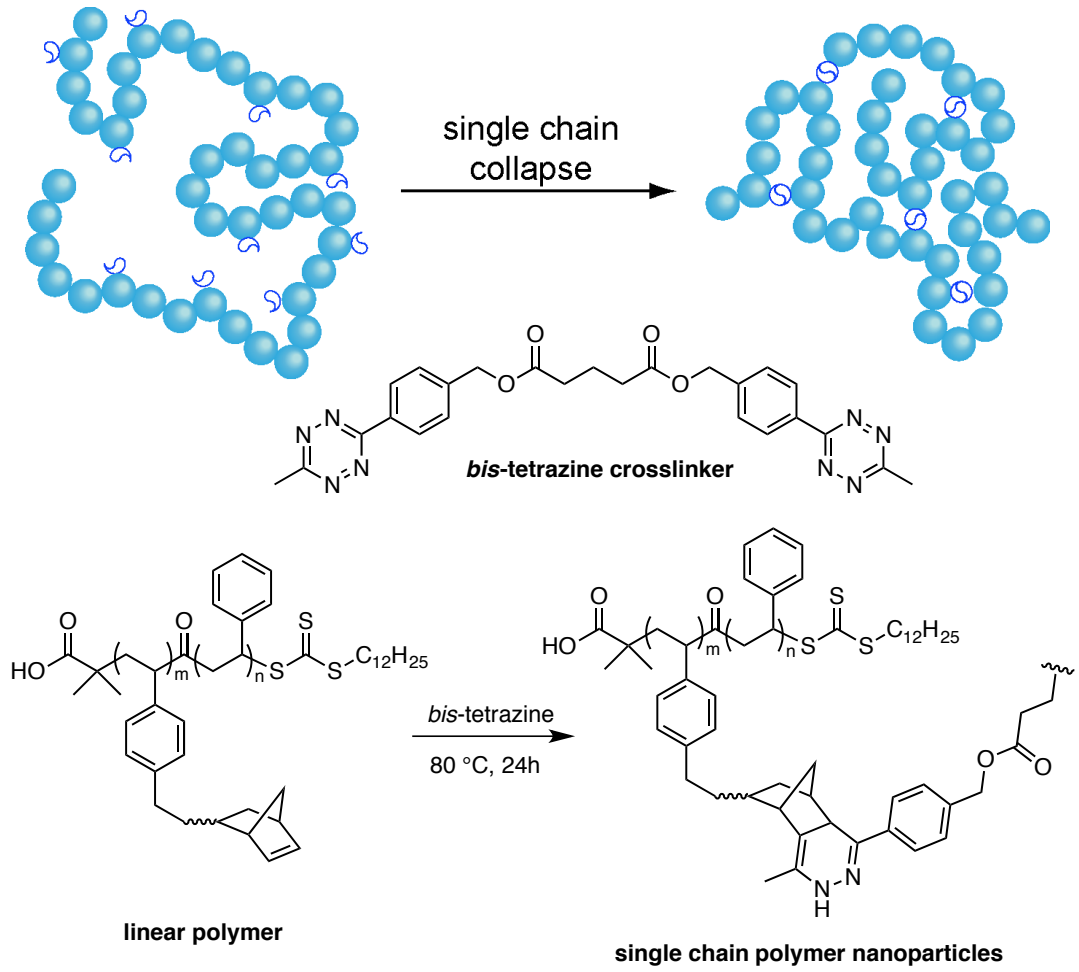

Figure 2.1: Single chain polymer nanoparticles formation *via* norbornene-tetrazine ligation Figure reprinted with permission from reference.[23] Copyright 2014 Royal Society of Chemistry.

Hydrogels are a class of materials consist with hydrophilic polymer chains and highly porous structures.[26] Hydrogels are highly absorbent and can contain a very large percentage (up to 99% or even higher) of water, yet behave like a solid due to the three-dimensional crosslinked network. Because of the biocompatibility and tunable mechanical properties, synthetic hydrogels have been widely used in constructing/mimicking extracellular matrix (ECM),[27] drug delivery[28,29] and tissue

engineering applications.[30-32] In the recent years, there has been a growing interest in utilizing bioorthogonal reactions in hydrogel formation, fabrication and further patterning.[25,33]

Anseth has created hydrogels using variety of bioorthogonal reactions, including norbornene-tetrazine ligation, to develop poly(ethylene glycol) (PEG)-based hydrogels for the creation of cell culture scaffolds.[22] By using a four-arm PEG-tetrazine and a cell degradable *bis*-norbornene crosslinker peptide, a hydrogel can be formed within 5 minutes. The hydrogel exhibits good cytocompatibility by showing 92% viability in 3D culture of hMSCs in 24 hours. Moreover, the formed hydrogel can be sequentially patterned *via* thiol-ene chemistry due to the orthogonality of tetrazine ligation.

Dove and coworkers reported an interesting one-step preparation of double network hydrogel using norbornene-tetrazine ligation and thiol-yne chemistry simultaneously (Figure 2.2C).[34] The first level of loose network was formed by reacting a norbornene-functionalized chitosan with a linear PEG-based *bis*-tetrazine crosslinker (Figure 2.2A) while another level of tough network was accomplished by adding a four-arm tetraalkyne and a linear PEG-dithiol crosslinker (Figure 2.2B). The formed hydrogel presents good mechanical performance: no fracture or hysteresis observed after repeated load of compressive stresses of 14 to 15 MPa at 98 compression, and it exhibits good cytocompatibility with excellent cell viability (> 99%) when hMSCs were 3d cultured for 48 hours.

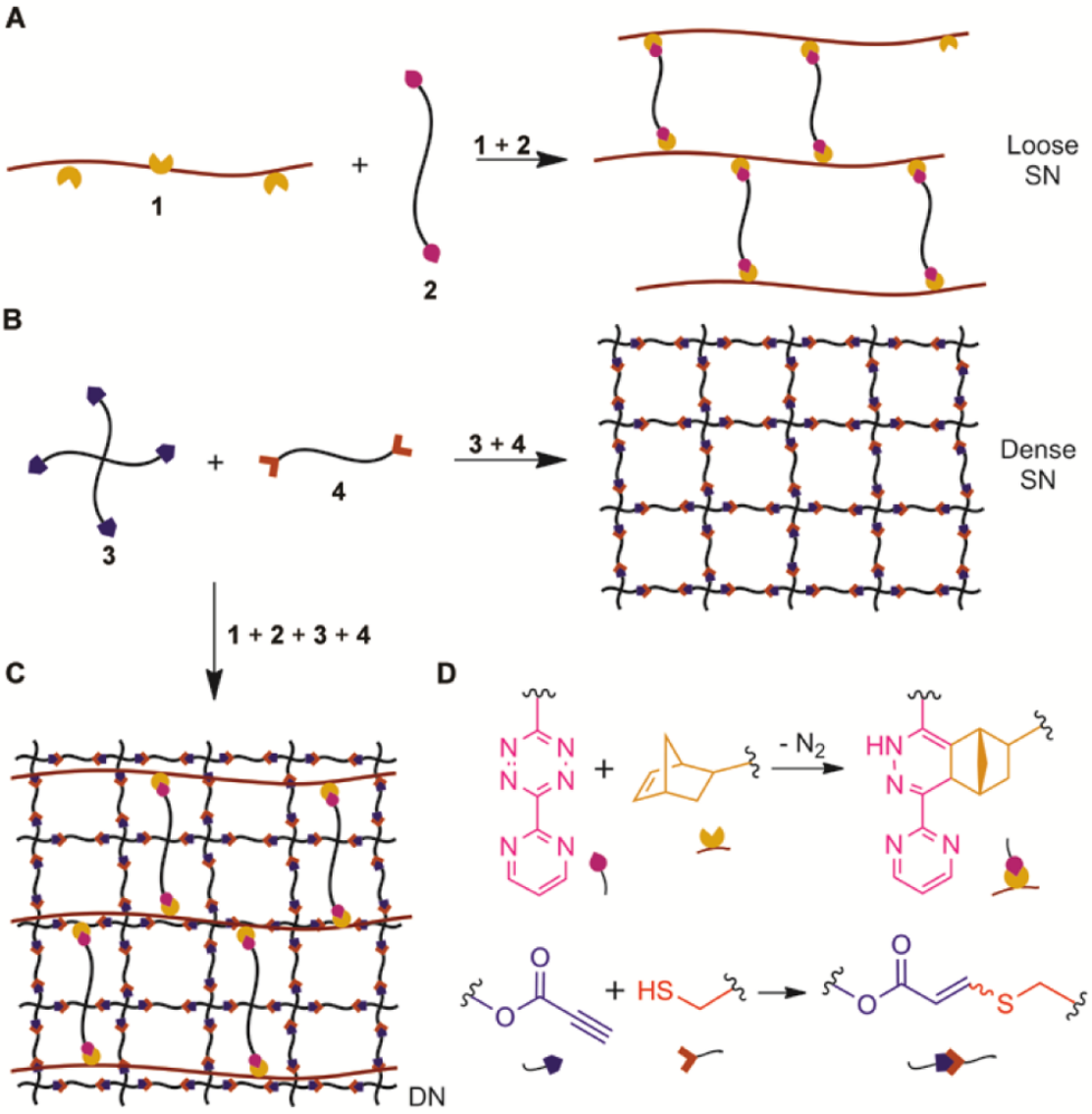

Figure 2.2: Schematic of double network (DN) hydrogel fabrication.[34] Reproduced with permission, Copyright 2015 American Chemical Society.

Aside from PEG, Joshi and coworkers reported an alginate-based hydrogel *via* norbornene-tetrazine ligation in 2015 (Figure 2.3).[24] Tetrazine and norbornene-functionalized alginates were synthesized separately and covalently crosslinked click alginate hydrogel were prepared by mixing the two kinds of alginates. Compared to the previous commonly used alginate hydrogels which were normally prepared from ionic crosslinking, the covalently crosslinked click alginate hydrogel had improved cytocompatibility and possessed tunable mechanical properties, which makes it attractive material to use in tissue engineering applications.

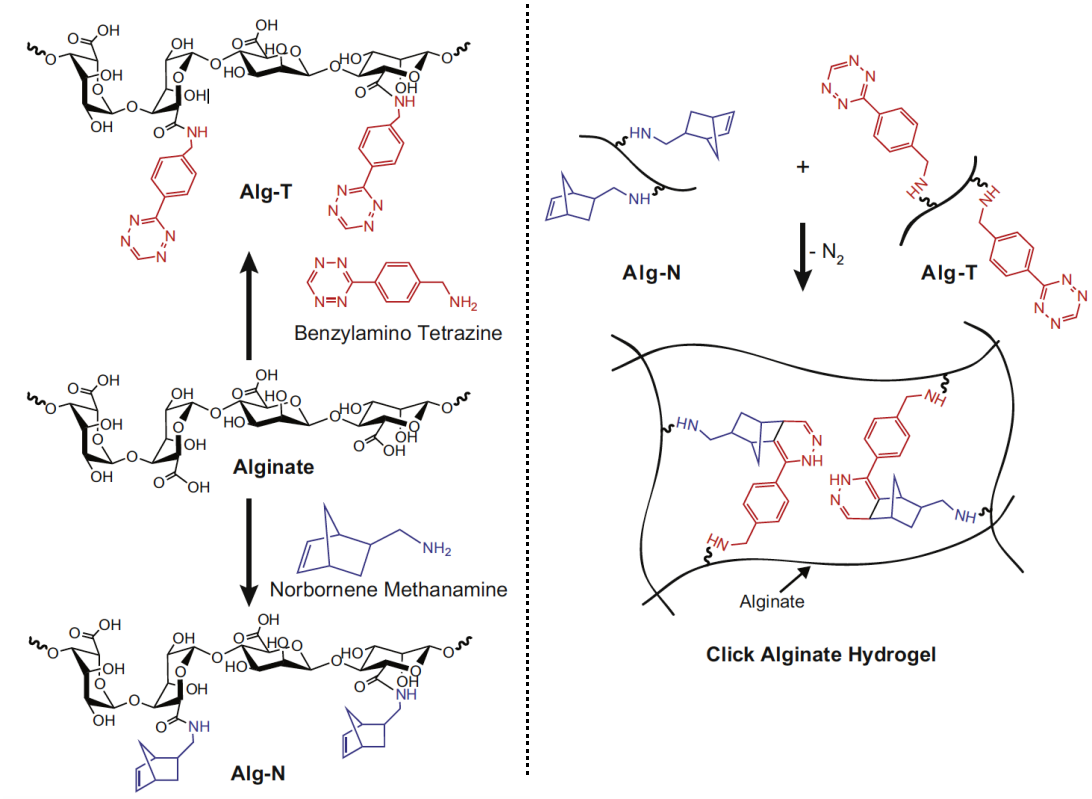

Figure 2.3: Left: synthesis of tetrazine and norbornene-functionalized alginates. Right: covalently crosslinked click alginate hydrogel network.[24] Reproduced with permission, Copyright 2015 Elsevier.

2.3 *trans*-Cyclooctene-Tetrazine Ligation-Enabled Interfacial Crosslinking

Unlike the norbornene-tetrazine ligation in biomaterials discovery, the *trans*-cyclooctene-tetrazine ligation had received relatively little attention in the area of biomaterials research. There had been reports using of TCO in nanoparticle bioconjugation,[35] but the TCO-tetrazine ligation has never been used for crosslinking or polymerization purposes.

Interfacial reactions have been extensively utilized in polymer science, with the preparation of Nylon as an archetypical example.[36,37] In the biomaterials realm, ionically crosslinked alginate hydrogel (microspheres produced by adding alginate solution into calcium bath) was employed in interfacial cell encapsulation purposes,[38,39] yet the lack of *in vivo* stability,[40,41] crosslinking homogeneity[42] and loss of mechanical integrity over time limited its development. Bowman and Anseth showed that enzyme-mediated interfacial radical chain polymerization can be used to create multilayered PEG-based hydrogel structures with micrometer-scale resolution and the incorporation of small molecules and nanoparticles into the hydrogel layers was achieved.[43]

We envisioned that with excellent bioorthogonality and unparalleled reaction kinetics, the TCO-tetrazine ligation could be used to crosslink and introduce molecular patterns into a functional hydrogel system with interfacial reaction kinetics.

Described below is the development of an interfacial bioorthogonal crosslinking method that can create and patterning hyaluronic acid (HA)-based hydrogel capsules and channels through a diffusion controlled gelation at the liquid-gel interface.

2.3.1 Hyaluronic Acid and Derivatives

The building block we chose hyaluronic acid to carry on the study of interfacial crosslinking process is Hyaluronic acid. Hyaluronic acid (HA), or hyaluronan, first isolated from vitreous humor of bovine eyes by Meyer and Palmer in 1934,[44] is a linear polysaccharide consisting of alternating repeats of $_D$-glucuronic acid and *N*-acetyl-$_D$-glucosamine (Scheme 2.8). The structure of hyaluronic acid was determined by Meyer in 1958.[45]

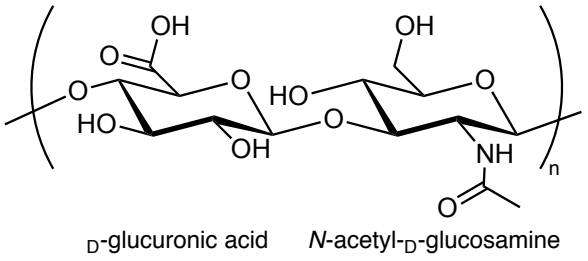

Scheme 2.8: Repeating disaccharide unit of hyaluronic acid.

The pK_a of the carboxylic acid on HA is 3 to 4. Under physiological conditions HA is a polyanion associated with counterions, frequently sodium (Na^+). Because of the high hydrophilicity and the abundant negative charge, HA is highly absorbent and can absorb a large amount of water and expand up to 1000 times its solid volume, forming a loose hydrated network.[46] HA is an essential component of the extracellular matrix (ECM) and plays important roles in a variety of biological processes including cellular signaling, wound healing, morphogenesis, and matrix organization.[47]

Because its biodegradable and immunoneutral properties, HA and its derivatives have been widely used clinically in medical products and in cosmetic preparations over the past decades.[48-50] Separately, HA has also been recognized as an

attractive building block for the creation and fabrication of biomaterials in recent years. Various chemical modifications[51-53] have been applied to HA to transform it into many physical forms with desirable performance (morphology, stiffness, bioactivity, etc.). Many of these transformations are accomplished by crosslinking HA with chemically modified pendant functional groups.

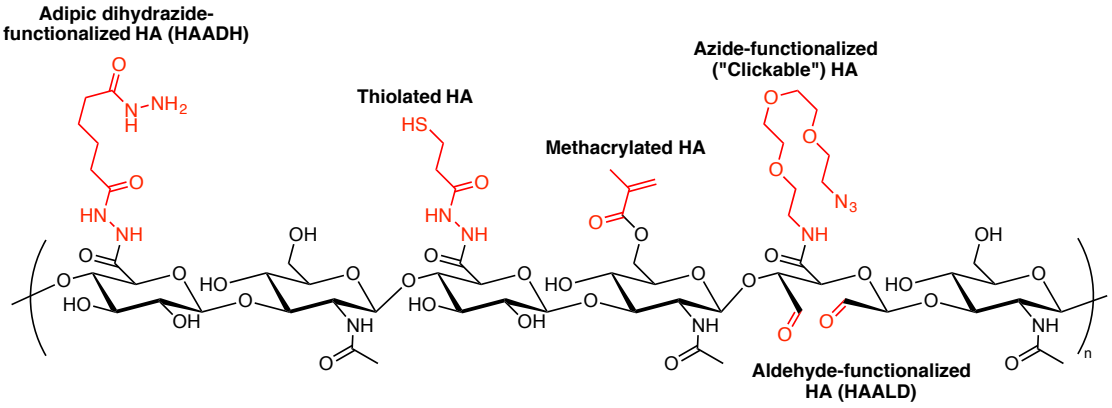

Scheme 2.9: A hypothetical composite structure illustrating representative chemical modification methods to create HA derivatives with pendant functionalities for crosslinking purposes.

As illustrated in Scheme 2.9, there are a number of established methods to create functional HA derivatives. Crosslinked HA hydrogel networks can be formed by introducing reactive handles (Michael-type addition, hydrazide-aldehyde condensation, radical polymerization, etc.) on different type HA derivatives and/or multifunctional crosslinkers. For example, methacrylated HA can be converted to an elastic hydrogel by radical polymerization using a photoinitiator in the presence of light.[54,55] PEG diacrylate can be used to crosslink thiolated HA *via* a Michael-type addition,[56] and aldehyde-derived HA (HAALD) hydrogels can be formed via

condensation reaction between hydrazide and aldehyde, with water being the only byproduct.[57,58]

It is worth mentioning that copper(I) mediated alkyne-azide cyclization (CuAAC) has been used to produce HA hydrogel. In 2007, Lamanna and coworkers reported the synthesis of azide and alkyne-functionalized HA where the HA carboxylates were modified *via* carbodiimide chemistry either as propargyl amides or 11-azido-triethyleneglycol amides (Scheme 2.10). By mixing the two HA derivatves, hydrogel can be formed in minutes using 0.01% CuCl as catalyst.[59] However, this first "clicked" HA hydrogel was impractical in clinical research because of the toxicity of copper catalyst.

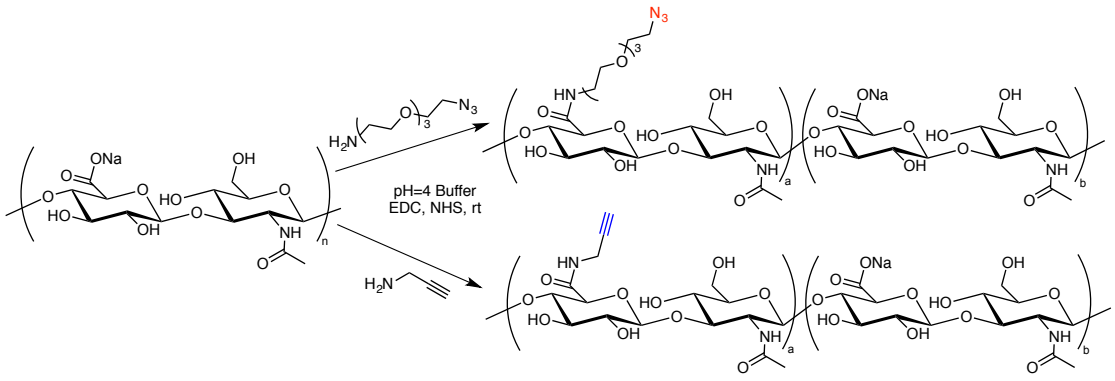

Scheme 2.10: "Clickable" HA modified with pendant alkyne and azide functionalities.

2.3.2 Preparation of Functionalized Hyaluronic Acid Derivatives, Crosslinkers and Fluorescent Tagging Agents

The TCO-tetrazine pair I selected are sTCO and diphenyltetrazine (Scheme 2.11). sTCO is the most reactive dienophile reported to date for TCO-tetrazine ligation reactions.[60,61] The diphenyltetrazine we chose exhibits good reactivity towards *trans*-cyclooctenes and possesses superior stability in organic solvents and in aqueous buffered environment. Both compounds can be easily synthesized on multigram scale. In water at 25 °C, I measured a second order rate constant k_2 284,000 M^{-1} s^{-1}. The rate constant was determined under pseudo first-order conditions.[62]

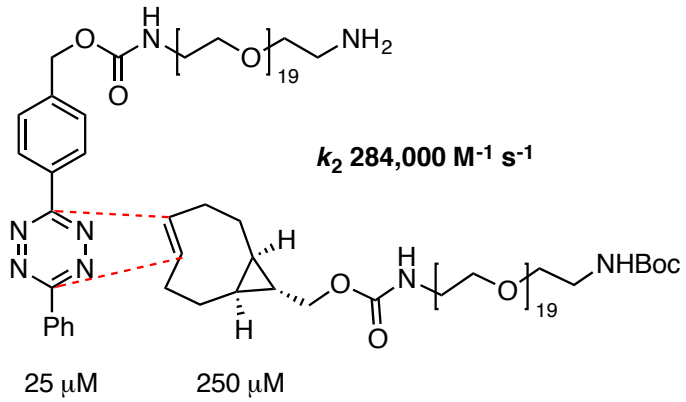

Scheme 2.11: Tetrazine-*trans*-cyclooctene pair selected for this study. The sTCO derivative was used in 10-fold excess, and stopped flow UV-vis spectrophotometer was used to monitor reaction progress.

Having selected the building block and the bioorthogonal reaction pair, I further started the preparation of functionalized HA derivative and corresponding crosslinker. I chose to attach the tetrazine functionality onto the backbone of HA while separately prepare a crosslinker molecule with sTCO endgroups.

Because of the hydrophobility of diphenyltetrazine moiety and the fact that the HA is only being soluble in water, I decided to transform the diphenyltetrazine into a PEG-conjugate (**2-3**) with terminal amine functionality, then further carry on the carbodiimide chemistry with carboxylate groups along the HA polymer chains (Scheme 2.12), affording tetrazine-modified HA (HA-Tz, **2-4**) with tetrazine incorporation percentage of 7%, analyzed by UV-vis spectroscopy and NMR.

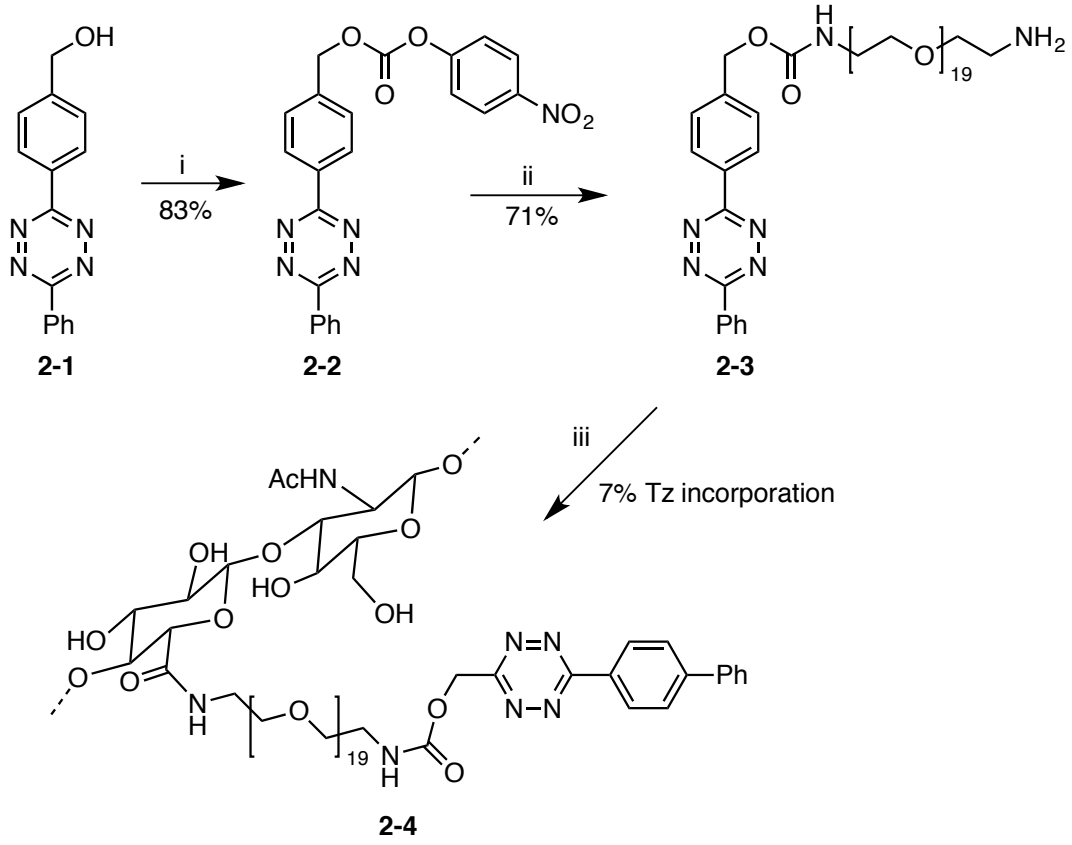

Scheme 2.12: Synthesis of tetrazine-modified HA (HA-Tz, **2-4**).(i) 4-nitrophenyl chloroformate, pyridine, DCM. (ii) *O*,*O*'-bis(2-aminoethyl)octadecaethylene glycol, DIPEA, DCM. (iii) HA-COONa, EDC, HOBt, DMSO/H_2O.

Synthesis of the *bis*-sTCO crosslinker was very straightforward by reacting sTCO-derived activated carbonate (**2-5**) with a *bis*-amino PEG oligomer to give the water soluble *bis*-sTCO crosslinker (**2-6**, Scheme 2.13).

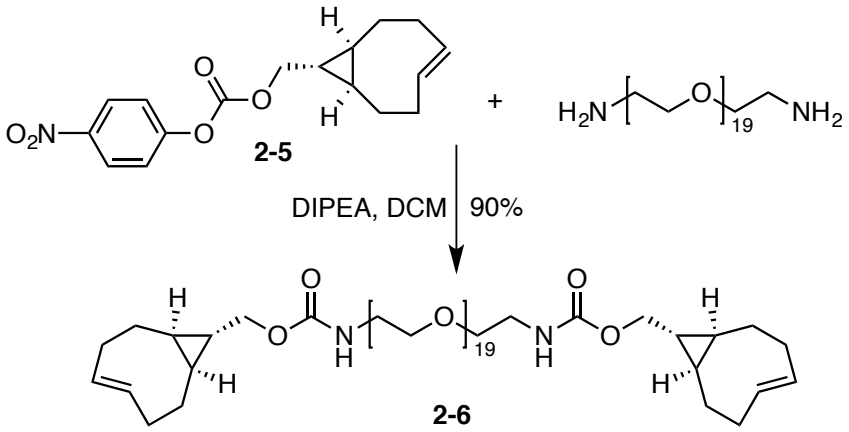

Scheme 2.13: Synthesis of *bis*-sTCO crosslinker **2-6**.

A fluorescent conjugate, Alexa Fluor® 647-sTCO (**2-7**) was synthesized (Scheme 2.14) for visualization purposes and as a proof-of-principle labeling/tagging agent.

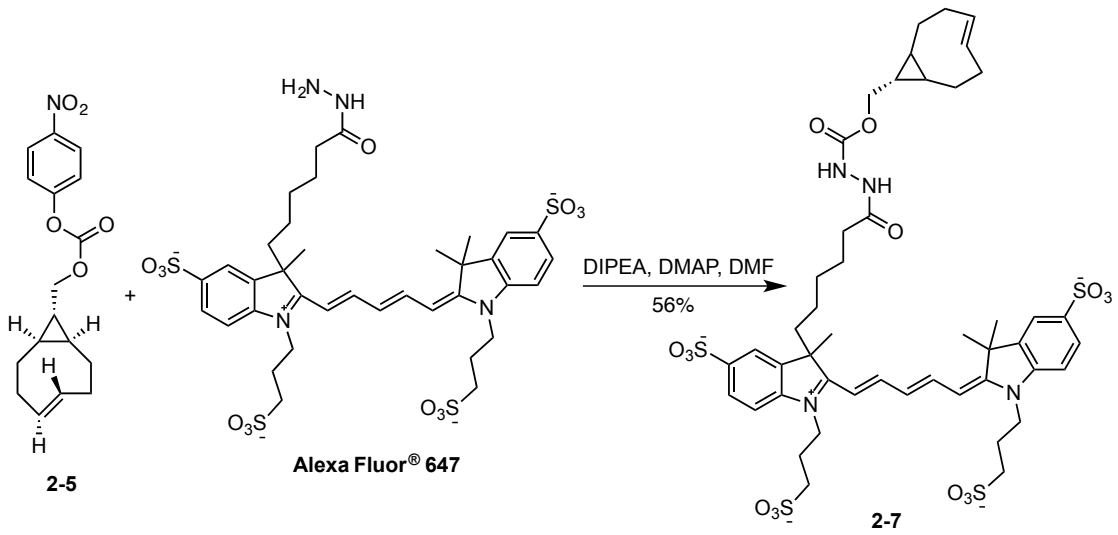

Scheme 2.14: Synthesis of Alexa Fluor® 647-sTCO conjugate **2-7**.

2.3.3 Interfacial Gelation and Hyaluronic Acid (HA) Hydrogel Microspheres

Having all the required materials readily prepared in hand, I moved on to conduct the interfacial gelation. The protocol of preparing a hyaluronic acid (HA) hydrogel microsphere is very straightforward: adding droplets of HA-Tz solution (2 wt% aqueous) into a bath of aqueous solution containing *bis*-sTCO crosslinker (400 μM), illustrated schematically in Figure 2.4:

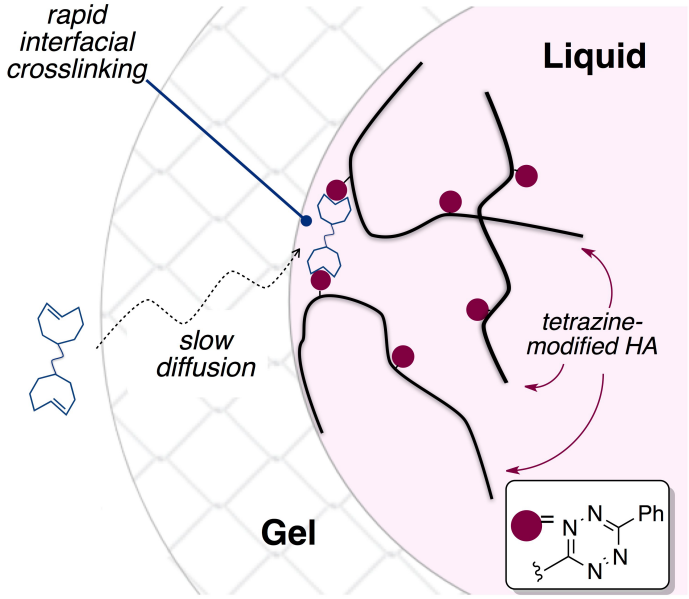

Figure 2.4: Schematic of the formation of a HA hydrogel microsphere from rapid interfacial crosslinking.

A thin layer of crosslinked hydrogels shell forms right after when the HA-Tz droplet makes contact to the crosslinker-containing bath solution, as evidenced by a colorless layer around the unreacted liquid core (Figure 2.6). Subsequent cross-linking is controlled by diffusion resulting in the inward advancement of a distinct gel/liquid interface. The *bis*-sTCO crosslinker (MW 1253) diffuses across the gel layer readily, while the high molecular weight HA-Tz (Mv 218 kDa) cannot. Thus, crosslinking takes place at the inner gel/liquid interface of the microsphere, with the volume of the un-crosslinked HA-Tz core steadily decreasing as the wall thickness increases. The whole process can be visually monitored by observing the disappearance of tetrazine moiety's pink chromophore (Figures 2.5 and 2.6). It takes a total of 2 hours for the crosslinker to diffuse all the way thru the HA-Tz droplet, forming a homogeneous,

transparent, nitrogen bubble-free HA hydrogel microsphere. The wall thickness increases linearly as function of crosslinking time over 2 hours.

The hydrogel microspheres are fully swollen after the crosslinking, with a equilibrium swelling ratio of 49 ± 2. Kevin Dicker, collaborating graduate student from the Jia group, performed oscillatory rheology study on the as-synthesized HA hydrogel microsphere by sandwiching the sample between the parallel plate geometry. Time sweep experiments (Figure 2.7, top) showed a stable plateau G' value of 135 ± 5 Pa with G" < 10 Pa after the initial decrease during the first 2 to 3 minutes, possibly because of the compression-induced network stiffening,[63] followed by network relaxation. The insensitivity of G′ (Figure 2.7, bottom) to frequency is consistent with an elastic, covalently crosslinked gel.

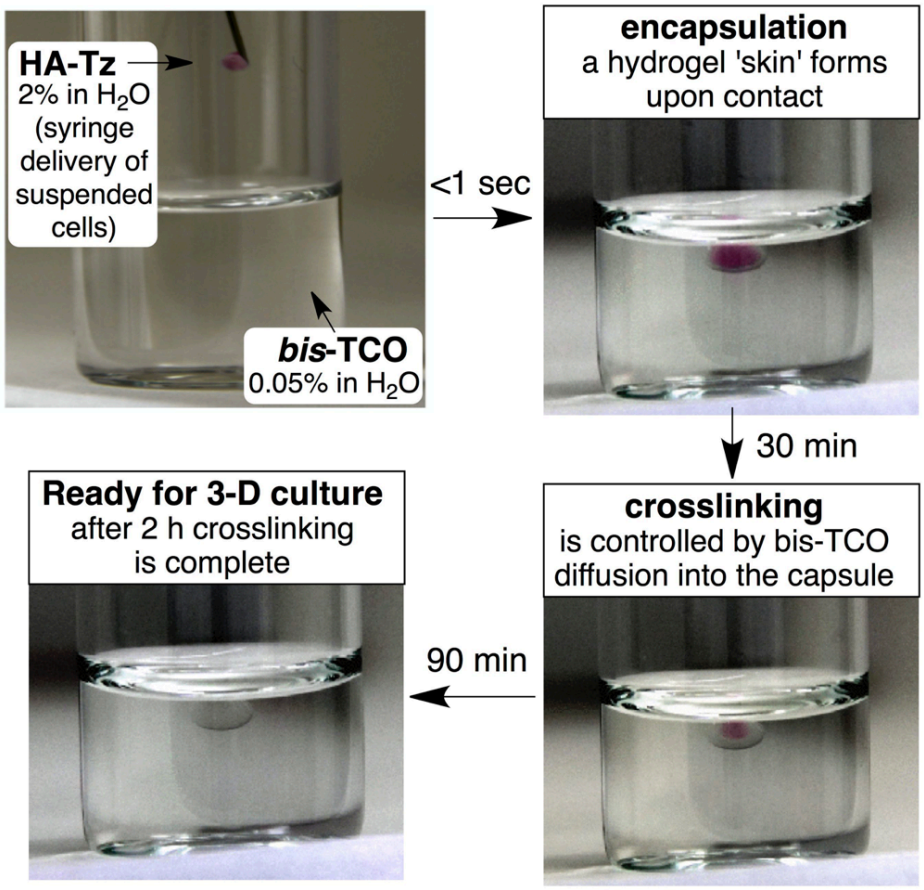

Figure 2.5: A fully crosslinked HA hydrogel microsphere forms from interfacial gelation in 2 hours.

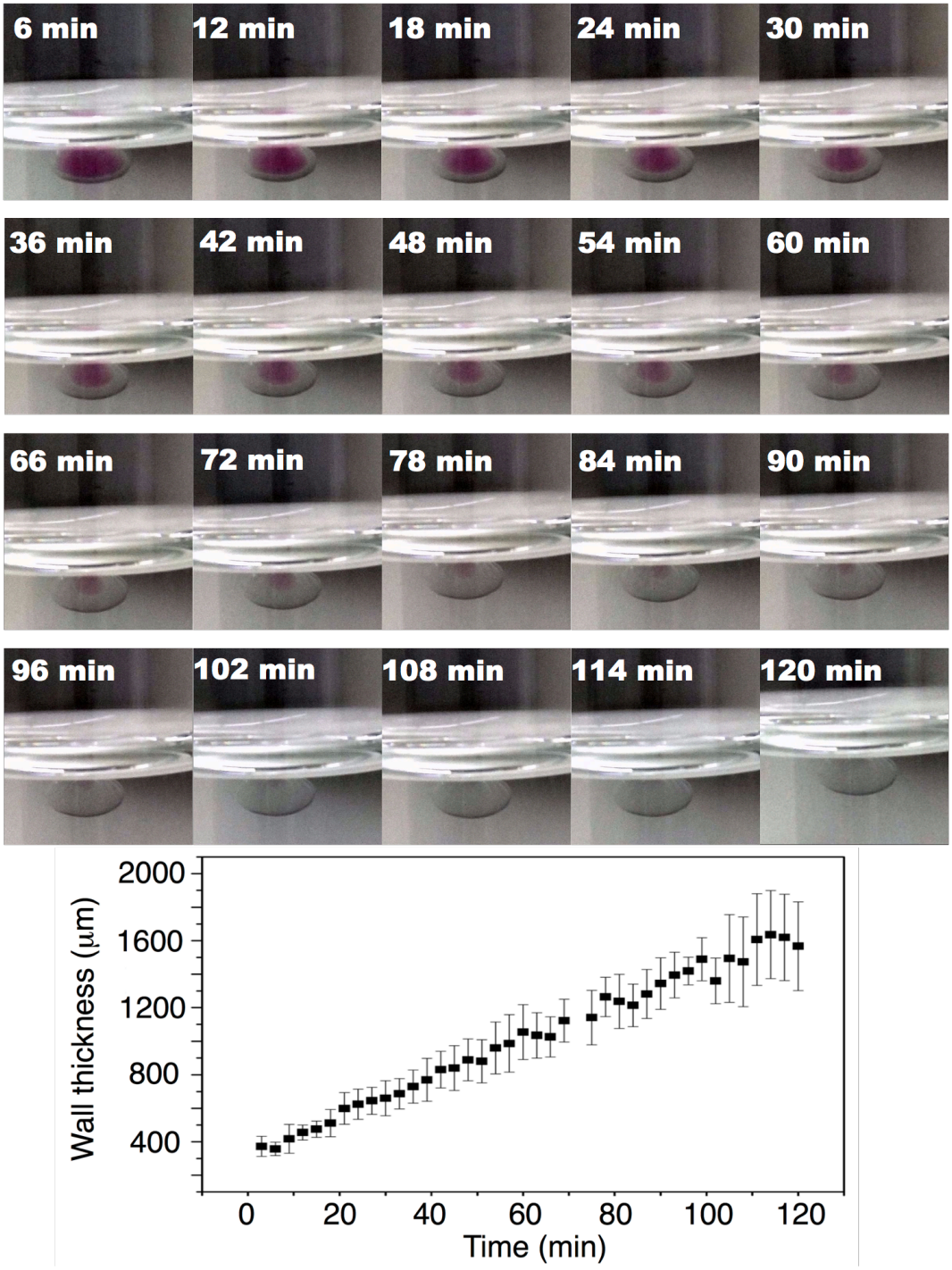

Figure 2.6: Top: Series of pictures taken at interval of 6 minutes through a duration of 2 hours when a HA hydrogel microsphere forms. Bottom: Crosslinked wall thickness as a function of diffusion time.

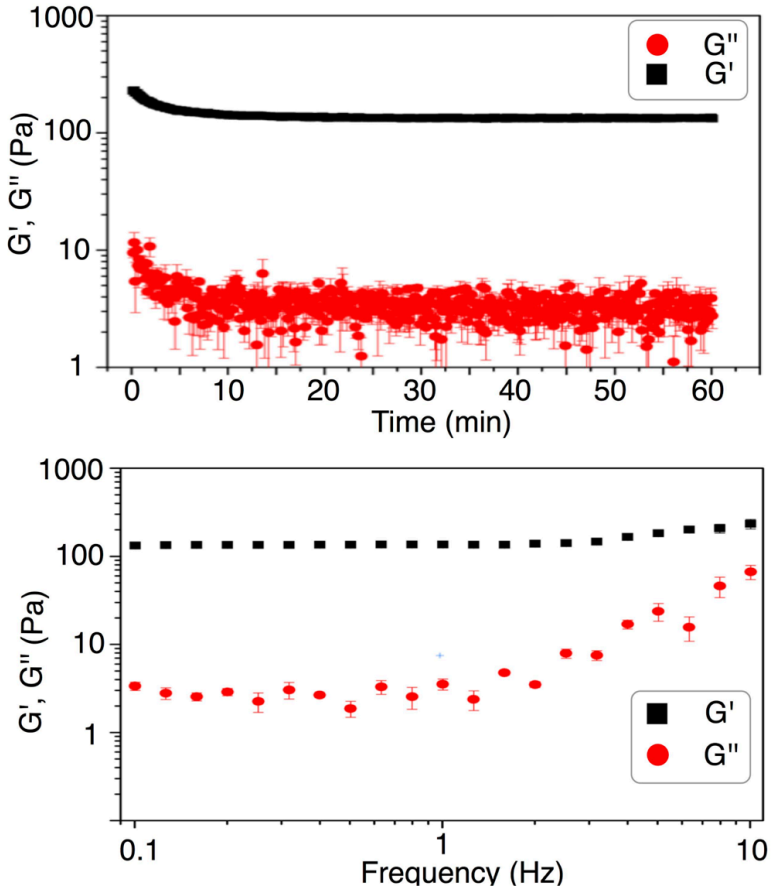

Figure 2.7: Rheological properties of interfacially crosslinked microspheres: G′, elastic modulus; G″, loss modulus.

2.3.4 Spatial and Temporal Controlled (Fluorophore) Tagging within Hydrogel Microspheres

Diffusion-controlled crosslinking also presented a very simple way to functionalize microspheres with spatial resolution. I envisioned that by blending diffusable TCO-conjugates into the crosslinker bath solution at an appropriate ratio (ratio not too high to compromise the crosslinking density and prevent the formation of efficient hydrogel networks), corresponding functionalities can be covalently introduced at the interface. Different functionalities can be introduced into various

layers by subsequently adopting crosslinker baths contain different kind of TCO conjugates. The thickness of the resulting "tagged" hydrogel layer would be a function of crosslinking time (Figure 2.8).

As proof of principle, I synthesized a fluorescent conjugate, Alexa Fluor® 647-sTCO (**2-7**) and used it as the "tagging" agent in the interfacial tagging experiments. Alexa Fluor® 647 is a very strong cyanine dye with a molar extinction coefficient as high as (approx.) 270,000 cm^{-1} M^{-1} so the usage of as low as 1 μM of the Alexa Fluor® 647-sTCO is sufficient for the imaging purpose.

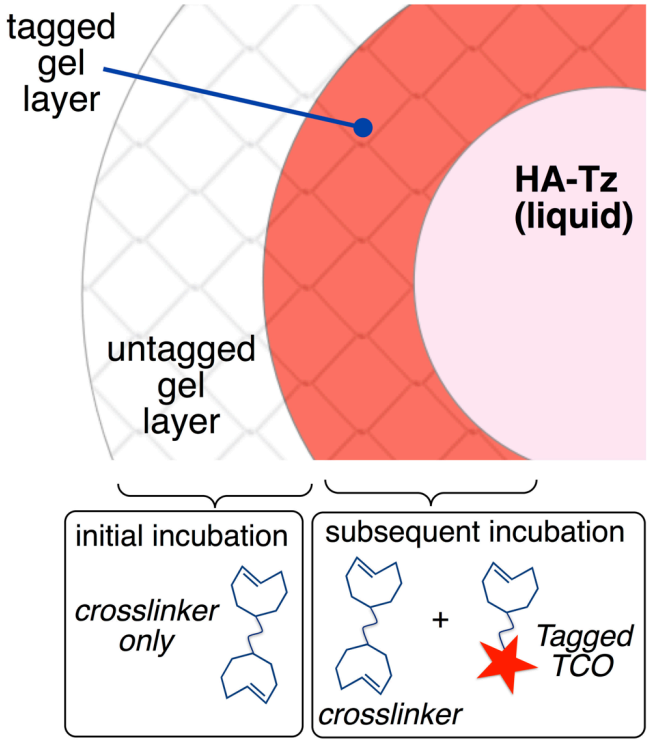

Figure 2.8: Schematic of interfacial covalent tagging of HA hydrogel microsphere.

By adding a droplet of HA-Tz (2 wt%) to *bis*-sTCO crosslinker (400 μM) bath containing Alexa Fluor® 647-sTCO conjugate (1 μM) and letting the crosslinking proceed for 30 minutes followed by 90 minutes crosslinking in dye-free *bis*-sTCO (400 μM), a hydrogel microsphere with only the outside ring tagged by Alexa Fluor® 647 can be prepared (Figure 2.9A). Alternatively, by simply switching the order and incubating the HA-Tz droplet first in a dye-free *bis*-sTCO bath for 1 hour then in a dye-containing bath, a hydrogel microsphere with only the core tagged can be prepared (Figure 2.9B). Microspheres tagged in a multilayered fashion can be achieved by simply alternating the presense/absence of Alexa Fluor® 647-sTCO conjugate during crosslinking (Figure 2.9 C-E).

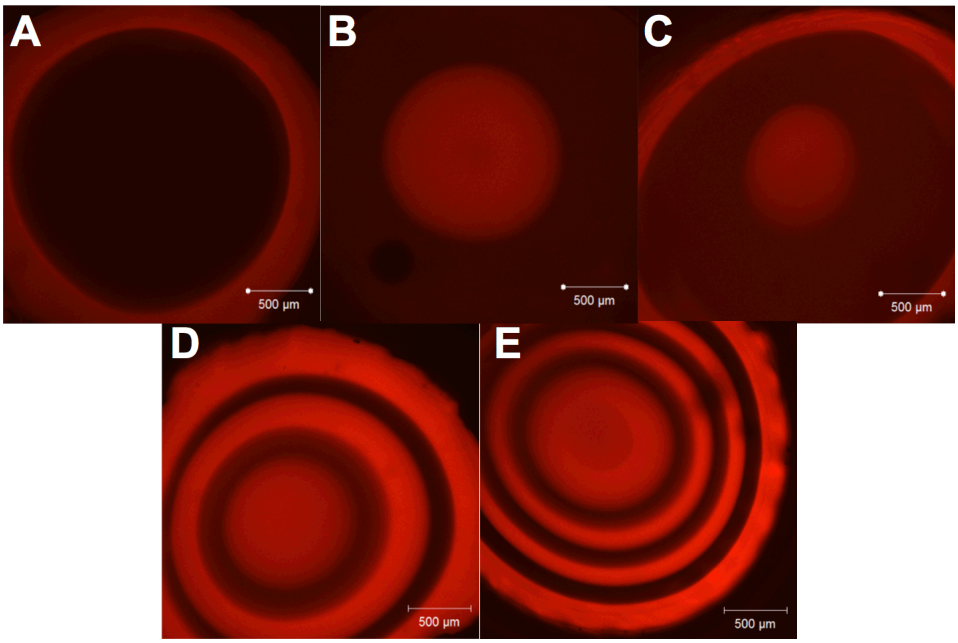

Figure 2.9: Confocal microscopy images of interfacial covalent tagging. (A) Interfacial crosslinking initially in the presence (30 min) then absence (90 min) of Alexa-TCO gave shell-labeled microspheres. (B) Crosslinking in the absence (60 min) and then presence (60 min) of Alexa-TCO gave core-labeled microspheres. (C-E) Onion-like structures by alternating the presence and absence of Alexa-TCO during the cross-linking procedure: three-, five-, and seven-layered gels are displayed.

Microspheres with radial gradients of fluorescent tag can be created by gradually introducing Alexa Fluor® 647-sTCO conjugate into the *bis*-sTCO bath during the crosslinking course, which can be simply achieved by the employment of a syringe pump. A gradient tagged microsphere (Figure 2.10, left) can be prepared by adding a HA-Tz droplet into *bis*-sTCO bath while increasing the concentration of Alexa Fluor® 647-sTCO conjugate from 0 to 0.47 µM using a syringe pump gradually over the course of 2 hours.

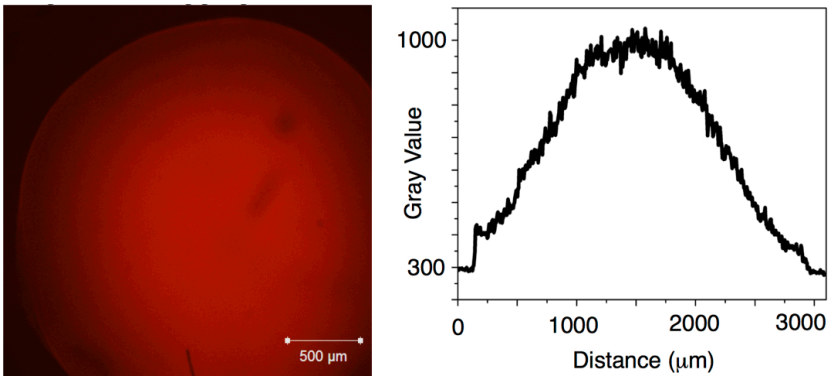

Figure 2.10: Left: confocal microscopy image of radial gradient covalent tagging; Right: color intensity across the diameter of the central slice of the microsphere.

These layered and gradient structures can be prepared without external triggers[64,65] or pre-existing templates,[65] and two independent chemistries[66] for cross-linking and patterning purposes are not required. With these tools, we envision use of bioorthogonal crosslinking for 3D covalent patterning of cell-instructive molecules that modulate cell adhesion, signaling and differentiation.

2.3.5 Construction of Water-Filled Hydrogel Channels

Separately, I also proved that the interfacial crosslinking can be used to prepare water-filled hydrogel channels (Figure 2.11) by a simple injection procedure without the need for pre-existing templates. When introducing *bis*-sTCO crosslinker solution into a bath of HA-Tz with a syringe, a crosslinked wall forms intantly following the path of the needle. The HA-Tz inside is excluded from penetrating into the channel due to large size while the crosslinker can diffuse out, therefore the crosslinking front extents outward and generates water-filled channels.

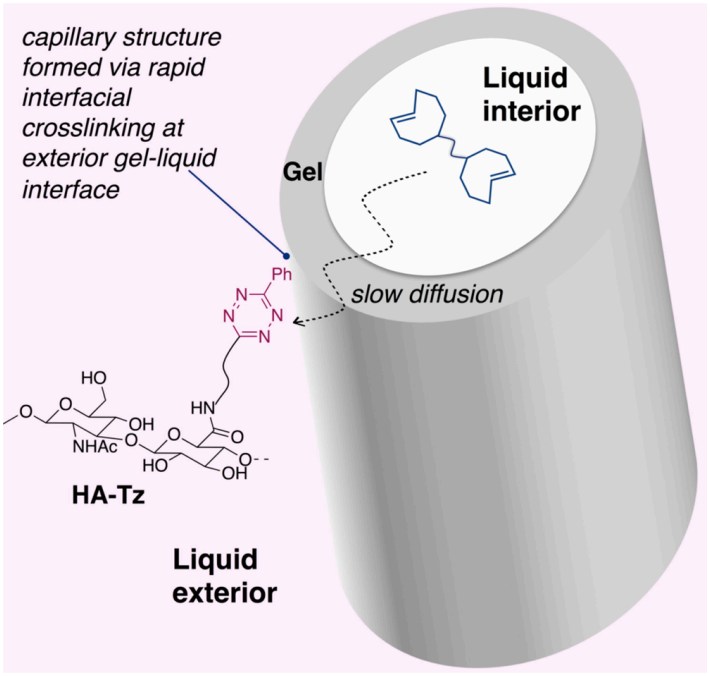

Figure 2.11: Schematic of the formation of a water-filled hydrogel channel from rapid interfacial crosslinking.

We again used Alexa Fluor® 647-sTCO conjugate as a visualization tool to monitor the process. A *bis*-sTCO (2 mM) solution containing Alexa Fluor® 647-sTCO

conjugate (2 μM) was injected to HA-Tz (2 wt%) bath *via* syringe. After 1 minute (Figure 2.12a), the channel wall thickness was 155 ± 13 μm while free Alexa Fluor® 647-sTCO and *bis*-sTCO remained in the interior (here we assume that the *bis*-sTCO and Alexa Fluor® 647-sTCO conjugate exhibit a similar rate of diffusion across the crosslinked shell). After 15 minutes (Figure 2.12b), the wall was 254 ± 18 μm thick and the fluorescence inside the channel decreased dramatically. The wall thickness at 30 and 60 minutes (Figure 2.12c) was 262 ± 18 μm with no significant increase thereafter because in this case the crosslinker within the lumen of the channel was the limiting reagent and the wall ceased to thicken when the crosslinker is depleted.

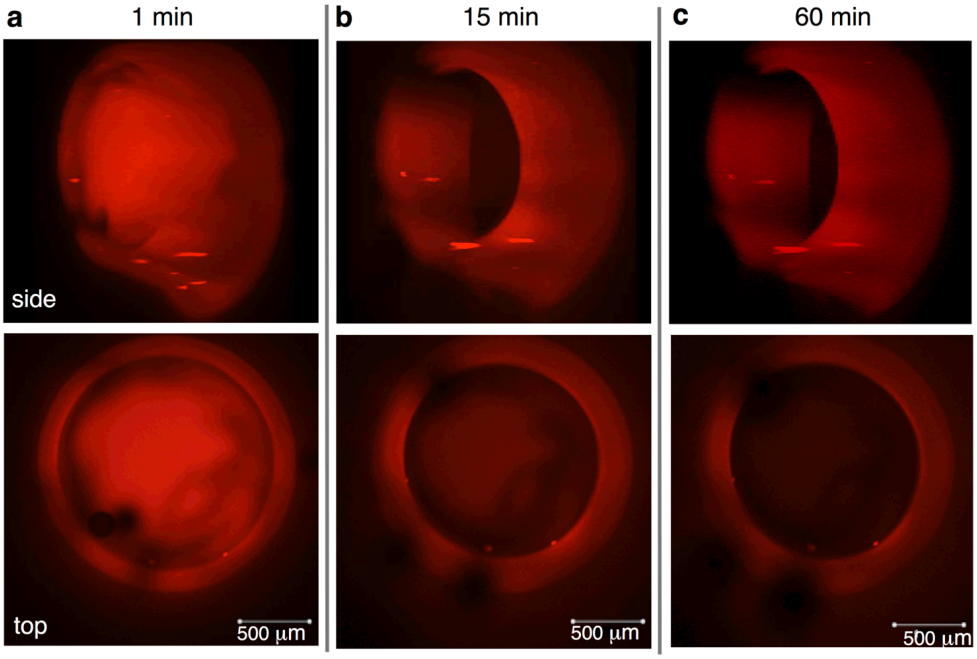

Figure 2.12: Top and side view of a water-filled hydrogel channel during its formation in a time course of 1 hour.

2.3.6 3D Culture of Human Prostate Cancer Cells (LNCaP)

Finally, we investigated if interfacial crosslink-created hydrogel microspheres could be used to engineer physiologically relevant *in vitro* tumor model. This part of work was carried out by my collaborator, Kevin Dicker.

Prostate cancer LNCaP cells suspended in HA-Tz could indeed be encapsulated in microspheres (Figure 2.13). The level of tetrazine incorporation (7%) gave soft, elastic gels appropriate for the 3D culture of LNCaP prostate cancer cells.[67,68] Live/dead staining (Figure 2.14) revealed 99 and 98% cell viability at days 1 and 5, respectively, confirming the cytocompatibility of tetrazine ligation. LNCaP cells initially entrapped homogeneously in a single cell state proliferated readily (Figure 2.13) and neighboring cell clusters merged within the microsphere. Cells in individual aggregates displayed rounded, clustered morphology with apparent cortical organization of actin. Individual microspheres were completely populated by over 200 dispersed tumor aggregates each greater than 50 μm (Figure 2.13b), showing great potential for application in construction of *in vitro* tumor models.

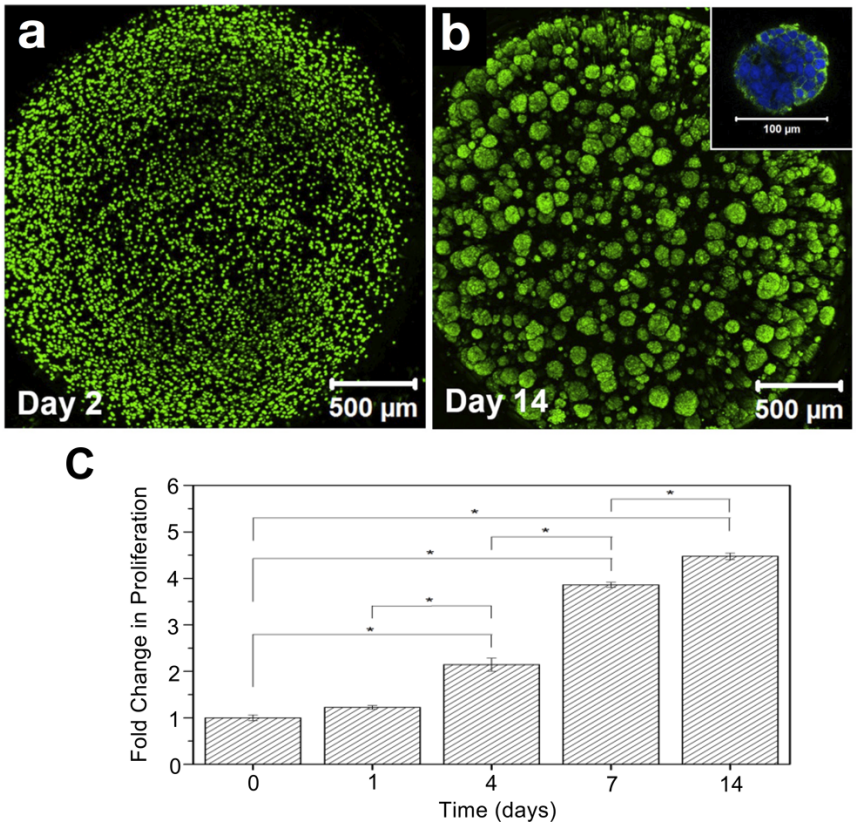

Figure 2.13: 3D culture of LNCaP inside interfacial crosslinked hydrogel microsphere. Confocal images after live/dead staining showing (a) individually dispersed LNCaP cells at day 2 and (b) dispersed tumoroids at day14. (c) cell proliferation assay (Trypan Blue exclusion), $*p < 0.05$.

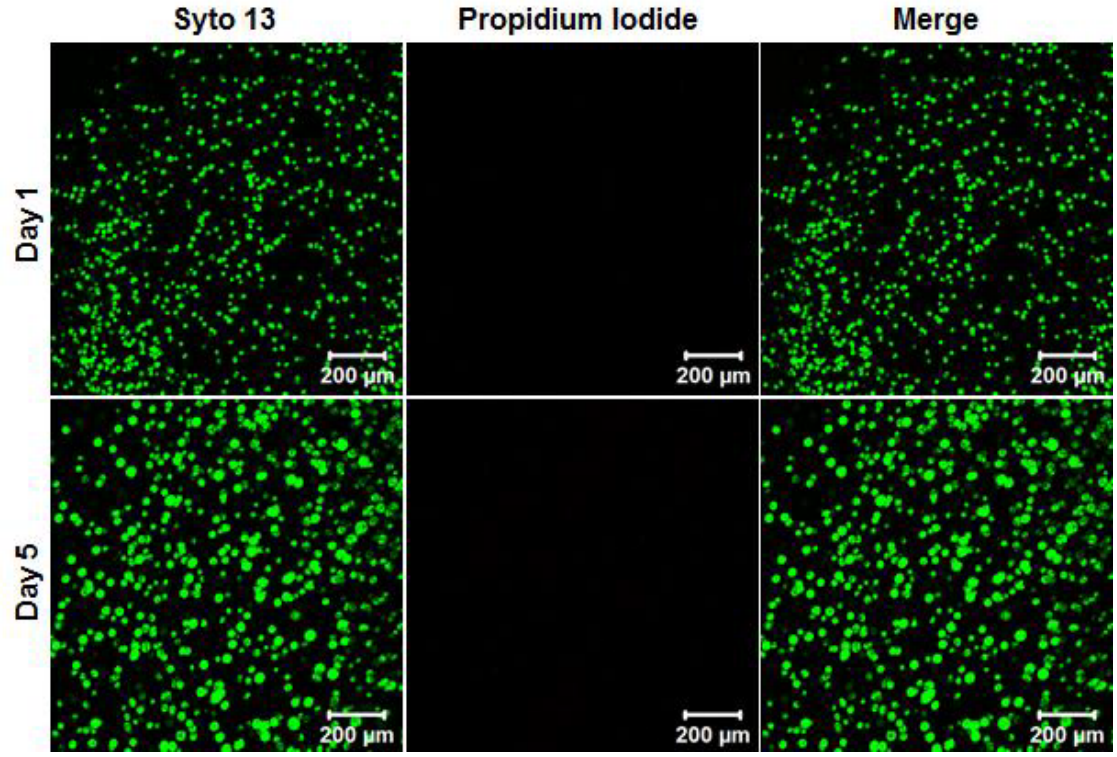

Figure 2.14: Live/dead staining of LNCaP cells cultured in HA hydrogel microspheres at day 1 and day 5. Live cells were stained green by Syto 13 and dead cells were stained red by propidium iodide.

2.3.7 Second Generation System for Interfacial Bioorthogonal Crosslinking of HA Hydrogels

Interfacial bioorthogonal crosslinking described above provides a new way to facile construction of cell culture matrices as well as tissue engineering scaffolds with 3D covalent patterning of cell-instructive functionality that could potentially modulate cell adhesion, signaling and differentiation.

Another attractive feature of the interfacial crosslinking method, while also an important aspect of the design of tissue engineering scaffolds is the ability of tuning mechanical property on-demand.

One intuitional idea of creating hydrogel structure with tunable stiffness would be introducing a "capped" TCO conjugate during the crosslinking course (Figure 2.15) in a similar fashion of introducing Alexa Fluor® 647-sTCO conjugate in previous experiments but at much higher loading ratio. Such capped TCO conjugates should be similar in size and hydrodynamic volume as to the *bis*-sTCO crosslinker to ensure the similar rate of diffusion across the crosslinked gel. Ideally, the capping agent will diffuse through the gel wall and competes with *bis*-sTCO crosslinker by "capping" the tetrazine moieties without crosslinking, thus brings in "defects" in the hydrogel network and leads to compromised crosslinking density and a softer hydrogel. In this manner, hydrogels with different stiffness distributed in layer can be achieved。

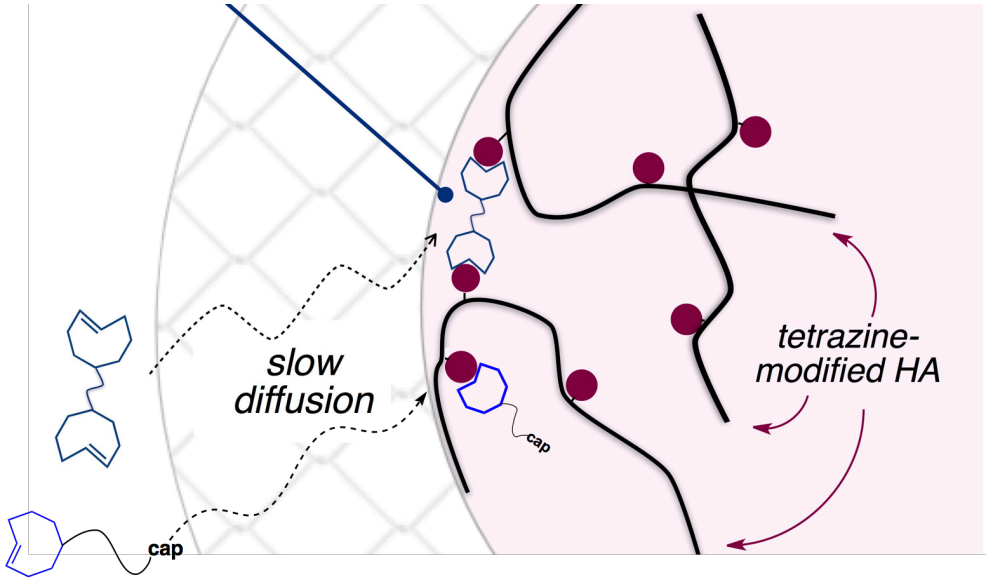

Figure 2.15: Schematic of the formation of hydrogel with tunable stiffness by introducing crosslink defect.

To accomplish such goal, we need HA-Tz with higher tetrazine modification to allow certain degree of "crosslinking defect" while still ensure effective gel network. Higher tetrazine incorporation rate will bring larger space for fine-tuning of stiffness.

However, the current version of HA-Tz is not without limits, the carbodiimide chemistry between carboxylate groups along the high MW HA polymer chains and the amino-functionalized PEGylated diphenyltetrazine (Scheme 2.12) was not proved to be very efficient, 5 equiv. of **2-3** (corresponding to carboxylate groups on HA) was used in the conjugation to afford merely 7% tetrazine incorporation. Besides the diamino-functionalized PEG oligomer to overcome the highly hydrophobic diphenyltetrazine was quite expensive. After the first report of interfacial bioorthogonal crosslinking, I put a lot effort on increasing the tetrazine incorporation such as tuning temperature and pH, substitution of PEGs with different sizes, running reaction in organic solvent after TBA cation exchange, etc. but none was proved to be effective.

Finally, I decided to move away from the highly hydrophobic diphenyltetrazine, therefore eliminating the need for expensive diamino-functionalized PEG oligomer. The methylphenyltetrazine (MPTz) has been widely used in applications utilizing IEDDA reactions recently, it is more hydrophilic than its diphenyl analog while possesses comparable reactivity towards *trans*-cyclooctene derivatives and is commercially available in forms of amine derivative and N-hydroxysuccinimide (NHS) ester.

The synthesis of my new version of HA-Tz (HAMPTz) started from commercially available N-hydroxysuccinimide (NHS) ester which can be transfer to a

hydrazide, which is readily soluble in DMSO/H_2O. The hydrazide derivative was then subjected to EDC coupling with HA under pH 4.75 to afford HAMPTz (**2-9**).

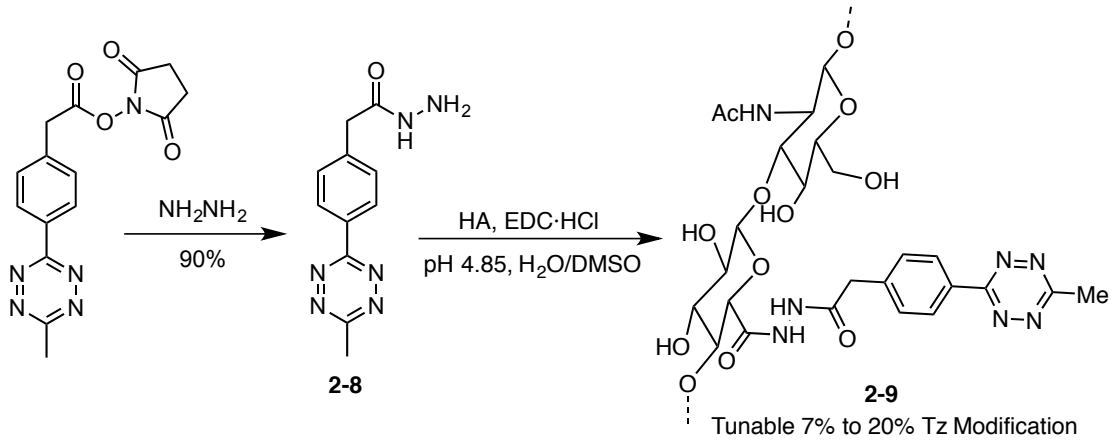

Scheme 2.15: Synthesis of 2nd generation of HA-Tz (HAMPTz, **2-9**).

The new synthesis (Scheme 2.15) was much more efficient and economical compared than before. Only 0.4 equiv. of tetrazine coupling agent (**2-8**) was needed to afford tetrazine incorporation percentage as high as 20% (the resulting HAMPTz tended to precipitate out of reaction mixture when more than 0.4 equiv. of **2-8** was used), a tunable modification rate of 7% to 20% could be achieved by simply tuning the equiv. of tetrazine **2-8** between 0.1 and 0.4.

The study towards the applications of HAMPTz was underway and was conducted in collaboration with Kevin Dicker and Yi Li. The higher tetrazine percentage indeed brought much better mechanical properties, hydrogel microspheres were prepared by introducing "capping" agents (Scheme 2.16), producing HAMPTz gels as much as 50 times stiffer than the original HA-Tz gels.

In an ongoing study, a variety types of cells were successfully encapsulated in the HAMPTz hydrogel microspheres and their behavior was studied while cell instructive signaling peptide sequence conjugate and crosslinker consists of cell degradable peptide (Scheme 2.16) were introduced interfacially to the cell culture hydrogel.

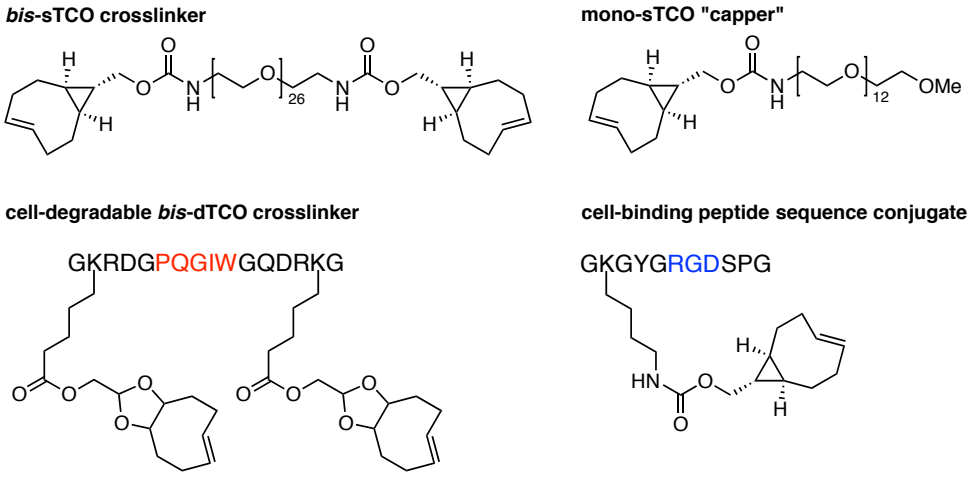

Scheme 2.16: Crosslinkers, "capper" agent and conjugates used in HAMPTz hydrogel fabrication

With help of higher tetrazine modification rate, water-filled channels made of HAMPTz were successfully acquired. Owing to their superior mechanical properties, the new generation of hydrogel channels are much more robust and elastic compared to the original version and can keep their shape during transportation and manipulation without being broken. As proof of principle, layers of tagging with different fluorescent conjugates was achieved (Figure 2.16). Ongoing interest lies in using HAMPTz hydrogel channels as supporting scaffolds for reconstruction of vascular

tissues by encapsulating and culturing different types of cells in separating layers throughout the HAMPTz hydrogel channels.

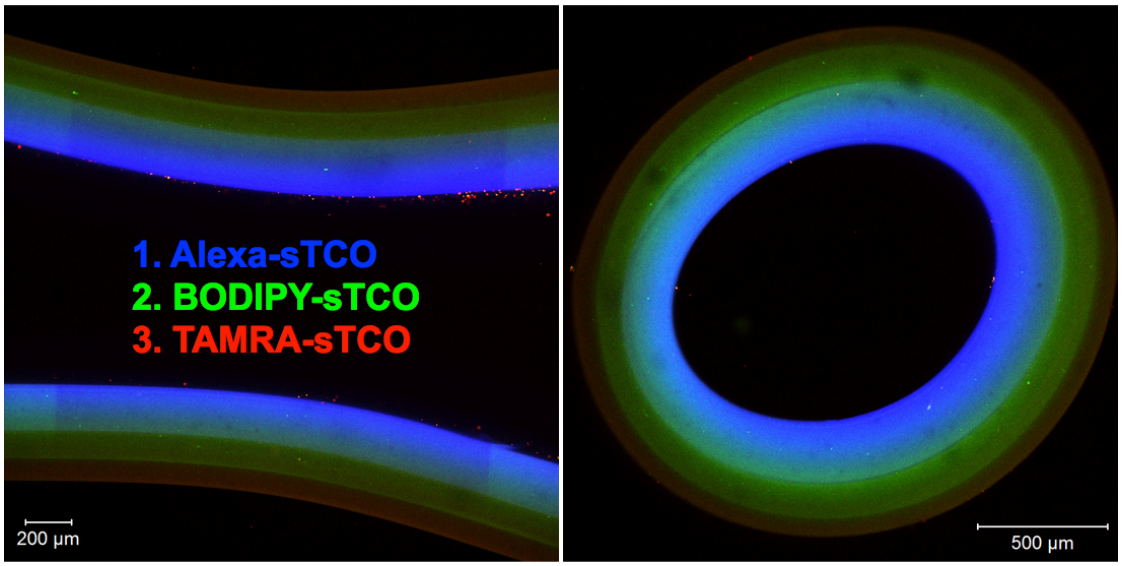

Figure 2.16: Confocal microscopic image of a HAMPTz hydrogel channel tagged with three kinds of fluorescent conjugates (Alexa Fluor® 647 in the inner layer, BODIPY in the middle layer and in the TAMRA outside layer)

2.4 Multiblock Copolymer Microfibers *via* Interfacial Bioorthogonal Polymerization

2.4.1 Multiblock Copolymers Derived from Bioorthogonal Chemsitries

Block copolymers are polymer made up of blocks of different polymerized monomers that consist of distinct chemical compositions and can exhibit superior physical, mechanical and biological properties over the properties of individual building blocks.[69]

Multiblock copolymers can be synthesized by linking polymeric precursors carrying complementary functional groups via a step-growth polymerization strategy. Bioorthogonal reactions provide an attractive approach for the construction of complex polymers with backbone diversity and complexity. The copper-catalyzed azide-alkyne cycloaddition (CuAAC) has been used in polymer chemistry. Matyjaszewski and coworkers used homobifunctional polystyrene prepared by atom transfer radical polymerization (ATRP) to synthesize step-growth copolymers (Scheme 2.1).[11] Green fluorescent protein (GFP) containing hybrid copolymers have also been prepared by CuAAC (Figure 2.17).[70]

Besides CuAAC, radical-mediated thiol/norbornene chemistry has been employed for the syntheses of mixed polystyrene (PS), poly(ethylene oxide) (PEO), and poly(dimethyl siloxane) (PDMS) multiblock copolymers.[71]

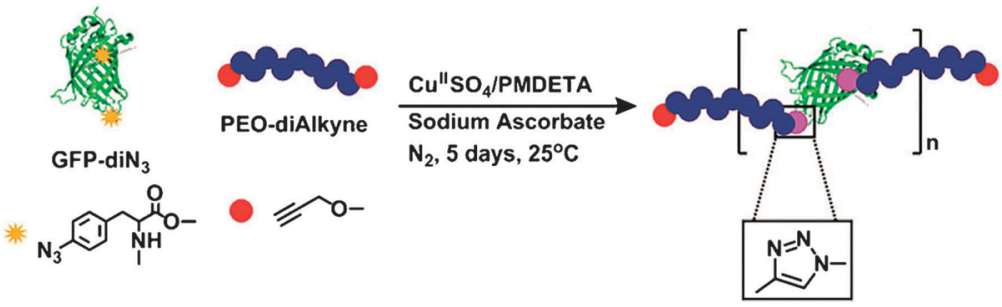

Figure 2.17: Protein–polymer hybrid multiblock copolymers synthesized by CuAAC chemistry.[70] Reproduced with permission, Copyright 2014, John Wiley & Sons, Inc.

The Jia group has explored utility of CuAAC for the construction of multiblock copolymers using diverse sets of synthetic and peptide building blocks.[72-75] Elastin–mimic hybrid multiblock copolymers consist of poly(*t*-butyl acrylate), polystyrene, poly(ethylene glycol) (PEG), and elastin-derived peptides were successfully synthesized using CuAAC reaction (Figure 2.18).

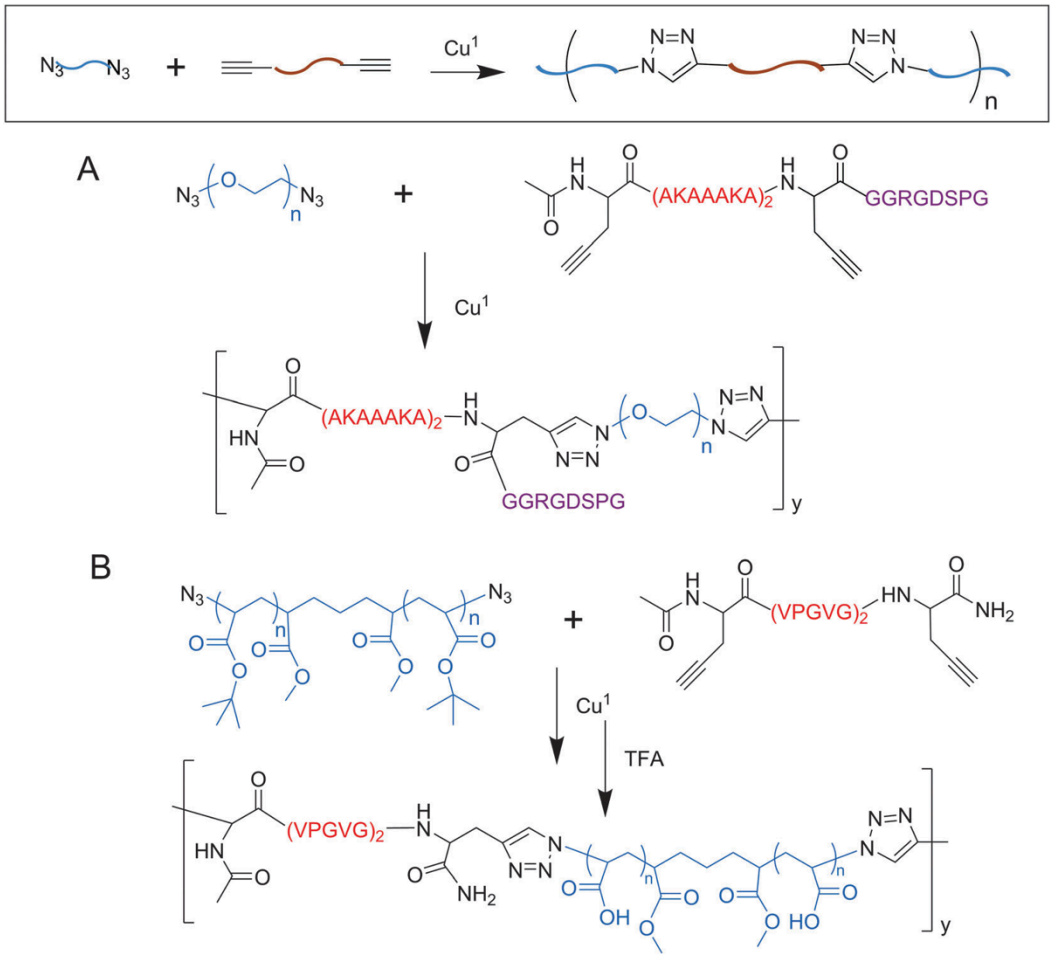

Figure 2.18: Elastin–mimic hybrid multiblock copolymers synthesized using CuAAC. Reproduced with permission, Copyright 2015, Royal Society of Chemistry.

The inverse-electron-demand Diels-Alder cycloaddition (IEDDA) has been used to synthesize diblock copolymers. O'Reilly and coworkers demonstrated that they can synthesize a variety of tetrazine or norbornene-terminal functionalized polymers including PS, PCL, PVL, PNIPAM and PEG.[76] Bioorthogonal reaction between polymer conjugates with counter functionalities lead to corresponding diblock copolymers.

There were no reports of using TCO-tetrazine ligation for polymerization purposes. We envisioned that the superior reaction kinetics of TCO-tetrazine ligation could make it an attractive tool in polymerization applications.

2.4.2 Interfacial Polymerization

Interfacial polymerization was first reported in two back-to-back papers by Wittbecker, Morgan and Kwolek in 1959,[36,37] in which it was describe as "interfacial polycondensation".

In their original study in 1959, sebacoyl chloride and hexamethylenediamine (Scheme 2.17) each dissolved in benzene and water reacted at the immiscible interface, forming poly(hexamethylene sebacamide) (Nylon-6,10) with high molecular weight. The most interesting part of this method is that a thin film of polymer can be formed at the interface if the interface between the two solvent were not disturbed and the film can be grasped and pulled out of the interface, more polymer can be formed instantly as the film was removed. A collapsed polyamide "rope" can be drawn out continuously.

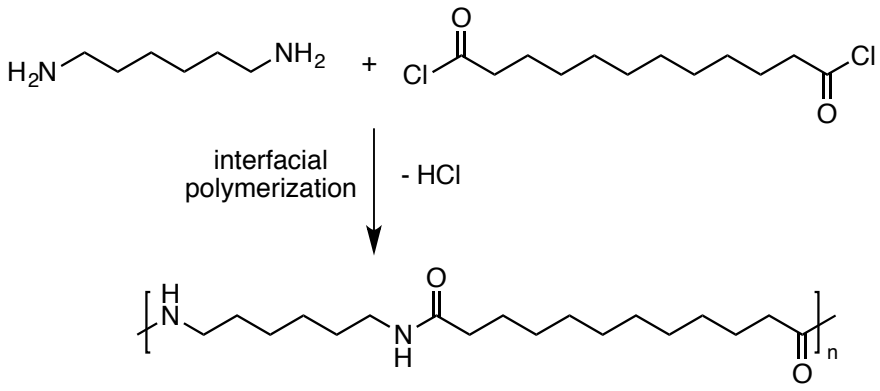

Scheme 2.17: Nylon-6,10 synthesized by interfacial polymerization.

This method has been proved to be particularly suitable for demonstration of condensation polymerization. The "Nylon rope trick" in which Nylon was produced in a beaker at room temperature,[77] has been performed in countless polymer chemistry teaching classes and labs all around the world for decades and is still the basis of a common classroom experiment.

Classically, interfacial polymerization is based on rapid but poorly selective reactions,[78] thereby excluding the possibility of incorporating biomolecules during the polymerization. On the other hand, the TCO-tetrazine ligation, as a highly selective bioorthogonal reaction while possessing extremely rapid reaction kinetics, should provide an elegant solution towards this question. In the following sections, I describe the first example of interfacial bioorthogonal polymerization in which multiblock copolymer fibers a prepared *via* rapid tetrazine ligation.

2.4.3 Tetrazine and *trans*-Cyclooctene-Containing Building Blocks

We chose the same sTCO-diphenyltetrazine pair as in the interfacial crosslinking project and the monomers for interfacial polymerization were prepared from precursors that are readily available on a multigram scale (Scheme 2.18). A *bis*-sTCO monomer (**2-10**) with a hydrophobic dodecyl spacer was designed to be soluble in organic solvent, *bis*-tetrazine monomer (**2-11**) with hydrophilic poly(ethyleneglycol) (PEG) spacer was designed to be soluble in aqueous solution. Separately, another water soluble *bis*-tetrazine monomer (**2-12**) containing a dangling fibronectin-derived cell adhesive peptide and PEG spacers was designed to enable the modular incorporation of biomolecules onto the multiblock copolymer during the polymerization. PEG spacers with molecular weights of 7.5 and 3.5 kDa were used to

prepare monomers **2-11** and **2-12**, respectively, providing comparable lengths for these monomers.

bis-sTCO (**2-10**):

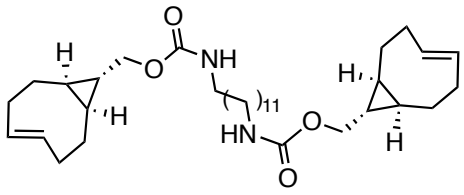

bis-Tz (**2-11**):

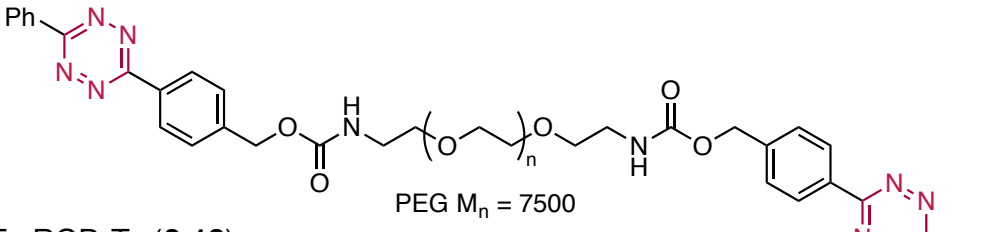

Tz-RGD-Tz (**2-12**):

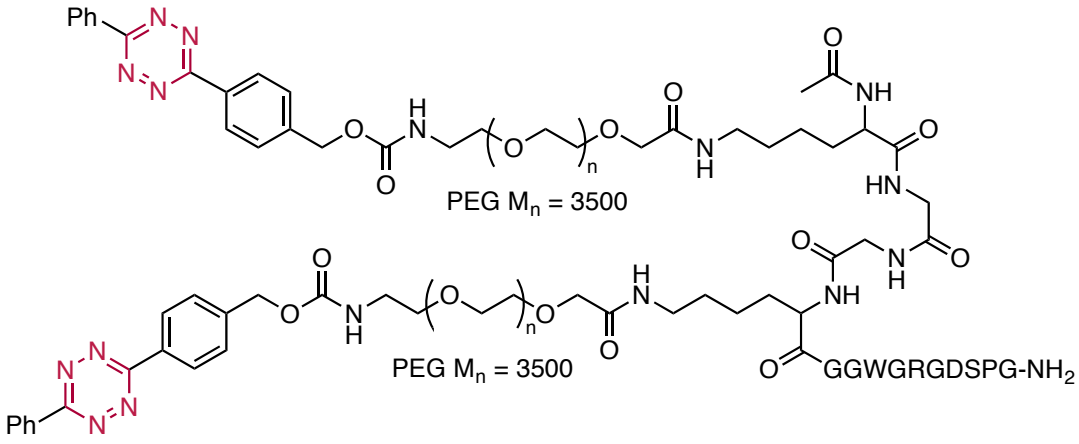

Scheme 2.18: Chemical structures of monomers for interfaicial polymerization.

2.4.4 Preparation of Copolymer Microfibers *via* Interfacial Polymerization

We postulated that the fast reactivity between tetrazine and TCO would enable interfacial polymerization, with the ability to draw (functionalized) multiblock copolymer fibers out of the liquid-liquid interface (Figure 2.20).

Several water-immiscible solvents including diethyl ether, ethyl acetate, hexanes, and toluene were evaluated for the interfacial polymerization procedure. All successfully gave polymer films at the interface, with ethyl acetate proving most conducive to fiber production due to its excellent solubility towards *bis*-sTCO (2-10) monomer and moderate volatility.

By overlaying an ethyl acetate solution of *bis*-sTCO (**2-10**) (3 mL, 3.6 mM) onto an aqueous solution of *bis*-Tz (**2-11**) (3 mL, 0.25 mM), a colorless multiblock copolymer film (Figure 2.19, left) was formed instantly at the interface between the two immiscible solutions and polymer fibers (Figure 2.19, right) can be continuously pulled out of the interface simply by a tweezer (Figure 2.21) and collected on a rotating frame at 20 RPM. Meter-long microfibers have been collected without breaking until approximately 70% of *bis*-Tz (**2-11**) was consumed, determined by monitoring the UV absorbance of the aqueous solution. Separately, peptide-containing microfibers were successfully prepared in the same interfacial fashion by using the Tz-RGD-Tz monomer **(2-13)**.

Ethyl acetate keeps the polymer film at the interface in a swollen state (as evidenced in which the dry fibers exhibited much smaller fiber diameters compared to the freshly drawn fibers), facilitating rapid monomer diffusion towards the polymer chain ends at the interface.

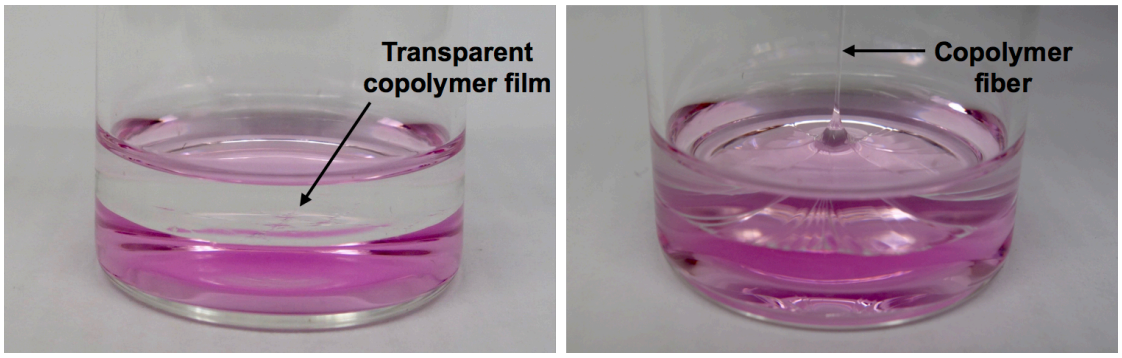

Figure 2.19: Close-up photographs showing copolymer film formed at the interface (left) and copolymer fibers being pulled out of the interface (right).

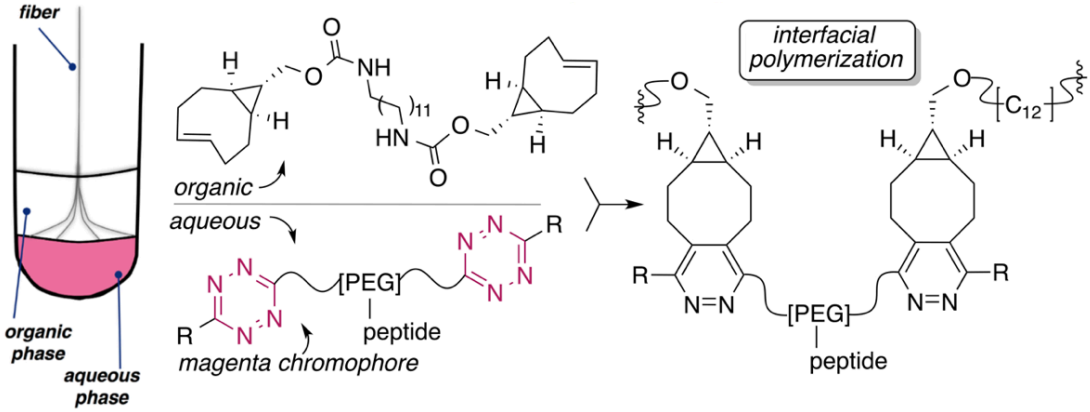

Figure 2.20: Schematic of interfacial bioorthogonal polymerization between phase-separated monomer solutions to produce multiblock copolymer fibers.

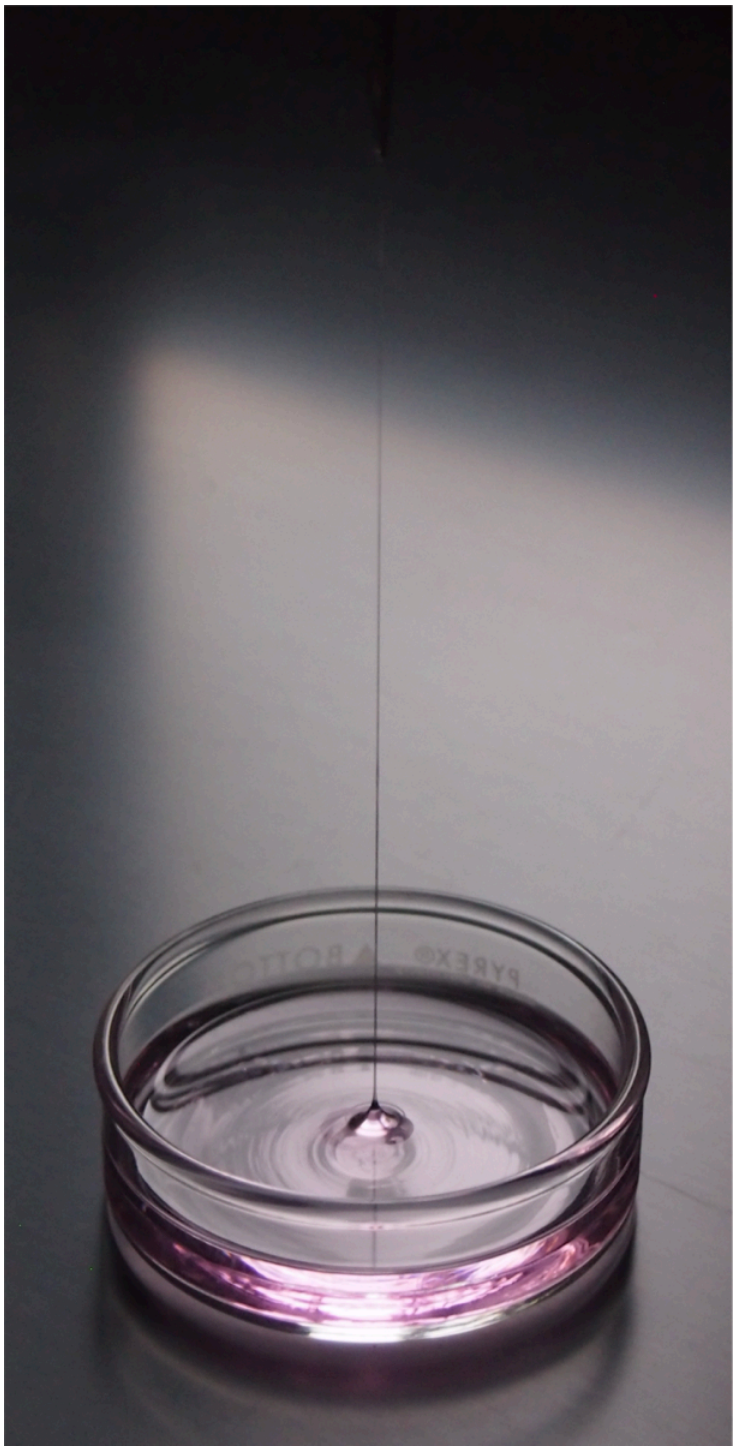

Figure 2.21: Meter-long multiblock copolymer fiber pulled out of aqueous/ethyl acetate interface from a petri dish by a tweezer.

2.4.5 Characterizations of Multiblock Copolymer Fibers

The characterizations of multiblock copolymer fibers, together with the evaluation of the peptide-containing copolymer fibers' ability to promote cell attachment and alignment, were conducted in collaboration with Dr. Shuang Liu. In this section, series of characterizations were performed on the "parent" (**2-13**) and peptide-containing (**2-14**) multiblock copolymer fibers (Scheme 2.19).

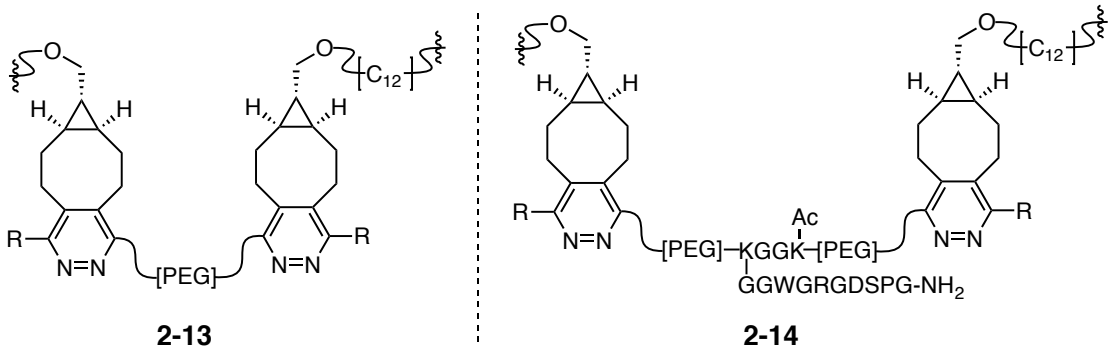

Scheme 2.19: Chemical structures of "parent" (left) and peptide-containing (right) interfacial polymerization products **2-13** and **2-14**.

2.4.5.1 Molecular Weight Characterization

The polymer fibers were first refluxed in THF to complete dissolve, then characterized gel permeation chromatography (GPC) using THF as mobile phase and commercial narrow disperse PEO as standards.

The "parent" polymer product **2-13** has a broad molecular weight distribution (Figure 2.22, top), as is characteristic for step-growth polymerization. The GPC trace was deconvoluted into two peaks, both with a Gaussian distribution. The respective number average molecular weights (M_n) calculated are 69.0 and 262.5 kDa, corresponding to an average of 7.5 and 28.7 repeating units, respectively. These values

are significantly higher than those calculated from previously reported step-growth polymers prepared from CuAAC or thiol/ene chemistry.

The incorporation of biological peptide did not compromise the polymerization process, as high molecular weight polymer 2-14 (M_n = 235 kDa) was also obtained using interfacial polymerization (Figure 2.22, bottom)

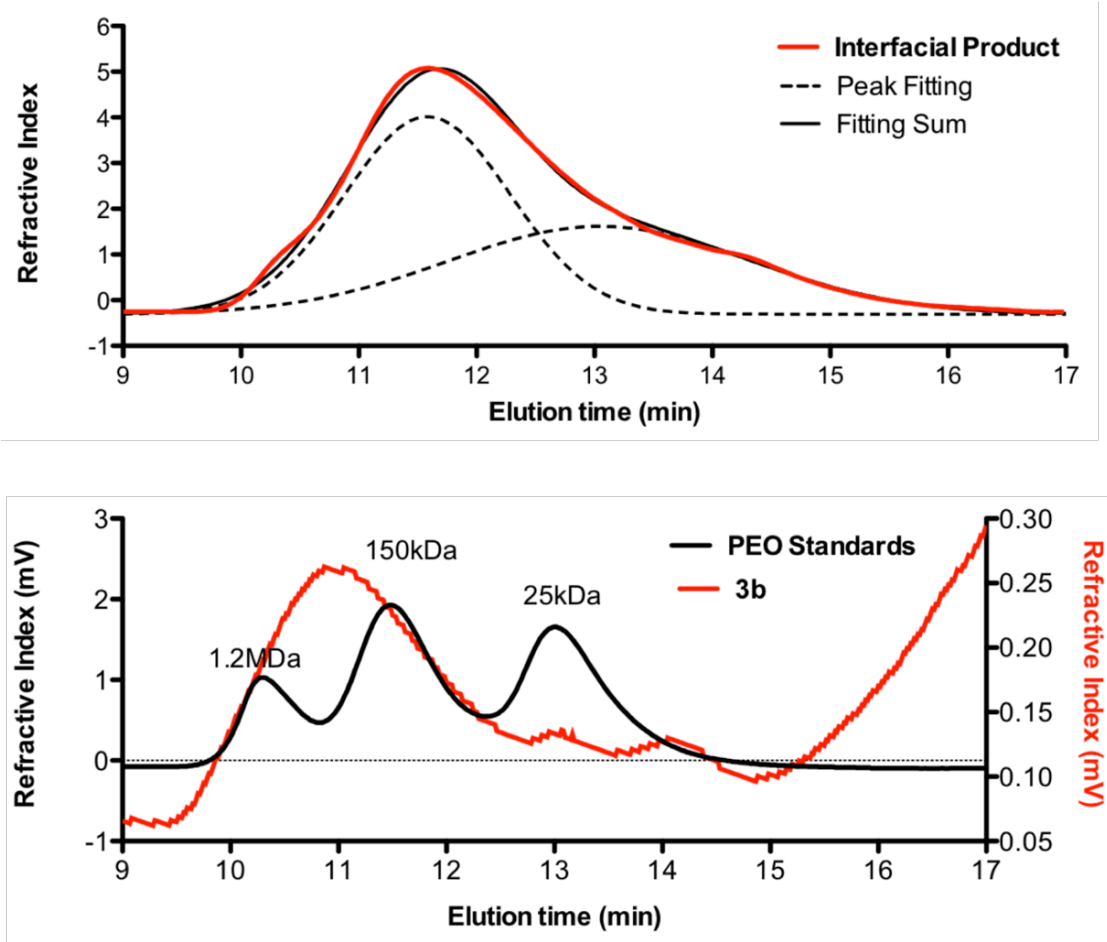

Figure 2.22: Top: GPC chromatographs of "parent" multiblock copolymer **2-13** from interfacial polymerization. Bottom: GPC chromatograph of peptide-containing multiblock copolymer **2-14** overlaid with PEO standards.

2.4.5.2 A Comparison Between Solution and Interfacial Polymerization

A solution polymerization using the equimolar amounts of monomer pair **2-10** and **2-11** (monomers dissolved in THF separately at a concentration of 2.0 mg/mL were mixed at a molar ratio of 1/1 to give a final monomer concentration of 0.23 mM) was carried in THF at concentrations comparable to the interfacial procedure and the subsequent polymerization products were compared (Table 2.1).

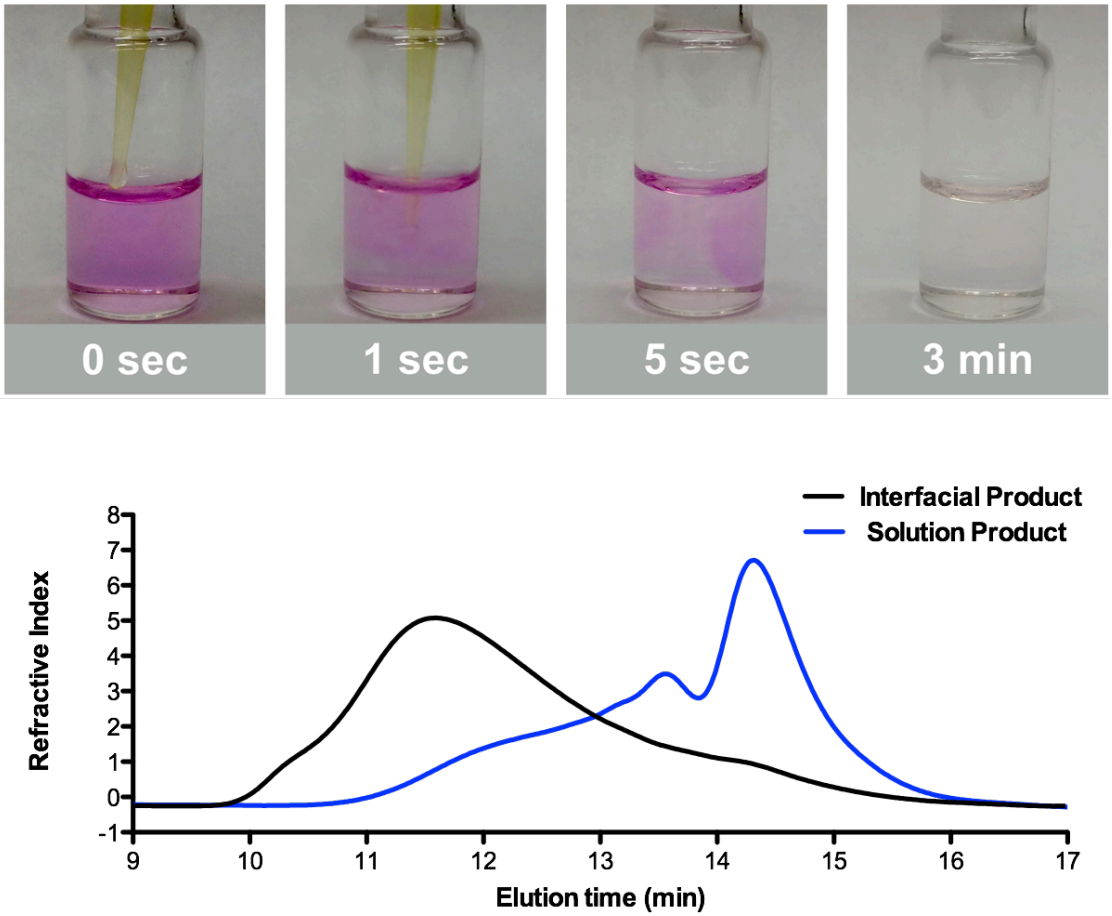

Figure 2.23: Top: Serial photographs showing the time course of solution (THF) polymerization of **2-10** and **2-11**. Bottom: GPC traces of **2-13** produced by interfacial (black) and solution (blue) polymerization.

As shown in Figure 2.23 (top), when **2-10** was first added to **2-11**, the initially pink solution instantaneously became colorless, indicating an immediate local consumption of the pink tetrazine chromophore. Within 3 min in the absence of any agitation, entire solution was nearly colorless. This is a clear evidence that the reaction of tetrazine with sTCO is significantly faster than the rate of diffusion. The GPC trace for the solution phase product (Figure 2.23, bottom) was deconvoluted into four peaks, with the highest molecular weight fraction having 8–10 repeating units, but representing only 24% of the polymeric product by integration. A major fraction (59% by integration) of the solution polymerization product even eluted at a longer retention time than the monomer **2-11**, possibly indicating the formation of cyclic byproducts[11] with smaller hydrodynamic volume compared to the monomer.

Table 2.1: GPC analyses of multiblock copolymer **2-13** synthesized by interfacial and solution phase polymerization

Polymerization Strategies	Interfacial			Solution				
	Overall	Deconvoluted Peaks		Overall	Deconvoluted Peaks			
M_n([kDa])[1]	180.1	69.0	262.5	22.0	3.4	9.7	11.9	76.1
M_w([kDa])	543.0			105.6				
Number of Repeats[2]	19.7	7.5	28.7	2.4	-	1.1	1.3	8.3
PDI	3.0			4.8				
Relative Percentage[3]	100%	45%	55%	100%	59%	6%	11%	24%

[1]The molecular weights (M_n and M_w) were calculated from GPC based on PEO standards; [2]The molecular weight of the repeating unit in the multiblock copolymer is calculated as 9142 Da.; [3]Relative percentages were calculated based on the areas under the GPC curves

2.4.5.3 Microscopic Characterizations

Fibers were collected in a consistent and reproducible fashion throughout the course of polymerization over the entire collecting frame (approximately 2 cm wide, Figure 2.24A, B). Crosshatched meshes (Figure 2.24D) were collected by simply changing the axis of rotation of the collecting frame. The collected fibers can be readily transferred to a glass supported silicone well (Figure 2.24C) for cell culture purposes (see **2.4.6** for detail).

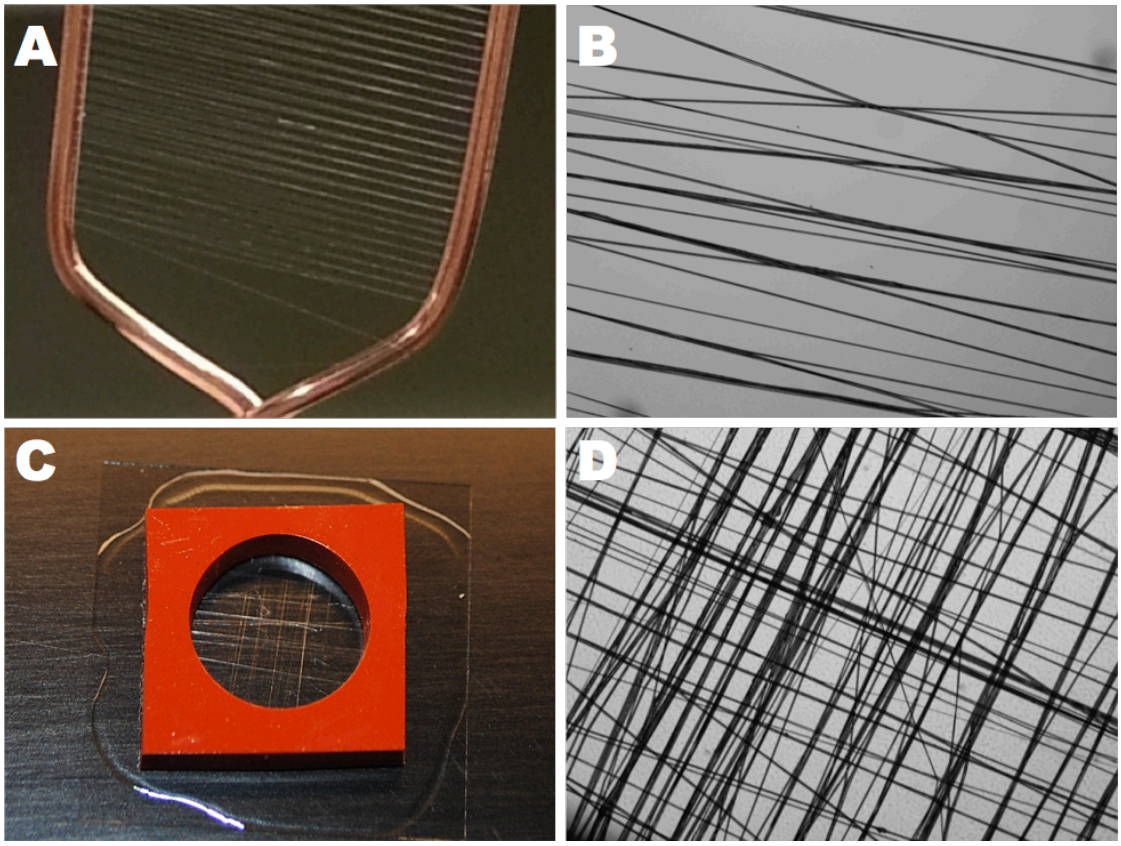

Figure 2.24: (A) Copolymer fibers collected on frame; (B, D) Dry fibers visualized under light microscope; (C) Copolymer fibers secured in a silicone well.

By rotating fiber orientation relative to polarized incident light, we observed change of fiber color (Figure 2.25), indicating the fibers are optically birefringent,[79] which implies the presence of locally ordered crystalline structures in the fibers, which were induced during the fiber pulling process.

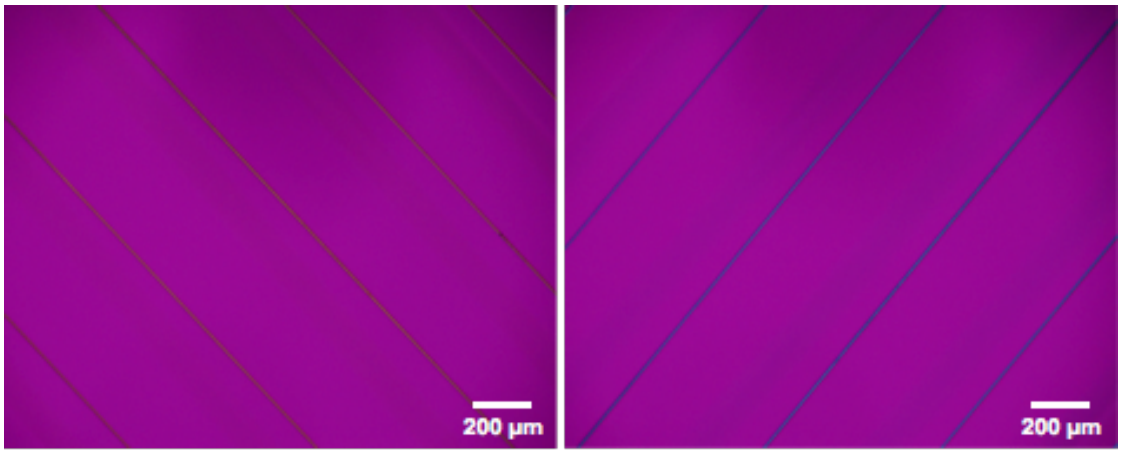

Figure 2.25: Polymer fibers imaged under polarized light. Fibers were aligned at a 45° angle relative to the polarizer. Fibers appear yellow (left) and blue (right) because of subtractive and additive interference, respectively.

Scanning electron microscopy (SEM) imaging (Figure 2.26) showed a similar morphology for "parent" (**2-13**) and peptide-containing (**2-14**) copolymer fibers, with majority of the fibers having diameters in the range of 6–11 µm (Figure 2.27) although a small population of thicker fibers is also present, possibly due to fiber merging during the pulling process.

Collectively, these findings illustrate how interfacial bioorthogonal polymerization can be used to fabricate aligned or woven fibers of uniform diameter through a simple pulling process.

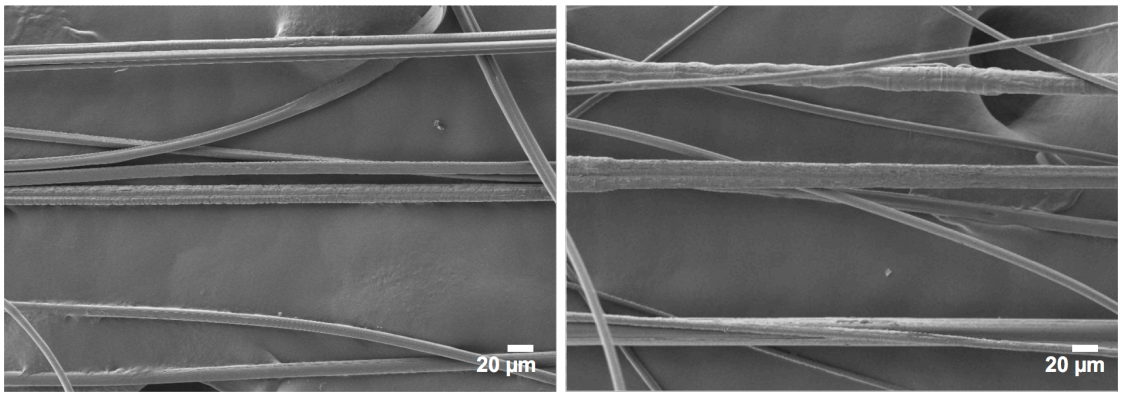

Figure 2.26: SEM micrographs of "parent" (left) and peptide-containing (right) fibers.

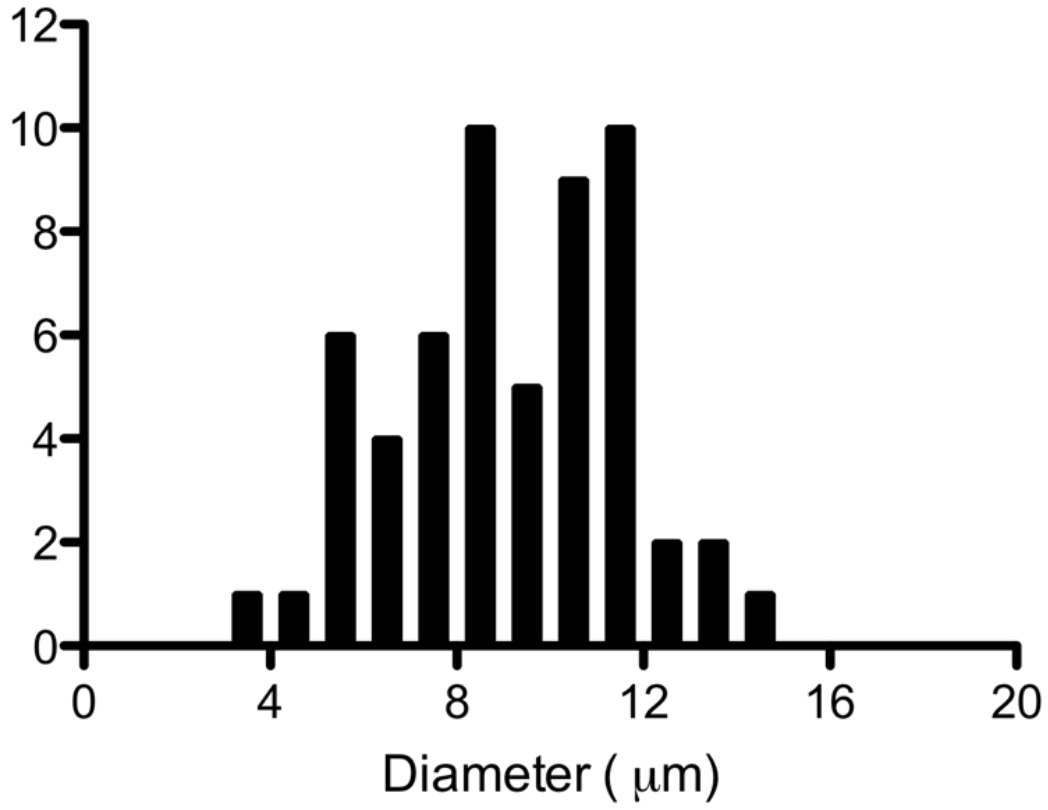

Figure 2.27: SEM histogram depicting the size distribution of "parent" multiblock copolymer fiber **2-13** (The histograms for **2-13** and **2-14** largely overlap).

2.4.5.4 Thermal, Morphological and Mechanical Characterizations

The polymer fibers were then subjected to thermal analysis. Differential scanning calorimetry (DSC) experiments revealed broad melting transitions centered around 53 and 34 °C, respectively (Figure 2.28), indicating a semicrystalline nature of the polymer fibers. The DSC thermograms of PEG-based *bis*-tetrazine monomers **2-11** and **2-12** show sharp endotherms at 55 and 43 °C, corresponding to the respective melting transition of the PEG chains while polymers **2-13** and **2-14** had a broader melting peak and a lower melting enthalpy (Figure 2.29). the second heating cycle of the *bis*-TCO monomer (**2-10**) did not reveal any melting endotherms. The results imply that the PEG and the aliphatic blocks contribute to the crystalline and the amorphous domains of the multiblock copolymers

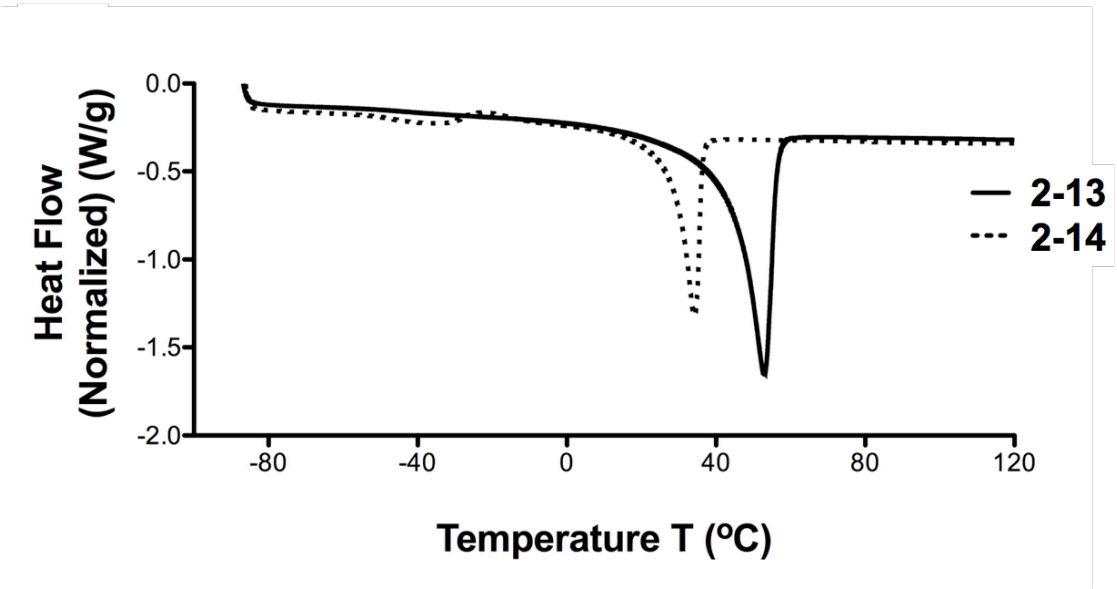

Figure 2.28: DSC thermograms of **2-13** and **2-14**.

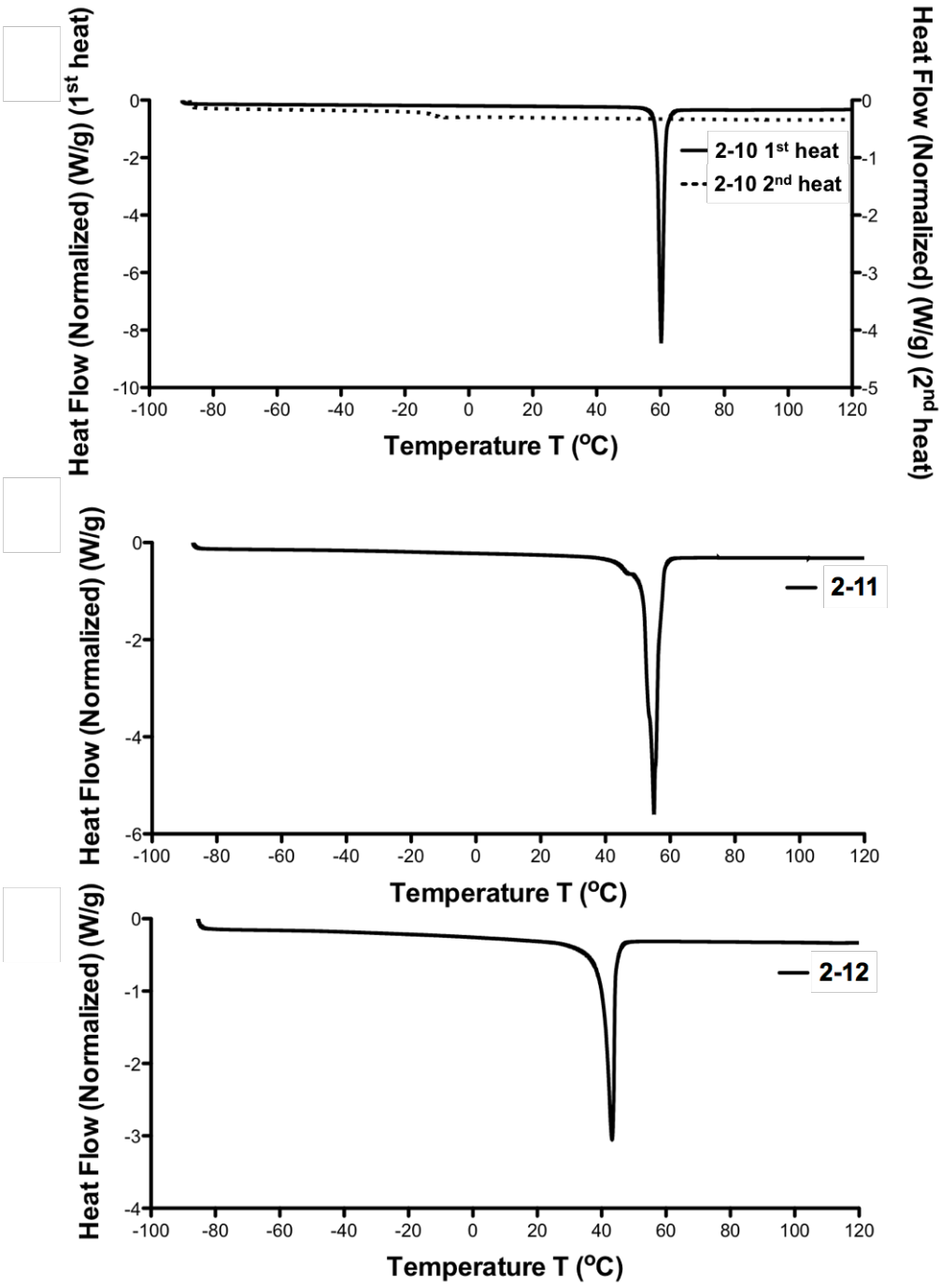

Figure 2.29: DSC thermograms of top: *bis*-sTCO monomer **2-10** (1st and 2nd heat cycles; middle: bistetrazine monomer **2-11** (2nd heat cycle) and bottom: **2-12** (2nd heat cycle) showing the respective melting transitions.

Finally, atomic force microscope (AFM), operated in PeakForce Tapping mode was employed for quantitative nanomechanical property mapping (QNM) of the polymer fibers.[80-82] The AFM height image for **2-13** fibers (Figure 2.30A) shows a semicrystalline polymer morphology with lamellar patterns, composed by densely packed crystalline domains appearing brighter than the surrounding amorphous interstitials. The uneven fiber surface introduced addition height difference across the scanned area. The surface of **2-14** fibers (Figure 2.30B) displays a more diffuse feature, with less discernible crystalline domains.

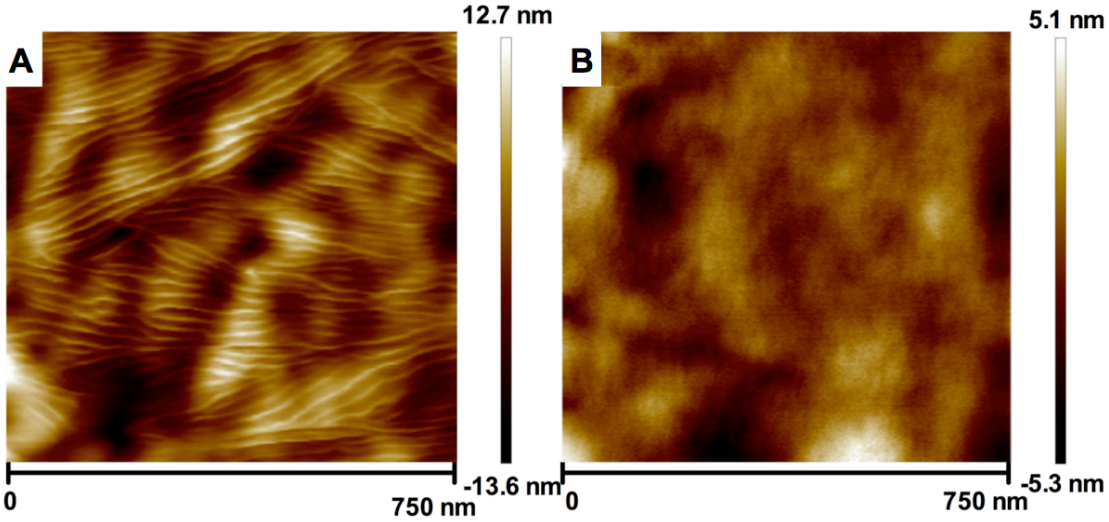

Figure 2.30: AFM height images of copolymer fibers **2-13** (A) and **2-14** (B).

AFM modulus mapping at a nanometer scale provides a measure of the local mechanical environment that is relevant to cells. The nanomechanical properties of the multiblock copolymer fibers were extrapolated from the AFM force-separation curves using a Hertzian model[83,84] and taking into consideration adhesive forces.

Young's modulus was calculated as 120±21 MPa for **2-13** fibers. The histogram for **2-14** fibers can be curve fitted into two populations with the estimated modulus of 106±12 and 74±5 MPa, respectively (Figure 2.31). The AFM results, in terms of the surface morphology and nanoscale stiffness, are in good agreement with our DSC observations regarding the crystallinity of the polymer fibers.

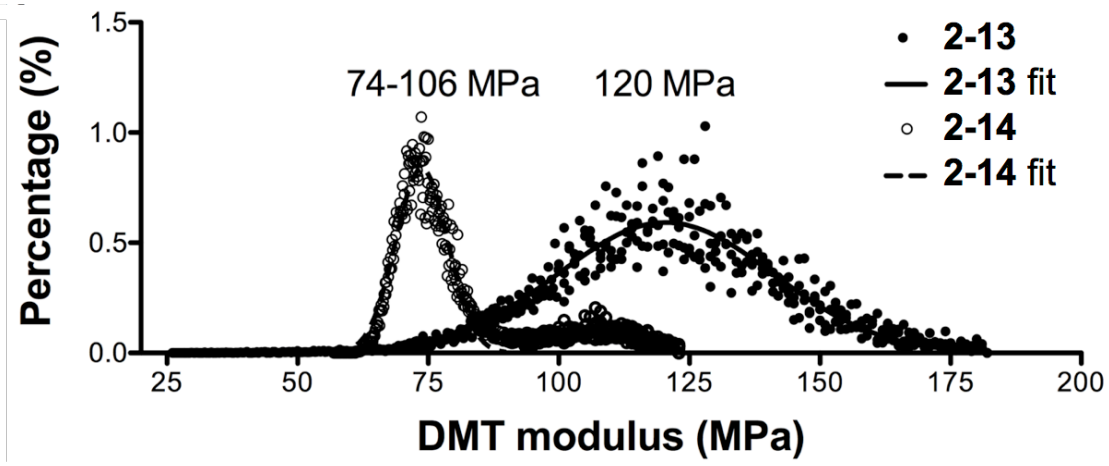

Figure 2.31: DMT modulus histograms for **2-13** and **2-14** fibers. Experimental data were curve-fitted with a Gaussian distribution

2.4.6 Evaluation of Peptide-Containing Microfibers' Ability to Promote Cell Attachment and Alignment

The peptide-containing copolymer fibers **2-14** were designed to simulate fibrous proteins found in native extracellular matrices (ECM) to provide biophysical and biochemical cues to cells. Dr. Shuang Liu evaluated the ability of the copolymer fibers to promote the attachment and alignment of fibroblast cell (NIH/3T3) and myoepithelial-like cells which were freshly isolated from healthy human salivary glands.

Fibers were immobilized on surface coated with poly(2-hydroxyethyl methacrylate) (PHEMA) and secured within silicone wells (Figure 2.24C). Fibroblasts attached to the peptide-containing fibers **2-14**, adopted a spindle shape, and oriented along the fibers 3 hours post seeding. Cells in close contact with the fiber developed exceptionally long and narrow processes (Figure 2.32B, white arrow) with actin stress fibers traversing the entire cell body. Those near fiber-anchored cells had a much smaller cell body and formed cell clusters bridging neighboring fibers. In areas of high cell density, cells aggregated to form branched and interconnected multicellular networks, and individual cells within the cluster exhibited a stellate morphology with no preferential cell orientation. Cells at the edge of the cluster extended short processes (Figure 2.32C, white arrow) to interrogate their surroundings for potential contacts even though the substrate in between the fibers is cell-repellent.

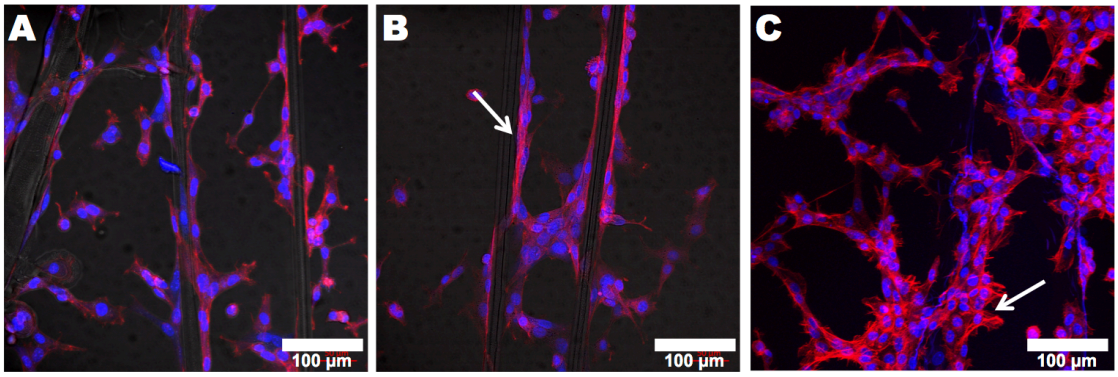

Figure 2.32: Confocal images of fibroblasts cultured in the presence of multiblock copolymer fibers **2-14** with cell-adhesive peptide. F-actin and nuclei were stained with Phalloidin (red) and DRAQ 5 (blue), respectively. Fibroblasts were cultured for 3 hours before being imaged with a confocal microscope.

The peptide-containing copolymer fibers could also support the attachment of myoepithelial-like cells. These cells did not attach to the synthetic fibers as rapidly as did fibroblasts; 24 hours post seeding, cells were loosely anchored on the fibers (Figure 2.33A), but had not undergone significant spreading. 60 hours post seeding, cells became more spread out, developed long and narrow lamellipodia and oriented parallel to the long axis of the fiber (Figure 2.33B, C). In some cases, multiple cells formed a cohesive blanket enclosing the fiber.

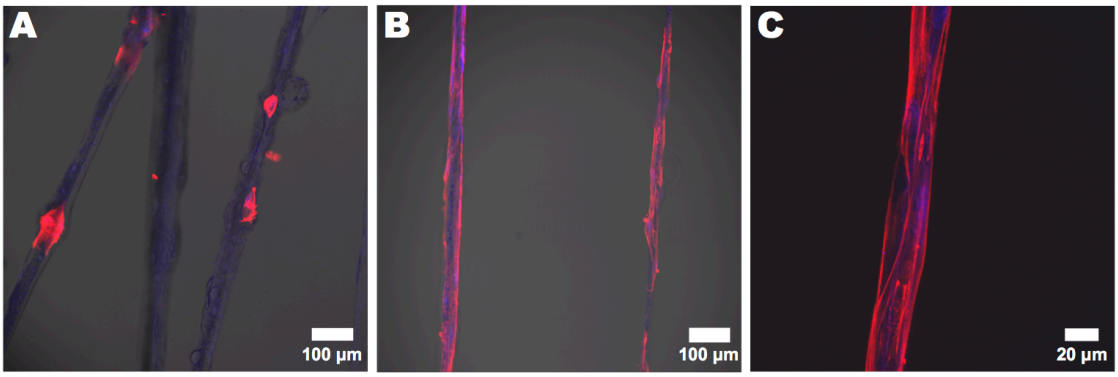

Figure 2.33: Confocal images of myoepithelial-like cells cultured in the presence of multiblock copolymer fibers **2-14** with cell-adhesive peptide. F-actin and nuclei were stained with Phalloidin (red) and DRAQ 5 (blue), respectively. Cells were cultured for 24 (A) and 60 (B-C) hours before being imaged with a confocal microscope.

In control experiemtns, when incubated with peptide free fibers **2-13**, both fibroblasts (Figure 2.34A) and myoepithelial-like cells (Figure 2.34B) remained round in suspension and on the substrate and the majority of unbound cells were washed off during the fixation process.

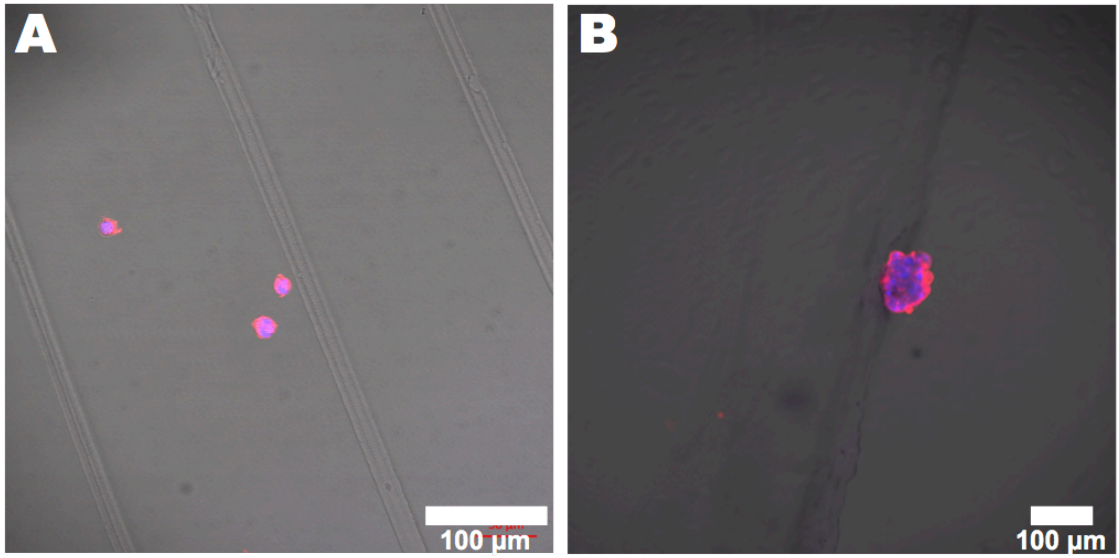

Figure 2.34: Confocal images of fibroblasts (A) and myoepithelial-like cells (B) cultured in the presence of multiblock copolymer fibers **2-13** without cell-adhesive peptide. F-actin and nuclei were stained with Phalloidin (red) and DRAQ 5 (blue), respectively. Fibroblasts were cultured for 3 hours and myoepithelial-like cells were cultured for 60 hours before being imaged with a confocal microscope.

Overall, the peptide-containing fibers could be prepared that present appropriate biochemical signals and topographical features for the anchorage and alignment of both fibroblasts and myoepithelial-like cells. The microfibers possess promising application on providing contact guidance for establishing appropriate cell–matrix and cell–cell interactions.

2.4.7 Crosslinked Hydrogel Fibers

As a result of being made of high molecular weight linear copolymer chains, the multiblock copolymer fibers inevitably swell, relax, and the individual polymer

chains tend to disassociate from each other when immersed in cell culture media during long-term cell culture (7 days). It is an attractive feature for applications where backbone dissociation was needed, for example, in drug release or as a degradable solid scaffold in tissue engineering applications. However, for applications in long-term cell culture, it is desirable to have more robust fibers

I proposed that a multi-armed monomer could be included in the interfacial polymerization procedure to provide fibers which are intrinsically crosslinked. Such fibers should still possess hydrogel-like properties and have better mechanical performance and stability against dissociation.

We further devised a 3-armed *tri*-sTCO monomer/crosslinker (Scheme 2-20) from commercially available *tris*(2-aminoethyl)amine as the hydrophobic building block in the organic phase for interfacial polymerization. For the hydrophilic block, we chose to continue using PEG-derived *bis*-diphenyltetrazine polymer **2-11** and **2-12**.

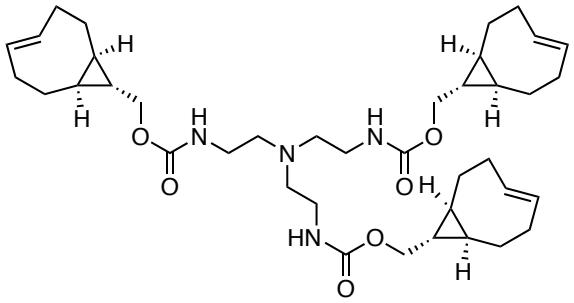

2-15

Scheme 2.20: Chemical structure of 3-armed *tris*-sTCO (**2-15**).

Again, meter-long microfibers were successfully drawn from the interface (Figure 2.35). The new crosslinked polymer fibers were smaller in diameter and swell less compared to linear copolymer fiber, possibly due to the tighter crosslinked structure.

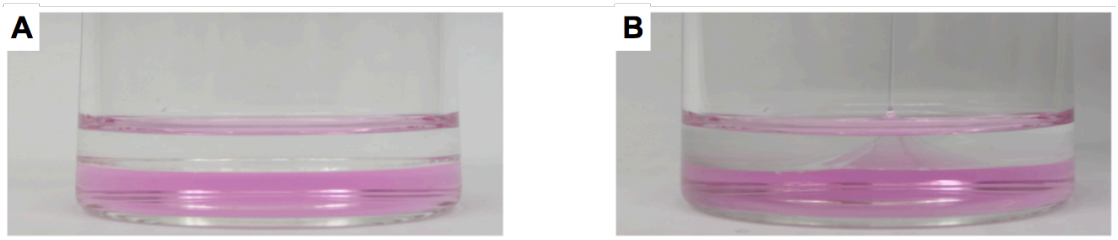

Figure 2.35: Photographs showing (A) phase separation between ethyl acetate and water solution; (B) crosslinked polymer fiber being drawn out of the interface.

The morphology change of linear and crosslinked polymer fibers incubated in water were monitored using optical microscopy (Figure 2.36). Upon incubation at 37 °C for 5 days, linear polymer chains in the fibers relaxed and disassociate from each other in the semicrystalline structure, fibers swelled further and morphology changed significantly, results in a bamboo-like morphology (Figure 2.36B). Fibers start to break in the weak points upon longer incubation, which make them not suitable for long-term cell culture.

On the other hand, the crosslinked polymer fibers exhibit the same morphology after incubation for 5, 14 and 21 days (Figure 2.36D-F). All fibers were smooth on the surface without defects and the diameters did not change significantly over time, enabling the long-term cell culture.

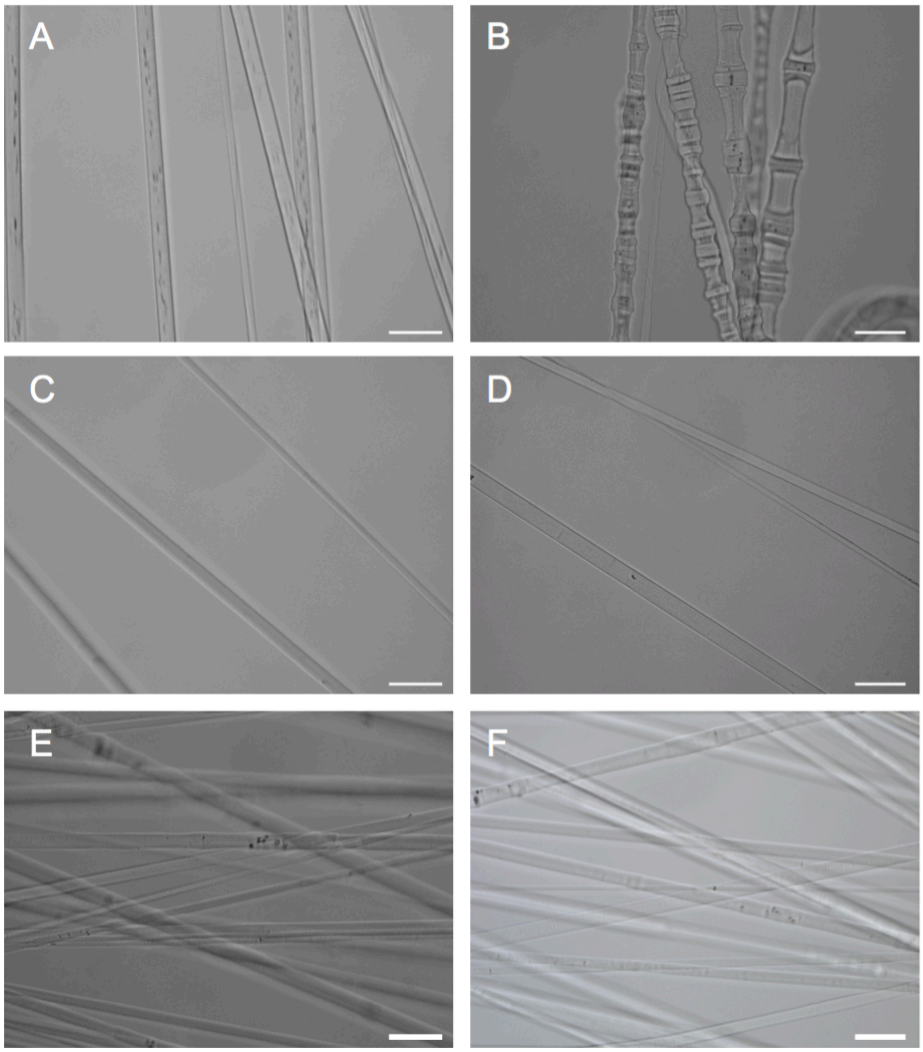

Figure 2.36: Surface morphology and stability in DI water of linear and crosslinked polymer fibers. Optical microscope images of linear polymer fibers incubated in DI water at day 0 (A) and day 5 (B); crosslinked polymer fibers incubated in water at 37 °C at day 0 (C) day 5 (D) day 14 (E) and day 21 (F). Scale Bar: 50 μm.

Further study towards the mechanical performance of crosslinked polymer fiber and its application on providing contact guidance and induce cell migration are underway, carried on by Dr. Shuang Liu.

2.5 Conclusions

In this chapter, I describe the first example of interfacial crosslinking using bioorthogonal TCO-tetrazine ligation. Bioocompatible hyaluronic acid-based hydrogel microspheres and channels were generated in a diffusion controlled fashion. These hydrogels can be covalently tagged with 3D resolution without the help of any external stimulus or triggers. An *in vitro* tumor model was achieved by 3D encapsulation and culture of LNCaP prostate cancer cells.

Separately, based on TCO-tetrazine ligation, a novel interfacial polymerization strategy was developed for the synthesis of hybrid multiblock copolymer. Meter-long copolymer fibers were pulled out of interface of two immiscible solutions. The unique modular approach enables the facile incorporation of functional peptides into the copolymer to fine-tune its biological properties. A fibronectin-derived peptide was successfully introduced onto the fibers during the polymerization and dramatically promoted the attachment and alignment of fibroblasts and myoepithelial-like cells.

Ongoing efforts has been made on the materials, a new generation of HA-Tz, HAMPTz, was developed to give more room for stiffness fine-tuning of the resulting hydrogel, while a crosslinked hydrogel fiber was synthesized by employment of 3-armed *tris*-sTCO block, resulting fibers with improved stability and suitable for long-term cell culture applications.

TCO-tetrazine ligation has emerged as a multifaceted strategy in polymer and biomaterials discovery, bringing promising results and exhilarating progress. The versatile materials we developed here will prove useful and become indispensable elements in the tissue engineering toolbox.

2.6 Experimental Procedures

2.6.1 General Considerations

All reactions were carried out in glassware that was flame-dried under vacuum and cooled under nitrogen. (rel-1R,8S,9R,4E)-Bicyclo[6.1.0]non-4-ene-9-ylmethanol was prepared following a known procedure.[60] *O,O*'-Bis(2-aminoethyl) octadecaethylene glycol (≥ 95% oligomer purity) and *O*-(2-Aminoethyl)-*O*-[2-(Boc-amino)ethyl] decaethylene glycol (≥ 90% oligomer purity) were purchased from Sigma Aldrich. Hyaluronic acid (sodium salt) was a generous gift from Genzyme Corporation. Dialysis membranes were purchased from Spectrum Labs (MWCO: 10 kDa). All 9-fluorenylmethoxycarbonyl (Fmoc)-protected amino acids were purchased from Protein Technologies (Tucson, AZ). 2-(1H-benzotriazole-1-yl)-1,1,3,3-tetramethyluronium hexafluorophosphate (HBTU) was purchased from Advanced Automated Peptide Protein Technologies (AAPPTEC, Louisville, KY). Rink Amide resin was ordered from EMD Millipore Corporation (Billerica, MA). Poly(ethylene glycol) diamine (M_n: 7,500 g/mol) and α-amino, ω-carboxyl poly(ethylene glycol) (M_n: 3,500 g/mol) were purchased from JenKem Technology USA (Plano, TX). Poly(2-hydroxyethyl methacrylate) (polyHEMA) was ordered from Sigma-Aldrich (St. Louis, MO). Flash Chromatography was performed using normal phase Silicycle silica gel (40-63D, 60Å). Deactivated silica gel was prepared by treating silica gel with EtSiCl3[85]. An APT pulse sequence was used for ^{13}C NMR spectra, where methylene and quaternary carbons appear 'up' (u), and methine and methyl carbons appear 'down' (d). The abbreviation 'app' stands for 'apparent.' Other reagents were purchased from commercial sources without additional purification.

2.6.2 Experimental Procedures of *trans*-Cyclooctene-Tetrazine Ligation-Enabled Interfacial Crosslinking

(4-(6-phenyl-1,2,4,5-tetrazin-3-yl)phenyl)methanol (2-1)

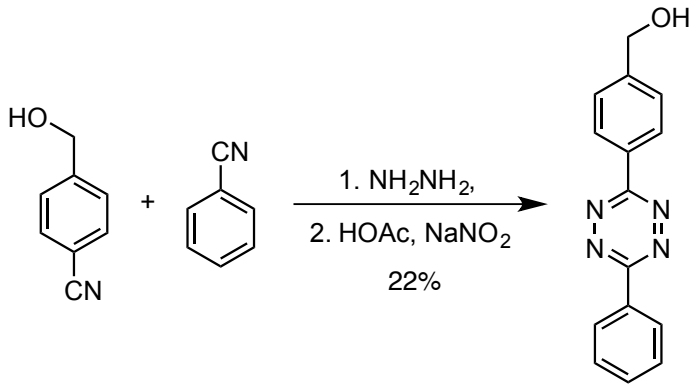

2-1

A dry round-bottomed flask was charged with 4-(hydroxymethyl)benzonitrile (5.80 g, 43.6 mmol), benzonitrile (18.0 g, 175 mmol) and anhydrous hydrazine (21.4 mL, 440 mmol). The flask was equipped with a reflux condenser, and the mixture was heated to 90 °C for 20 h behind a blast shield. The mixture was allowed to cool down to room temperature and was diluted with ethyl acetate (300 mL), washed twice with H_2O (150 mL), and dried over $MgSO_4$. The solution was filtered and the filtrate was concentrated under reduced pressure. The residual solid was dissolved in acetic acid (84 mL), and an aqueous solution of $NaNO_2$ (23.2 mL of a 9.40 M solution, 218 mmol) was added at 0 °C via Pasteur pipette. After stirring for 30 min at room temperature, the mixture was diluted with dichloromethane (300 mL). An aqueous solution of saturated $NaHCO_3$ was added then carefully added to neutralize the acetic acid. The mixture was partitioned and the organic phase was washed three times with saturated $NaHCO_3$ aqueous solution, and then dried over $MgSO_4$, filtered, and concentrated onto silica gel using a rotary evaporator. Column chromatography using

a gradient (0-70 %) of acetone in hexanes afforded 2.46 g (9.32 mmol, 22%) of **2-1** as a purple solid. ^{1}H NMR (DMSO-d_6, 400 MHz, δ): 8.40-8.60 (m, 4H), 7.58-7.75 (m, 5H), 5.46 (t, J=5.7 Hz 1H), 4.65 (d, J=5.6 Hz, 2H). ^{13}C NMR (DMSO-d_6, 100 MHz, δ): 163.4 (u, 1C), 163.3 (u, 1C), 147.7 (u, 1C), 132.6 (d, 1C), 132.0 (u, 1C), 130.2 (u, 1C), 129.6 (d, 2C), 127.6 (d, 2C), 127.5 (d, 2C), 127.2 (d, 2C), 62.5 (u, 1C). HRMS (ESI) [M+H]: calcd. for $C_{15}H_{13}N_4O^+$, 265.1084; found 265.1098.

4-nitrophenyl 4-(6-phenyl-1,2,4,5-tetrazin-3-yl)benzyl carbonate (2-2)

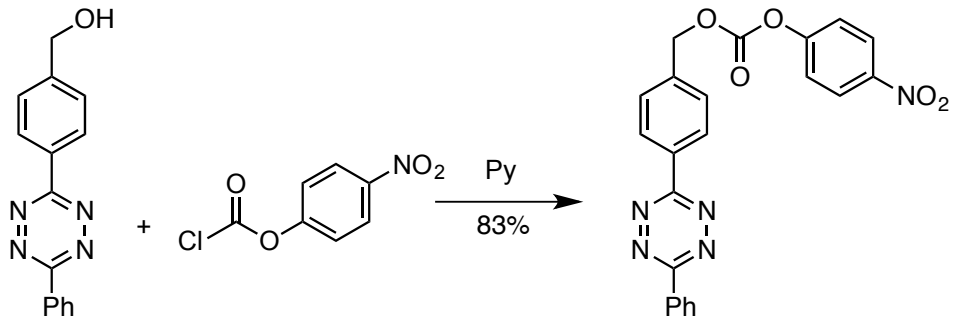

2-1 **2-2**

A dry round-bottled flask was charged with (4-(6-phenyl-1,2,4,5-tetrazin-3-yl)phenyl)methanol **2-1** (157 mg, 0.595 mmol). Anhydrous dichloromethane (12 mL) and pyridine (0.12 mL, 1.5 mmol) were added to the flask. A solution of 4-nitrophenylchloroformate (180 mg, 0.892 mmol) in anhydrous dichloromethane (3 mL) was added to the flask via syringe and the solution was stirred for 2 h at room temperature. Saturated NH_4Cl aqueous solution was added to the mixture and the layers were separated, and the aqueous layer was extracted twice with dichloromethane. The organic layers were combined, dried with $MgSO_4$, filtered, and concentrated onto silica gel using a rotary evaporator. Column chromatography using a gradient (30-70%) of dichloromethane in hexanes afforded 0.211 g (0.492 mmol,

83%) of **3** as a purple solid. ^{1}H NMR ($CDCl_3$, 400 MHz, δ): 8.63-8.76 (m, 4H), 8.26-8.34 (m, 2H), 7.60-7.75 (m, 5H), 7.38-7.46 (m, 2H), 5.43 (s, 2H). ^{13}C NMR ($CDCl_3$, 100 MHz, δ): 164.2 (u, 1C) 163.7 (u, 1C) 155.5 (u, 1C) 152.7 (u, 1C) 145.6 (u, 1C) 138.9 (u, 1C) 133.0 (d, 1C) 132.5 (u, 1C) 131.8 (u, 1C) 129.5 (d, 2C) 129.2 (d, 2C) 128.5 (d, 2C) 128.2 (d, 2C) 125.5 (d, 2C) 121.9 (d, 2C) 70.3 (u, 1C). HRMS (ESI) [M+H]: calcd. for $C_{22}H_{16}N_5O_5^+$, 430.1146; found 430.1154.

Tetrazine-OEG-amine (2-3)

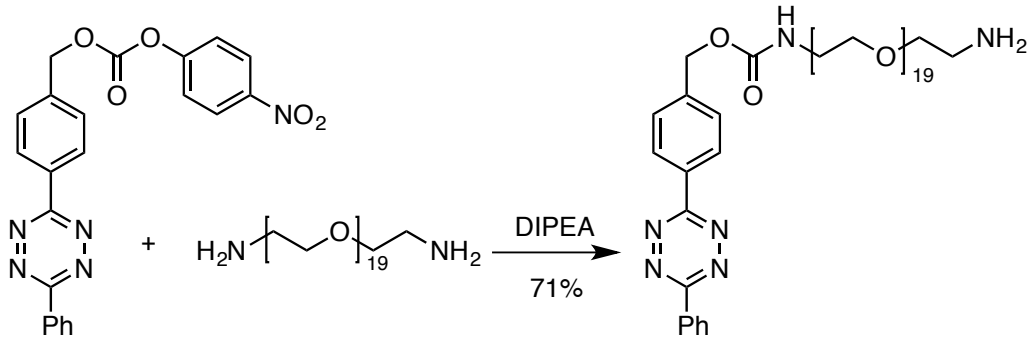

2-2 **2-3**

A dry round-bottled flask was charged with a solution of *O,O*'-bis(2-aminoethyl)octadecaethylene glycol (141 mg, 0.157 mmol) in anhydrous dichloromethane (4 mL) and *N,N*-diisopropylethylamine (DIPEA, 36.5 µL, 0.209 mmol). A solution of 4-nitrophenyl 4-(6-phenyl-1,2,4,5-tetrazin-3-yl)benzyl carbonate (**2-2**, 45 mg, 0.11 mmol) in anhydrous dichloromethane (6 mL) was added to the flask via a syringe pump over 3 h. The mixture was then allowed to stir overnight at room temperature. The solvent was removed with a rotary evaporator and the residue was washed three times with hexanes. Column chromatography on deactivated silica gel[2] using a gradient 30-100% acetone in hexanes followed by 10% methanol in dichloromethane afforded 88 mg (0.074 mmol, 71%) of **2-3** as a water-soluble purple

solid. ^{1}H NMR ($CDCl_3$, 400 MHz, δ): 8.55-8.75 (m, 4H), 7.86-7.99 (br, 2H), 7.50-7.70 (m, 5H), 5.50-5.61 (br, 1H), 5.21 (s, 2H), 3.91 (m, 2H), 3.59-3.73 (m, 74H), 3.41 (m, 2H), 3.10-3.24 (m, 2H). ^{13}C NMR ($CDCl_3$, 100 MHz, δ): 164.1(1C), 163.8(1C), 156.4(1C), 141.8(1C), 132.9(1C), 131.8(1C), 131.4(1C), 129.5(2C), 128.6(2C), 128.2(2C), 128.1(2C), 70.7-70.0(35C), 69.9(1C), 69.7(1C), 66.8(1C), 66.0(1C), 41.1(1C), 40.7(1C). HRMS (ESI) [M+H]: calcd. for $C_{56}H_{95}N_6O_{21}^+$, 1187.6545; found 1187.6541. UV-vis (27.5 μM in H_2O): λ_{max} 300 nm.

HA-Tz (2-4)

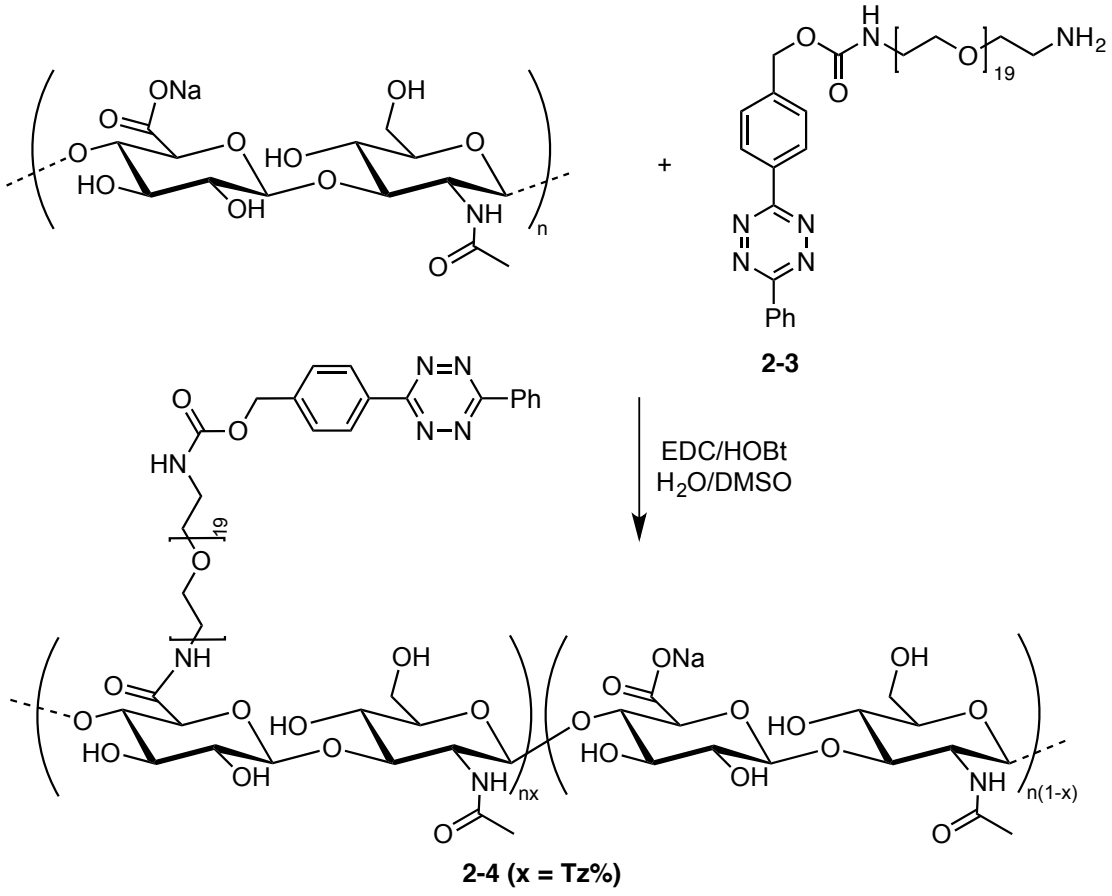

2-4 (x = Tz%)

Hyaluronic acid (30.1 mg, 79.2 μmol) was dissolved in H_2O (6.7 mL) at a concentration of 4.5 mg/mL. Tetrazine-OEG-amine (**4**) (447 mg, 0.376 mmol) dissolved in H_2O (3.2 mL) was then added dropwise to the HA solution. To this mixture was slowly added a solution of 1-ethyl-3-[3-(dimethylamino)propyl]-carbodiimide (EDC) (57.8 mg, 301 μmol) in DMSO/H_2O (1:1, 302 μL), followed by a solution of 1-hydroxybenzotriazole (HOBt) (40.6 mg, 301 μmol) in DMSO/H_2O (1:1, 302 μL). The resulting mixture was stirred at 37 °C for 24 h. The HA derivative was then precipitated in ice-cold ethanol (100 mL, 10 vol. excess). The precipitates were then collected by centrifugation at 4,000 rpm for 8 min. The pellet was then re-dissolved in H_2O at approximately 3 mg/mL and exhaustively dialyzed (Spectra 10 kDa MWCO) against H_2O. The purified product was lyophilized to afford 29 mg (0.063 mmol, 80%) HA-Tz as a pink fluffy solid. The product was stored at 4 °C prior to use.

(rel-1R,8S,9R,4E)-Bicyclo[6.1.0]non-4-ene-9-ylmethanol

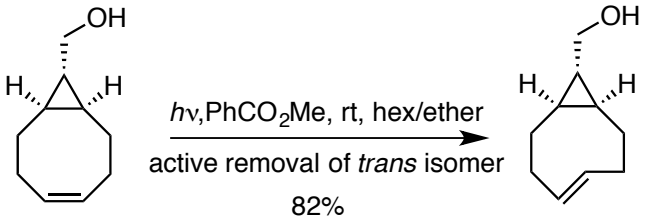

The continuous flow apparatus described previously was used for the photoisomerization[86], Biotage SNAP cartridges (Biotage part no. FSK0-1107-0050) was filled with a bed of unmodified silica gel that was topped with 14.5 g of silica gel which was impregnated with $AgNO_3$(1.45 g, 8.55 mmol). (1R,8S,9R,4Z)-Bicyclo [6.1.0]non-4-ene-9-ylmethanol(1.00 g, 6.58 mmol) and methyl benzoate (1.80g, 13.2

mmol) were placed in a quartz flask and dissolved in 500 mL of 1:1 Et_2O:hexanes. Dodecane (1.12g, 6.58 mmol) was also added to the flask to allow for GC monitoring. The solution was equilibrated through the continuous flow system at a 100 mL/min flow rate. The solution in the quartz flask was then irradiated (254nm) under continuous flow conditions (100 mL/min) for 4 hours, at which point GC analysis indicated that the reaction was complete. The SNAP cartridges were flushed with 400 mL of 1:1 Et_2O/hexanes and then dried with compressed air. To the dried silica gel was sequentially added NH_4OH (200 mL) and methylene chloride (200 mL) and the resulting mixture was filtered. The filtrate was transferred to a separatory funnel and partitioned. The aqueous layer was extracted twice with methylene chloride. The organic layers were combined, washed twice with water then dried with magnesium sulfate and filtered. The solvent was removed with a rotary evaporator, column chromatography (20% ethyl acetate/hexanes) afforded 820 mg of 7 (82%) (rel-1R,8S,9R,4E)-Bicyclo [6.1.0]non-4-ene-9-ylmethanol as a colorless oil. ^{1}H and ^{13}C NMR data agreed with the previously reported data.

(rel-1R,8S,9R,4E)-Bicyclo[6.1.0]non-4-ene-9-ylmethyl (4-nitrophenyl) carbonate (2-5)

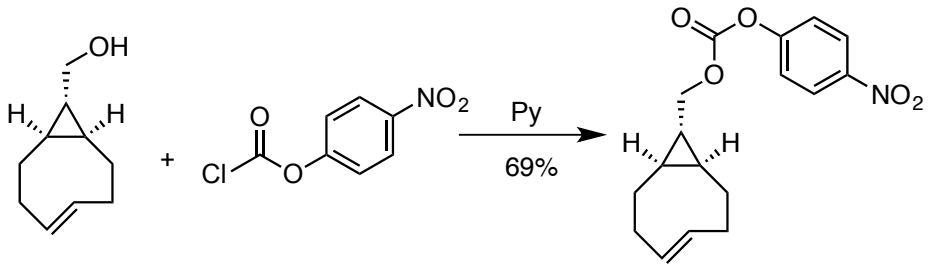

2-5

A dry round-bottled flask was charged with (rel-1R,8S,9R,4E)-bicyclo [6.1.0]non-4-ene-9-ylmethanol (820 mg, 5.39 mmol). Anhydrous dichloromethane (100 mL) and pyridine (1.09 mL, 13.5 mmol) were added to the flask. A solution of 4-nitrophenylchloroformate (1.30 g, 6.47 mmol) in anhydrous dichloromethane (14 mL) was added to the flask via syringe and the solution was stirred for 1 h at room temperature. Saturated NH_4Cl aqueous solution was added to the mixture and the layers were separated, and the aqueous layer was extracted twice with dichloromethane. The organic layers were combined, dried with $MgSO_4$, filtered, solvent was removed using a rotary evaporator. Purification by column chromatography (5% ethyl actetate/hexanes) yielded afforded 1.18 g (3.72 mmol, 69%) of (rel-1R,8S,9R,4E)-Bicyclo[6.1.0]non-4-ene-9-ylmethyl (4-nitrophenyl) carbonate **2-5** as a white solid. ^{1}H and ^{13}C NMR data agreed with the previously reported data.

"*bis*-sTCO" (2-6)

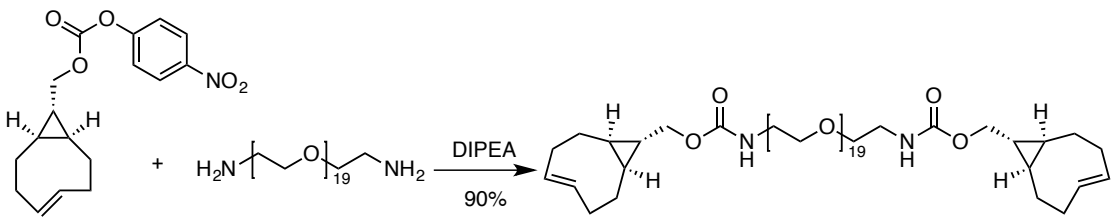

2-5 **2-6**

A dry round-bottled flask was sequentially charged via syringe with a solution of *O,O*'-Bis(2-aminoethyl)octadecaethylene glycol (64 mg, 0.071 mmol) in anhydrous dichloromethane (2 mL) and *N,N*-diisopropylethylamine (49.9 µL, 0.29 mmol), followed by a solution of (1*R*,8*S*,9*R*,4*E*)-bicyclo[6.1.0]non-4-en-9-ylmethyl(4-nitrophenyl) carbonate (**2-5**, 50 mg, 0.16 mmol) in anhydrous dichloromethane (3

mL). The mixture was stirred overnight at room temperature. The solvent was removed with a rotary evaporator. Purification by column chromatography using 0-5% methanol in dichloromethane yielded 80 mg (0.064 mmol, 90%) of *bis*-sTCO **2-6** as a water-soluble clear oil. ^{1}H NMR ($CDCl_3$, 400 MHz, δ): 5.77-5.90 (m, 2H), 5.17-5.31 (m, 2H), 5.04-5.16 (m, 2H), 3.86-3.97 (m, 4H), 3.48-3.68 (m, 72H), 3.50-3.56 (m, 4H), 3.30-3.38 (m, 4H), 2.29-2.38 (m, 2H), 2.12-2.29 (m, 6H), 1.82-1.97 (m, 4H), 0.75-0.88 (m, 2H), 0.47-0.60 (m, 4H), 0.32-0.46 (m, 4H). ^{13}C NMR ($CDCl_3$, 100 MHz, δ): 157.0 (u, 2C), 138.5 (d, 2C), 131.4 (d, 2C), 70.7-70.5 (u, 34C), 70.4 (u, 2C), 70.2 (u, 2C), 69.5 (u, 2C), 40.8 (u, 2C), 38.8 (u, 2C), 33.9 (u, 2C), 32.7 (u, 2C), 27.7 (u, 2C), 24.8 (d, 2C), 22.0 (d, 2C), 21.0 (d, 2C). HRMS (ESI) [M+H]: calcd. for $C_{62}H_{113}N_2O_{23}^{+}$, 1253.7729; found 1253.7745.

Alexa Fluor® 647-sTCO conjugate (2-7)

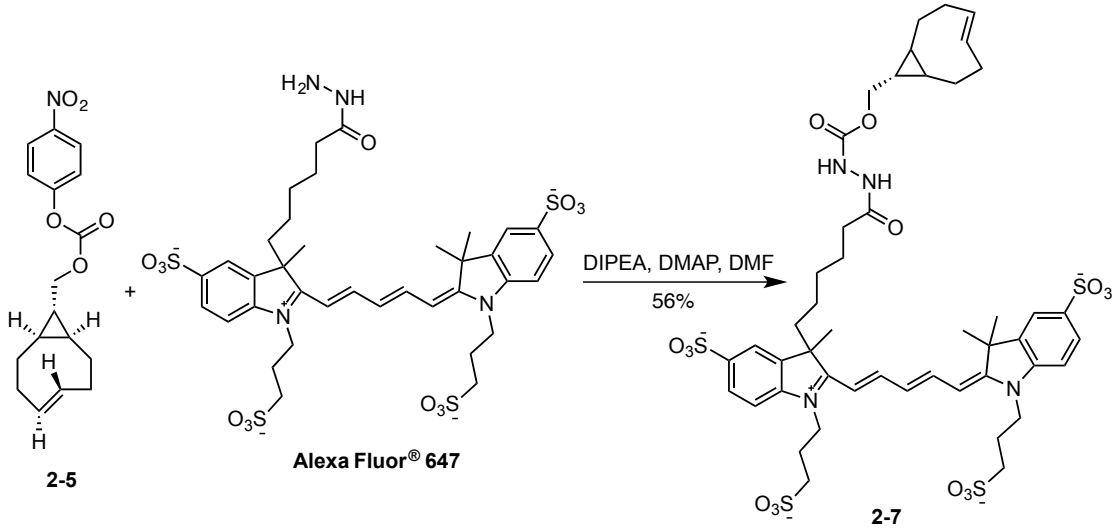

(1*R*,8*S*,9*R*,4*E*)-Bicyclo[6.1.0]non-4-en-9-ylmethyl(4-nitrophenyl) carbonate (**2-5**, 1.3 mg, 4.2 μmol) was added to a vial that contained Alexa Fluor® 647 hydrazide, tris(triethylammonium) salt (1.0 mg, 0.83 μmol). A DMF solution (200 μL,

anhydrous) containing *N,N*-diisopropylethylamine (215 μg, 1.67 μmol) and 4-dimethylaminopyridine (DMAP, 50 μg, 0.41 μmol) was added to the vial. The mixture was stirred overnight at ambient temperature and was purified with reverse phase HPLC, generating 0.49 mg (47 μmol, 56%) of **2-7** as a blue solid. MS and HPLC analyses indicated that the purity of a compound with a mass of 1047 Da. was >98%.

Determination of percent tetrazine incorporation in HA-Tz.

The percent tetrazine incorporation in HA-Tz was determined collectively by UV-vis and ^{1}H NMR analyses. UV-vis quantification was based on the tetrazine absorption at λ_{max} 300 nm employing Beer-Lambert law. Using an aqueous solution of compound **4** at a concentration of 27.5 μM as the standard (Figure 2.37, top), the molar extinction coefficient of the tetrazine moiety (ε_{Tz}) was determined as 3.2×10^4 L Mol^{-1} cm^{-1}. Taking into consideration the change of the molecular weight for HA disaccharide repeats after tetrazine incorporation, the degree of tetrazine incorporation in HA-Tz was calculated as 7% (Figure 2.37, bottom). By ^{1}H NMR, the degree of modification was analyzed by comparing the integration between the aromatic protons (7.4-8.4 ppm) to that the acetamido moiety of the N-acetyl-d-glucosamine residue of HA.

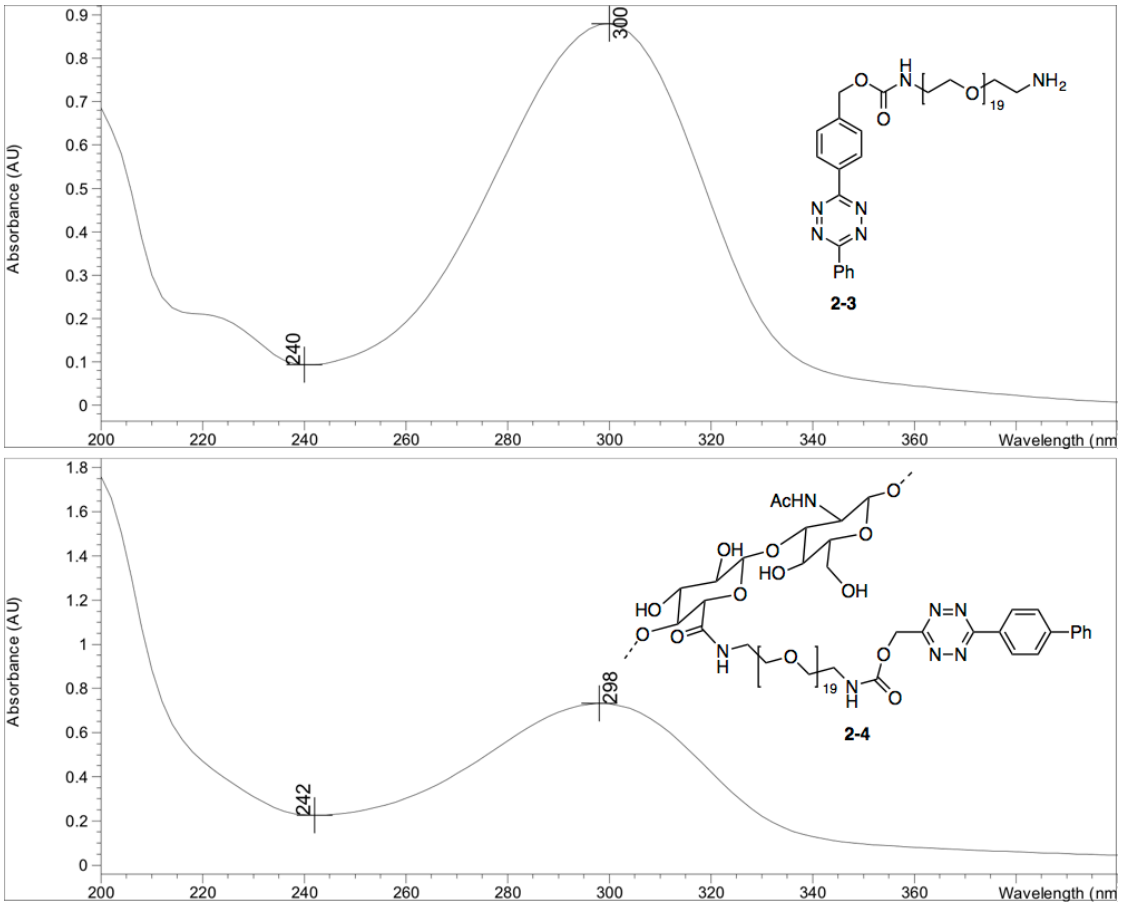

Figure 2.37: UV-vis spectra of aqueous solutions of (top) compound **2-3** at a concentration of 27.5 μM and (bottom) HA-Tz **2-4** at a concentration of 0.153 g/L. In both measurements, a UV cuvette with a path length of 1 cm was used.

Determination of molecular weight and solution viscosity and rheological characterization were carried out by Kevin Dicker as described in reference[62].

Preparation of hyaluronic acid (HA) hydrogel microspheres

HA-Tz and bis-TCO were separately dissolved in PBS at a concentration of 2 wt% and 400 μM, respectively. To prepare HA microspheres, HA-Tz was dropped via

a 25G syringe into a 500 μL solution of *bis*-sTCO solution in a 48 well plate (BD Falcon™). The interfacial crosslinking was allowed to occur at 37 °C for 2 hours without any agitation. The *bis*-sTCO solution was then replaced with fresh PBS. The gel particles were dehydrated in graded ethanol solutions and vacuum dried. The swelling ratio, reported as an average of three repeats, was determined as the ratio of the initial weight of the wet gel to the weight of the dry product. The microsphere wall thickness was measured by capturing an image of the microsphere during crosslinking every 3 minutes for the 2 hour gelation period. The wall thickness was then quantified by using imageJ to measure the thickness of the crosslinked wall of the microsphere as a function of time.

Preparation of water-filled HA hydrogel channels

To prepare crosslinked hydrogel channels while simultaneously monitoring the channel formation via confocal microscopy, a glass cylinder (I.D. = 5 mm, h = 10 mm), mounted onto an imaging chamber (Lab-Tek™), was filled with ~200 μL HA-Tz (2 wt%). A syringe containing 2 mM *bis*-sTCO and 2 μM Alexa-sTCO was inserted to the bottom of the HA-Tz-filled cylinder. The syringe was pulled out of the cylinder while injecting ~ 30 μL of the solution, leaving behind a liquid channel. The channel was monitored and imaged for 60 minutes using a Zeiss 510 NLO confocal microscope (Carl Zeiss, Maple Grove, MN).

Selective interfacial tagging

Selective interfacial tagging was achieved by timed exposure of the crosslinking HA-Tz droplet, originally dissolved in PBS at 2 wt%, to aqueous baths of *bis*-sTCO (400 μM) alone or *bis*-sTCO (400 μM and 1 μM Alexa-sTCO) in an alternating fashion. The total exposure time was maintained at 2 hours to ensure complete gelation. For example, alternating exposure of the HA-Tz droplet to the dye-free and dye-containing baths for 15 min each for 3 cycles, followed by a 30-min exposure to the dye-containing bath resulted in a crosslinked microsphere with 7 distinct layers. To tag the microspheres with Alexa-sTCO in a gradient fashion, HA-Tz was dropped into a *bis*-sTCO bath (1 mL, 400 μM) and Alexa-sTCO was added to the bath using a syringe pump gradually over the course of 2 hours, reaching a final concentration of 0.47 μM. A control experiment was performed by dropping 2 wt% HA-Tz into bath of 400 μM *bis*-sTCO and 0.47 μM alexa-sTCO and allowed to crosslink for 2 hours. Upon completion of the tagging experiment, the bath was replaced with PBS and the gels were images using a Zeiss 510 NLO confocal microscope.

Interfacial cell encapsulation and 3D culture was carried out by Kevin Dicker as described in reference[62].

2.6.3 Experimental Procedures of Multiblock Copolymer Microfibers via Interfacial Bioorthogonal Polymerization

***bis*-sTCO monomer**

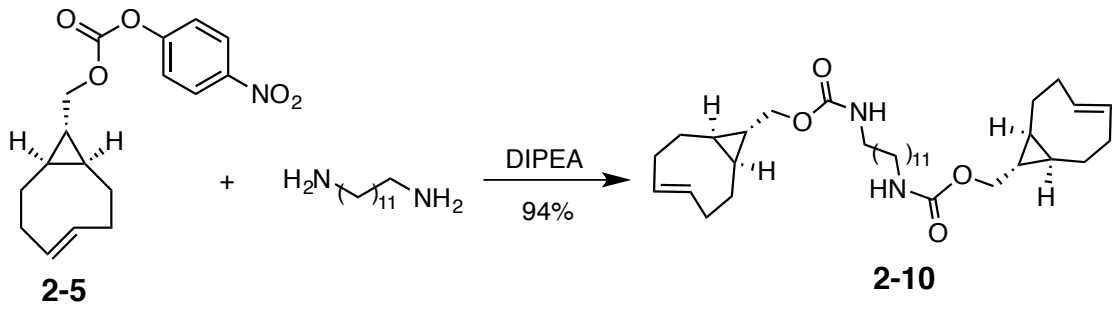

A dry round-bottom flask was sequentially charged *via* syringe with a solution of 1,12-diaminododecane (143 mg, 0.72 mmol) in anhydrous dichloromethane (10 mL) followed by triethylamine anhydrous (400 µL, 2.87 mmol) and a solution of (1R,8S,9R,4E)-bicyclo[6.1.0]non-4-en-9-ylmethyl(4-nitrophenyl) carbonate (**2-5**, 500 mg, 1.58 mmol), prepared following a known procedure, in anhydrous dichloromethane (2 mL). The mixture was stirred overnight at room temperature, diluted with dichloromethane (30 mL) followed by exhaustive aqueous wash (8×30 mL). The organic layer was dried with $MgSO_4$, filtered and then the solvent was removed with a rotary evaporator. Purification by column chromatography using 10% ethyl acetate in hexanes yielded *bis*-sTCO **2-10** (376 mg, 0.66 mmol, 94%) as a white solid. ^{1}H NMR (600 MHz, $CDCl_3$, δ): 5.83-5.90 (m, 2H), 5.07-5.15 (m, 2H), 4.62 (s, 2H), 3.90-3.96 (m, 4H), 3.12-3.18 (m, 4H), 2.34-2.39 (m, 2H), 2.30-2.18 (m, 6H), 1.96-1.87 (m, 4H), 1.52-1.45 (m, 4H), 1.33-1.23 (m, 16H), 0.79-0.90 (m, 2H), 0.60-0.50 (m, 4H), 0.46-0.38 (m, 4H). ^{13}C NMR ($CDCl_3$, 100 MHz, δ): 156.9 (u, 2C), 138.5 (d, 2C), 131.4 (d, 2C), 69.5 (u, 2C), 41.1 (u, 2C), 38.8 (u, 2C), 33.9 (u, 2C), 32.7(u, 2C), 30.2 (u, 2C), 29.7 (u, 4C), 29.4 (u, 2C), 27.8 (u, 2C), 26.9 (u, 2C), 24.9 (d, 2C),

22.1 (d, 2C), 21.0 (d, 2C). HRMS (ESI) [M+H]: calcd. for $C_{34}H_{57}N_2O_4^+$, 557.4313 found 557.4310.

PEG-based *bis*-tetrazine monomer (2-11)

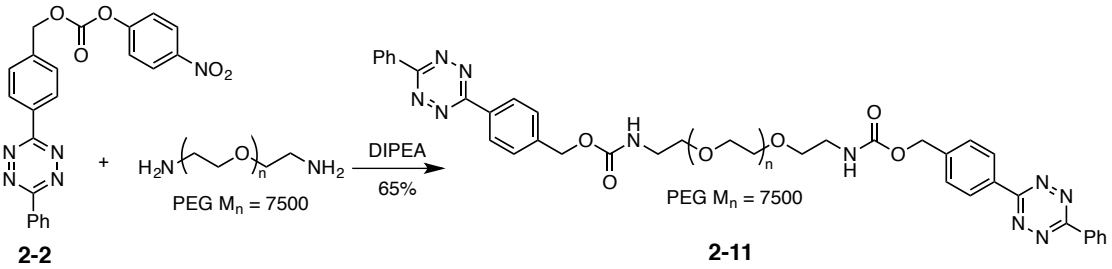

2-2 **2-11**

A dry round-bottom flask was sequentially charged with a solution of PEG diamine (M_n 7,500 g/mol, 1.00 g, approx. 0.13 mmol) in anhydrous dichloromethane (20 mL) followed by triethylamine (74.2 µL, 0.53 mmol). 4-Nitrophenyl 4-(6-phenyl-1,2,4,5-tetrazin-3-yl)benzyl carbonate (229 mg, 0.53 mmol) was added to the flask. The mixture was then allowed to stir overnight at room temperature. The reaction mixture was divided into 8 centrifuge tubes each containing ethyl ether (50 mL). The crude product was obtained by precipitation followed by centrifugation (5,000 rpm, 6 min). Crude PEG *bis*-tetrazine was purified with reverse-phase high-performance liquid chromatography (HPLC) on a Waters preparative HPLC (Waters, Milford, MA) equipped with a fraction collector and UV-vis detector using a Phenomenex® C18 Column (100 Å, 5 µm, 250 × 21.2 mm) at 25°C. A water/acetonitrile gradient as solvent system and a flow rate of 10 mL/min were used and the tetrazine chromophore (absorbance at 300 nm) was used to monitor the product elution. Crude products were dissolved in water and a 2 mL solution was injected each time. Collected fractions were lyophilized using a -80°C freeze dryer (Labconco, Kansas City, MO) and stored in -20°C freezer. Analytical HPLC was used to characterize the purity of molecules on

a Shimadzu HPLC instrument with a Phenomenex® C18 Column (100 Å, 5 μm, 250 × 4.6 mm) at 40°C with a flow rate of 1 mL/min. The elution gradient started from 95% A and 5% B for 3 min and ramped to 20% A and 80% B in 97 min. HPLC purification afforded monomer **2-11** (700 mg, approx. 0.086 mmol, 65%) as a pink solid. An analytical HPLC chromatogram of **2-11** is shown in Appendix B. The major peak represented 99% of the integrated HPLC trace, monitored at either 254 or 300 nm. ^{1}H NMR ($CDCl_3$, 600 MHz, δ): 8.69-8.63 (m, 8H), 7.75-7.60 (m, 10H), 7.68-7.59 (m, 2H), 5.53 (s, 2H) 5.24 (s, 4H), 3.85-3.80 (m, 4H), 3.73-3.55 (m, approx. 680H), 3.47-3.40 (m, 8H). ^{13}C NMR ($CDCl_3$, 100 MHz, δ): 164.1(2C), 163.8(2C), 156.4(2C), 141.8(2C), 132.9(2C), 131.8(2C), 131.4(2C), 129.4(4C), 128.6(4C), 128.2(4C), 128.1(4C), 70.7 (major PEG carbons), 70.4(2C), 70.1(2C), 66.0(2C), 41.1(2C).

The synthesis and characterization of fibronectin-derived peptide KGGKGGWGRGDSPG was carried out by Dr. Shuang Liu as described in reference[87].

Peptide-containing *bis*-tetrazine monomer (2-12)

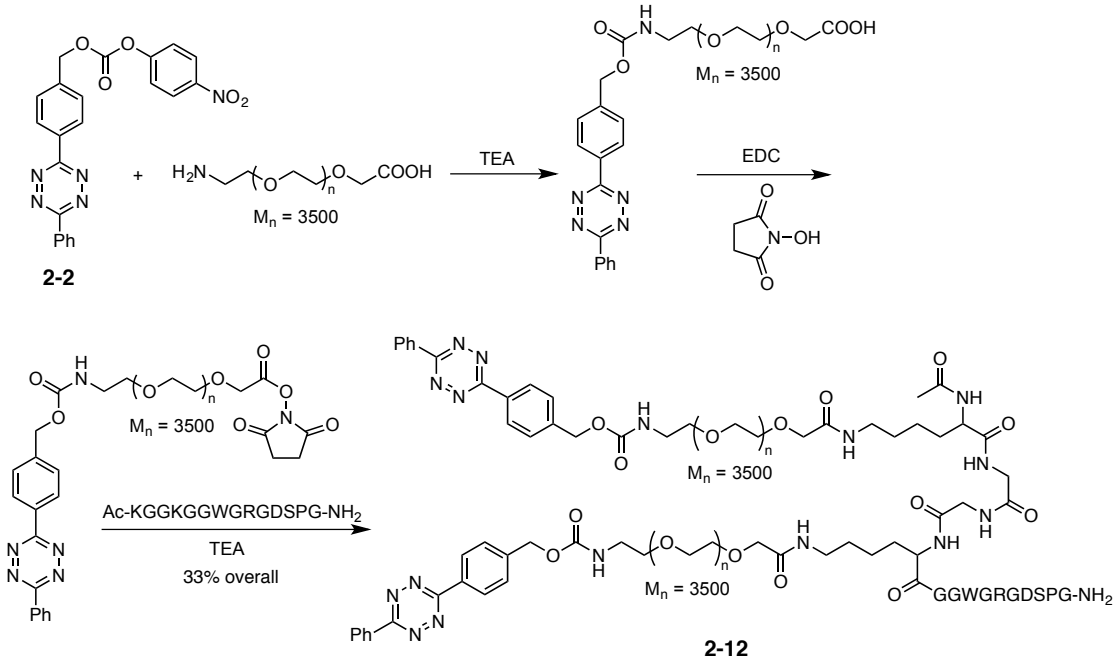

The purified peptide was used to prepare peptide-containing *bis*-tetrazine (**2-12**). A dry round-bottom flask was charged with a solution of PEG amino acid (M_n 3,500, 300 mg, approx. 0.086 mmol) in anhydrous dichloromethane (6 mL) and triethylamine (47.7 μL, 0.34 mmol). 4-Nitrophenyl 4-(6-phenyl-1,2,4,5-tetrazin-3-yl)benzyl carbonate (**2-2**, 73.5 mg, 0.17 mmol) was added to the flask. The mixture was then allowed to stir overnight at room temperature. The reaction mixture was divided into 3 centrifuge tubes each containing ethyl ether (40 mL). The crude product was obtained by precipitation, followed by centrifugation (5,000 rpm, 6 min). The material was then re-dissolved in anhydrous dichloromethane (4 mL), and to this solution was added *N*-hydroxysuccinimide (NHS, 19.7 mg, 0.17 mmol) and *N*-(3-dimethylaminopropyl)-*N*'-ethylcarbodiimide hydrochloride (EDC·HCl, 32.9 mg, 0.17 mmol). The crude NHS ester was precipitated by adding diethyl ether (~120 mL), and the resulting suspension was allowed to stir overnight at room temperature. After

centrifugation (5,000 rpm, 6 min), the crude NHS ester was dissolved in anhydrous DMF (6 mL), and sequentially added were the purified peptide (46 mg, 0.034 mmol) and triethylamine (18.9 μL, 0.14 mmol). The Tz-PEG-NHS ester was used in excess (2.5 fold) relative to the peptide to ensure a complete substitution of the two lysine residues. The mixture was then allowed to stir overnight at room temperature. The crude peptide-containing monomer **2-12** was precipitated by adding diethyl ether (~120 mL), followed by centrifugation (5,000 rpm, 6 min). Monomer **2-12** was purified and analyzed using the same methods described above for monomer **2-11**. HPLC purification afforded monomer **2-12** (100 mg, approx. 0.011 mmol, 33%) as a pink solid. The purity of **2-12** was analyzed by HPLC. The major peak represented 99% of the integrated HPLC trace, monitored at either 254 or 300 nm. Structure of monomer **2-12** was confirmed by ^{1}H NMR spectrum analysis.

Interfacial polymerization

bis-sTCO (**1**) was dissolved in ethyl acetate at a concentration of 3.6 mM and the bis-tetrazine monomer (**2a** or **2b**) was dissolved in water at a concentration of 0.25 mM. To a 60-mm diameter petri dish was added the aqueous solution (3 mL) of the appropriate bis-tetrazine monomer (**2a** or **2b**). The solution of **1** (3 mL) in ethyl acetate was carefully poured over the aqueous phase without disturbing the interface. Upon contact, a polymer thin film formed at the interface. The thin film was grasped gently using sharp tweezers and was connected to a collecting frame that was driven by a motor at a speed of 20 rpm for continuous fiber collection. As controls, solution polymerizations were carried out in THF with a 1:1 sTCO/Tz molar ratio. In one experiment (referred to as ‘solution polymerization 1’ in Figure S6 and Table S1), the

reaction was carried out by adding **1** (0.069mL of 3.6 mM THF solution) to **2a** (1 mL of 0.25 mM THF solution), giving a final concentration of 0.23 mM. In a second experiment (designated as 'solution polymerization 2' in Figure S6 and table S1), the reaction was carried out by adding **1** (0.139 mL of 3.6 mM THF solution) to **2a** (1 mL of 0.50 mM THF solution), giving a final concentration of 0.44 mM. GPC was used to analyze the solution polymerization products as displayed in Figure S6.

The following experiments were carried out by Dr. Shuang Liu as described in reference:[87]

Gel permeation chromatography (GPC) analysis

Optical birefringence

Differential scanning calorimetry (DSC)

Atomic force microscopy (AFM)

Cell culture and immunostaining

REFERENCES

(1) Binder, W. H.; Sachsenhofer, R. 'Click' Chemistry in Polymer and Materials Science. *Macromol. Rapid Commun.* **2007**, *28*, 15-54.

(2) Binder, W. H.; Sachsenhofer, R. 'Click' Chemistry in Polymer and Material Science: An Update. *Macromol. Rapid Commun.* **2008**, *29*, 952-981.

(3) Meldal, M.; Tornøe, C. W. Cu-Catalyzed Azide−Alkyne Cycloaddition. *Chem. Rev.* **2008**, *108*, 2952-3015.

(4) Evans, R. A. The Rise of AzideAlkyne 1,3-Dipolar Click Cycloaddition and its Application to Polymer Science and Surface Modification. *Aust. J. Chem.* **2007**, *60*, 384-395.

(5) Golas, P. L.; Matyjaszewski, K. Marrying click chemistry with polymerization: expanding the scope of polymeric materials. *Chem. Soc. Rev.* **2010**, *39*, 1338-1354.

(6) Hvilsted, S. Facile design of biomaterials by 'click' chemistry. *Polym. Int.* **2012**, *61*, 485-494.

(7) Hoyle, C. E.; Lowe, A. B.; Bowman, C. N. Thiol-click chemistry: a multifaceted toolbox for small molecule and polymer synthesis. *Chem. Soc. Rev.* **2010**, *39*, 1355-1387.

(8) Hoyle, C. E.; Bowman, C. N. Thiol–Ene Click Chemistry. *Angew. Chem. Int. Ed.* **2010**, *49*, 1540-1573.

(9) Rostovtsev, V. V.; Green, L. G.; Fokin, V. V.; Sharpless, K. B. A Stepwise Huisgen Cycloaddition Process: Copper(I)-Catalyzed Regioselective "Ligation" of Azides and Terminal Alkynes. *Angew. Chem. Int. Ed.* **2002**, *41*, 2596-2599.

(10) Tornøe, C. W.; Christensen, C.; Meldal, M. Peptidotriazoles on Solid Phase: [1,2,3]-Triazoles by Regiospecific Copper(I)-Catalyzed 1,3-Dipolar Cycloadditions of Terminal Alkynes to Azides. *J. Org. Chem.* **2002**, *67*, 3057-3064.

(11) Tsarevsky, N. V.; Sumerlin, B. S.; Matyjaszewski, K. Step-Growth "Click" Coupling of Telechelic Polymers Prepared by Atom Transfer Radical Polymerization. *Macromolecules* **2005**, *38*, 3558-3561.

(12) Malkoch, M.; Vestberg, R.; Gupta, N.; Mespouille, L.; Dubois, P.; Mason, A. F.; Hedrick, J. L.; Liao, Q.; Frank, C. W.; Kingsbury, K.; Hawker, C. J. Synthesis of well-defined hydrogel networks using Click chemistry. *Chem. Commun.* **2006**, 2774.

(13) Gondi, S. R.; Vogt, A. P.; Sumerlin, B. S. Versatile Pathway to Functional Telechelics via RAFT Polymerization and Click Chemistry. *Macromolecules* **2007**, *40*, 474-481.

(14) Lutz, J.-F.; Börner, H. G.; Weichenhan, K. Combining Atom Transfer Radical Polymerization and Click Chemistry: A Versatile Method for the Preparation of End-Functional Polymers. *Macromol. Rapid Commun.* **2005**, *26*, 514-518.

(15) Sumerlin, B. S.; Tsarevsky, N. V.; Louche, G.; Lee, R. Y.; Matyjaszewski, K. Highly Efficient "Click" Functionalization of Poly(3-azidopropyl methacrylate) Prepared by ATRP. *Macromolecules* **2005**, *38*, 7540-7545.

(16) Ladmiral, V.; Mantovani, G.; Clarkson, G. J.; Cauet, S.; Irwin, J. L.; Haddleton, D. M. Synthesis of Neoglycopolymers by a Combination of "Click Chemistry" and Living Radical Polymerization. *J. Am. Chem. Soc.* **2006**, *128*, 4823-4830.

(17) Blackman, M. L.; Royzen, M.; Fox, J. M. Tetrazine Ligation: Fast Bioconjugation Based on Inverse-Electron-Demand Diels−Alder Reactivity. *J. Am. Chem. Soc.* **2008**, *130*, 13518-13519.

(18) Devaraj, N. K.; Weissleder, R.; Hilderbrand, S. A. Tetrazine-Based Cycloadditions: Application to Pretargeted Live Cell Imaging. *Bioconjugate Chem.* **2008**, *19*, 2297-2299.

(19) Patterson, D. M.; Nazarova, L. A.; Xie, B.; Kamber, D. N.; Prescher, J. A. Functionalized cyclopropenes as bioorthogonal chemical reporters. *J. Am. Chem. Soc.* **2012**, *134*, 18638-18643.

(20) Yang, J.; Šečkutė, J.; Cole, C. M.; Devaraj, N. K. Live-Cell Imaging of Cyclopropene Tags with Fluorogenic Tetrazine Cycloadditions. *Angew. Chem. Int. Ed.* **2012**, *51*, 7476-7479.

(21) Chen, W.; Wang, D.; Dai, C.; Hamelberg, D.; Wang, B. Clicking 1,2,4,5-tetrazine and cyclooctynes with tunable reaction rates. *Chem. Commun. (Camb.)* **2012**, *48*, 1736-1738.

(22) Alge, D. L.; Azagarsamy, M. A.; Donohue, D. F.; Anseth, K. S. Synthetically tractable click hydrogels for three-dimensional cell culture formed using tetrazine-norbornene chemistry. *Biomacromolecules* **2013**, *14*, 949-953.

(23) Hansell, C. F.; Lu, A.; Patterson, J. P.; O'Reilly, R. K. Exploiting the tetrazine-norbornene reaction for single polymer chain collapse. *Nanoscale* **2014**, *6*, 4102-4107.

(24) Desai, R. M.; Koshy, S. T.; Hilderbrand, S. A.; Mooney, D. J.; Joshi, N. S. Versatile click alginate hydrogels crosslinked via tetrazine-norbornene chemistry. *Biomaterials* **2015**, *50*, 30-37.

(25) Azagarsamy, M. A.; Anseth, K. S. Bioorthogonal Click Chemistry: An Indispensable Tool to Create Multifaceted Cell Culture Scaffolds. *ACS Macro Lett.* **2013**, *2*, 5-9.

(26) Hoffman, A. S. Hydrogels for biomedical applications. *Adv. Drug Del. Rev.* **2002**, *54*, 3-12.

(27) Geckil, H.; Xu, F.; Zhang, X.; Moon, S.; Demirci, U. Engineering hydrogels as extracellular matrix mimics. *Nanomedicine* **2010**, *5*, 469-484.

(28) Nochi, T.; Yuki, Y.; Takahashi, H.; Sawada, S.-i.; Mejima, M.; Kohda, T.; Harada, N.; Kong, I. G.; Sato, A.; Kataoka, N.; Tokuhara, D.; Kurokawa, S.;

Takahashi, Y.; Tsukada, H.; Kozaki, S.; Akiyoshi, K.; Kiyono, H. Nanogel antigenic protein-delivery system for adjuvant-free intranasal vaccines. *Nat. Mater.* **2010**, *9*, 572-578.

(29) He, C.; Kim, S. W.; Lee, D. S. In situ gelling stimuli-sensitive block copolymer hydrogels for drug delivery. *J. Control. Release* **2008**, *127*, 189-207.

(30) Lutolf, M. P.; Gilbert, P. M.; Blau, H. M. Designing materials to direct stem-cell fate. *Nature* **2009**, *462*, 433-441.

(31) Yu, L.; Ding, J. Injectable hydrogels as unique biomedical materials. *Chem. Soc. Rev.* **2008**, *37*, 1473-1481.

(32) Lyon, L. A.; Meng, Z.; Singh, N.; Sorrell, C. D.; St. John, A. Thermoresponsive microgel-based materials. *Chem. Soc. Rev.* **2009**, *38*, 865-874.

(33) Zhu, H.; Wu, H.; Wu, M.; Gong, Q. Tetrazine Bioorthogonal Reaction: A Novel Scheme for Polymer and Biomaterials. *Curr. Org. Chem.* **2016**, *20*, 1756-1767.

(34) Truong, V. X.; Ablett, M. P.; Richardson, S. M.; Hoyland, J. A.; Dove, A. P. Simultaneous Orthogonal Dual-Click Approach to Tough, in-Situ-Forming Hydrogels for Cell Encapsulation. *J. Am. Chem. Soc.* **2015**, *137*, 1618-1622.

(35) Haun, J. B.; Devaraj, N. K.; Hilderbrand, S. A.; Lee, H.; Weissleder, R. Bioorthogonal chemistry amplifies nanoparticle binding and enhances the sensitivity of cell detection. *Nat. Nanotechnol.* **2010**, *5*, 660-665.

(36) Wittbecker, E. L.; Morgan, P. W. Interfacial polycondensation. I. *J. Polym. Sci.* **1959**, *40*, 289-297.

(37) Morgan, P. W.; Kwolek, S. L. Interfacial polycondensation. II. Fundamentals of polymer formation at liquid interfaces. *J. Polym. Sci.* **1959**, *40*, 299-327.

(38) Lim, F.; Sun, A. M. Microencapsulated islets as bioartificial endocrine pancreas. *Science* **1980**, *210*, 908.

(39) Augst, A. D.; Kong, H. J.; Mooney, D. J. Alginate Hydrogels as Biomaterials. *Macromol. Biosci.* **2006**, *6*, 623-633.

(40) Shoichet, M. S.; Li, R. H.; White, M. L.; Winn, S. R. Stability of hydrogels used in cell encapsulation: An in vitro comparison of alginate and agarose. *Biotechnol. Bioeng.* **1996**, *50*, 374-381.

(41) Chan, G.; Mooney, D. J. Ca2+ released from calcium alginate gels can promote inflammatory responses in vitro and in vivo. *Acta Biomater.* **2013**, *9*, 9281-9291.

(42) Kuo, C. K.; Ma, P. X. Ionically crosslinked alginate hydrogels as scaffolds for tissue engineering: Part 1. Structure, gelation rate and mechanical properties. *Biomaterials* **2001**, *22*, 511-521.

(43) Johnson, L. M.; Deforest, C. A.; Pendurti, A.; Anseth, K. S.; Bowman, C. N. Formation of three-dimensional hydrogel multilayers using enzyme-mediated redox chain initiation. *ACS Appl. Mater. Interfaces.* **2010**, *2*, 1963-1972.

(44) Meyer, K.; Palmer, J. W. THE POLYSACCHARIDE OF THE VITREOUS HUMOR. *J. Biol. Chem.* **1934**, *107*, 629-634.

(45) Meyer, K. Chemical structure of hyaluronic acid. *Fed. Proc.* **1958**, *17*, 1075-1077.

(46) Laurent, T. C.; Fraser, J. R. Hyaluronan. *FASEB J.* **1992**, *6*, 2397-2404.

(47) Fraser, J. R. E.; Laurent, T. C.; Laurent, U. B. G. Hyaluronan: its nature, distribution, functions and turnover. *J. Intern. Med.* **1997**, *242*, 27-33.

(48) Chong, B. F.; Blank, L. M.; McLaughlin, R.; Nielsen, L. K. Microbial hyaluronic acid production. *Appl. Microbiol. Biotechnol.* **2005**, *66*, 341-351.

(49) Rice, K. G. The Chemistry, Biology, and Medical Applications of Hyaluronan and Its Derivatives Edited by T. C. Laurent. Portland Press, London, U.K. 1998. xvi + 341 pp. 17 × 25 cm. ISBN 1-85578-119-0. $127.50. *J. Med. Chem.* **1998**, *41*, 5336-5336.

(50) Lapčík, L.; Lapčík, L.; De Smedt, S.; Demeester, J.; Chabreček, P. Hyaluronan: Preparation, Structure, Properties, and Applications. *Chem. Rev.* **1998**, *98*, 2663-2684.

(51) Burdick, J. A.; Prestwich, G. D. Hyaluronic acid hydrogels for biomedical applications. *Adv. Mater.* **2011**, *23*, H41-56.

(52) Xu, X.; Jha, A. K.; Harrington, D. A.; Farach-Carson, M. C.; Jia, X. Hyaluronic Acid-Based Hydrogels: from a Natural Polysaccharide to Complex Networks. *Soft Matter* **2012**, *8*, 3280-3294.

(53) Dicker, K. T.; Gurski, L. A.; Pradhan-Bhatt, S.; Witt, R. L.; Farach-Carson, M. C.; Jia, X. Hyaluronan: A simple polysaccharide with diverse biological functions. *Acta Biomater.* **2014**, *10*, 1558-1570.

(54) Burdick, J. A.; Chung, C.; Jia, X.; Randolph, M. A.; Langer, R. Controlled Degradation and Mechanical Behavior of Photopolymerized Hyaluronic Acid Networks. *Biomacromolecules* **2005**, *6*, 386-391.

(55) Ifkovits, J. L.; Burdick, J. A. Review: photopolymerizable and degradable biomaterials for tissue engineering applications. *Tissue Eng.* **2007**, *13*, 2369-2385.

(56) Vanderhooft, J. L.; Mann, B. K.; Prestwich, G. D. Synthesis and Characterization of Novel Thiol-Reactive Poly(ethylene glycol) Cross-Linkers for Extracellular-Matrix-Mimetic Biomaterials. *Biomacromolecules* **2007**, *8*, 2883-2889.

(57) Jia, X.; Colombo, G.; Padera, R.; Langer, R.; Kohane, D. S. Prolongation of sciatic nerve blockade by in situ cross-linked hyaluronic acid. *Biomaterials* **2004**, *25*, 4797-4804.

(58) Jha, A. K.; Hule, R. A.; Jiao, T.; Teller, S. S.; Clifton, R. J.; Duncan, R. L.; Pochan, D. J.; Jia, X. Structural Analysis and Mechanical Characterization of Hyaluronic Acid-Based Doubly Cross-Linked Networks. *Macromolecules* **2009**, *42*, 537-546.

(59) Crescenzi, V.; Cornelio, L.; Di Meo, C.; Nardecchia, S.; Lamanna, R. Novel Hydrogels via Click Chemistry: Synthesis and Potential Biomedical Applications. *Biomacromolecules* **2007**, *8*, 1844-1850.

(60) Taylor, M. T.; Blackman, M. L.; Dmitrenko, O.; Fox, J. M. Design and synthesis of highly reactive dienophiles for the tetrazine-trans-cyclooctene ligation. *J. Am. Chem. Soc.* **2011**, *133*, 9646-9649.

(61) Darko, A.; Wallace, S.; Dmitrenko, O.; Machovina, M. M.; Mehl, R. A.; Chin, J. W.; Fox, J. M. Conformationally Strained trans-Cyclooctene with Improved Stability and Excellent Reactivity in Tetrazine Ligation. *Chem. Sci.* **2014**, *5*, 3770-3776.

(62) Zhang, H.; Dicker, K. T.; Xu, X.; Jia, X.; Fox, J. M. Interfacial Bioorthogonal Cross-Linking. *ACS Macro Lett* **2014**, *3*, 727-731.

(63) Erk, K. A.; Henderson, K. J.; Shull, K. R. Strain Stiffening in Synthetic and Biopolymer Networks. *Biomacromolecules* **2010**, *11*, 1358-1363.

(64) Luo, Y.; Shoichet, M. S. A photolabile hydrogel for guided three-dimensional cell growth and migration. *Nat. Mater.* **2004**, *3*, 249-253.

(65) Bajaj, P.; Marchwiany, D.; Duarte, C.; Bashir, R. Patterned Three-Dimensional Encapsulation of Embryonic Stem Cells using Dielectrophoresis and Stereolithography. *Adv. Healthcare Mater.* **2013**, *2*, 450-458.

(66) DeForest, C. A.; Polizzotti, B. D.; Anseth, K. S. Sequential click reactions for synthesizing and patterning three-dimensional cell microenvironments. *Nat. Mater.* **2009**, *8*, 659-664.

(67) Xu, X.; Gurski, L. A.; Zhang, C.; Harrington, D. A.; Farach-Carson, M. C.; Jia, X. Recreating the tumor microenvironment in a bilayer, hyaluronic acid hydrogel construct for the growth of prostate cancer spheroids. *Biomaterials* **2012**, *33*, 9049-9060.

(68) Xu, X.; Sabanayagam, C. R.; Harrington, D. A.; Farach-Carson, M. C.; Jia, X. A hydrogel-based tumor model for the evaluation of nanoparticle-based cancer therapeutics. *Biomaterials* **2014**, *35*, 3319-3330.

(69) Ruzette, A.-V.; Leibler, L. Block copolymers in tomorrow's plastics. *Nat. Mater.* **2005**, *4*, 19-31.

(70) Averick, S.; Karácsony, O.; Mohin, J.; Yong, X.; Moellers, N. M.; Woodman, B. F.; Zhu, W.; Mehl, R. A.; Balazs, A. C.; Kowalewski, T.; Matyjaszewski, K. Cooperative, Reversible Self-Assembly of Covalently Pre-Linked Proteins into Giant Fibrous Structures. *Angew. Chem. Int. Ed.* **2014**, *53*, 8050-8055.

(71) Walker, C. N.; Sarapas, J. M.; Kung, V.; Hall, A. L.; Tew, G. N. Multiblock Copolymers by Thiol Addition Across Norbornene. *ACS Macro Lett.* **2014**, *3*, 453-457.

(72) Grieshaber, S. E.; Farran, A. J. E.; Lin-Gibson, S.; Kiick, K. L.; Jia, X. Synthesis and Characterization of Elastin−Mimetic Hybrid Polymers with Multiblock, Alternating Molecular Architecture and Elastomeric Properties. *Macromolecules* **2009**, *42*, 2532-2541.

(73) Greene, A. C.; Zhu, J.; Pochan, D. J.; Jia, X.; Kiick, K. L. Poly(Acrylic Acid-b-Styrene) Amphiphilic Multiblock Copolymers as Building Blocks for the Assembly of Discrete Nanoparticles. *Macromolecules* **2011**, *44*, 1942-1951.

(74) Grieshaber, S. E.; Farran, A. J.; Bai, S.; Kiick, K. L.; Jia, X. Tuning the properties of elastin mimetic hybrid copolymers via a modular polymerization method. *Biomacromolecules* **2012**, *13*, 1774-1786.

(75) Grieshaber, S. E.; Paik, B. A.; Bai, S.; Kiick, K. L.; Jia, X. Nanoparticle Formation from Hybrid, Multiblock Copolymers of Poly(Acrylic Acid) and VPGVG Peptide. *Soft Matter* **2013**, *9*, 1589-1599.

(76) Hansell, C. F.; Espeel, P.; Stamenović, M. M.; Barker, I. A.; Dove, A. P.; Du Prez, F. E.; O'Reilly, R. K. Additive-Free Clicking for Polymer Functionalization and Coupling by Tetrazine–Norbornene Chemistry. *J. Am. Chem. Soc.* **2011**, *133*, 13828-13831.

(77) Morgan, P. W.; Kwolek, S. L. The nylon rope trick: Demonstration of condensation polymerization. *J. Chem. Educ.* **1959**, *36*, 182.

(78) Odian, G.: Principles of Polymerization. John Wiley & Sons, Inc., 2004.

(79) Gindl, W.; Martinschitz, K. J.; Boesecke, P.; Keckes, J. Changes in the Molecular Orientation and Tensile Properties of Uniaxially Drawn Cellulose Films. *Biomacromolecules* **2006**, *7*, 3146-3150.

(80) Schön, P.; Bagdi, K.; Molnár, K.; Markus, P.; Pukánszky, B.; Julius Vancso, G. Quantitative mapping of elastic moduli at the nanoscale in phase separated polyurethanes by AFM. *Eur. Polym. J.* **2011**, *47*, 692-698.

(81) Sweers, K. K. M.; van der Werf, K. O.; Bennink, M. L.; Subramaniam, V. Spatially resolved frequency-dependent elasticity measured with pulsed force microscopy and nanoindentation. *Nanoscale* **2012**, *4*, 2072-2077.

(82) Hernández, J. J.; Rueda, D. R.; García-Gutiérrez, M. C.; Nogales, A.; Ezquerra, T. A.; Soccio, M.; Lotti, N.; Munari, A. Structure and Morphology of Thin Films of Linear Aliphatic Polyesters Prepared by Spin-Coating. *Langmuir* **2010**, *26*, 10731-10737.

(83) Derjaguin, B. V.; Muller, V. M.; Toporov, Y. P. Effect of contact deformations on the adhesion of particles. *J. Colloid Interface Sci.* **1975**, *53*, 314-326.

(84) Yang, X.; Cui, C.; Tong, Z.; Sabanayagam, C. R.; Jia, X. Poly(ε-caprolactone)-based copolymers bearing pendant cyclic ketals and reactive acrylates for the fabrication of photocrosslinked elastomers. *Acta Biomater.* **2013**, *9*, 8232-8244.

(85) Panne, P.; Fox, J. M. Rh-Catalyzed Intermolecular Reactions of Alkynes with α-Diazoesters That Possess β-Hydrogens: Ligand-Based Control over Divergent Pathways. *J. Am. Chem. Soc.* **2007**, *129*, 22-23.

(86) Royzen, M.; Yap, G. P. A.; Fox, J. M. A Photochemical Synthesis of Functionalized trans-Cyclooctenes Driven by Metal Complexation. *J. Am. Chem. Soc.* **2008**, *130*, 3760-3761.

(87) Liu, S.; Zhang, H.; Remy, R. A.; Deng, F.; Mackay, M. E.; Fox, J. M.; Jia, X. Meter-long multiblock copolymer microfibers via interfacial bioorthogonal polymerization. *Adv. Mater.* **2015**, *27*, 2783-2790.

Chapter 3

CATALYTIC TURN-ON OF BIOORTHOGONAL TETRAZINE LIGATION

Work described here has already been published (Zhang, H.; Trout, W. S.; Liu, S.; Andrade, G. A.; Hudson, D. A.; Scinto, S. L.; Dicker, K. T.; Li, Y.; Lazouski, N.; Rosenthal, J.; Thorpe, C.; Jia, X.; Fox, J. M., Rapid Bioorthogonal Chemistry Turn-on through Enzymatic or Long Wavelength Photocatalytic Activation of Tetrazine Ligation. *J Am Chem Soc* **2016,** *138* (18), 5978-83.). It is reprinted in this chapter with permissions of *Journal of American Chemical Society* (Copyright 2016 American Chemical Society).

3.1 Previous Bioorthogonal Chemistry Turn-on Methods

There has been a growing interest in inducing bioorthogonal reactivity using external stimulus, especially using light as trigger. The use of photo-triggered bioorthogonal reactivity can provides opportunities of spatial and temporal control during the labeling process.[1-3] In 2006, Popik and coworkers discovered that the cyclopropenones can be photodecarbonylated in a two-photon process (Scheme 3.1), generating "clickable" alkynes that are reactive towards azides.[4,5] In further study, they reported selective labeling of live cells by *in-situ* photo-triggered click chemistry based on masked dibenzocyclooctynes (Scheme 3.2).[6] Azide-tagged cells were placed in medium containing biotinylated cyclopropenone and exposed to 350 nm light while the cells in the control group were kept in dark, subsequent treatment with an avidin-

fluorophore conjugate showed selective cell labeling while low fluorescence intensities were measured in the control group.

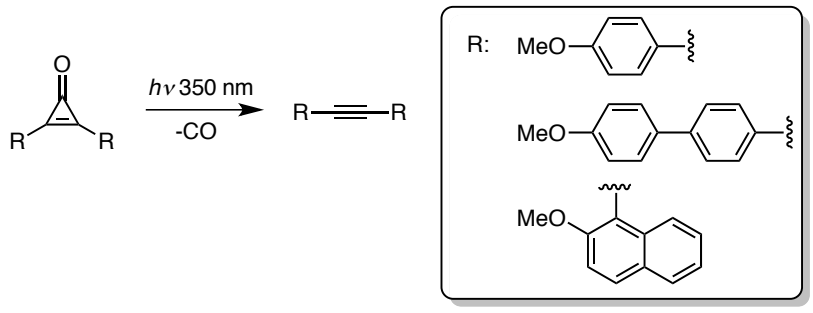

Scheme 3.1: Photodecarbonylation of cyclopropenones.

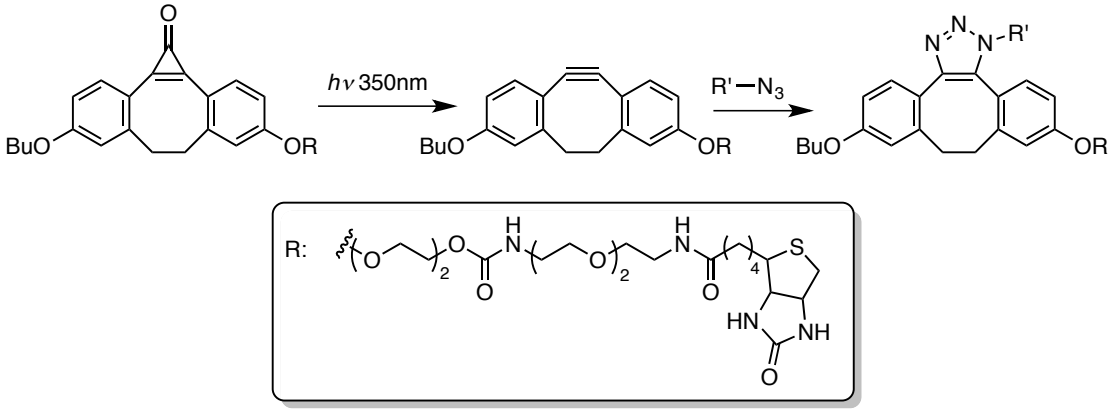

Scheme 3.2: Photochemical initiation of SPAAC.

Lin and coworkers developed a photo-induced 1,3-dipolar cycloaddition reaction between tetrazoles and alkenes. Reactive nitrile imine dipoles can be photo-generated from diaryltetrazoles for efficient cycloaddition reactions with alkenes to form fluorescent pyrazoline cycloadducts (Scheme 3.3).[1,7,8] Extraordinarily rapid

reaction kinetics as high as k_2 10^4 M^{-1} s^{-1} have been achieved when strained alkenes (e.g. 3,3-disubstituted cyclopropenes[9] or spiro[2.3]hex-1-enes[10]) were used. This "photoclick chemistry" has been applied in peptide side chain crosslinking,[11] modification of proteins *in vitro*,[12] visualization of proteins in living cells,[9,13] as well as *in situ* hydrogel formation.[14,15]

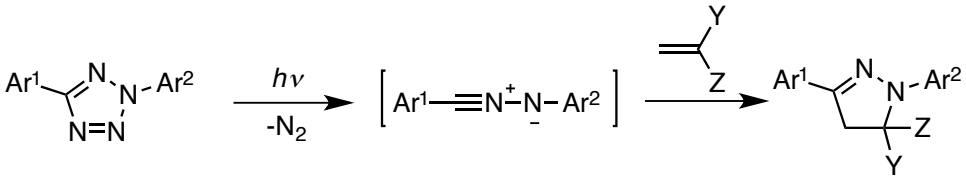

Scheme 3.3: Photoactivated 1,3-dipolar cycloaddition reaction.

One advantage of Lin's method was that the tunable photoactivation wavelength. The initial photoclick chemistry was performed under irradiation band centered at 302 nm or 365 nm. UV light in these regions may pose considerable phototoxicity to living cells. Fortunately, further improvements have been made by tailoring the substitutions on tetrazole precursors. A series of tetrazoles with different photoactivation wavelengths were developed.[16-18]

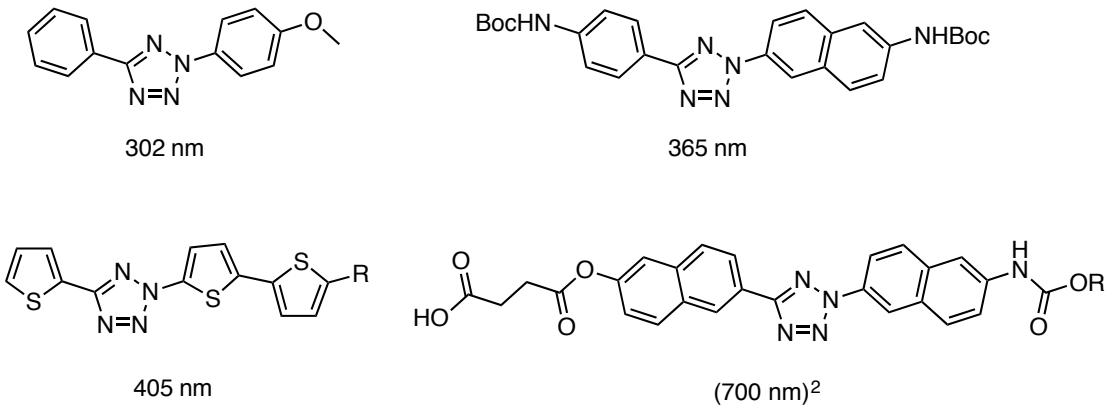

Scheme 3.4: Tetrazoles with variable photoactivation wavelengths.

Compared to UV and near UV light which has limited ability to penetrate tissue and has issues of phototoxicity,[19] red and near-IR light is more physiology-friendly and can deeply penetrate tissues to several centimeters.[20] However, there had been no reports on directly using red or near-IR light to activate bioorthogonal reactivity. There are studies in which cyclopropenone and tetrazole-based photoclick chemistries were activated by two-photon near-IR irradiation. While two-photon methods provide excellent spatial resolution, their practical applications were limited by the very small focal volumes. Near-IR photodecaging processes have been described based on cyanine,[21] BODIOY[22] and phthalocyanine dyes,[23,24] but these methods suffer from relatively slow decaging kinetics.

3.2 Dihydrotetrazine (DHTz) and Its Role in Tetrazine Synthesis

Besides the numerous applications in bioorthogonal chemistry and biomedical research, *s*-tetrazines have seen significant applications in the areas of coordination chemistry,[25-27] explosive materials research,[28,29] and natural product synthesis.[30-32]

The most convenient method for tetrazine synthesis was introduced in the last century via the addition of hydrazine to aromatic nitriles, forming symmetric or asymmetric dihydrotetrazine intermediate, followed by oxidation to yield tetrazine products (Scheme 3.5).[33-35]

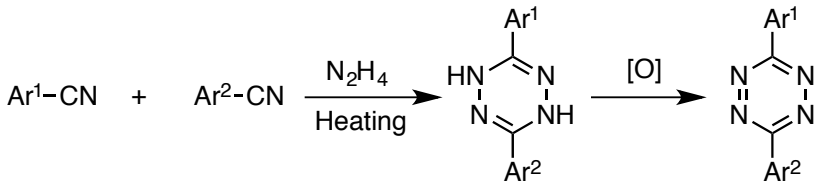

Scheme 3.5: Classical tetrazine synthesis.

Recently, Devaraj and coworkers reported a metal catalyzed tetrazine synthesis method in which nickel or zinc triflates were used to catalyze the formation of dyhidrotetrazine, which were subsequently oxidized by nitrous acid (Scheme 3.5).[36] The method is successful for alkyl substituted tetrazines, which were challenging to prepare by alternate routes.

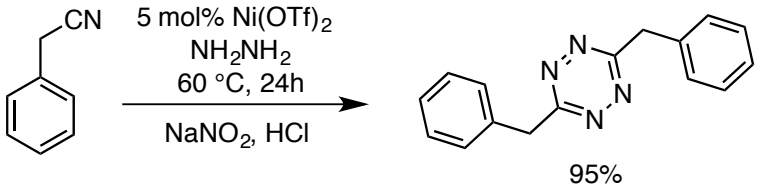

Scheme 3.6: Representative example of Devaraj's tetrazine synthesis.

As shown above, all these *s*-tetrazine synthesis involve the preparation and oxidation of dihydrotetrazine precursors. Commonly, nitrous reagents (e.g. HONO, $NaNO_2$) are used in the oxidation. There are also reports in which CrO_3[37] and DDQ[38,39] were used as oxidation agents for converting dihydrotetrazine into tetrazine. Dr. Selvaraj from our group demonstrated that phenyliodonium diacetate (PIDA) can be utilized as a mild and effective oxidant for aryl and alkyl dihydrotetrazine oxidation.[40] Very recently, Hu and coworkers described the synthesis of alkyl tetrazine derivative from *gem*-difluoroalkenes under aerobic conditions at room temperature in which they used air to oxidize the dialkyl-dihydrotetrazine intermediates.[41]

3.3 Catalytic Turn-on of Tetrazine Ligation from Latent Dihydrotetrazine

Dihydrotetrazines are not reactive towards strained dienophile (e.g. *trans*-cyclooctene, cyclooctyne, norbornene, etc.). We envisioned that dihydrotetrazines could be utilized as latent precursors for later "turn-on" of bioorthogonal reactivity (Figure 3.1) if it were possible to identify controllable and physiology-friendly oxidation methods.

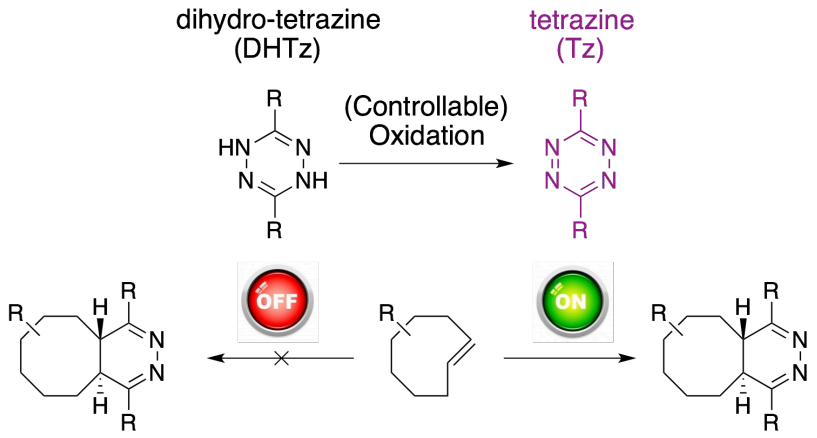

Figure 3.1: Turn-on of bioorthogonal reactivity thru controllable oxidation of dihydrotetrazine.

3.3.1 Choosing the Appropriate Dihydrotetrazine/Tetrazine Pair

Our work started by choosing a suitable dihydrotetrazine (DHTz) and tetrazine (Tz) pair that would be stable in both oxidation states. The stability of DHTz and Tz largely depends on the substitution on the core structure, dihydrotetrazines substituted by electron withdrawing groups possess good stability towards background oxidation but the corresponding tetrazines are too reactive toward water and other nucleophiles. On the other hand, when substituted by electron donating groups, the oxidized tetrazines will have excellent stability in aqueous condition while the corresponding dihydrotetrazine being too readily oxidized even when exposed in air (Figure 3.2).

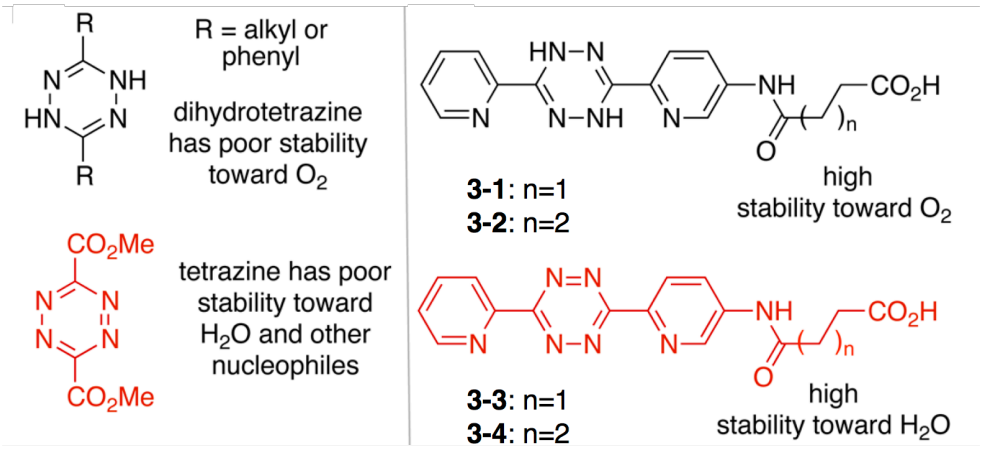

Figure 3.2: Identification of a DHTz/Tz pair with high stability.

We chose the dipyridyl-DHTz/Tz pair for good stability in both oxidation states and the investigations of the stability of the redox pair using UV-vis spectroscopy were conducted in collaboration with graduate student William Trout.

Dihydrotetrazine **3-1** and **3-3** are highly resilient toward background oxidation, as a 35 μM solution, **3-1** in MeOH was shown to retain 99% and 98% of the DHTz oxidation state after 1 and 2 h, respectively in UV-vis analysis (Figure 3.3A). Aqueous solutions of **3-1** were handled in glassware that had been first rinsed with 2.0 mM EDTA in PBS to remove adventitious metal impurities and 99% and 96% DHTz integrity were obtained in PBS buffer in the dark after time periods of 0.5 and 2.5 h, respectively (97% and 94% after 1 and 2 h when in ambient light). Dipyridyl-tetrazine derivative have been described previously and used broadly for applications in nuclear medicine and cell imaging. In PBS buffer at 25 °C tetrazine **3-3** (800 μM) shows 98% and 83% fidelity after 2 and 24 h, respectively (Figure 3.3B).

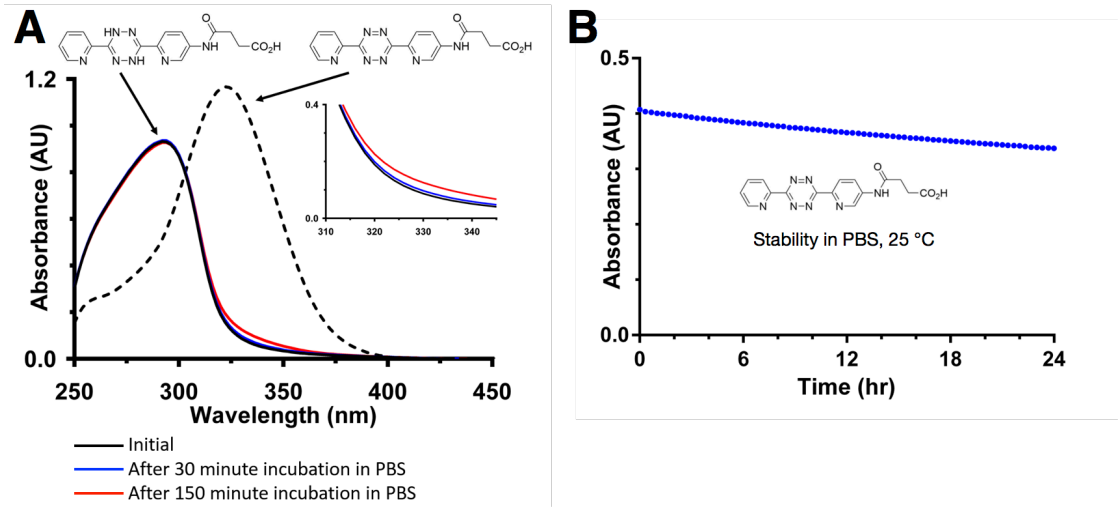

Figure 3.3: (A) Oxidative stability of **3-1** in dark in PBS monitored by recording absorbance at 0, 0.5 and 2.5 hours. (B) Hydrolytic stability of **3-3** in PBS at 25 °C was monitored every 20 minutes at 525 nm.

3.3.2 Electrochemical Characterization of Oxidation of Dihydrotetrazine

The electrochemical oxidation of **3-1** in phosphate buffer was performed by Gabriel Andrade, graduate student from the Rosenthal group at the University of Delaware. The voltammogram displays a single peak centered at 0.02 V.

Under mildly oxidizing conditions (0.18 V relative to Ag/AgCl), a 1.1 mM solution of **3-1** visually turned pink (Figure 3.4, left) and the oxidation to **3-3** proceeds cleanly with an isosbestic point at 303 nm as monitored by UV-vis (Figure 3.4, right).

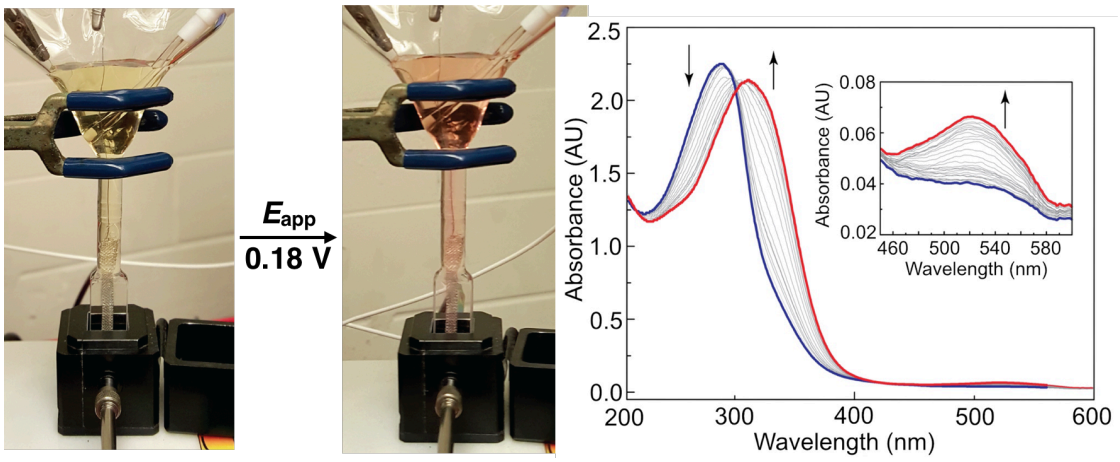

Figure 3.4: Left: aqueous solution of **3-1** (1.1 mM) undergoes a visible color change from pale yellow to pink, indicating the formation of tetrazine. Right: spectral change during electrochemical conversion of **3-1** (blue trace) (1.1 mM) to **3-3** (red trace).

3.3.3 Long Wavelength Photocatalytic Activation of Tetrazine Ligation

I started the photocatalytic oxidation experiment from applying $Ru(bpy)_3(PF_6)_2$ to multiblock copolymer fiber contains DHTz (this part of studies will be elaborate in detail later in chapter **3.4**), preliminary result with the use of 1 mM of $Ru(bpy)_3(PF_6)_2$ and a 200W incandescent bulb was positive: the activated fibers were visually pink and after treatment of Alexa Fluor® 647-sTCO solution I can observe the fiber turing blue (color of Alexa Fluor® 647 dye) under light microscope. However, later attempts to confirm and characterize the photocatalytic oxidation of DHTz small molecules were unsuccessful because the strong absorption of 1 mM $Ru(bpy)_3(PF_6)_2$ which overlaped with absorption of DHTz.

Following on my initial success with $Ru(bpy)_3(PF_6)_2$, William Trout joined this project and studied other photo sensitizers. Several photosensitizers were found to catalyze the oxidation of **3-1** to **3-3** in the presence of long wavelength visible light.

Of those studied, methylene blue was considered an attractive sensitizer because of its low molecular weight, low toxicity, good solubility and the absorption spectrum (λ_{max} 665 nm) that extends to the near-IR.[42]

Dipyridyl-dihydrotetrazine **3-1** has maximum absorption in the UV-vis spectrum at 292 nm, and the oxidized tetrazine **3-3** at 325 nm with a less intense peak at 525 nm, thus these signature absorptions were used to analyze and quantify the redox transformation. Experiments were conducted at 25 °C in a thermostated cuvette with stirring capability and an interchangeable single top-mounted LED. A custom 3D printed light fixture was used to mount the LED directly above the cuvette and block ambient light.

In the photooxidation experiment, irradiation of dihydrotetrazine **3-1** (21 μM) with a single 660 nm LED (9.1 mW/cm^2) in the presence of methylene blue (4 μM) in pH 7.4 PBS caused conversion to tetrazine **3-3** with quantitative yield within 200 s (Figure 3.5B). The same isosbestic point at 303 nm was observed during the course of photooxidation (Figure 3.5D). The light dependence of the methylene blue catalyzed oxidation was demonstrated by turning the LED on and off (Figure 3.5C). Similar light dependent on/off behavior was exhibited with either rose bengal or carboxyfluorescein with irradiation centered at 528 nm.

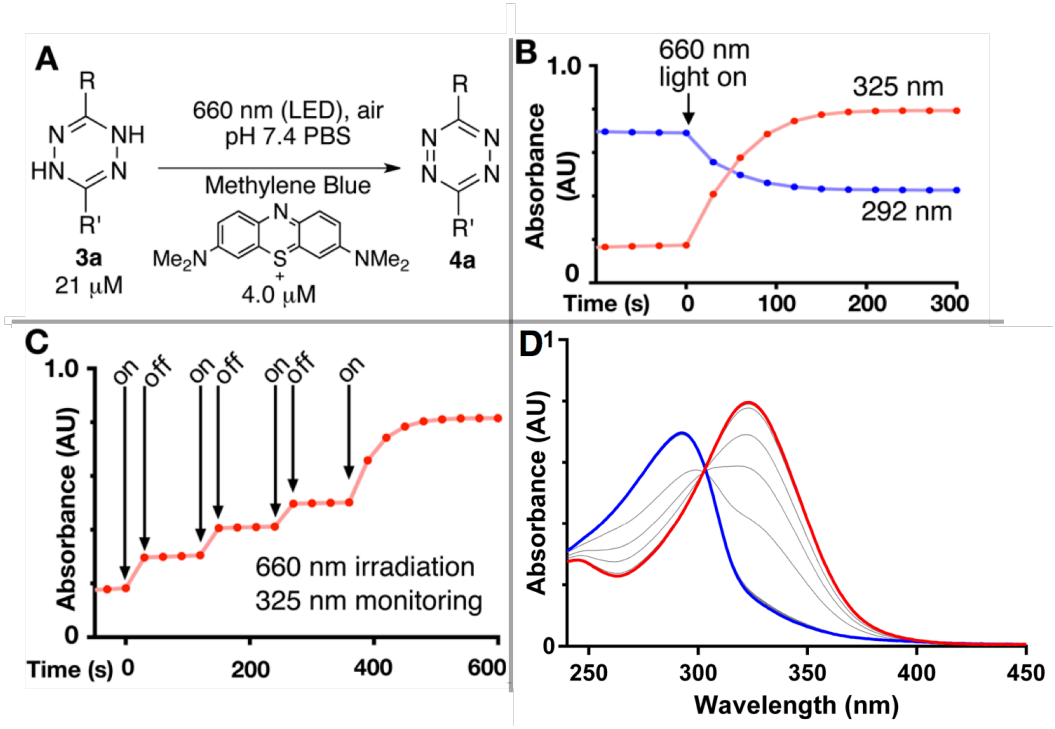

Figure 3.5: (A) Methylene blue catalyzed photooxidation of **3-1** to **3-3**. (B) After the onset of irradiation, reaction progress was monitored every 30 s at 325 nm, which increased with formation of **3-3**, and 292 nm, which decreased upon consumption of **3-1**. (C) The reaction progress requires irradiation and stalls when the LED is turned off. (D) The photooxidation of **3-1** to **3-3** displays an isosbestic point at 303 nm

Both methylene blue and rose bengal are known $^1O_2$ sensitizers, and we therefore queried the influence of a $^1O_2$ quencher on the oxidation rate of **3-1**. Neither the methylene blue nor the rose bengal catalyzed photooxidations are impeded by the addition of 60 mM NaN_3.

Besides methylene blue, rose bengal and carboxyfluorescein discussed above, other sensitizers found to be capable of catalyzing photooxidation of dihydrotetrazine to tetrazine include acridine orange, coomassie brilliant blue, rhodamine B, BODIPY, safranin and phenol red.

3.3.4 Enzymatic Activation of Tetrazine Ligation

As a complement to these photooxidation reactions, we observed that horseradish peroxidase (HRP) can efficiently catalyze the oxidation of **3-1** in the dark at low enzyme concentration.

HRP is an enzyme extensively used in biochemical assays by oxidizing phenols and other organic substrates.[43,44] While H_2O_2 is typically required as the terminal oxidant, HRP can oxidize certain substrates (e.g., indole-3-acetic acid,[45,46] NADH,[47] and hydroquinones[48]) in the absence of peroxide.

The addition of HRP (15 nM) to a peroxide-free solution of **3-1** (30 μM) in PBS led to the rapid formation of **3-3** (Figure 3.6). Again, an isosbestic point at 303 nm was observed during the enzymatic oxidation. The formation of **3-3** was significantly slowed down in the presence of 2 mM H_2O_2 and was near baseline in the presence of H_2O_2 but absence of HRP (Figure 3.6B). It was observed that the oxidation of **3-1** by HRP follows Michaelis-Menten kinetics, with $K_m = 1.0 \times 10^{-4}$ M, $k_{cat} = 27\ s^{-1}$, and $k_{cat}/K_m = 2.7 \times 10^5\ M^{-1}\ s^{-1}$.

Neither cytochrome *c* nor hemoglobin were effective catalysts of DHTz oxidation, with only slow conversion of **3-1** to **3-3** even with heme concentrations that were nearly 3 orders of magnitude higher than that used with HRP. The addition of superoxide dismutase (SOD, 770 nM) does not suppress the rate of the oxidation of **3-1** by HRP, providing evidence that superoxide is not responsible for the oxidation.

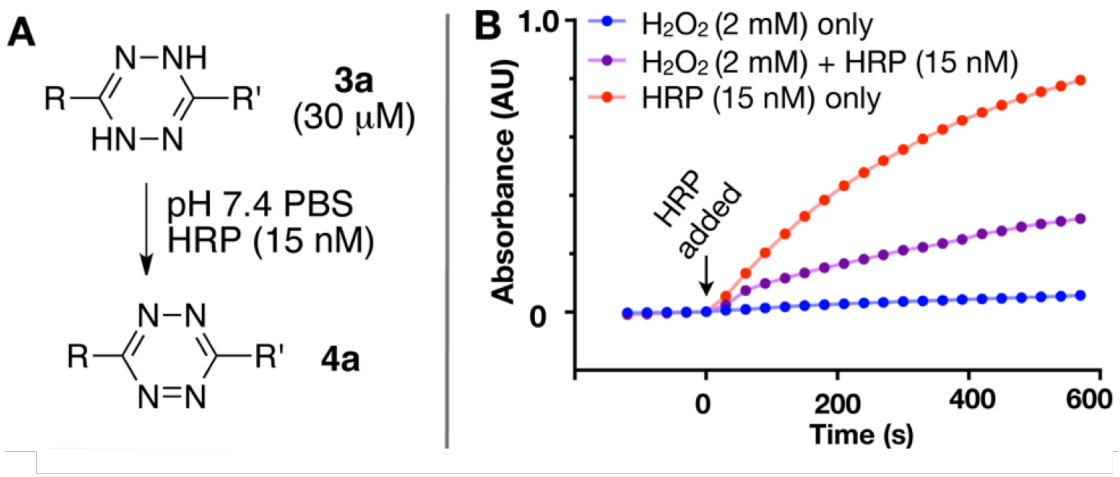

Figure 3.6: (A) Horseradish peroxidase catalyzed oxidation of **3-1** to **3-3**. (B) Enzymatic oxidation is most efficient in the absence of peroxide and is suppressed upon addition of peroxide. Hydrogen peroxide without catalyst is not an effective oxidant of **3-1**.

3.4 Dihydrotetrazine-Incorporated Multiblock Copolymer Fibers

We envisioned that the light and enzyme-catalyzed reactions developed above will be promising tools to functionalize the polymeric materials, especially in a post-synthetic modification. The multiblock copolymer fiber generated from interfacial polymerization (described in chapter 2) developed earlier from our group[49] is an ideal platform to test out the "turn-on" of tetrazine ligation reactivity.

The modular approach enabled us to incorporate cell-instructive molecules (e.g. RGD sequence) onto the polymer chain during the process of polymerization and the resulting microfibers exhibited dramatic increase in the ability to promote cell attachment and alignment. However, fabrication of protein-containing fibers was not achieved due to the possibility of protein denaturation by the required organic solvent and the large amount of protein conjugates that would be required for an interfacial polymerization.

We hypothesized that dihydrotetrazine-containing copolymer fibers can be prepared in a similar interfacial polymerization approach by adopting a dihydrotetrazine-containing monomer (Figure 3.7, top). The dihydrotetrazine functionality can be subsequently activated by light or enzyme-catalyzed oxidation conditions, affording tetrazine functionality and enabling further modification including conjugation of protein derivatives (Figure 3.7, bottom).

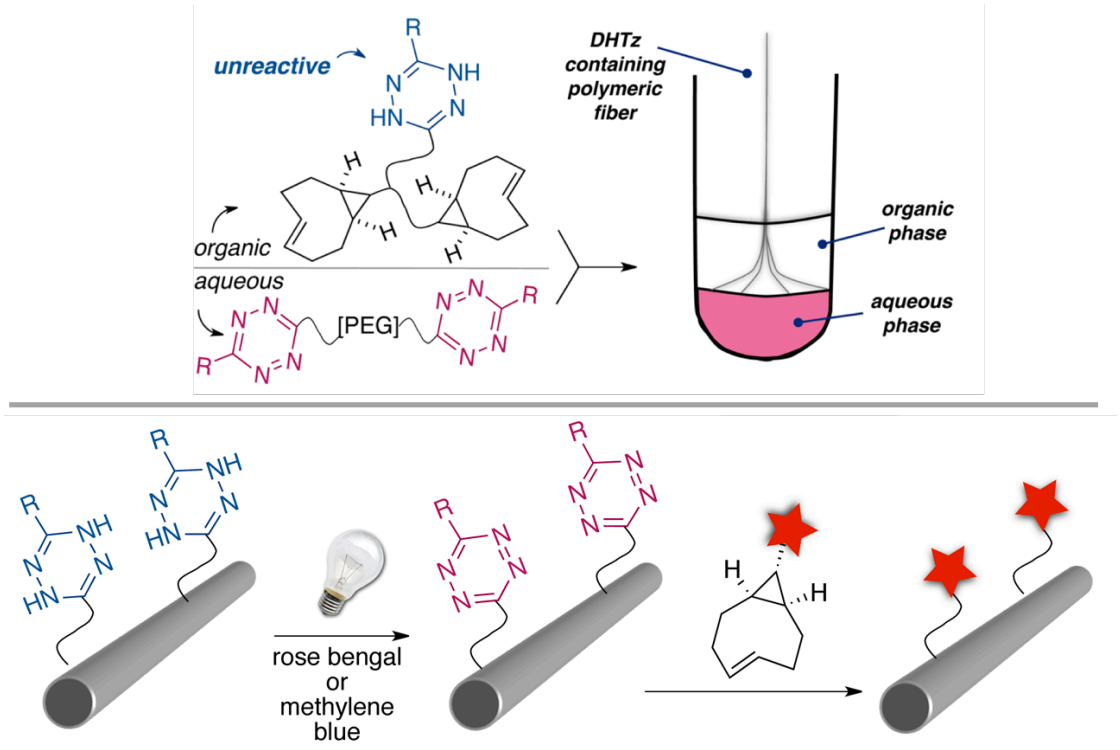

Figure 3.7: Top: Schematic representation of interfacial polymerization with a dihydrotetrazine-derived monomer. Bottom: Schematic representation of copolymer fiber activation and subsequent conjugation.

3.4.1 Dihydrotetrazine-Containing Block Monomer and Preparation of Dihydrotetrazine-Containing Copolymer Fibers

I sought to introduce the dihydrotetrazine functionality into the aliphatic *bis*-sTCO monomer and keep using the hydrophilic *bis*-tetrazine monomer **2-11** described in chapter 2. A building block monomer **3-5** contains two sTCO and one dipyridyl-dihydrotetrazine was derived from 1,3-diamino-2-propanol. Notably, compound **3-5** was readily purified stored and handled without special precautions, indicating the good stability of dipyridyl-dihydrotetrazine towards background oxidation.

I again used Alexa Fluor® 647-sTCO conjugate **2-7** as a visualization molecule for small molecule tagging, a Clover[50]-sTCO conjugate was prepared for the experiment of post-synthetic protein modification, a fibronectin-derived RGD-sTCO conjugate was also synthesized, structures of monomers and tagging agent used in the experiment are included in figure 3.8.

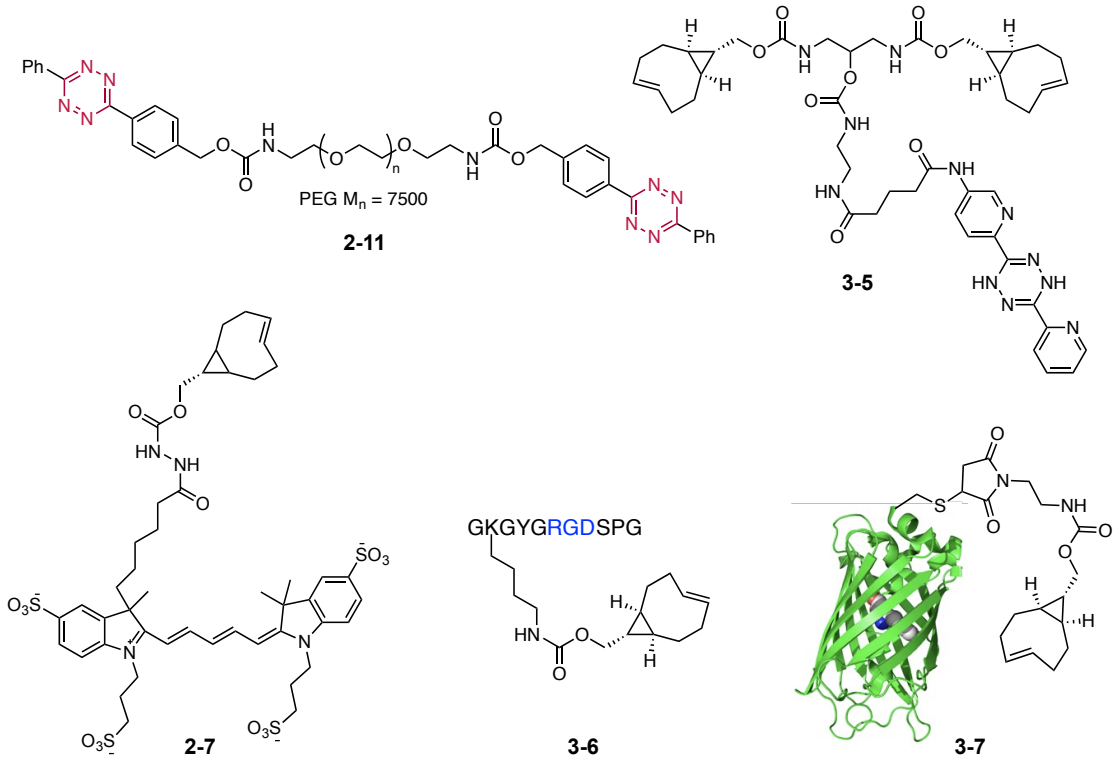

Figure 3.8: Monomers **2-11** and **3-5** were used for interfacial polymerization. sTCO conjugates of the green fluorescent protein variant Clover (**3-7**), the dye Alexa Fluor® 647 (**2-7**), and an RGD peptide (**3-6**) were used to modify the fibers.

Following a similar procedure described before (Chapter 2), meter-long, mechanically robust polymer fibers were continuously pulled from the liquid-liquid interface without breakage. The DHTz-containing fibers were collected and dried affixed onto pre-cleaned glass slides using adhesive silicon isolators where further activation and subsequent modifications were conducted.

3.4.2 Post-Synthetic Activation of Bioorthogonal Reactivity

To examine the postsynthetic activation and modification of the DHTz-containing fibers, the fibers were generally immersed in 100 μM sensitizer in PBS and

irradiated with a simple incandescent bulb for 5 min. After irradiation, the fibers were rinsed and then allowed to react with an sTCO conjugate for 1 min, and rinsed again. Methylene blue was used to activate fibers toward conjugations of Clover-sTCO or RGD-sTCO, and in Alexa Fluor® 647-sTCO conjugation experiments, rose bengal was used due to the spectral overlap of the Alexa Fluor® 647 with methylene blue.

Fibers that were activated and modified with Alexa Fluor® 647-sTCO and Clover-sTCO were characterized by confocal microscope. The confocal images showed clear labeling by Alexa dye (Figure 3.9-10) and Clover protein (Figure 3.14-15) localized to the exterior of the fibers which were also illustrated by the confocal Z-stack images (Figure 3.18). The control experiments illustrated that dye conjugation was not efficient if the sensitizer (Figure 3.12-13, 16-17) or light (Figure 3.11) was excluded.

HRP-catalyzed oxidation of dihydrotetrazines can also be used to activate fibers toward bioconjugation (Figure 3.19-20); however, in this instance photocatalytic activation is faster and more efficient.

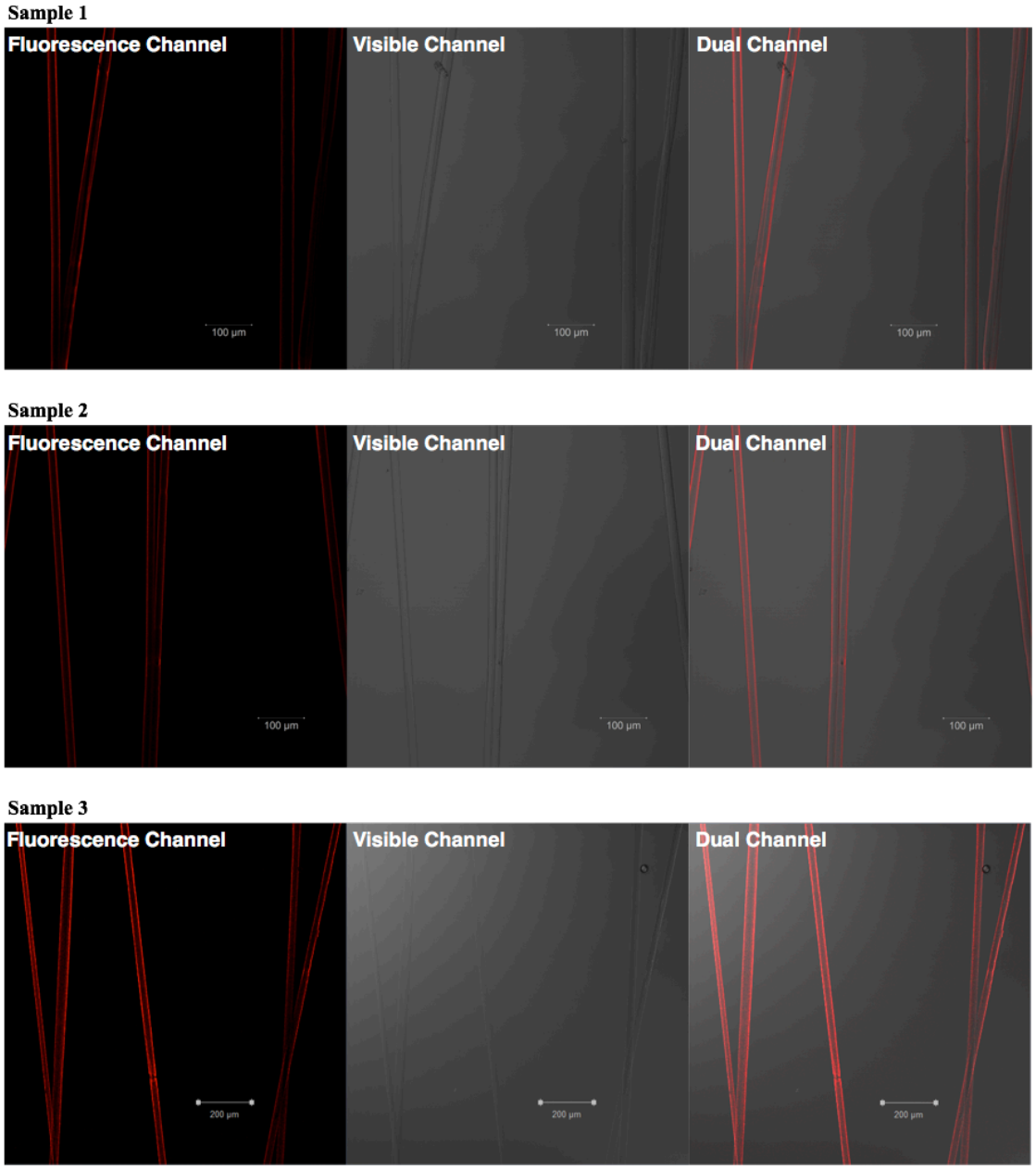

Figure 3.9: Confocal images of Alexa Fluor® 647 tagging experiment: positive sets.

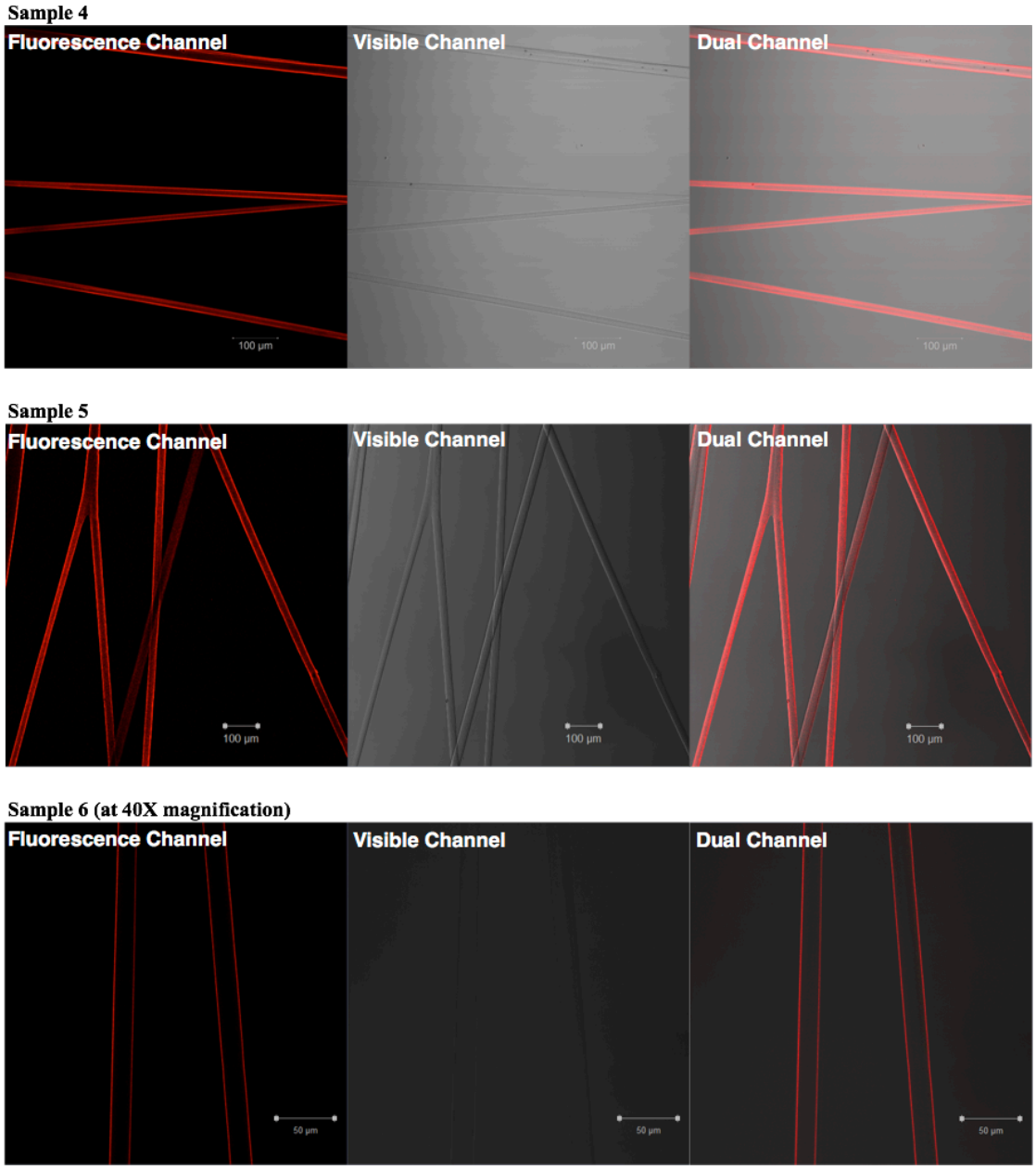

Figure 3.10: Confocal images of Alexa Fluor® 647 tagging experiment: positive sets.

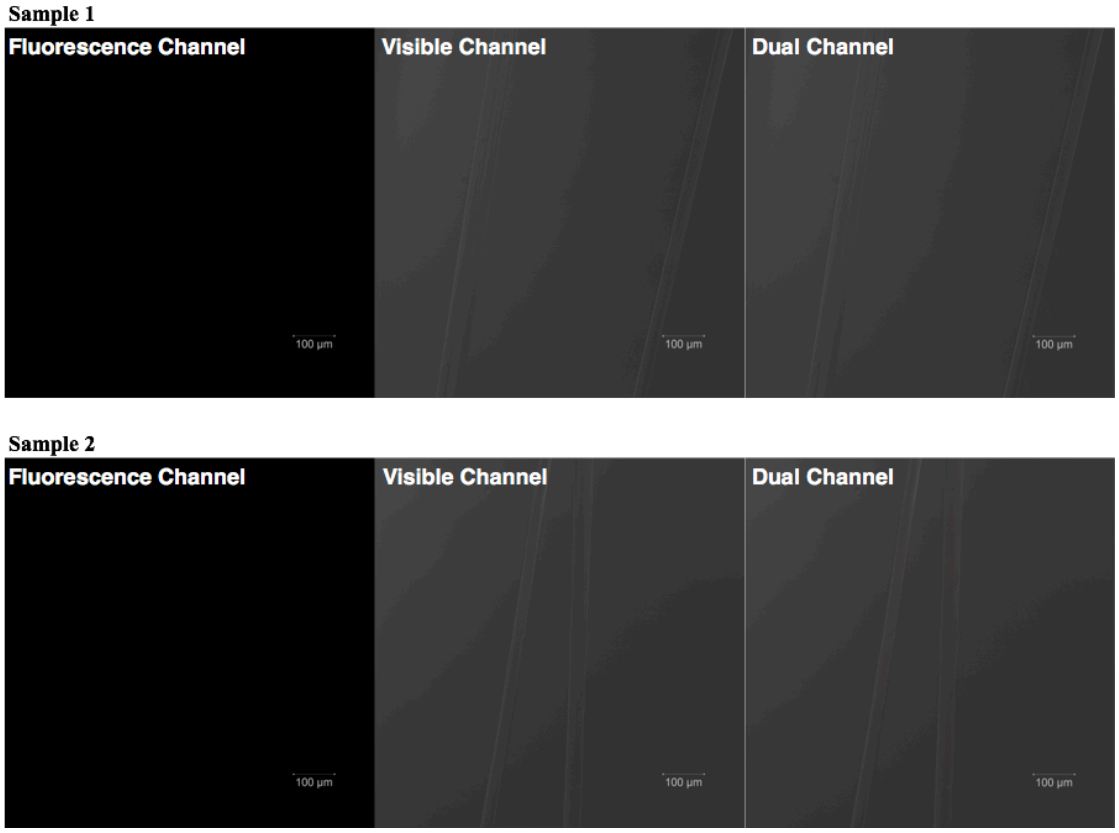

Figure 3.11: Confocal images of Alexa Fluor® 647 tagging experiment: control sets without light.

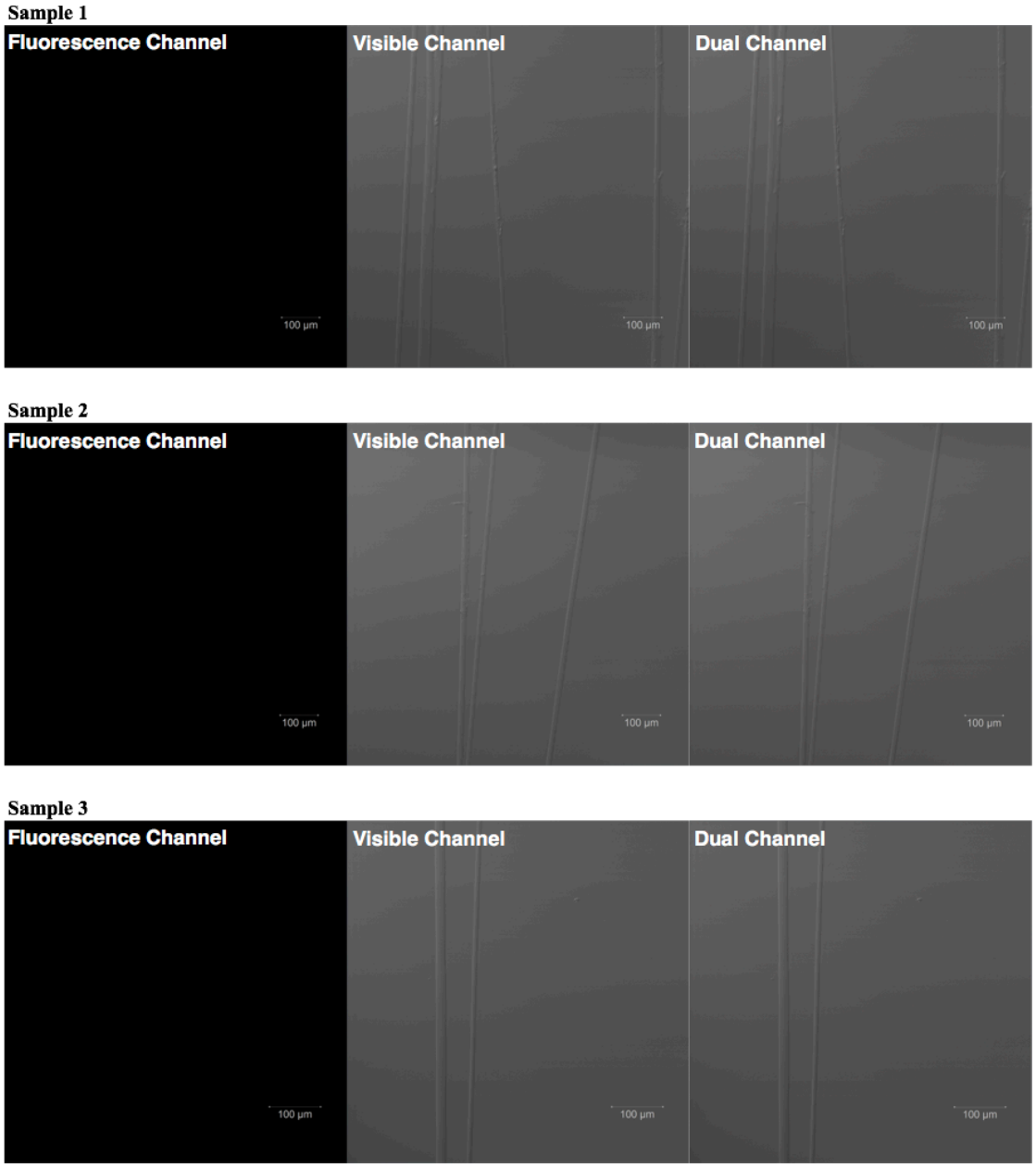

Figure 3.12: Confocal images of Alexa Fluor® 647 tagging experiment: control sets without sensitizer.

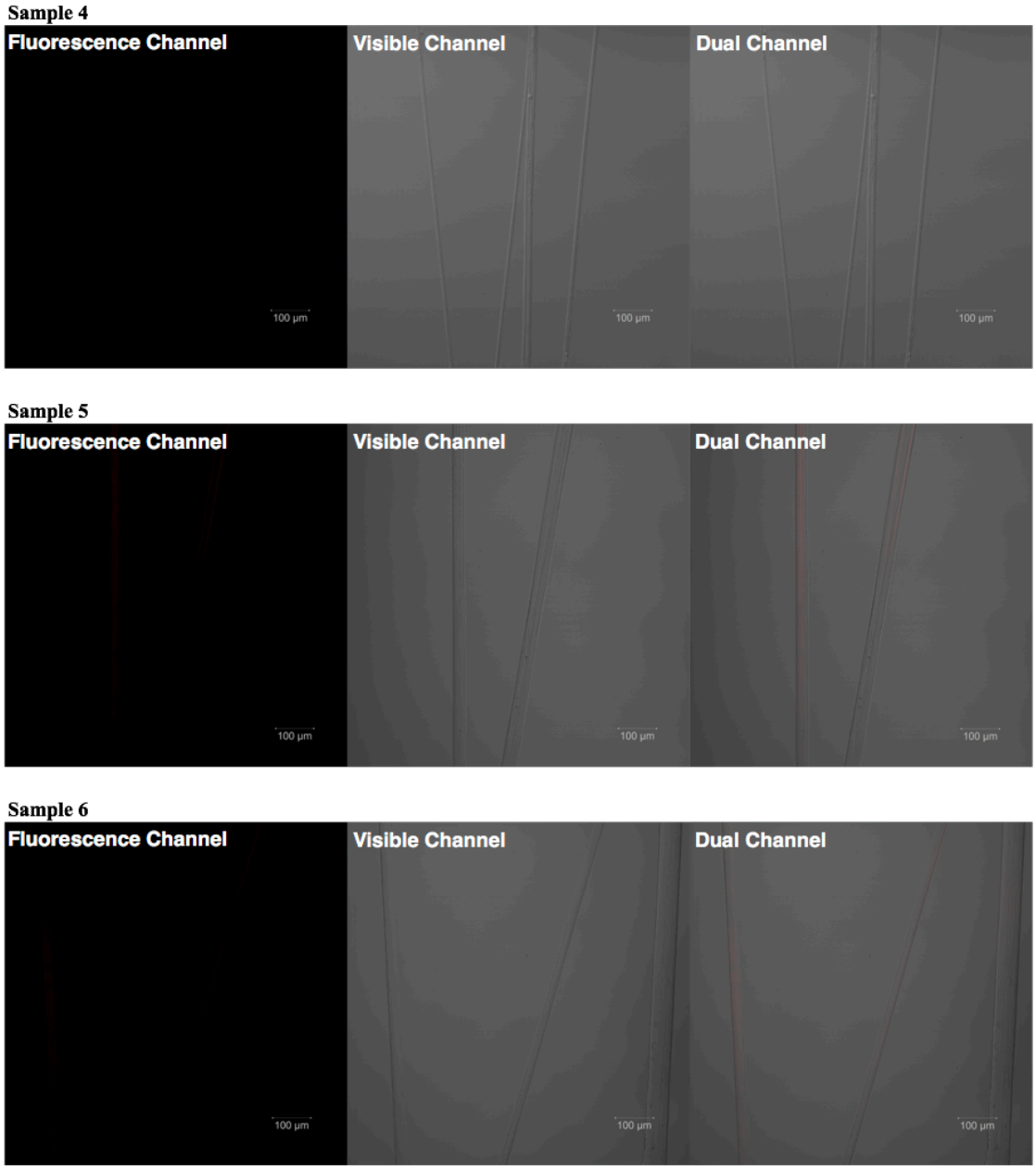

Figure 3.13: Confocal images of Alexa Fluor® 647 tagging experiment: control sets without sensitizer.

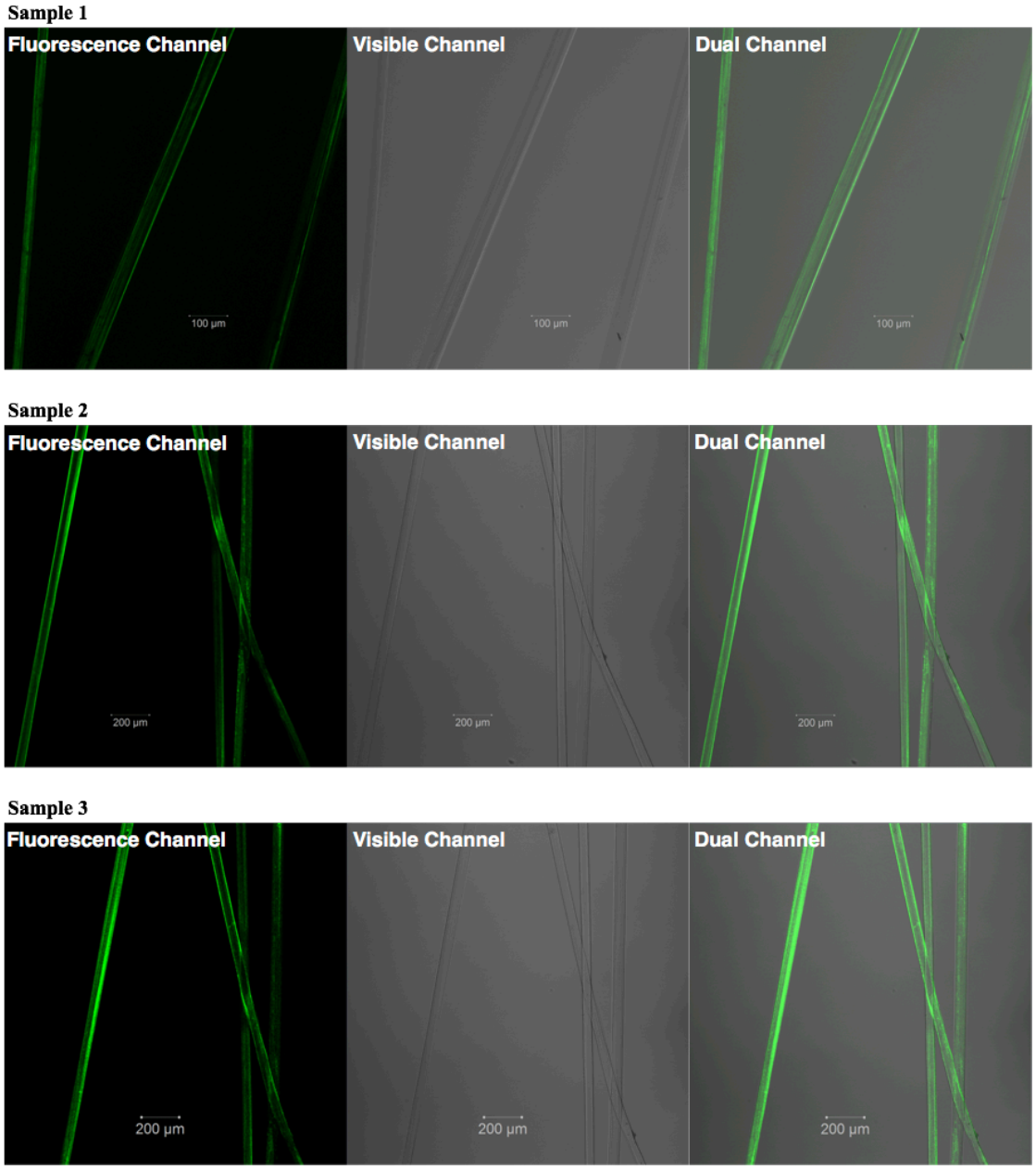

Figure 3.14: Confocal images of Clover protein tagging experiment: positive sets.

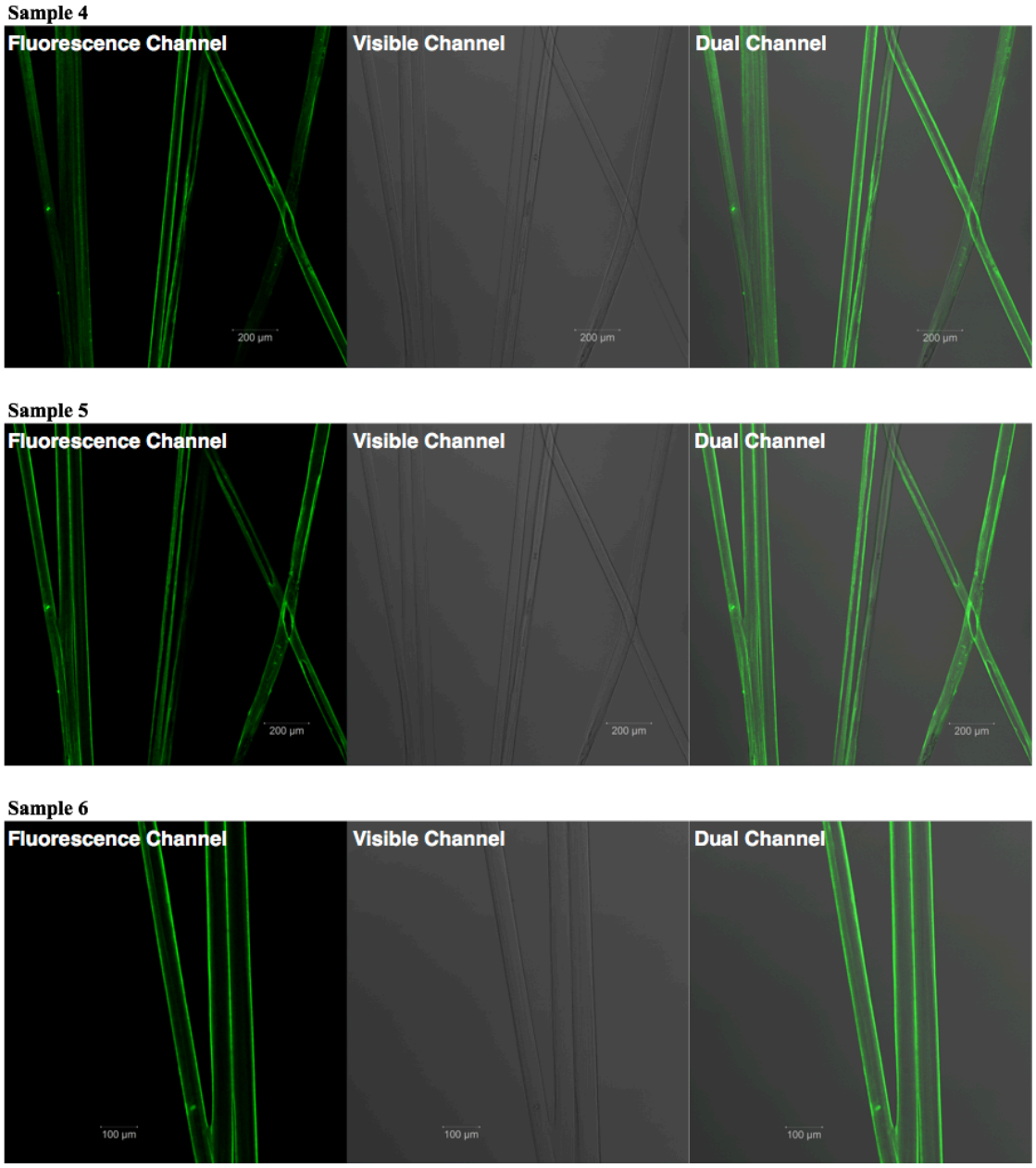

Figure 3.15: Confocal images of Clover protein tagging experiment: positive sets.

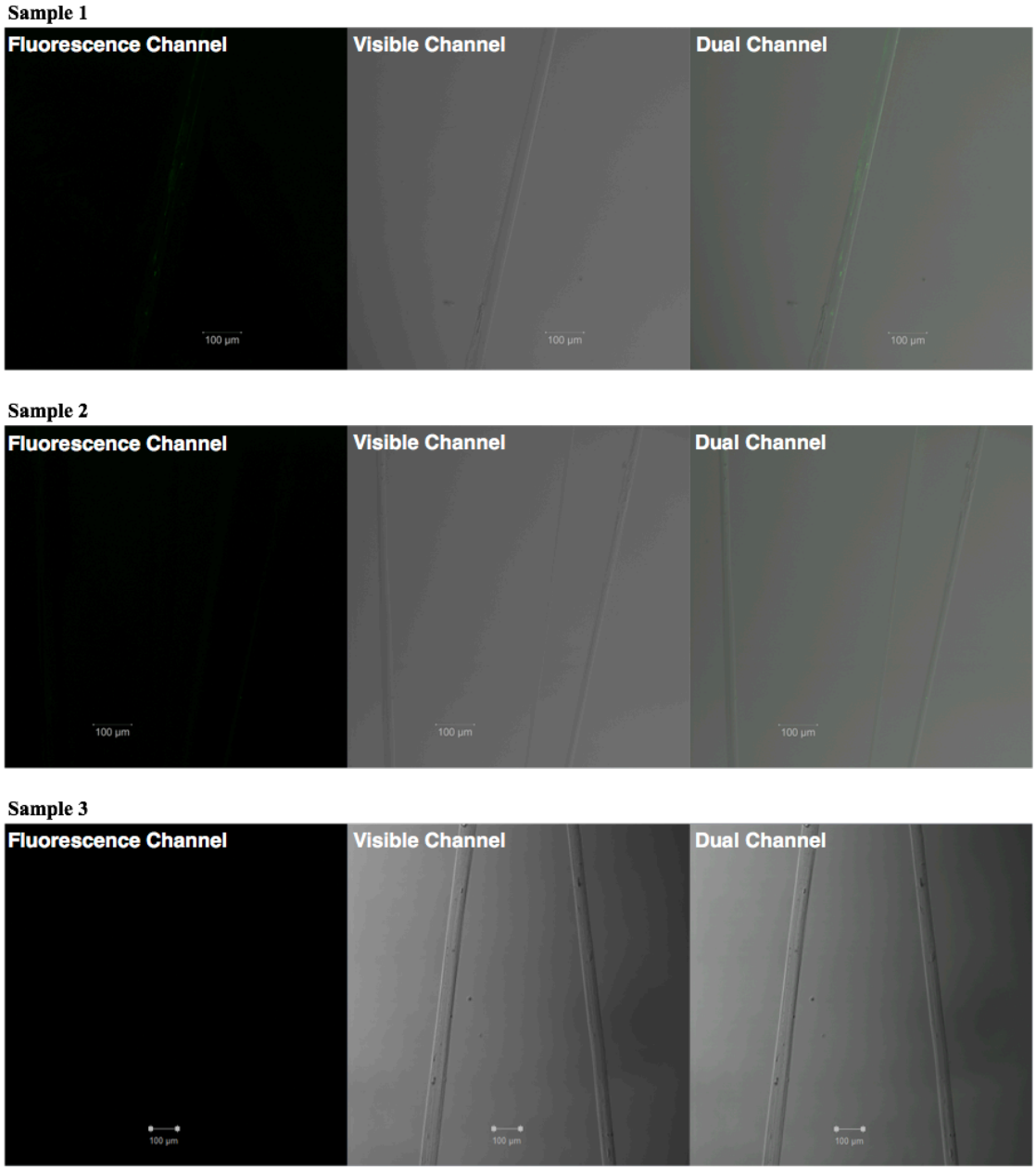

Figure 3.16: Confocal images of Clover protein tagging experiment: control sets without sensitizer.

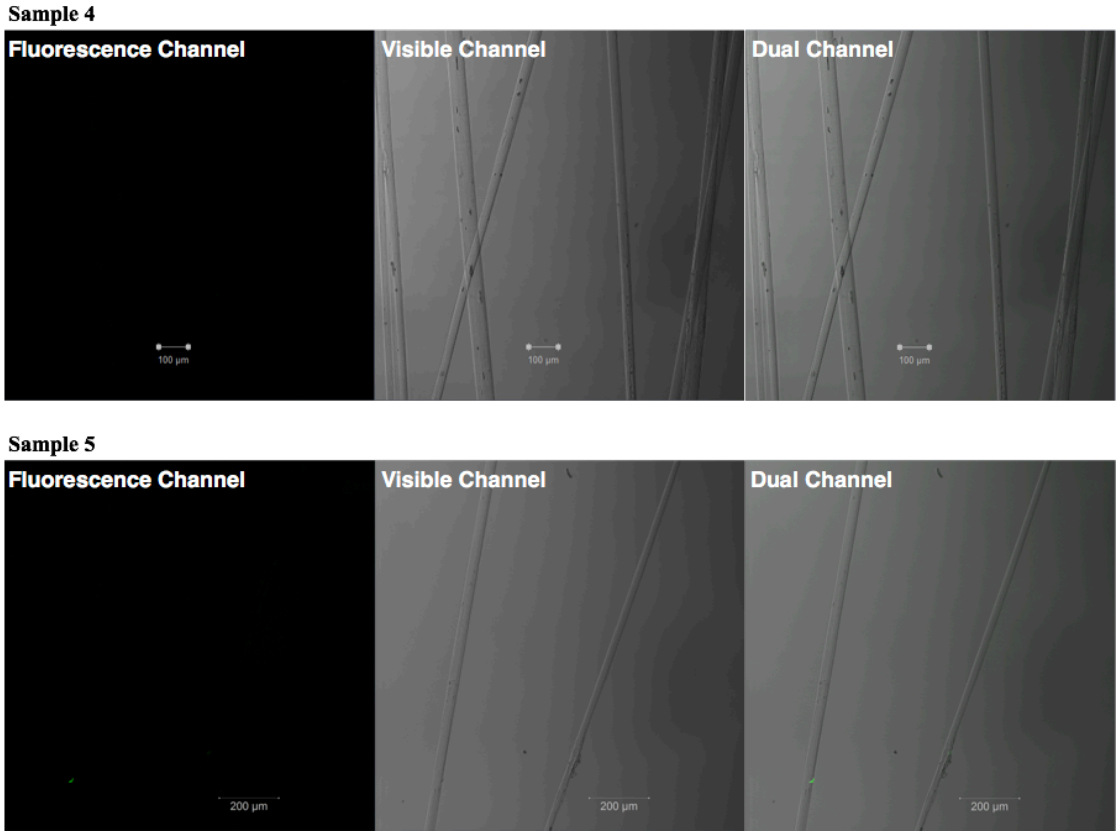

Figure 3.17: Confocal images of Clover protein tagging experiment: control sets without sensitizer.

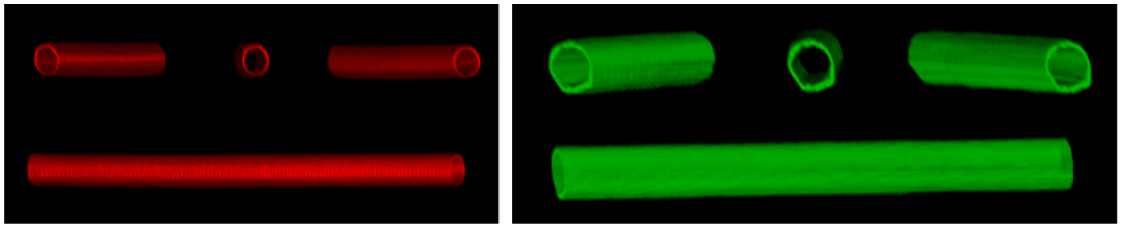

Figure 3.18: Reconstructed confocal z-stack images of activated fibers that were conjugated with Alexa Fluor® 647-sTCO (Left) and Clover-sTCO (Right).

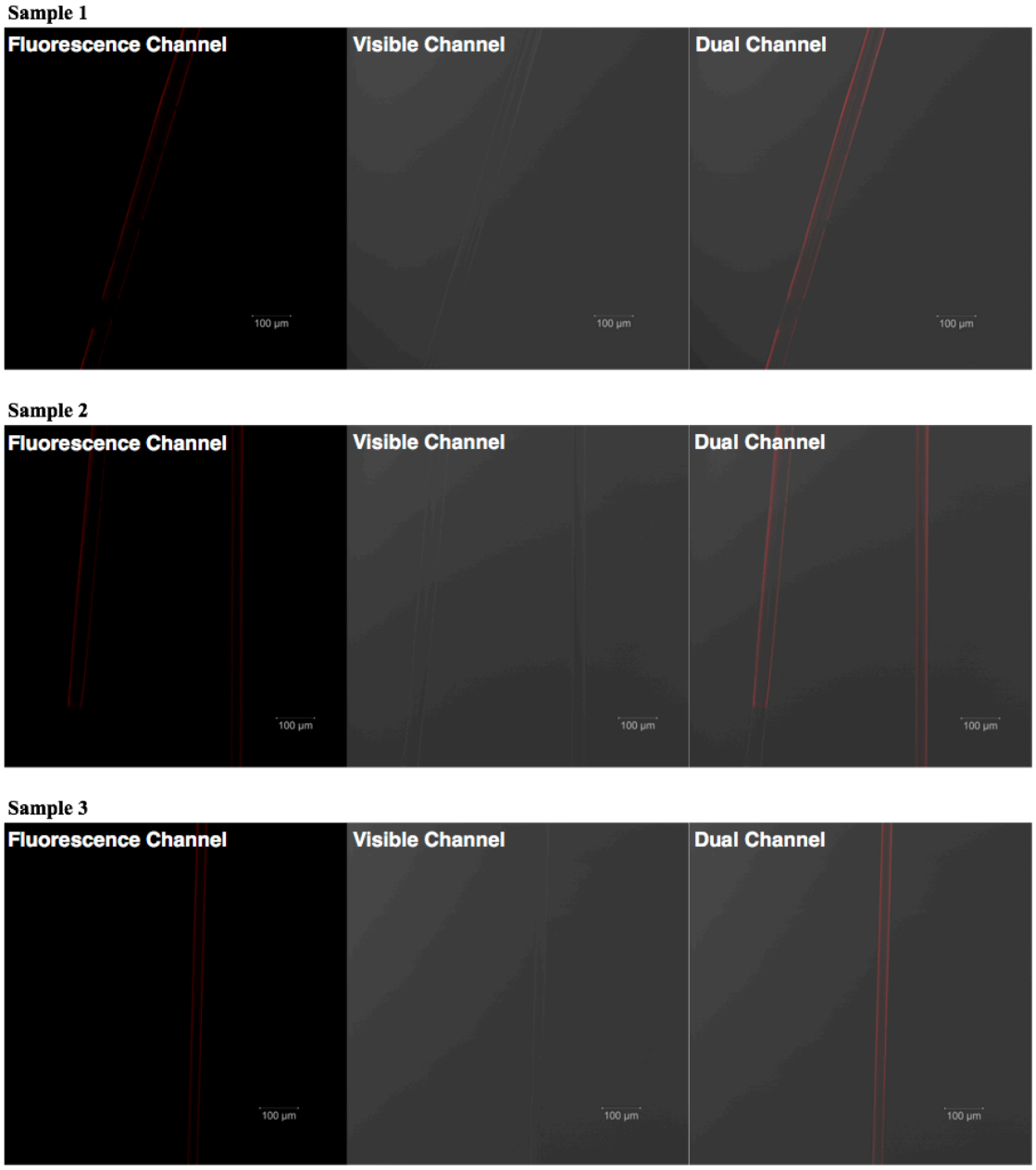

Figure 3.19: Confocal images of oxidizing DHTz-microfibers by horseradish peroxidase (HRP): positive sets.

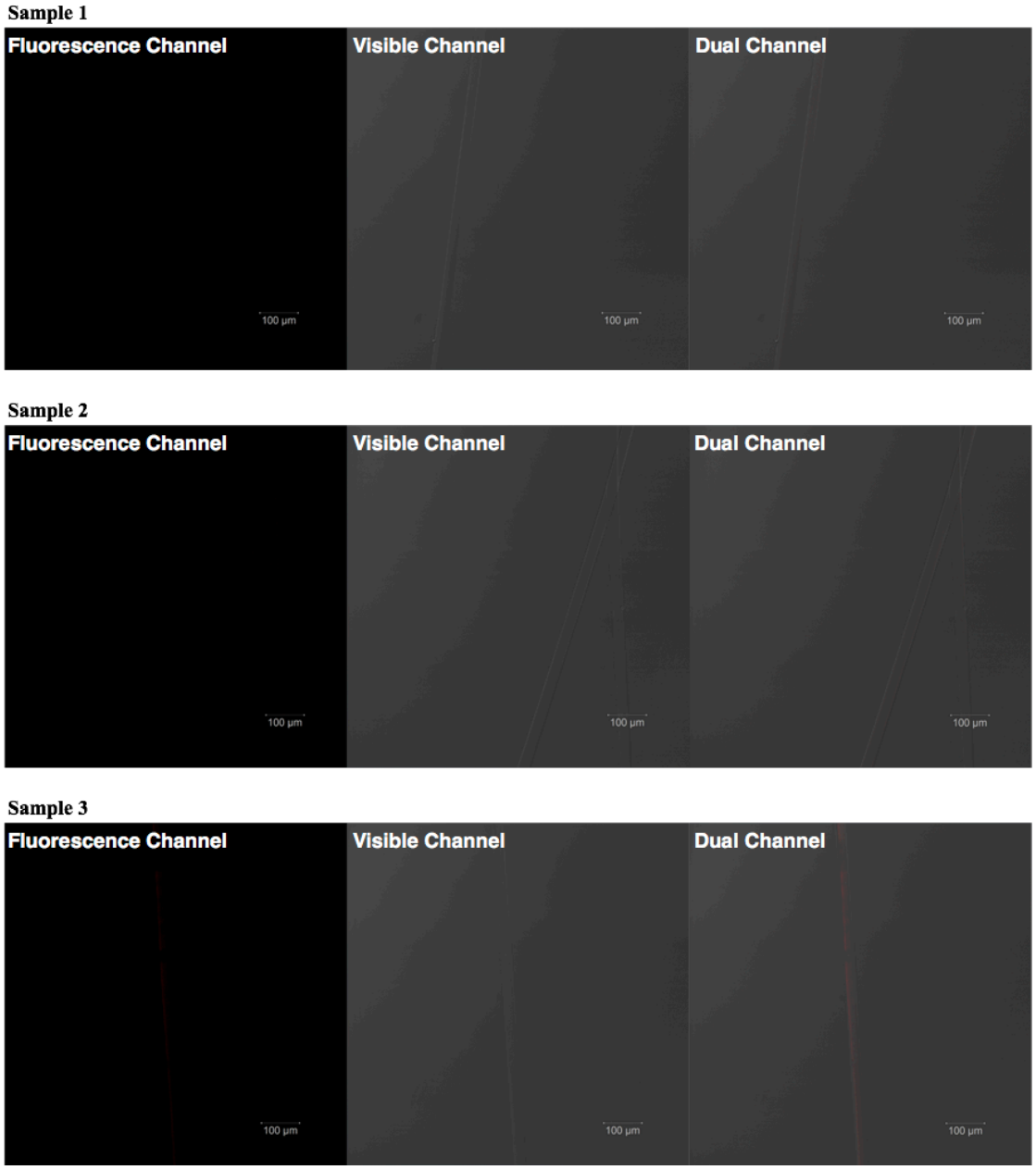

Figure 3.20: Confocal images of oxidizing DHTz-microfibers by horseradish peroxidase (HRP): control sets without HRP

The photocatalytic activation of tetrazines was also employed in the post-synthetic modification of the fibers with peptidic cues that promote cell adhesion and contact guidance. RGD-sTCO was conjugated to activated fibers through tetrazine ligation, and the resulting fibers were immobilized in silicone wells coated with poly(2-hydroxyethyl methacrylate) to eliminate cellular adhesion to the culture wells. Cell culture experiments conducted by Dr. Shuang Liu showed fibroblasts selectively attached to RGD-tagged fibers and elongated along the long axis of the fibers, adopting a healthy fibroblastic morphology (Figure 3.21). Cell attachment and spreading was not observed in control experiments (Figure 3.22-24) where the sensitizer and/or the RGD-sTCO were excluded. These studies demonstrate the ability to functionalize biomimetic fibers with molecules that can enable visualization or promote cell adhesion.

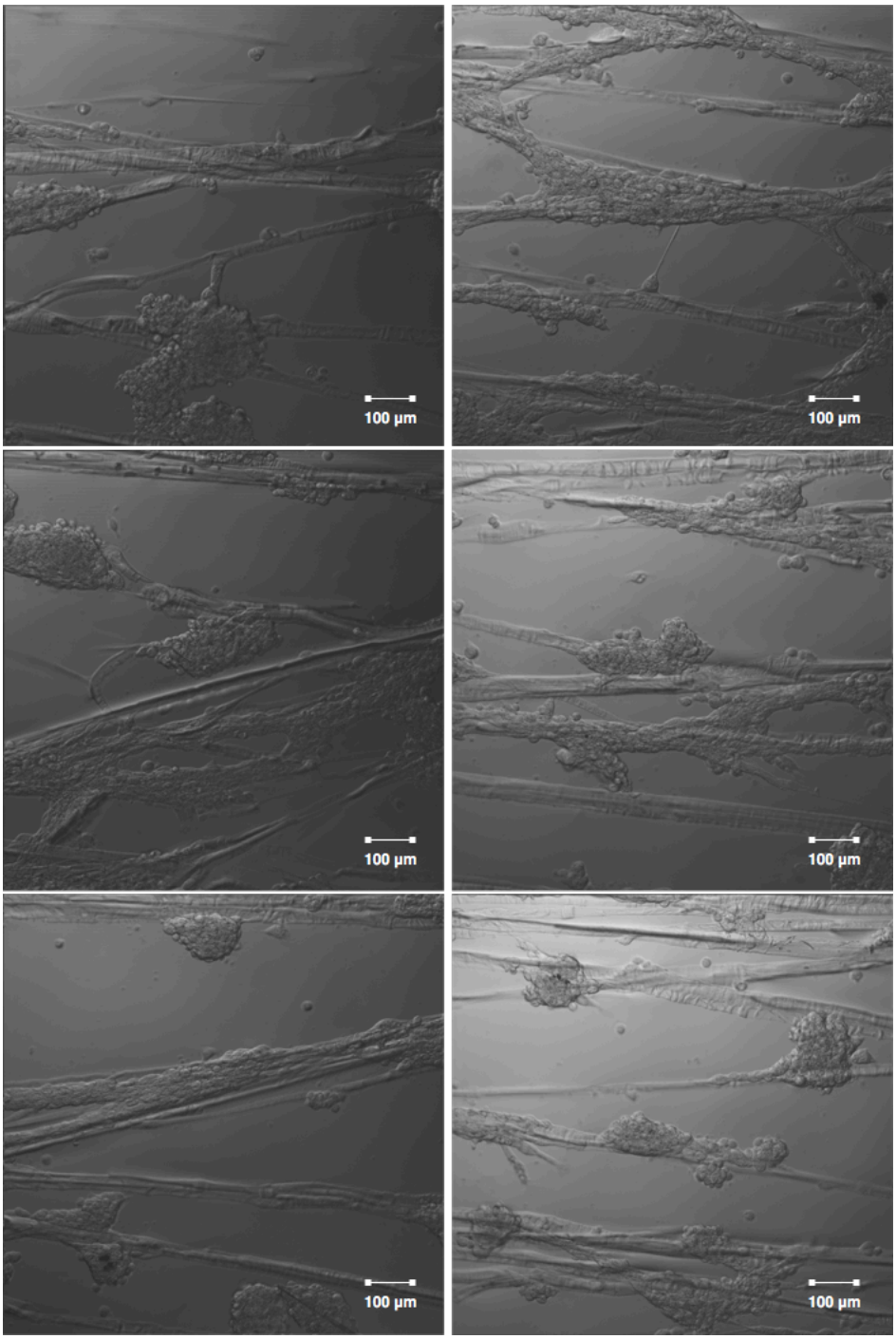

Figure 3.21: Confocal images of RGD peptide tagging experiment: positive sets.

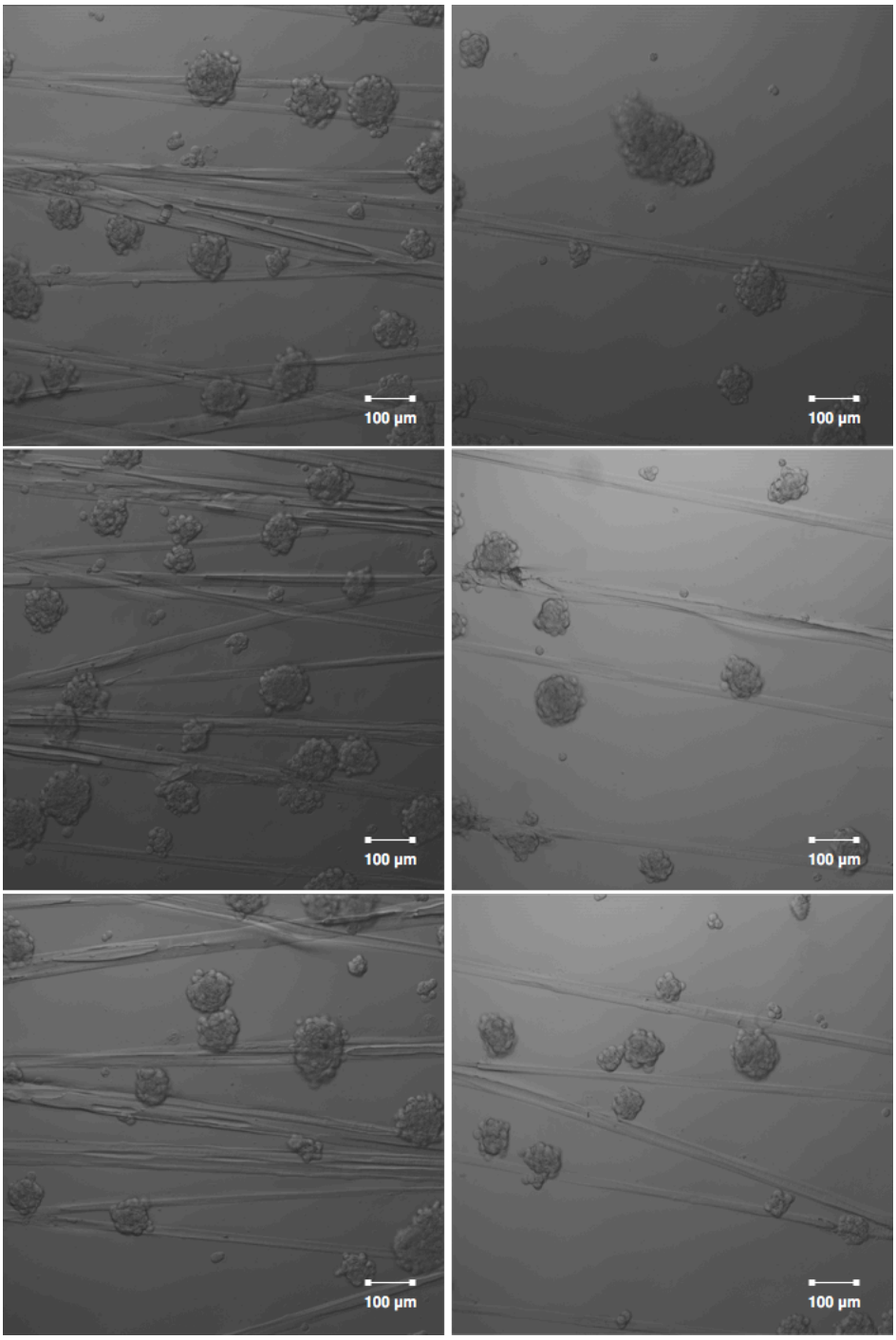

Figure 3.22: Confocal images of RGD peptide tagging experiment: control sets without sensitizer.

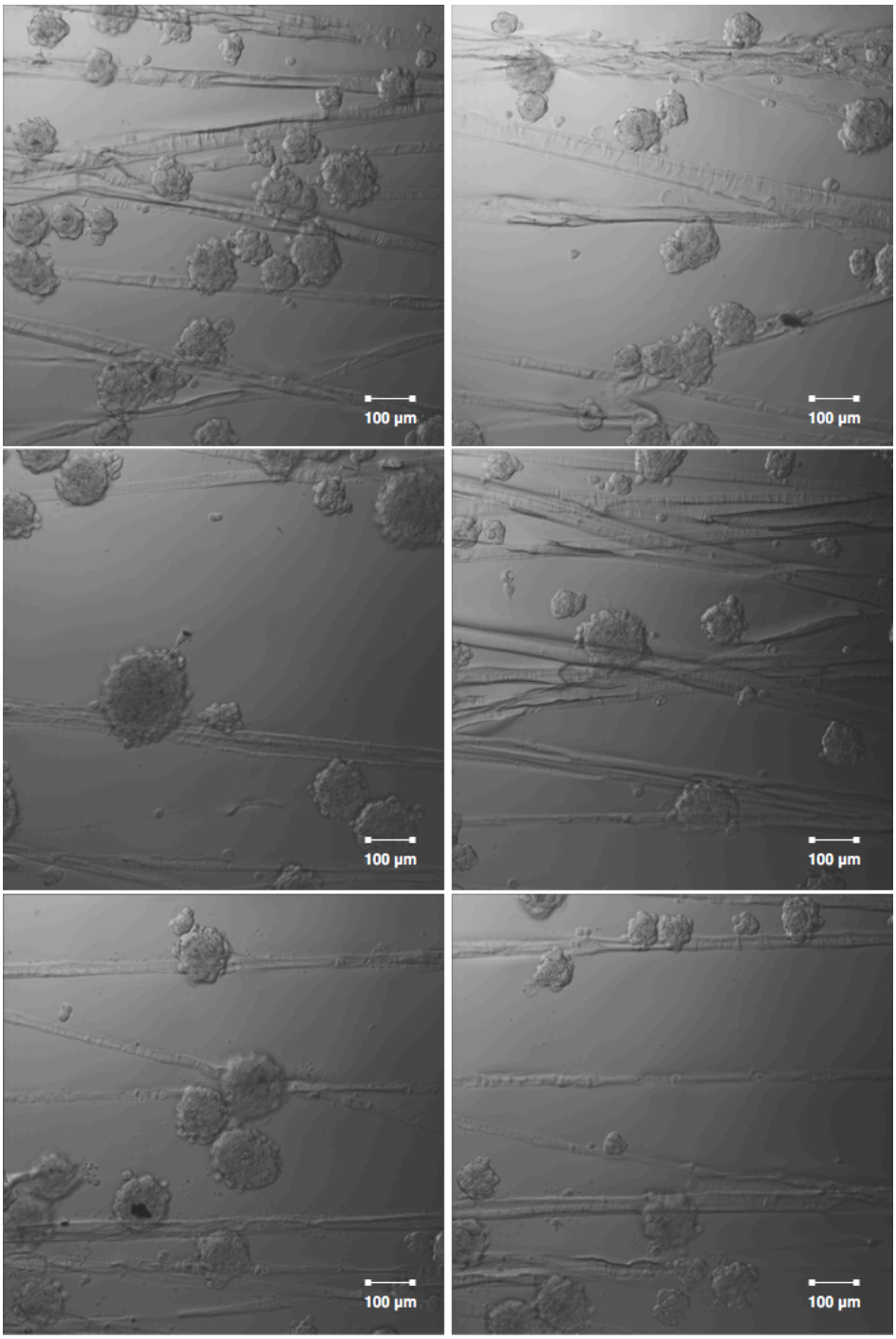

Figure 3.23: Confocal images of RGD peptide tagging experiment: control sets without sensitizer.

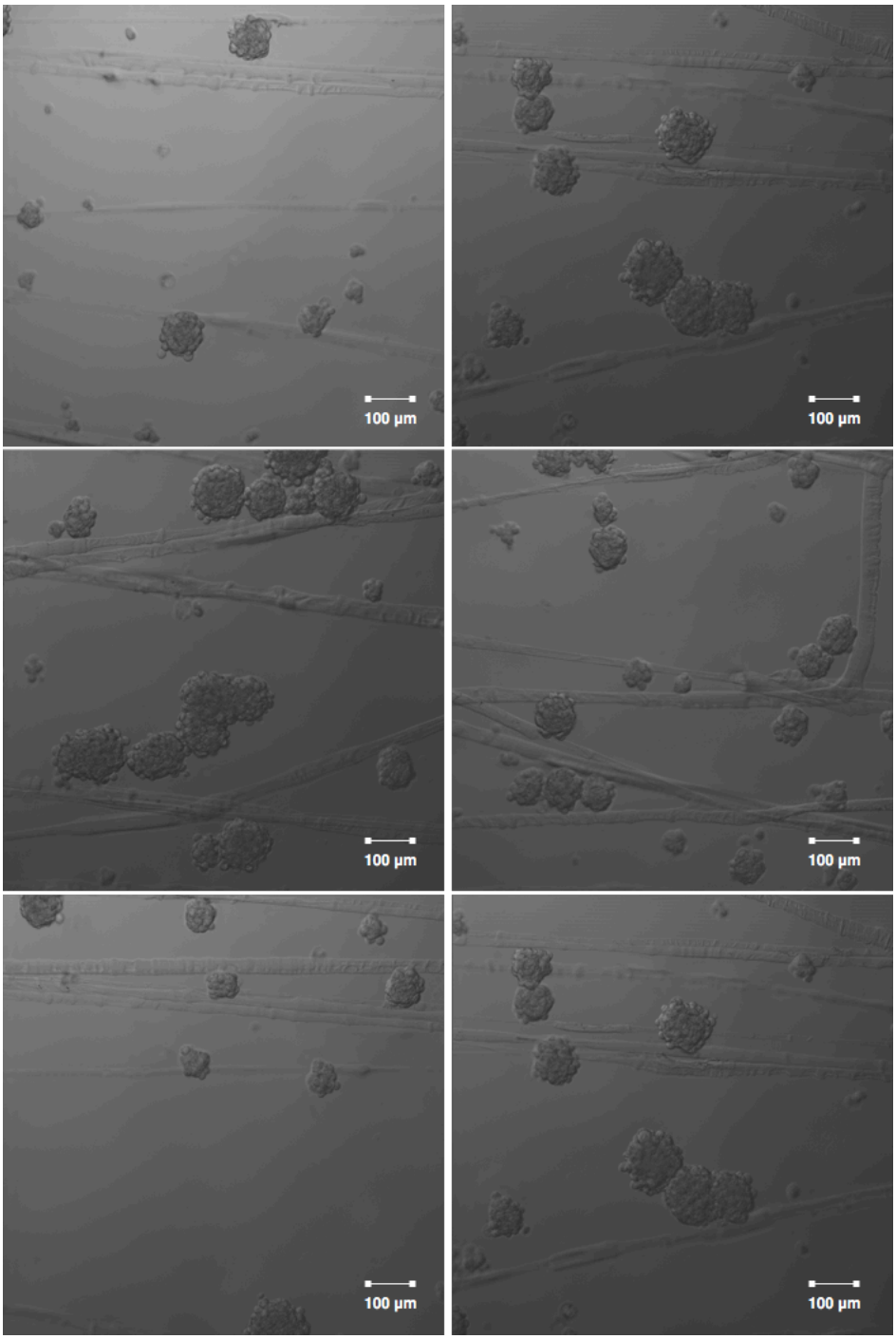

Figure 3.24: Confocal images of RGD peptide tagging experiment: control sets without RGD or sensitizer.

3.5 Conclusions

In this chapter, I described a novel method in which near-IR light or HRP enzyme can be used to activate rapid bioorthogonal reactivity catalytically. This was achieved by catalytic conversion of an unreactive, latent dihydrotetrazine to reaction-ready tetrazine functionality.

Series of long wavelength photosensitizers were found to catalyze the oxidation of DHTz to Tz effieciently in the presence of light and air. Horseradish peroxidase (HRP) was found to catalyze the oxidation at nanomolar concentrations in absence of peroxide. Our methods can provide a milder and more physiology-friendly way to "turn-on" rapid tetrazine ligation reactivity with great promise in extending to a wide range of applications in materials, cellular, and in vivo systems.

Moreover, based on the previous bioorthogonal interfacial polymerization developed from our group, I successfully incorporated DHTz functionality onto the copolymer fibers, which can be activated postsynthetically by either light or an HRP enzyme. Conjugations with small molecule fluorophores, cell-instructive peptide sequences and fluorescent proteins were accomplished, providing a new tool for modulating the cell adhesive properties of a biomaterial.

Future directions include pursuing of more stable DHTz/Tz pairs and exploring further applications in cell imaging, pretargeted prodrug activation and tissue engineering.

3.6 Experimental Procedures

3.6.1 General Considerations

All reactions were carried out in glassware that was flame-dried under vacuum and cooled under nitrogen. THF was purified by distillation from Na/benzophenone. Flash Chromatography was performed using normal phase Silicycle silica gel (40-63D, 60Å). An APT pulse sequence was used for ^{13}C NMR spectra, where methylene and quaternary carbons appear 'up' (u), and methine and methyl carbons appear 'down' (dn). (1R,8S,9R,4E)-bicyclo[6.1.0]non-4-en-9-ylmethyl(4-nitrophenyl) carbonate[51], (rel-1R,8S,9R,4E)-Bicyclo [6.1.0]non-4-ene-9-ylmethyl-N-2maleimidoethyl carbamate,[51] 6-(6-(pyridin-2-yl)-1,4-dihydro-1,2,4,5-tetrazin-3-yl)pyridin-3-amine,[40] 6-(6-(pyridin-2-yl)-1,2,4,5-tetrazin-3-yl)pyridin-3-amine[40] and ((1*R*,8*S*,9*r*,*E*)-bicyclo[6.1.0]non-4-en-9-yl)methyl *tert*-butyl (3,6,9,12,15,18,21,24,27,30,33-undecaoxapentatriacontane-1,35-diyl)dicarbamate[52](**3-12**) were prepared following known procedures. Other solvents and reagents were purchased from commercial sources without additional purification.

3.6.2 Synthetic Procedures

4-oxo-4-((6-(6-(pyridin-2-yl)-1,4-dihydro-1,2,4,5-tetrazin-3-yl)pyridin-3-yl)amino)butanoic acid (3-1)

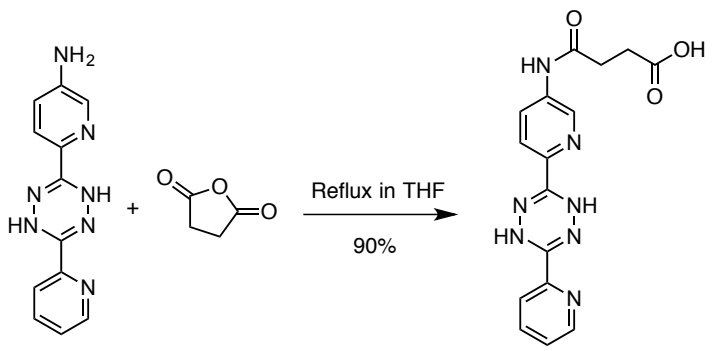

3-1

To a dry round-bottom flask was added 6-(6-(pyridin-2-yl)-1,4-dihydro-1,2,4,5-tetrazin-3-yl)pyridin-3-amine(200 mg, 0.79 mmol),[40] succinic anhydride (400 mg, 4.00 mmol) and anhydrous THF (8 mL). The mixture was refluxed for 24 hours at 60 °C and then cooled by an ice bath. The precipitate was filtered and sequentially washed by THF (2 mL) and ethyl acetate (3×3 mL) and dried to yield the title compound **3-1** (251 mg, 0.71 mmol, 90%) as an orange solid. ^{1}H NMR (400 MHz, DMSO-d_6, δ): 12.20 (br, 1H), 10.47 (s, 1H), 8.95 (s, 1H), 8.89 (s, 1H), 8.82 (d, J = 2.4 Hz, 1H), 8.71 – 8.58 (m, 1H), 8.14 (dd, J = 8.8, 2.5 Hz, 1H), 8.01 – 7.85 (m, 3H), 7.53 (ddd, J = 6.9, 4.8, 1.6 Hz, 1H), 2.63 (t, J = 6.6 Hz, 2H), 2.54 (t, J = 6.9 Hz, 2H). ^{13}C NMR (100 MHz, DMSO-d_6, δ): 173.83 (u, 1C), 171.10 (u, 1C), 148.67 (dn, 1C), 147.36 (u, 1C), 146.42 (u, 1C), 146.15 (u, 1C), 141.43 (u, 1C), 138.75 (dn, 1C), 137.48 (dn, 1C), 137.33 (u, 1C), 126.55 (dn, 1C), 125.38 (dn, 1C), 121.49 (dn, 1C), 121.02 (dn, 1C), 31.07 (u, 1C), 28.63 (u, 1C). HRMS (LIFDI) [M^+]: calcd. for $C_{16}H_{15}N_7O_3^+$, 353.1236 found 353.1277.

5-oxo-5-((6-(6-(pyridin-2-yl)-1,4-dihydro-1,2,4,5-tetrazin-3-yl)pyridin-3-yl)amino)pentanoic acid (3-2)

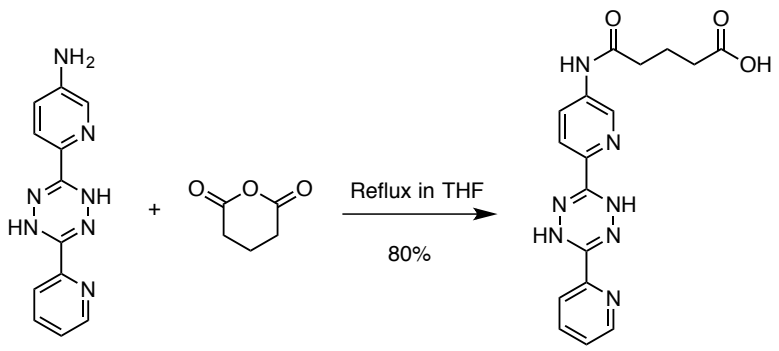

3-2

To a dry round-bottom flask was added 6-(6-(pyridin-2-yl)-1,4-dihydro-1,2,4,5-tetrazin-3-yl)pyridin-3-amine(1.87 g, 7.39 mmol),[40] glutaric anhydride (1.01 g, 8.87 mmol) and anhydrous THF (70 mL). The mixture was refluxed for 24 hours at 60 °C and then cooled by an ice bath. The precipitate was filtered on a Buchner funnel and sequentially rinsed by THF (10 mL) and ethyl acetate (3×10 mL) and dried to yield the title compound **3-2** (2.16 g, 5.89 mmol, 80%) as a orange solid. ^{1}H NMR (600 MHz, DMSO-d_6, δ): 12.22 (br, 1H), 10.40 (s, 1H), 8.95 (s, 1H), 8.90 (s, 1H), 8.81 (d, J = 2.4 Hz, 1H), 8.67 – 8.58 (m, 1H), 8.16 (dd, J = 8.8, 2.5 Hz, 1H), 8.02 – 7.85 (m, 3H), 7.53 (ddd, J = 6.9, 4.8, 1.6 Hz, 1H), 2.42 (t, J = 7.4 Hz, 2H), 2.29 (t, J = 7.3 Hz, 2H), 1.89 – 1.76 (m, 2H). ^{13}C NMR (100 MHz, DMSO-d_6, δ): 174.25 (u, 1C), 171.68 (u, 1C), 148.66 (dn, 1C), 147.35 (u, 1C), 146.42 (u, 1C), 146.15 (u, 1C), 141.45 (u, 1C), 138.91 (dn, 1C), 137.47 (dn, 1C), 137.31 (u, 1C), 126.69 (dn, 1C), 125.37 (dn, 1C), 121.45 (dn, 1C), 121.02 (dn, 1C), 35.36 (u, 1C), 32.96 (u, 1C), 20.24 (u, 1C). HRMS (LIFDI) [M^+]: calcd. for $C_{17}H_{17}N_7O_3^+$, 367.1393 found 367.1403.

4-oxo-4-((6-(6-(pyridin-2-yl)-1,2,4,5-tetrazin-3-yl)pyridin-3-yl)amino)butanoic acid (3-3)

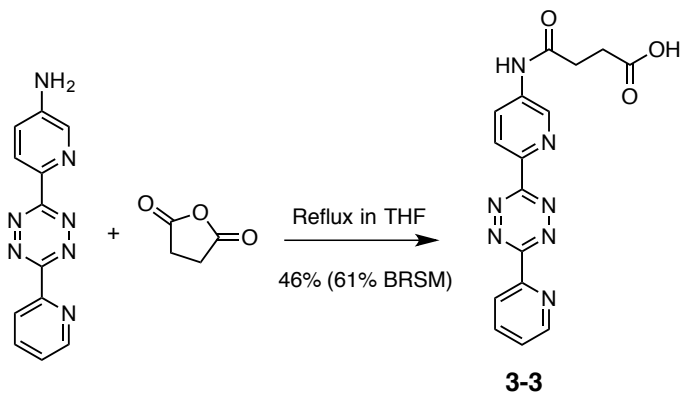

3-3

This synthesis was carried out by William Trout as described in reference.[53]

2,5-dioxopyrrolidin-1-yl 5-oxo-5-((6-(6-(pyridin-2-yl)-1,4-dihydro-1,2,4,5-tetrazin-3-yl)pyridin-3-yl)amino)pentanoate (3-8)

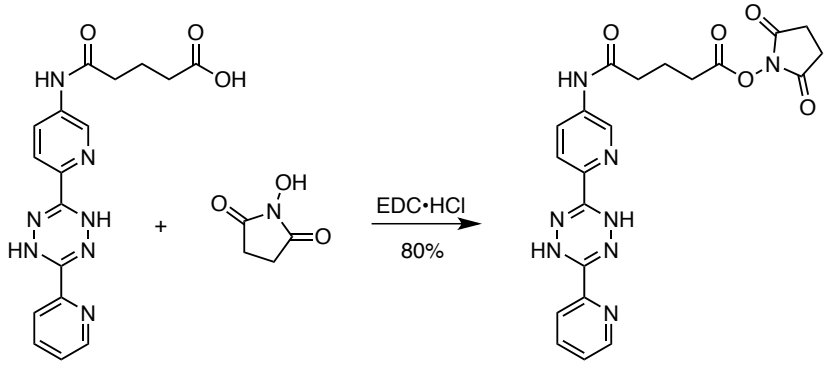

3-2 **3-8**

To a dry round-bottom flask was added **3-2** (200 mg, 0.54 mmol), *N*-hydroxysuccinimide (125 mg, 1.09 mmol), *N*-(3-dimethylaminopropyl)-*N'*-ethylcarbodiimide hydrochloride (209 mg, 1.09 mmol) and anhydrous DMF (2 mL). The mixture was stirred for 1 hour at room temperature. DMF was removed by rotary evaporation at 50 °C using an efficient vacuum pump (<1 torr). The crude product was dissolved in acetone and then concentrated onto silica gel. Purification by column chromatography using a gradient (10%-70%) of acetone in hexanes yielded 202 mg (0.44 mmol, 80%) of the title compound **3-8** as an orange solid. ^{1}H NMR (600 MHz,

$CDCl_3$, δ): 8.61 (d, *J* = 2.5 Hz, 1H), 8.57 (dd, *J* = 4.8, 1.4 Hz, 1H), 8.53 (s, 1H), 8.48 (s, 1H), 8.31 (s, 1H), 8.20 (dd, *J* = 8.8, 2.6 Hz, 1H), 8.10 – 7.96 (m, 2H), 7.78 – 7.70 (m, 1H), 7.35 (dd, *J* = 7.5, 4.9 Hz, 1H), 2.97 – 2.90 (m, 4H), 2.76 – 2.70 (m, 2H), 2.55 – 2.50 (m, 2H), 2.28 – 2.19 (m, 2H). ^{13}C NMR (100 MHz, $CDCl_3$, δ): 170.70 (u, 1C), 169.86 (u, 2C), 168.44 (u, 1C), 148.53 (dn, 1C), 147.60 (u, 1C), 146.91 (u, 1C), 146.48 (u, 1C), 142.80 (u, 1C), 139.32 (dn, 1C), 136.86 (dn, 1C), 136.26 (u, 1C), 127.29 (dn, 1C), 125.02 (dn, 1C), 121.75 (dn, 1C), 121.35 (dn, 1C), 35.47 (u, 1C), 29.94 (u, 1C), 25.80 (u, 2C), 21.41 (u, 1C). HRMS (LIFDI) [M^+]: calcd. for $C_{21}H_{20}N_8O_5^+$, 464.1557 found 464.1541.

bis(((E)-bicyclo[6.1.0]non-4-en-9-yl)methyl) (2-hydroxypropane-1,3-diyl)dicarbamate (3-9)

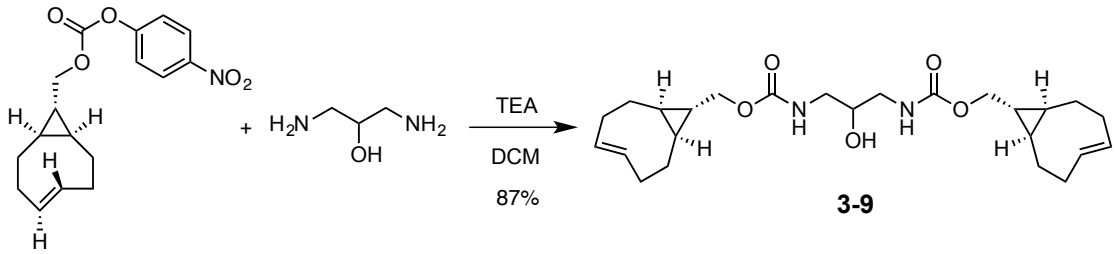

A dry round-bottom flask was sequentially charged *via* syringe with a solution of 1,3-diamino-2-propanol (120 mg, 1.33 mmol) in anhydrous dichloromethane (20 mL) followed by anhydrous triethylamine (744 µL, 5.37 mmol) and (1R,8S,9R,4E)-bicyclo[6.1.0]non-4-en-9-ylmethyl(4-nitrophenyl) carbonate(930 mg, 2.93 mmol).[51] The mixture was stirred overnight at room temperature, diluted with dichloromethane (30 mL) followed by exhaustive aqueous wash (5×50 mL). The organic layer was dried with $MgSO_4$, filtered and then the solvent was removed with a rotary evaporator.

Purification by column chromatography first using 10% ethyl acetate in hexanes then switching to 30% acetone in hexanes yielded the title compound **3-9** (520 mg, 1.16 mmol, 87%) as a colorless oil. ^{1}H NMR (600 MHz, $CDCl_3$, δ): 5.82 (ddd, *J* = 16.1, 9.3, 6.1 Hz, 2H), 5.29 (br, 2H), 5.12 (ddd, *J* = 16.1, 10.6, 3.4 Hz, 2H), 3.94 (d, *J* = 6.3 Hz, 4H), 3.74 – 3.80 (m, 1H), 3.47 (br, 1H), 3.35 – 3.15 (m, 4H), 2.39 – 3.32 (m, 2H), 2.30 – 2.24 (m, 4H), 2.24 – 2.14 (m, 2H), 2.00 – 1.86 (m, 4H), 0.90 – 0.78 (m, 2H), 0.60 – 0.50 (m, 4H), 0.45 – 0.36 (m, 4H).^{13}C NMR (100 MHz, $CDCl_3$, δ): 158.26 (u, 2C), 138.49 (dn, 2C), 131.43 (dn, 2C), 71.10 (dn, 1C), 70.11 (u, 2C), 43.82 (u, 2C), 38.78 (u, 2C), 33.89 (u, 2C), 32.70 (u, 2C), 27.76 (u, 2C), 24.69 (dn, 2C), 22.14 (dn, 2C), 21.12 (dn, 2C). HRMS (LIFDI) [M^+]: calcd. for $C_{25}H_{38}N_2O_5^+$, 446.2781 found 446.2791.

bis(((E)-bicyclo[6.1.0]non-4-en-9-yl)methyl) (2-(((4-nitrophenoxy)carbonyl) oxy)propane-1,3-diyl)dicarbamate (3-10)

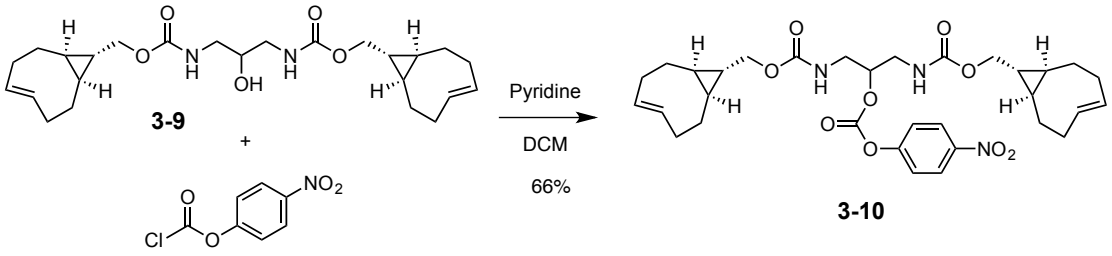

A dry round-bottled flask was charged with **3-9** (500 mg, 1.12 mmol). Anhydrous dichloromethane (30 mL) and pyridine (0.23 mL, 2.80 mmol) were added to the flask. A solution of 4-nitrophenylchloroformate (271 mg, 1.34 mmol) in anhydrous dichloromethane (4 mL) was added to the flask via syringe and the solution was stirred for 1 h at room temperature. Saturated aq. NH_4Cl was added to the mixture and the layers were separated, and the aqueous layer was extracted twice with

dichloromethane. The organic layers were combined, dried with $MgSO_4$ and filtered, and the solvent was removed using a rotary evaporator. Purification by column chromatography (10% to 30% ethyl actetate/hexanes) yielded 450 mg (0.74 mmol, 66%) of the title compound **3-10** as a white solid. ^{1}H NMR (600 MHz, $CDCl_3$, δ): 8.28 (d, *J* = 9.2 Hz, 2H), 7.41 (d, *J* = 9.2 Hz, 2H), 5.85 (ddd, *J* = 16.0, 9.3, 6.2 Hz, 2H), 5.41 – 5.22 (m, 2H), 5.11 (ddd, *J* = 16.8, 10.5, 3.9 Hz, 2H), 4.83 – 4.75 (m, 1H), 3.96 (d, *J* = 6.5 Hz, 4H), 3.79 – 3.17 (m, 4H), 2.40 – 2.30 (m, 2H), 2.30 – 2.15 (m, 6H), 2.01 – 1.80 (m, 4H), 0.90 – 0.75 (m, 2H), 0.62 – 0.48 (m, 4H), 0.45 – 0.35 (m, 4H). ^{13}C NMR (100 MHz, $CDCl_3$, δ): 157.49 (u, 2C), 155.51 (u, 1C), 151.85 (u, 1C), 145.59 (u, 1C), 138.45 (dn, 2C), 131.41 (dn, 2C), 125.48 (dn, 2C), 122.00 (dn, 2C), 76.95 (dn, 1C), 70.19 (u, 2C), 40.06 (u, 2C), 38.75 (u, 2C), 33.86 (u, 2C), 32.67 (u, 2C), 27.73 (u, 2C), 24.69 (dn, 2C), 22.14 (dn, 2C), 21.13 (dn, 2C). HRMS (LIFDI) [M^+]: calcd. for $C_{32}H_{41}N_3O_9^+$, 611.2843 found 611.2837.

bis(((E)-bicyclo[6.1.0]non-4-en-9-yl)methyl) (2-(((2-aminoethyl)carbamoyl) oxy)propane-1,3-diyl)dicarbamate (3-11)

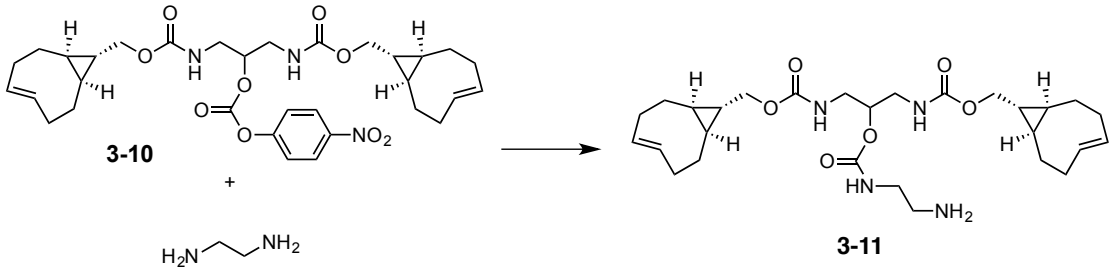

A dry round-bottom flask was sequentially charged *via* syringe with ethylenediamine (218 μL, 3.27 mmol) followed by a solution of **3-10** (100 mg, 0.16 mmol) in anhydrous dichloromethane (4 mL). The solution was stirred for 1 h at room

temperature, diluted with dichloromethane (15 mL) and followed by exhaustive aqueous washes (5×30 mL). The organic layer was dried with $MgSO_4$, filtered and concentrated down with a rotary evaporator to afford the title compound **3-11** (80 mg, 92% crude yield) as a pale yellow solid. The crude product was carried to the next step of synthesis without further purification.

bis(((E)-bicyclo[6.1.0]non-4-en-9-yl)methyl) (2-(((2-(5-oxo-5-((6-(6-(pyridin-2-yl)-1,4-dihydro-1,2,4,5-tetrazin-3-yl)pyridin-3-yl)amino)pentanamido)ethyl) carbamoyl)oxy)propane-1,3-diyl)dicarbamate (3-5)

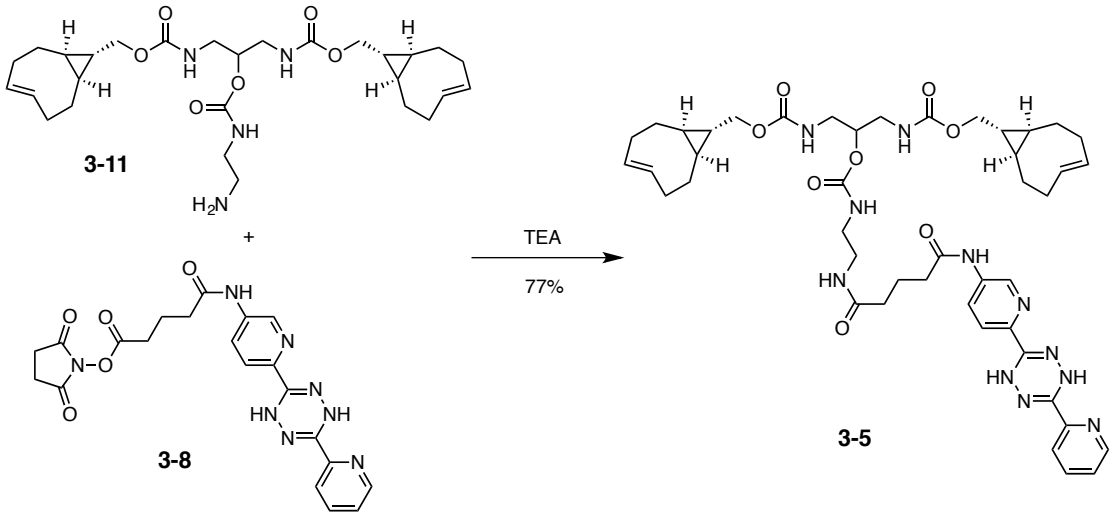

To a dry round-bottom flask was added **3-11** (39 mg, 73.3 μmol), **3-8** (25 mg, 53.9 μmol) and a solution of triethylamine (17 μL, 0.12 mmol) in dichloromethane (2 mL). The mixture was stirred for 1 hour under room temperature and then concentrated onto silica gel using a rotary evaporator. Purification by column chromatography using a gradient (20%-70%) of acetone in hexanes yielded the title compound **3-5** (37 mg, 42.0 μmol, 77%) as an orange solid. ^{1}H NMR (400 MHz,

MeOH-d_4, δ): 8.85 (d, J = 2.4 Hz, 1H), 8.64 (dt, J = 5.0, 1.3 Hz, 1H), 8.16 (dd, J = 8.7, 2.6 Hz, 1H), 8.06 (d, J = 7.9 Hz, 1H), 8.01 (d, J = 8.7 Hz, 1H), 7.89 (td, J = 7.7, 1.7 Hz, 1H), 7.48 (ddd, J = 7.5, 4.9, 1.1 Hz, 1H), 5.85 (ddd, J = 16.2, 9.3, 6.2 Hz, 2H), 5.11 (ddd, J = 16.6, 10.2, 3.7 Hz, 2H), 4.75 – 4.65 (m, 1H), 4.02 – 3.79 (m, 4H), 3.43 – 3.27 (m, 4H), 3.27 – 3.12 (m, 4H), 2.54 – 2.44 (m, 2H), 2.39 – 2.28 (m, 4H), 2.28 – 2.11 (m, 6H), 2.08 – 1.97 (m, 2H) 1.98 – 1.80 (m, 4H), 0.94 – 0.79 (m, 2H), 0.68 – 0.49 (m, 4H), 0.49 – 0.35 (m, 4H).^{13}C NMR (100 MHz, MeOH-d_4, δ): 175.67 (u, 1C), 174.17 (u, 1C), 159.44 (u, 1C), 158.42 (u, 2C), 149.82 (dn, 1C), 148.86 (u, 1C), 148.32 (u, 1C), 148.06 (u, 1C), 143.49 (u, 1C), 140.85 (dn, 1C), 139.19 (dn, 2C), 138.51 (u, 1C), 138.26 (dn, 1C), 132.18 (dn, 2C), 128.34 (dn, 1C), 126.36 (dn, 1C), 122.62(dn, 1C), 122.39(dn, 1C), 73.76(dn, 1C), 70.60(u, 2C), 42.28(u, 1C), 41.47(u, 1C), 40.32 (u, 2C), 39.68 (u, 2C), 36.85 (u, 1C), 36.10 (u, 1C), 34.67 (u, 2C), 33.64 (u, 2C), 28.55 (u, 2C), 25.96 (dn, 2C), 23.26 (dn, 2C), 22.63 (u, 1C), 22.21 (dn, 2C). HRMS (ESI) [MH^+]: calcd. for $C_{45}H_{60}N_{11}O_8^+$, 882.4626 found 882.4635.

3.6.3 DHTz-Containing Copolymer Fiber Fabrication Experiments

Preparation of DHTz-microfibers

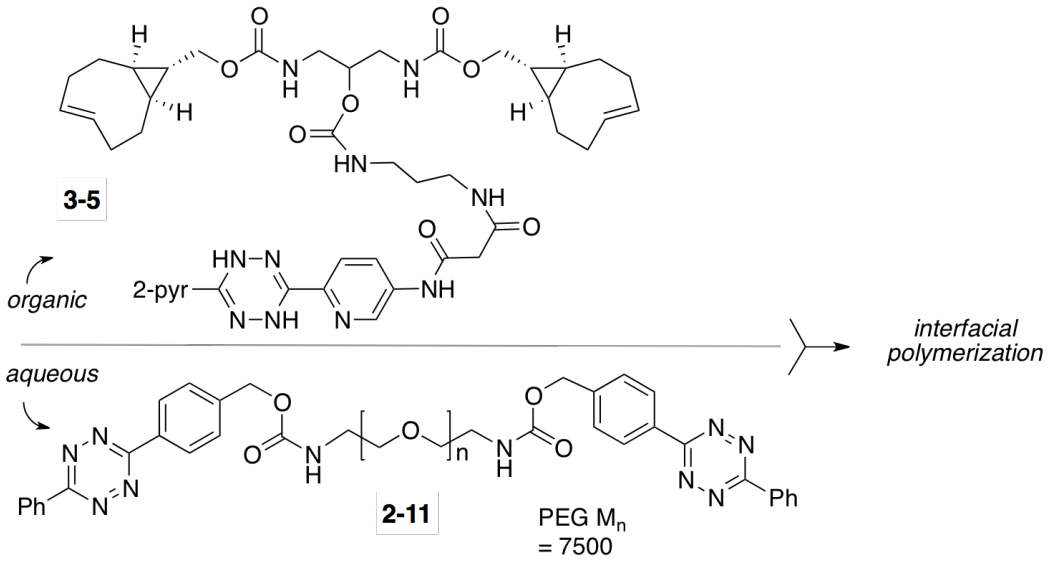

Interfacial polymerization was conducted in accord with our previously described procedure.[49] The DHTz-containing *bis*-sTCO monomer **3-5** was dissolved in ethyl acetate at a concentration of 1.2 mM. The known PEG-based *bis*-tetrazine monomer **2-11** was dissolved in water at a concentration of 0.15 mM. To a 60-mm diameter petri dish was added 3 mL of the aqueous solution of the *bis*-tetrazine monomer **2-11**. The solution of **3-5** (3 mL) in ethyl acetate was carefully added over the aqueous phase without disturbing the interface. Upon contact, a polymer thin film formed at the interface. The thin film was grasped gently using sharp tweezers and the fiber that was pulled from the interface was connected to a collecting frame that was constructed of copper wire. The fiber was collected by manually rotating the frame. The microfibers were dried affixed onto pre-cleaned glass slides using adhesive silicon isolators (Purchased from Grace Bio-Labs, product #665301).

To 'cap' any unreacted tetrazine endgroups from the monomer **2-11**, the fibers were treated with the water soluble sTCO derivative **3-12**[52] (shown below, synthesized following a known procedure). Thus, to a silicon isolator containing DHTz-enriched microfibers was added PBS solution of **3-12** (1 mM). The microfibers were allowed to soak in the solution for 1 minute before the capping solution was removed. The microfibers were then rinsed using PBS solution for 3 times.

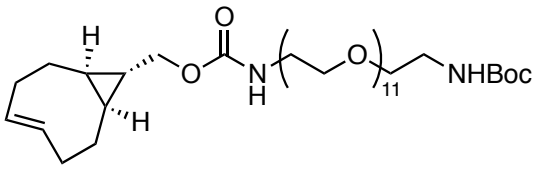

3-12

Alexa Fluor® 647 tagging experiment and control experiments

To silicon isolator containing DHTz-functionalized microfibers was added a PBS solution of rose bengal (100 μM). The microfibers were allowed to soak in the solution for 5 minutes before rose bengal solution was removed. The microfibers were then rinsed three times with PBS buffer (~3×200 μL). The red microfibers were then immersed in PBS solution and irradiated with a 200-watt incandescent lamp for 5 minutes followed by rinsing with three portions of PBS buffer (~3×200 μL). The microfibers were then treated with a PBS solution of Alexa Fluor® 647-sTCO (1 μM) for 1 minute followed by rinsing with three portions of PBS buffer (~3×200 μL). Samples were imaged with a Zeiss LSM 5 Live DuoScan high-speed confocal microscope (Carl Zeiss, Maple Grove, MN).

Control without light: The procedure was identical to that described above, except that the fibers were prepared in a dark room without exposure to light.

Control without sensitizer: The microfibers were immersed in PBS buffer and irradiated with a 200-watt incandescent lamp for 5 minutes and subsequently rinsed three times with PBS buffer (~3×200 μL). The microfibers were then treated with a PBS solution of Alexa Fluor® 647-sTCO (1 μM) for 1 minute followed by three rinses with PBS buffer (~3×200 μL). Samples were imaged with a Zeiss LSM 5 Live DuoScan highspeed confocal microscope (Carl Zeiss, Maple Grove, MN).

Clover protein tagging experiment and control experiment

In a silicon isolator, DHTz-functionalized microfibers were immersed in a PBS solution of methylene blue (100 μM) and irradiated with a 200-watt incandescent lamp for 5 minutes. The microfibers were then rinsed with three portions of PBS buffer (~3×200 μL) and treated with a PBS solution of Clover-sTCO (5 μM) for 1 minute followed by rinsing with three portions of PBS buffer (~3×200 μL). Samples were imaged with a Zeiss LSM 5 Live DuoScan high-speed confocal microscope (Carl Zeiss, Maple Grove, MN).

Control without sensitizer: The microfibers were immersed in PBS solution and irradiated with a 200-watt incandescent lamp for 5 minutes followed by rinsing with three portions of PBS buffer (~3×200 μL). The microfibers were then treated by PBS solution of Clover-sTCO (5 μM) for 1 minute followed by rinsing with three portions of PBS buffer (~3×200 μL). Samples were imaged with a Zeiss LSM 5 Live DuoScan high-speed confocal microscope (Carl Zeiss, Maple Grove, MN).

Oxidation of DHTz-microfibers by horseradish peroxidase (HRP)

To silicon isolator containing DHTz-microfibers was added a PBS solution of HRP (10 μM). After the microfibers had been immersed in the solution for 1 hour, they were rinsed with three portions of PBS buffer (~3×200 μL). The microfibers were then treated with a PBS solution of Alexa Fluor® 647-sTCO (1 μM) for 1 minute followed by rinsing with three portions of PBS buffer (~3×200 μL). Samples were imaged with a Zeiss LSM 5 Live DuoScan high-speed confocal microscope (Carl Zeiss, Maple Grove, MN).

Control without HRP: The microfibers were submerged in PBS solution for 1 hour followed by PBS solution rinsing for 3 times. The microfibers were then treated by PBS solution of Alexa Fluor® 647-sTCO (1 μM) for 1 minute followed by rinsing with three portions of PBS buffer (~3×200 μL). Samples were imaged with a Zeiss LSM 5 Live DuoScan high-speed confocal microscope (Carl Zeiss, Maple Grove, MN).

RGD peptide tagging experiment and control experiments

DHTz-microfibers were affixed to a silicone well (9 mm diameter) supported on a poly(2-hydroxyethyl methacrylate) (pHEMA)-coated 1-well Nunc® chamber using silicone isolators (Grace Bio-Labs, product #665301). The fibers were immersed in a solution of methylene blue (100 μM) in PBS, and then irradiated with a 200-watt incandescent lamp for 5 minutes followed by rinsing with three portions of PBS buffer (~3×200 μL). The microfibers were then immersed in a PBS solution of RGD-sTCO (10 μM) for 1 min followed by rinsing with three portions of PBS buffer (~3×200 μL).

Control without sensitizer: In a silicone well, the DHTz-microfibers were immersed in PBS buffer and irradiated with a 200-watt incandescent lamp for 5

minutes followed by rinsing with three portions of PBS buffer (~3×200 μL). The microfibers were then immersed in a PBS solution of RGD-sTCO (10 μM) for 1 min followed by rinsing with three portions of PBS buffer (~3×200 μL).

Control without RGD: The DHTz-microfibers were immersed in a solution of methylene blue (100 μM) in PBS, and irradiated with a 200-watt incandescent lamp for 5 minutes followed by rinsing with three portions of PBS buffer (~3×200 μL).

Control without RGD or sensitizer: The DHTz-microfibers were immersed in PBS and irradiated with a 200-watt incandescent lamp for 5 minutes followed by rinsing with three portions of PBS buffer (~3×200 μL).

Cell culture and confocal imaging

Fibroblasts (NIH 3T3, ATCC, Manassas, VA) were maintained in DMEM media supplemented with 10% fetal bovine serum (FBS) and 1% Pen-Strep (Invitrogen, Carlsbad, CA). DHTz-microfibers were affixed to a silicone well (9 mm diameter) supported on a poly(2-hydroxyethyl methacrylate) (pHEMA)-coated 1-well Nunc® chamber using silicone isolators (Grace Bio-labs, Bend, OR). The fibers were washed with sterile PBS and cell culture media three times respectively before being sterilized under UV for 15 minutes. A 200 μL suspension of cells with a density of 0.5 × 10^6 cells/mL was added into each well and cultured at 37°C for 20 hours before confocal imaging under transmitted light. Samples were imaged with a Zeiss LSM 5 Live DuoScan high-speed confocal microscope (Carl Zeiss, Maple Grove, MN).

REFERENCES

(1) Lim, R. K. V.; Lin, Q. Photoinducible Bioorthogonal Chemistry: A Spatiotemporally Controllable Tool to Visualize and Perturb Proteins in Live Cells. *Acc. Chem. Res.* **2011**, *44*, 828-839.

(2) Grim, J. C.; Marozas, I. A.; Anseth, K. S. Thiol-ene and photo-cleavage chemistry for controlled presentation of biomolecules in hydrogels. *J. Control. Release* **2015**, *219*, 95-106.

(3) Tasdelen, M. A.; Yagci, Y. Light-Induced Click Reactions. *Angew. Chem. Int. Ed.* **2013**, *52*, 5930-5938.

(4) Urdabayev, N. K.; Poloukhtine, A.; Popik, V. V. Two-photon induced photodecarbonylation reaction of cyclopropenones. *Chem. Commun.* **2006**, 454-456.

(5) Arumugam, S.; Orski, S. V.; Mbua, N. E.; McNitt, C.; Boons, G.-J.; Locklin, J.; Popik, V. V. Photo-click chemistry strategies for spatiotemporal control of metal-free ligation, labeling, and surface derivatization. *Pure Appl. Chem.* **2013**, *85*, 1499-1513.

(6) Poloukhtine, A. A.; Mbua, N. E.; Wolfert, M. A.; Boons, G.-J.; Popik, V. V. Selective Labeling of Living Cells by a Photo-Triggered Click Reaction. *J. Am. Chem. Soc.* **2009**, *131*, 15769-15776.

(7) Song, W.; Wang, Y.; Qu, J.; Madden, M. M.; Lin, Q. A Photoinducible 1,3-Dipolar Cycloaddition Reaction for Rapid, Selective Modification of Tetrazole-Containing Proteins. *Angew. Chem. Int. Ed.* **2008**, *47*, 2832-2835.

(8) Ramil, C. P.; Lin, Q. Photoclick chemistry: a fluorogenic light-triggered in vivo ligation reaction. *Curr. Opin. Chem. Biol.* **2014**, *21*, 89-95.

(9) Yu, Z.; Pan, Y.; Wang, Z.; Wang, J.; Lin, Q. Genetically Encoded Cyclopropene Directs Rapid, Photoclick-Chemistry-Mediated Protein Labeling in Mammalian Cells. *Angew. Chem. Int. Ed.* **2012**, *51*, 10600-10604.

(10) Yu, Z.; Lin, Q. Design of Spiro[2.3]hex-1-ene, a Genetically Encodable Double-Strained Alkene for Superfast Photoclick Chemistry. *J. Am. Chem. Soc.* **2014**, *136*, 4153-4156.

(11) Madden, M. M.; Rivera Vera, C. I.; Song, W.; Lin, Q. Facile synthesis of stapled, structurally reinforced peptide helices via a photoinduced intramolecular 1,3-dipolar cycloaddition reaction. *Chem. Commun.* **2009**, 5588-5590.

(12) Wang, J.; Zhang, W.; Song, W.; Wang, Y.; Yu, Z.; Li, J.; Wu, M.; Wang, L.; Zang, J.; Lin, Q. A Biosynthetic Route to Photoclick Chemistry on Proteins. *J. Am. Chem. Soc.* **2010**, *132*, 14812-14818.

(13) Song, W.; Wang, Y.; Qu, J.; Lin, Q. Selective Functionalization of a Genetically Encoded Alkene-Containing Protein via "Photoclick Chemistry" in Bacterial Cells. *J. Am. Chem. Soc.* **2008**, *130*, 9654-9655.

(14) He, M.; Li, J.; Tan, S.; Wang, R.; Zhang, Y. Photodegradable Supramolecular Hydrogels with Fluorescence Turn-On Reporter for Photomodulation of Cellular Microenvironments. *J. Am. Chem. Soc.* **2013**, *135*, 18718-18721.

(15) Fan, Y.; Deng, C.; Cheng, R.; Meng, F.; Zhong, Z. In Situ Forming Hydrogels via Catalyst-Free and Bioorthogonal "Tetrazole–Alkene" Photo-Click Chemistry. *Biomacromolecules* **2013**, *14*, 2814-2821.

(16) An, P.; Yu, Z.; Lin, Q. Design of oligothiophene-based tetrazoles for laser-triggered photoclick chemistry in living cells. *Chem. Commun.* **2013**, *49*, 9920-9922.

(17) Yu, Z.; Ohulchanskyy, T. Y.; An, P.; Prasad, P. N.; Lin, Q. Fluorogenic, Two-Photon-Triggered Photoclick Chemistry in Live Mammalian Cells. *J. Am. Chem. Soc.* **2013**, *135*, 16766-16769.

(18) An, P.; Yu, Z.; Lin, Q. Design and Synthesis of Laser-Activatable Tetrazoles for a Fast and Fluorogenic Red-Emitting 1,3-Dipolar Cycloaddition Reaction. *Org. Lett.* **2013**, *15*, 5496-5499.

(19) Klán, P.; Šolomek, T.; Bochet, C. G.; Blanc, A.; Givens, R.; Rubina, M.; Popik, V.; Kostikov, A.; Wirz, J. Photoremovable Protecting Groups in Chemistry and Biology: Reaction Mechanisms and Efficacy. *Chem. Rev.* **2013**, *113*, 119-191.

(20) Yang, Y.; Mu, J.; Xing, B. Photoactivated drug delivery and bioimaging. *Wiley Interdisciplinary Reviews: Nanomedicine and Nanobiotechnology* **2017**, *9*, n/a-n/a.

(21) Gorka, A. P.; Nani, R. R.; Zhu, J.; Mackem, S.; Schnermann, M. J. A Near-IR Uncaging Strategy Based on Cyanine Photochemistry. *J. Am. Chem. Soc.* **2014**, *136*, 14153-14159.

(22) Palao, E.; Slanina, T.; Muchová, L.; Šolomek, T.; Vítek, L.; Klán, P. Transition-Metal-Free CO-Releasing BODIPY Derivatives Activatable by Visible to NIR Light as Promising Bioactive Molecules. *J. Am. Chem. Soc.* **2016**, *138*, 126-133.

(23) Nkepang, G.; Bio, M.; Rajaputra, P.; Awuah, S. G.; You, Y. Folate Receptor-Mediated Enhanced and Specific Delivery of Far-Red Light-Activatable Prodrugs of Combretastatin A-4 to FR-Positive Tumor. *Bioconj. Chem.* **2014**, *25*, 2175-2188.

(24) Olejniczak, J.; Carling, C.-J.; Almutairi, A. Photocontrolled release using one-photon absorption of visible or NIR light. *J. Control. Release* **2015**, *219*, 18-30.

(25) Kaim, W. The coordination chemistry of 1,2,4,5-tetrazines. *Coord. Chem. Rev.* **2002**, *230*, 127-139.

(26) Hassink, M.; Liu, X.; Fox, J. M. Copper-Catalyzed Synthesis of 2,4-Disubstituted Allenoates from α-Diazoesters. *Org. Lett.* **2011**, *13*, 2388-2391.

(27) Xue, M.; Ma, S.; Jin, Z.; Schaffino, R. M.; Zhu, G.-S.; Lobkovsky, E. B.; Qiu, S.-L.; Chen, B. Robust Metal−Organic Framework Enforced by Triple-

Framework Interpenetration Exhibiting High H2 Storage Density. *Inorg. Chem.* **2008**, *47*, 6825-6828.

(28) Chavez, D. E.; Hiskey, M. A.; Gilardi, R. D. 3,3′ -Azobis(6-amino-1,2,4,5-tetrazine): A Novel High-Nitrogen Energetic Material. *Angew. Chem. Int. Ed.* **2000**, *39*, 1791-1793.

(29) Wei, T.; Zhu, W.; Zhang, X.; Li, Y.-F.; Xiao, H. Molecular Design of 1,2,4,5-Tetrazine-Based High-Energy Density Materials. *J. Phys. Chem. A* **2009**, *113*, 9404-9412.

(30) Boger, D. L.; Hong, J. Asymmetric Total Synthesis of ent-(−)-Roseophilin: Assignment of Absolute Configuration. *J. Am. Chem. Soc.* **2001**, *123*, 8515-8519.

(31) Hamasaki, A.; Zimpleman, J. M.; Hwang, I.; Boger, D. L. Total Synthesis of Ningalin D. *J. Am. Chem. Soc.* **2005**, *127*, 10767-10770.

(32) Boger, D. L.; Panek, J. S. Formal total synthesis of streptonigrin. *J. Org. Chem.* **1983**, *48*, 621-623.

(33) Hofmann, K. A.; Ehrhart, O. Einwirkung von Hydrazin auf Dicyandiamid. *Ber. Dtsch. Chem. Ges.* **1912**, *45*, 2731-2740.

(34) Abdel, N. O.; Kira, M. A.; Tolba, M. N. A direct synthesis of dihydrotetrazines. *Tetrahedron Lett.* **1968**, *9*, 3871-3872.

(35) Clavier, G.; Audebert, P. s-Tetrazines as Building Blocks for New Functional Molecules and Molecular Materials. *Chem. Rev.* **2010**, *110*, 3299-3314.

(36) Yang, J.; Karver, M. R.; Li, W.; Sahu, S.; Devaraj, N. K. Metal-Catalyzed One-Pot Synthesis of Tetrazines Directly from Aliphatic Nitriles and Hydrazine. *Angew. Chem. Int. Ed.* **2012**, *51*, 5222-5225.

(37) Sauer, J.; Pabst, Gunther R.; Holland, U.; Kim, H.-S.; Loebbecke, S. 3,6-Bis(2H-tetrazol-5-yl)-1,2,4,5-tetrazine: A Versatile Bifunctional Building Block for the Synthesis of Linear Oligoheterocycles. *Eur. J. Org. Chem.* **2001**, *2001*, 697-706.

(38) M. Asselin, C.; C. Fraser, G.; K. Hall Jr, H.; Edward Lindsell, W.; B. Padias, A.; N. Preston, P. Synthesis and metallation of ferrocenylimines derived from ligating diaminoheteroarenes. *J. Chem. Soc., Dalton Trans.* **1997**, 3765-3772.

(39) Blackman, M. L.; Royzen, M.; Fox, J. M. Tetrazine Ligation: Fast Bioconjugation Based on Inverse-Electron-Demand Diels−Alder Reactivity. *J. Am. Chem. Soc.* **2008**, *130*, 13518-13519.

(40) Selvaraj, R.; Fox, J. M. An efficient and mild oxidant for the synthesis of s-tetrazines. *Tetrahedron Lett.* **2014**, *55*, 4795-4797.

(41) Fang, Z.; Hu, W.-L.; Liu, D.-Y.; Yu, C.-Y.; Hu, X.-G. Synthesis of tetrazines from gem-difluoroalkenes under aerobic conditions at room temperature. *Green Chem.* **2017**.

(42) Schirmer, R. H.; Adler, H.; Pickhardt, M.; Mandelkow, E. "Lest we forget you — methylene blue …". *Neurobiol. Aging* **2011**, *32*, 2325.e2327-2325.e2316.

(43) Azevedo, A. M.; Martins, V. C.; Prazeres, D. M. F.; Vojinović, V.; Cabral, J. M. S.; Fonseca, L. P.: Horseradish peroxidase: a valuable tool in biotechnology. In *Biotechnol. Ann. Rev.*; Elsevier, 2003; Vol. 9; pp 199-247.

(44) Veitch, N. C. Horseradish peroxidase: a modern view of a classic enzyme. *Phytochemistry* **2004**, *65*, 249-259.

(45) Folkes, L. K.; Wardman, P. Oxidative activation of indole-3-acetic acids to cytotoxic species— a potential new role for plant auxins in cancer therapy1. *Biochem. Pharmacol.* **2001**, *61*, 129-136.

(46) Wardman, P. Indole-3-Acetic Acids and Horseradish Peroxidase: A New Prodrug / Enzyme Combination for Targeted Cancer Therapy. *Curr. Pharm. Des.* **2002**, *8*, 1363.

(47) Yokota, K.; Yamazaki, I. Analysis and computer simulation of aerobic oxidation of reduced nicotinamide adenine dinucleotide catalyzed by horseradish peroxidase. *Biochemistry* **1977**, *16*, 1913-1920.

(48) Klapper, M. H.; Hackett, D. P. The Oxidatic Activity of Horseradish Peroxidase: I. OXIDATION OF HYDRO- AND NAPHTHOHYDROQUINONES. *J. Biol. Chem.* **1963**, *238*, 3736-3742.

(49) Liu, S.; Zhang, H.; Remy, R. A.; Deng, F.; Mackay, M. E.; Fox, J. M.; Jia, X. Meter-long multiblock copolymer microfibers via interfacial bioorthogonal polymerization. *Adv. Mater.* **2015**, *27*, 2783-2790.

(50) Lam, A. J.; St-Pierre, F.; Gong, Y.; Marshall, J. D.; Cranfill, P. J.; Baird, M. A.; McKeown, M. R.; Wiedenmann, J.; Davidson, M. W.; Schnitzer, M. J.; Tsien, R. Y.; Lin, M. Z. Improving FRET dynamic range with bright green and red fluorescent proteins. *Nat. Methods.* **2012**, *9*, 1005-1012.

(51) Taylor, M. T.; Blackman, M. L.; Dmitrenko, O.; Fox, J. M. Design and synthesis of highly reactive dienophiles for the tetrazine-trans-cyclooctene ligation. *J. Am. Chem. Soc.* **2011**, *133*, 9646-9649.

(52) Zhang, H.; Dicker, K. T.; Xu, X.; Jia, X.; Fox, J. M. Interfacial Bioorthogonal Cross-Linking. *ACS Macro Lett* **2014**, *3*, 727-731.

(53) Zhang, H.; Trout, W. S.; Liu, S.; Andrade, G. A.; Hudson, D. A.; Scinto, S. L.; Dicker, K. T.; Li, Y.; Lazouski, N.; Rosenthal, J.; Thorpe, C.; Jia, X.; Fox, J. M. Rapid Bioorthogonal Chemistry Turn-on through Enzymatic or Long Wavelength Photocatalytic Activation of Tetrazine Ligation. *J. Am. Chem. Soc.* **2016**, *138*, 5978-5983.

APPENDIX

Appendix A

SPECTRAL DATA FOR CHAPTER 1

^{1}H NMR (600 MHz, $CDCl_3$)

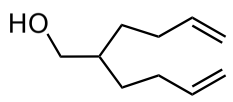

1-17

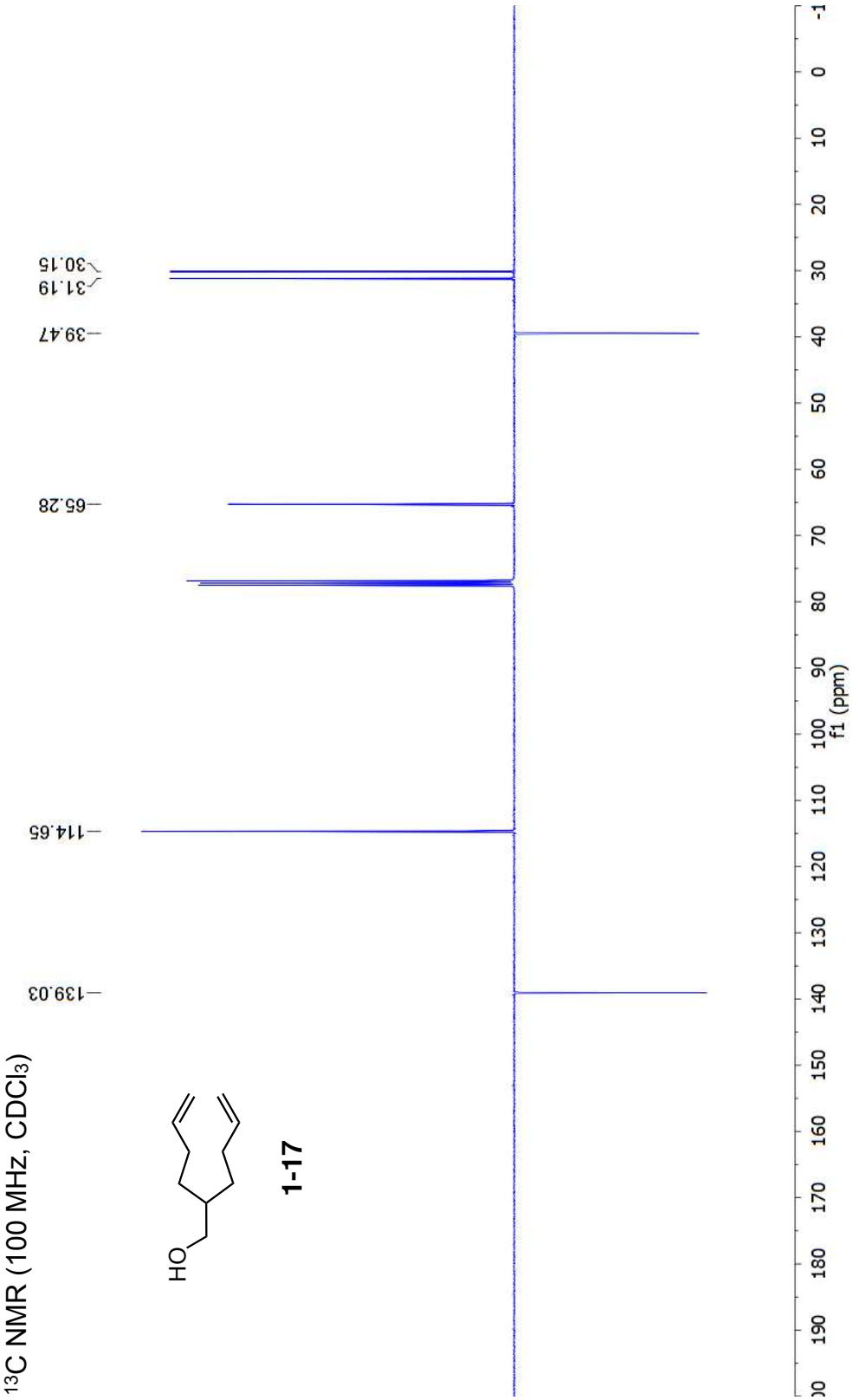
^{13}C NMR (100 MHz, $CDCl_3$)
139.03
114.65
65.28
39.47
31.19
30.15
HO
1-17
f1 (ppm)

^{1}H NMR (600 MHz, $CDCl_3$)

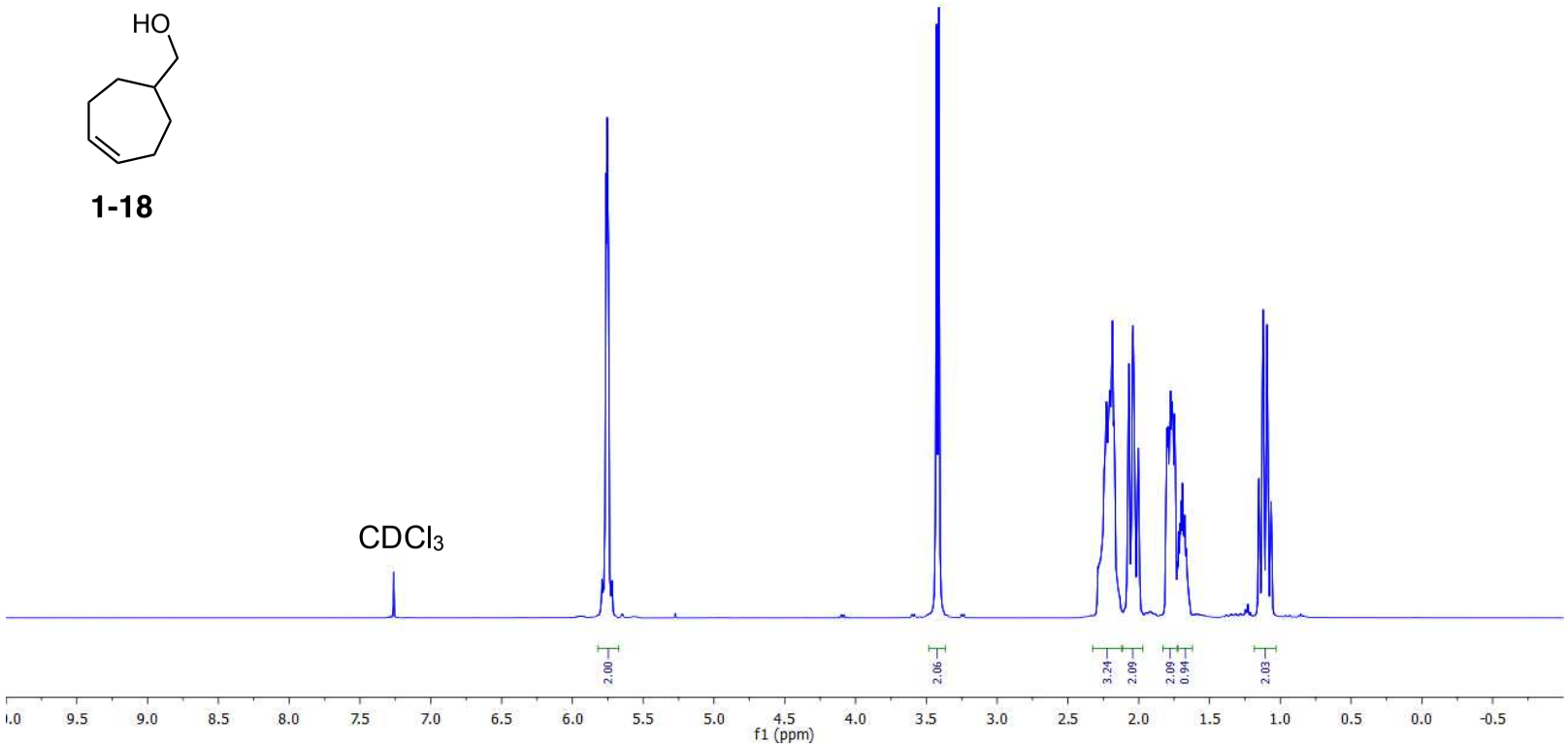

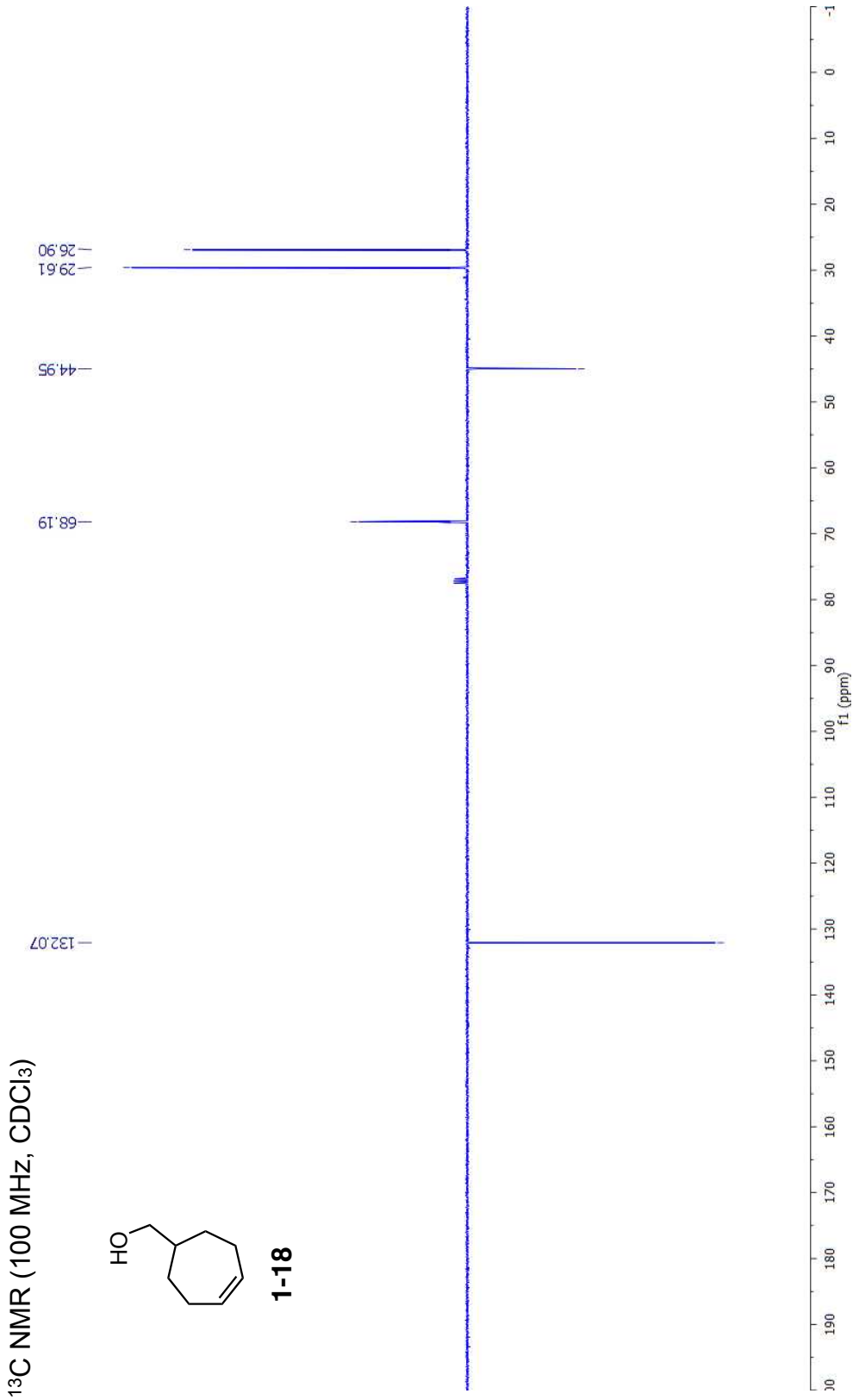
^{13}C NMR (100 MHz, $CDCl_3$)
HO
1-18
132.07
68.19
44.95
29.61
26.90
f1 (ppm)

^{1}H NMR (400 MHz, $CDCl_3$)

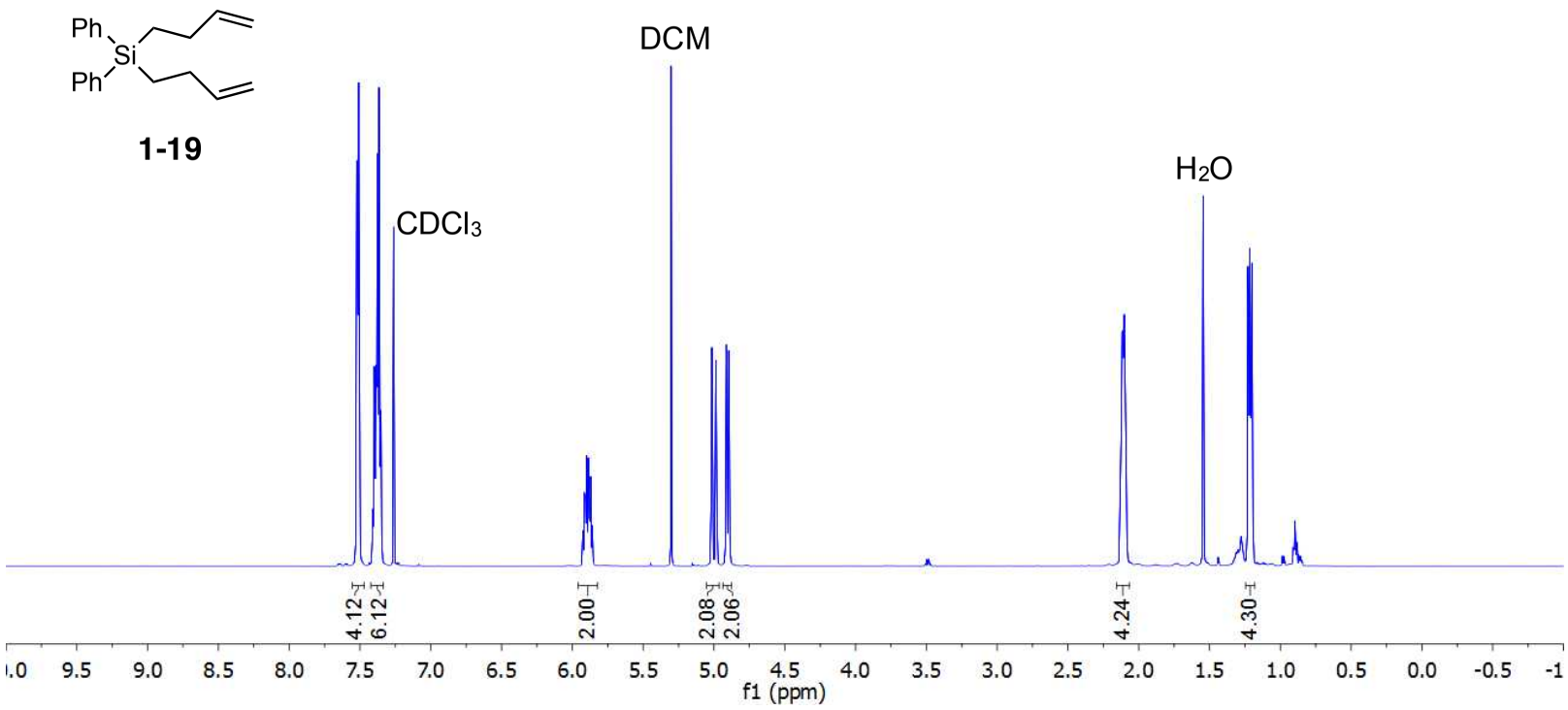

^{13}C NMR (100 MHz, $CDCl_3$)

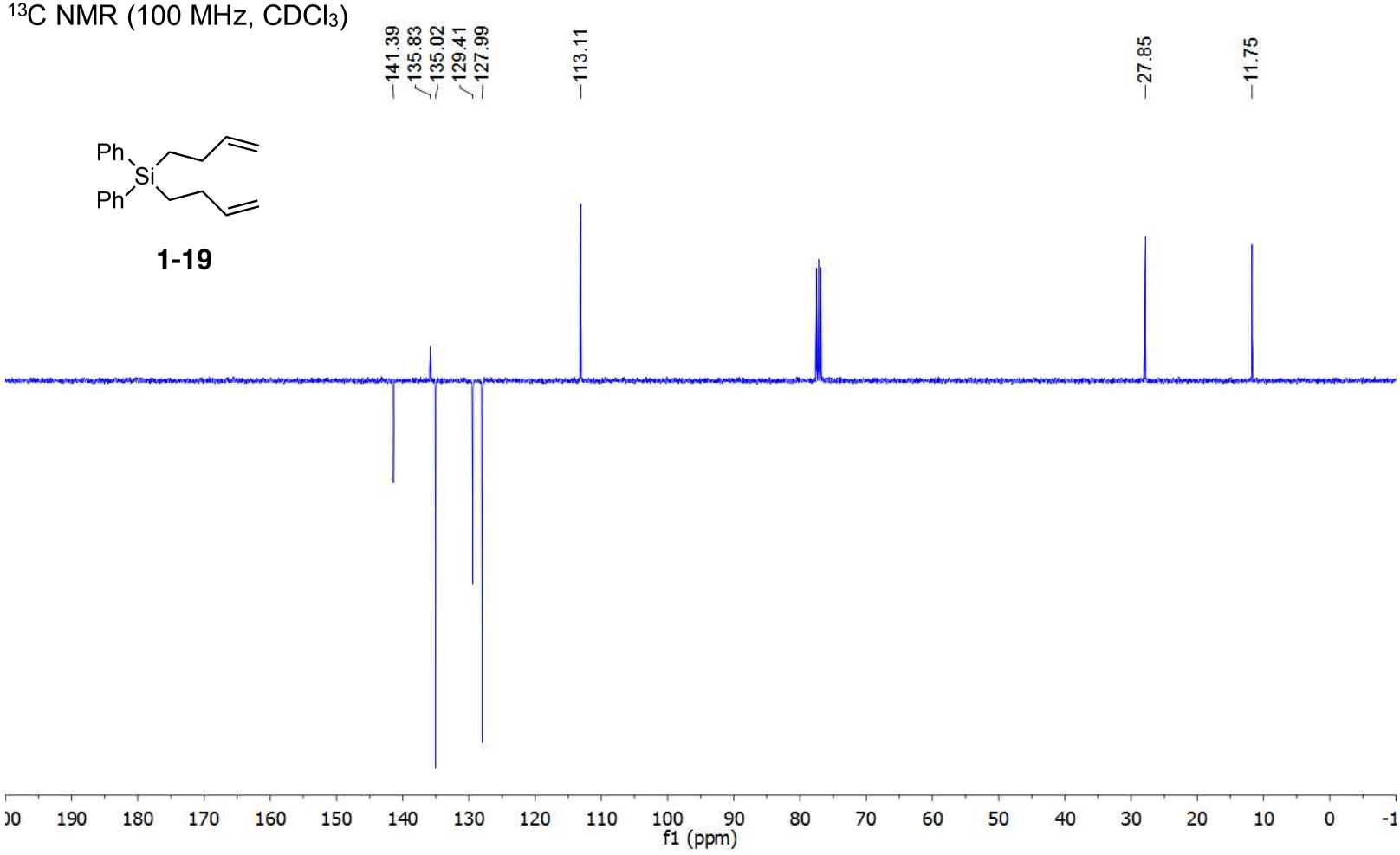

^{1}H NMR (400 MHz, $CDCl_3$)

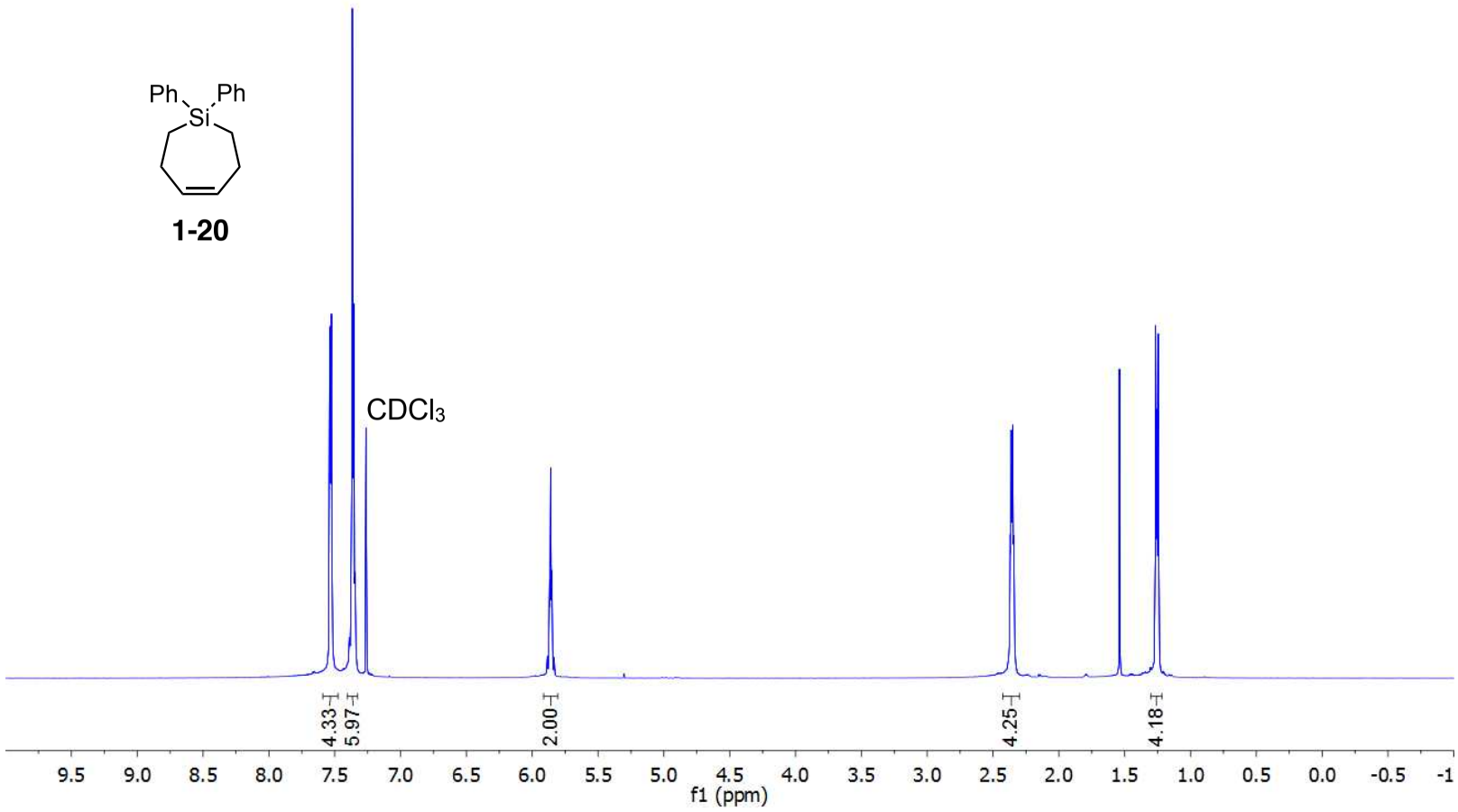

^{13}C NMR (100 MHz, $CDCl_3$)

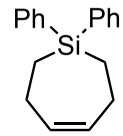

1-20

^{1}H NMR (400 MHz, CD_3OD)

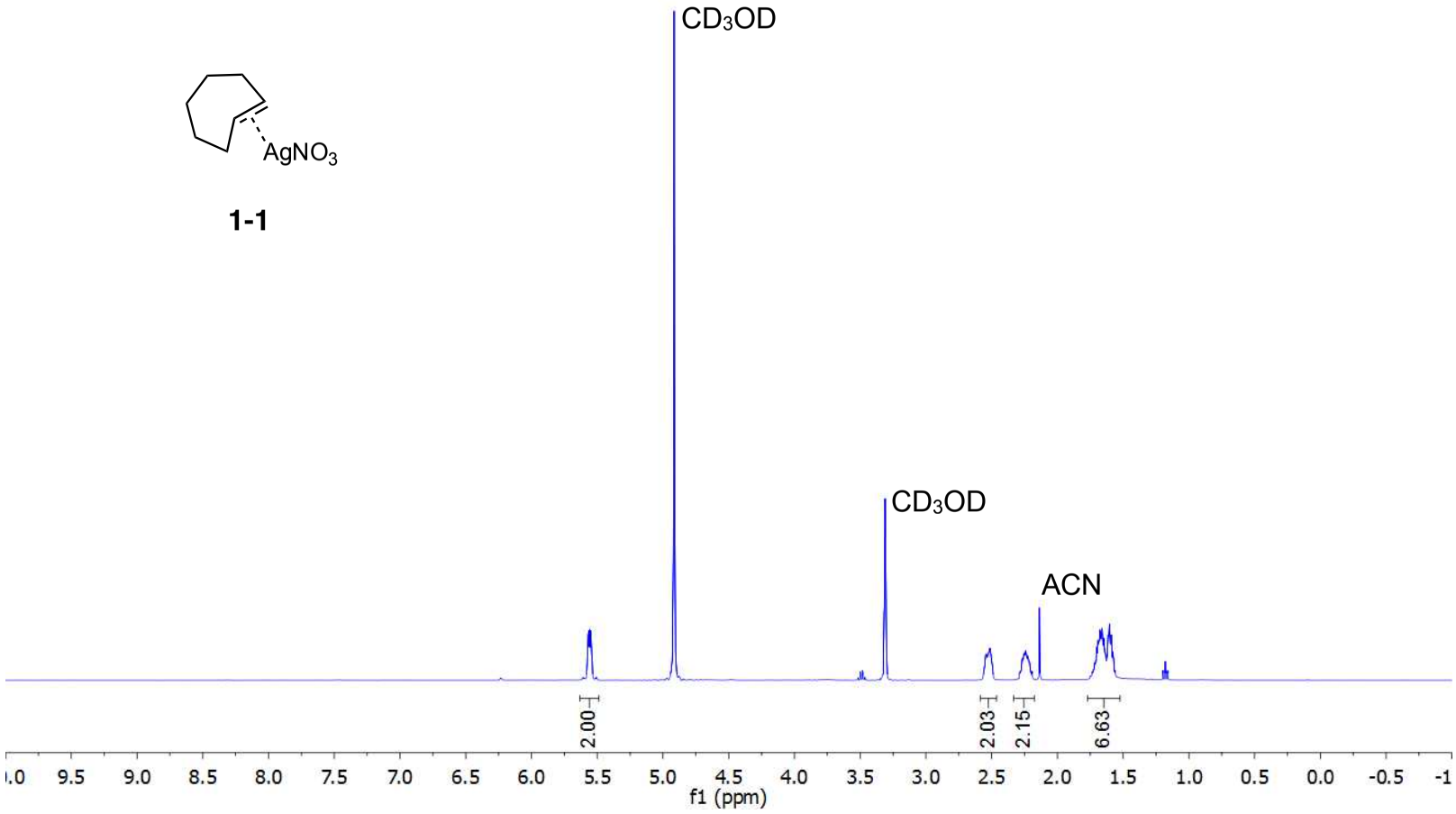

^{13}C NMR (100 MHz, CD_3OD)

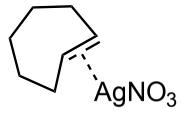

1-1

^{1}H NMR (400 MHz, CD_3OD)

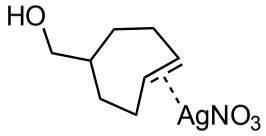

1-2

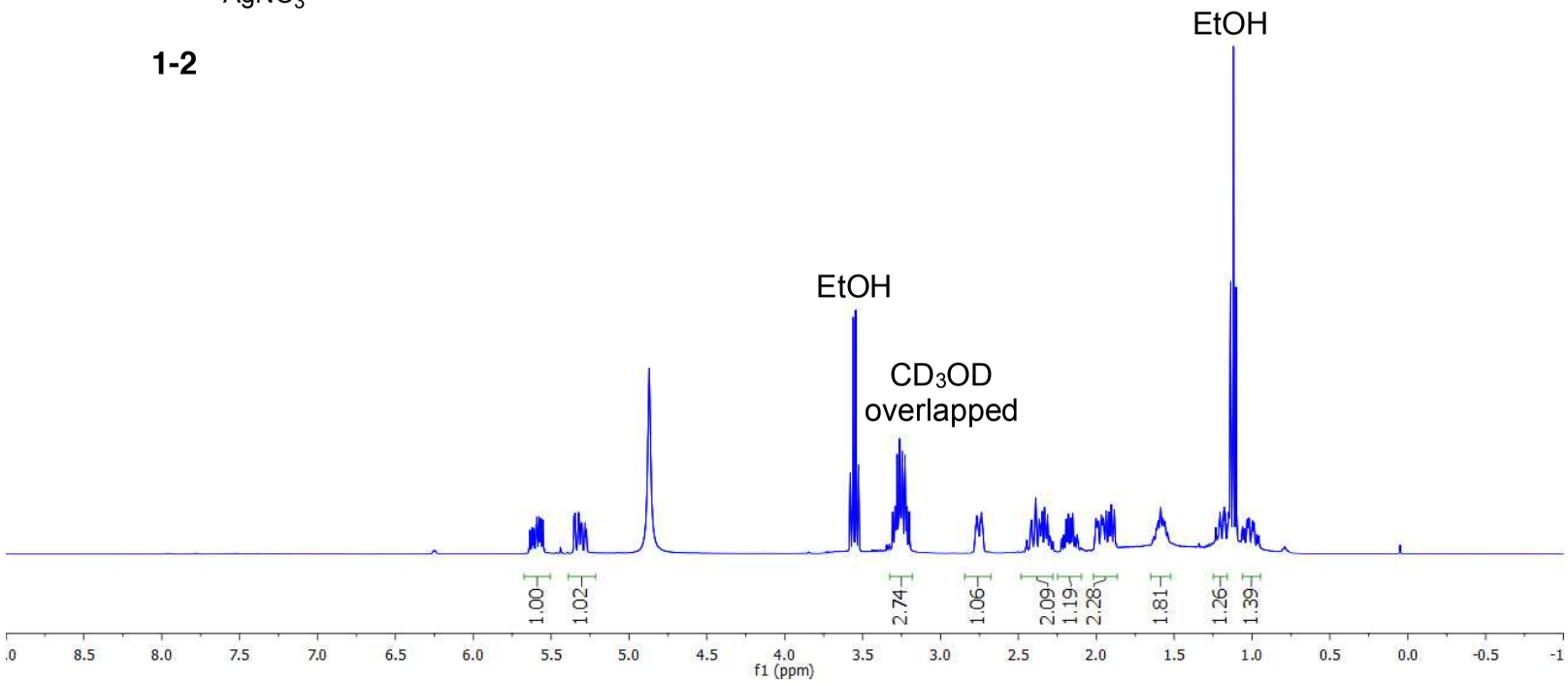

^{13}C NMR (100 MHz, CD_3OD)

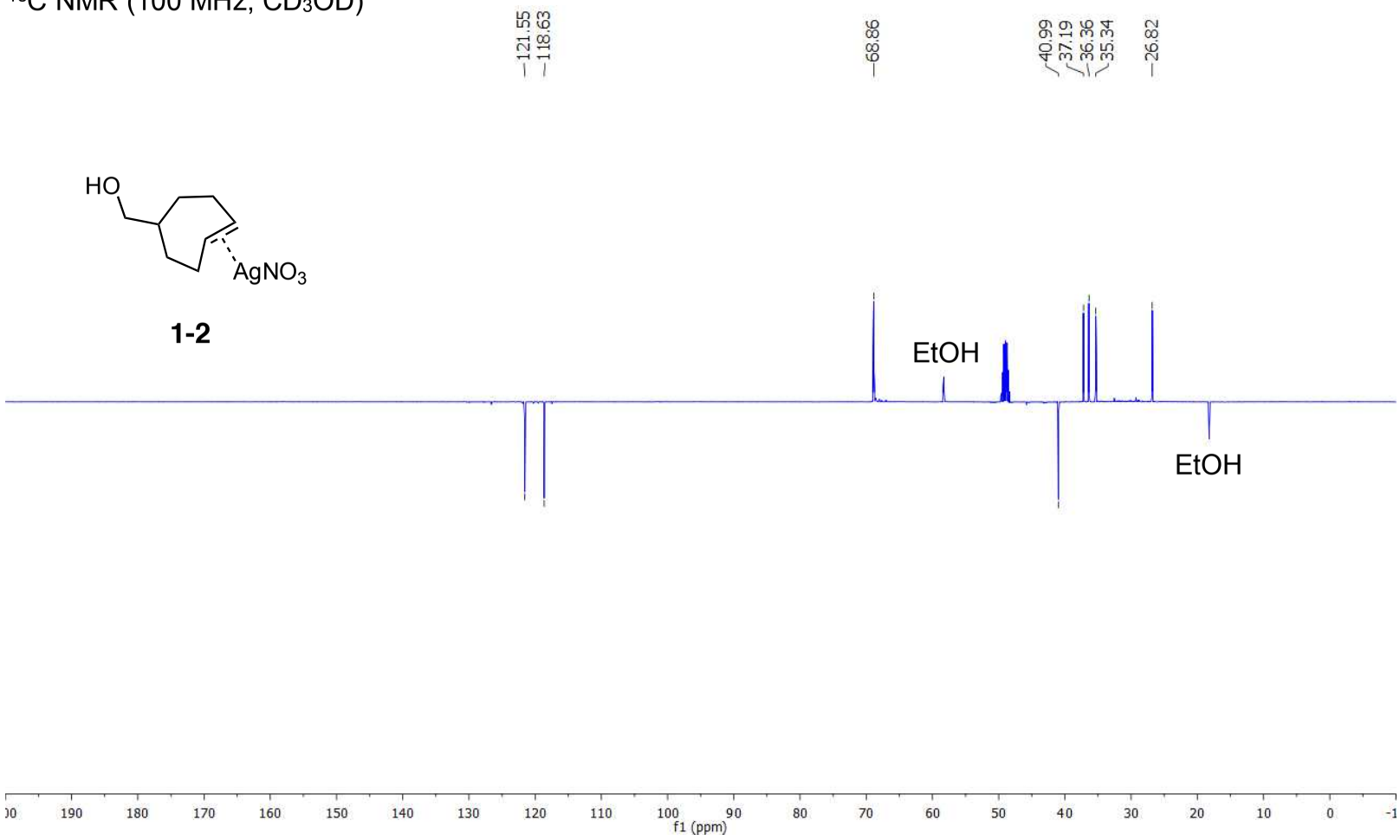

1-2

^{1}H NMR (400 MHz, CD_3OD)

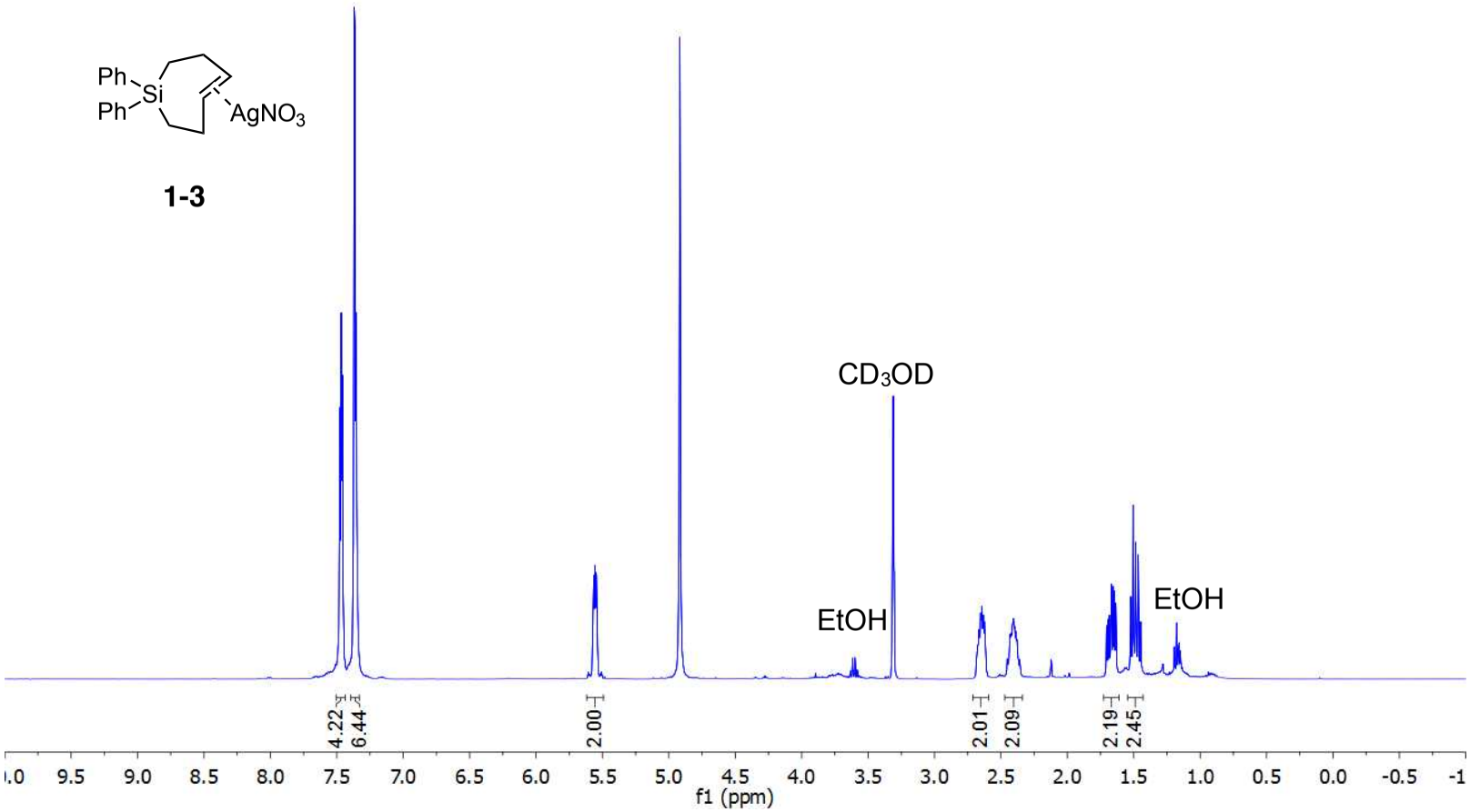

^{13}C NMR (100 MHz, CD_3OD)

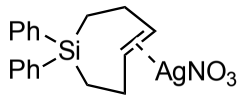

1-3

^{1}H NMR (600 MHz, $CDCl_3$)

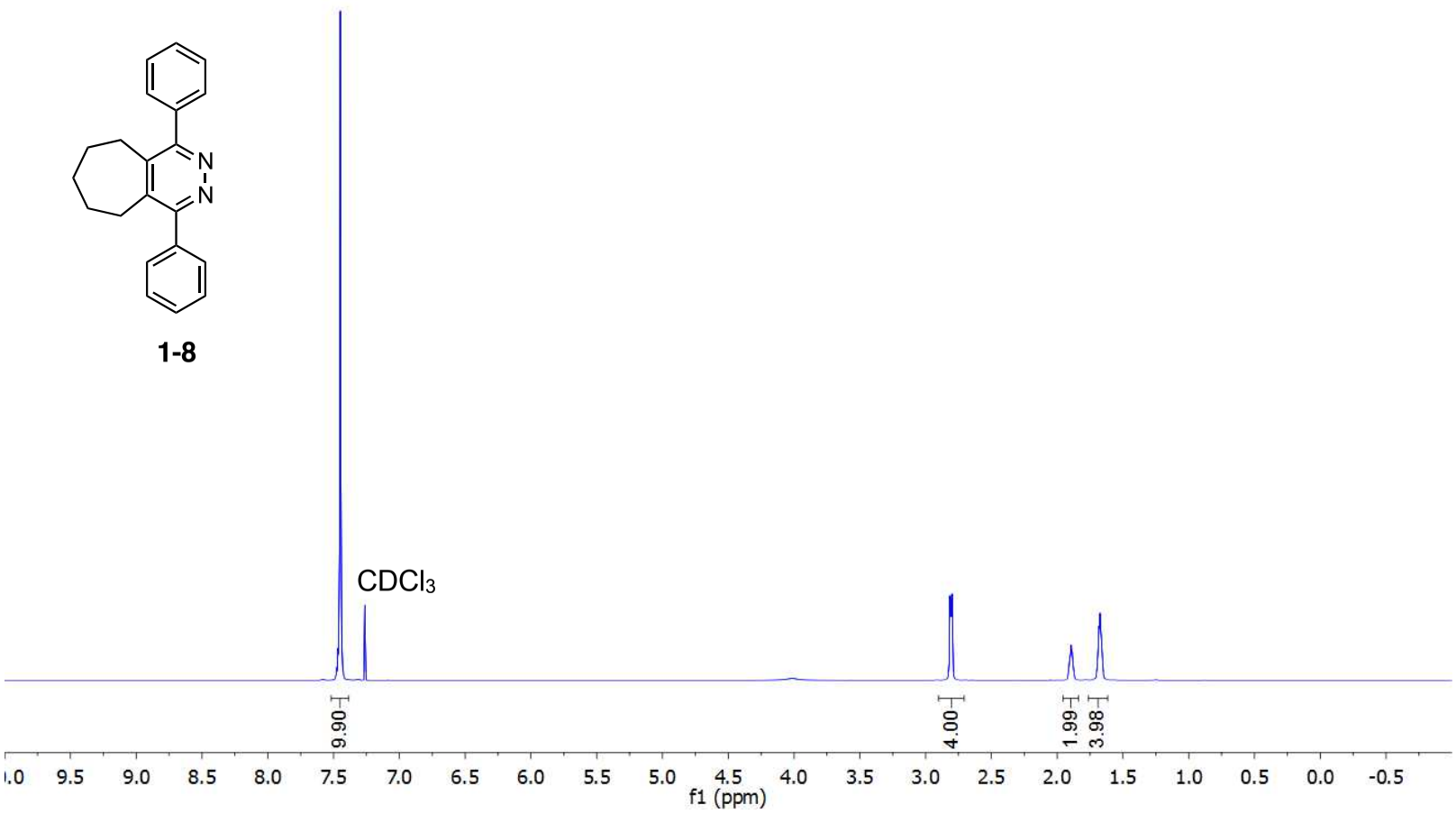

1-8

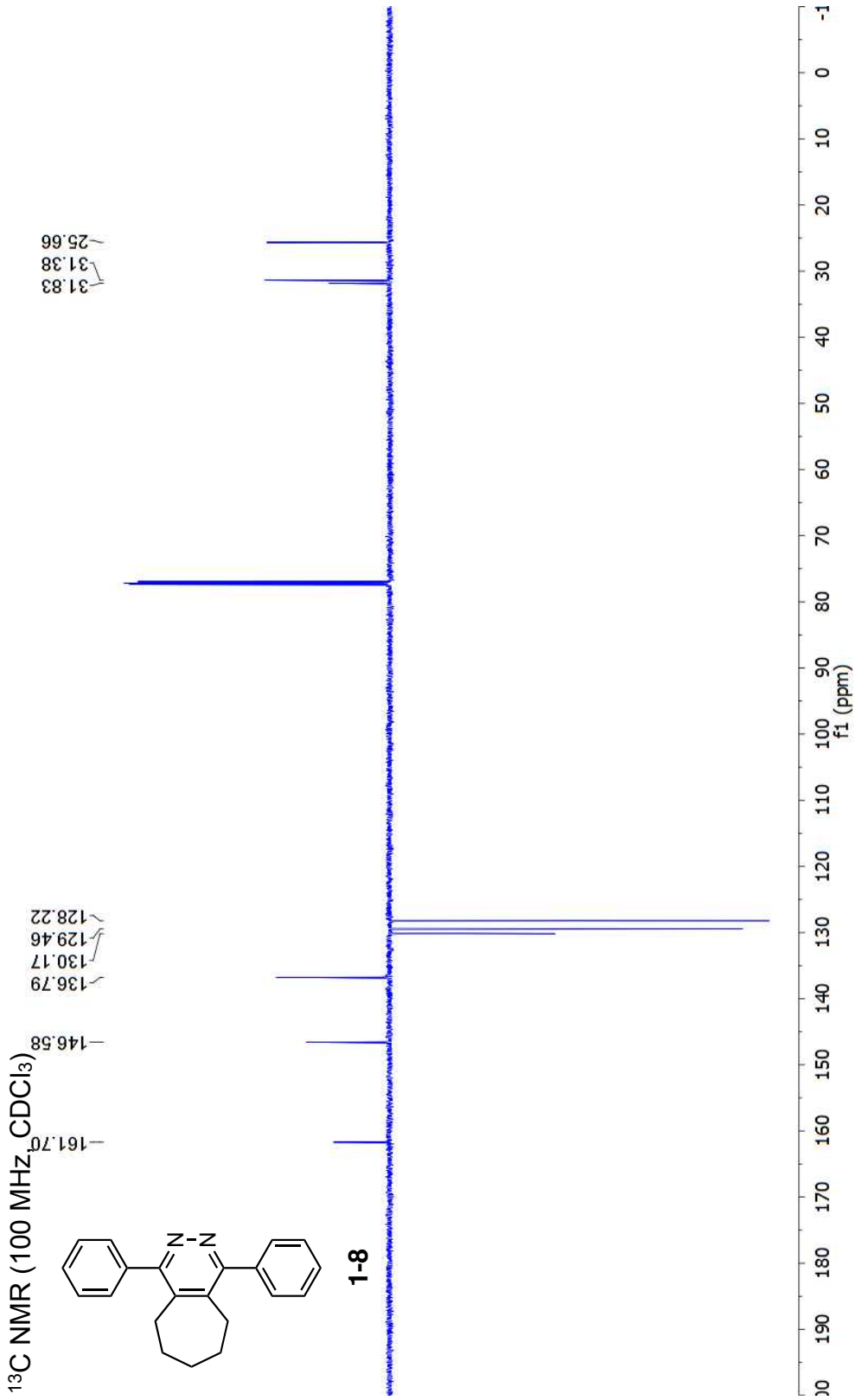
^{13}C NMR (100 MHz, CDCl$_3$)
1-8
161.70
146.58
136.79
130.17
129.46
128.22
31.83
31.38
25.66
f1 (ppm)

^{1}H NMR (400 MHz, $CDCl_3$)

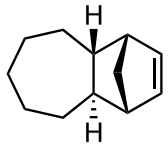

1-9

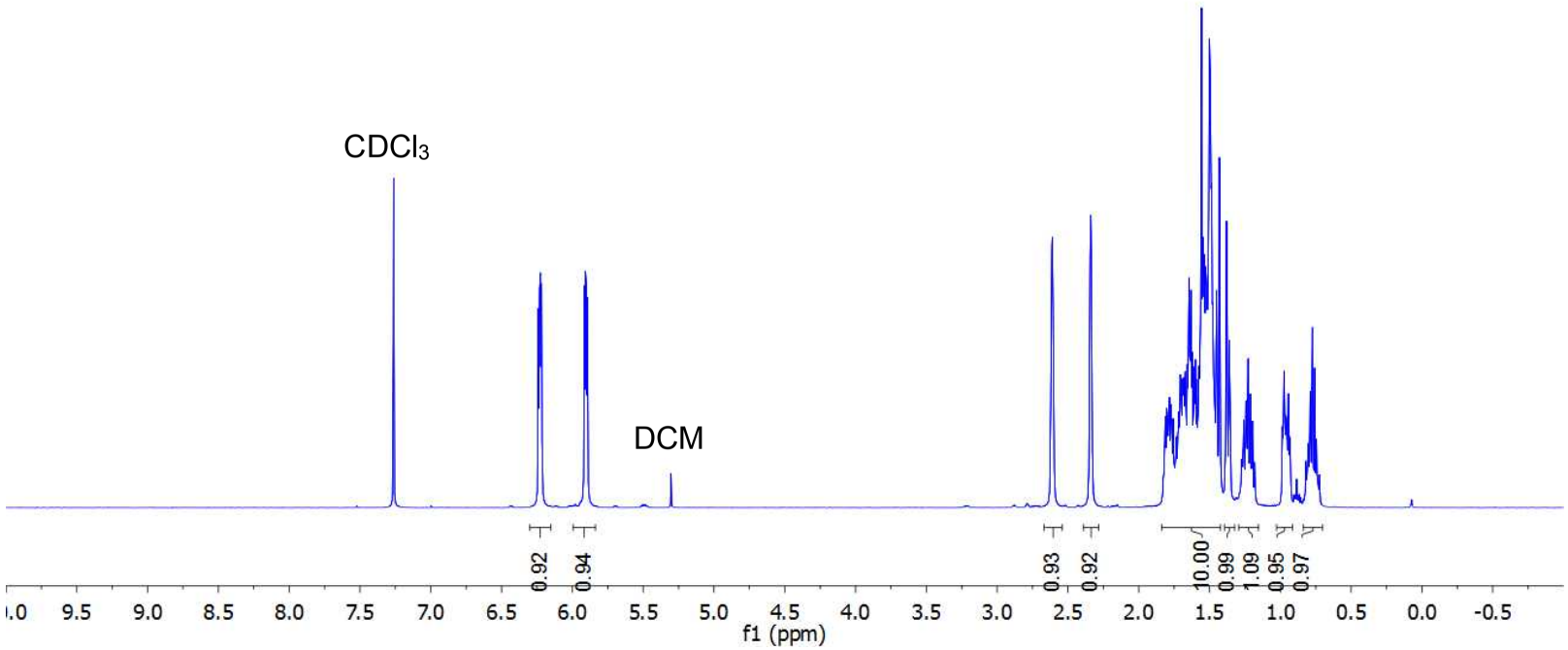

^{13}C NMR (100 MHz, $CDCl_3$)

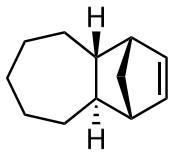

1-9

^{1}H NMR (600 MHz, $CDCl_3$)

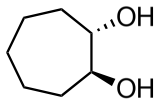

1-10

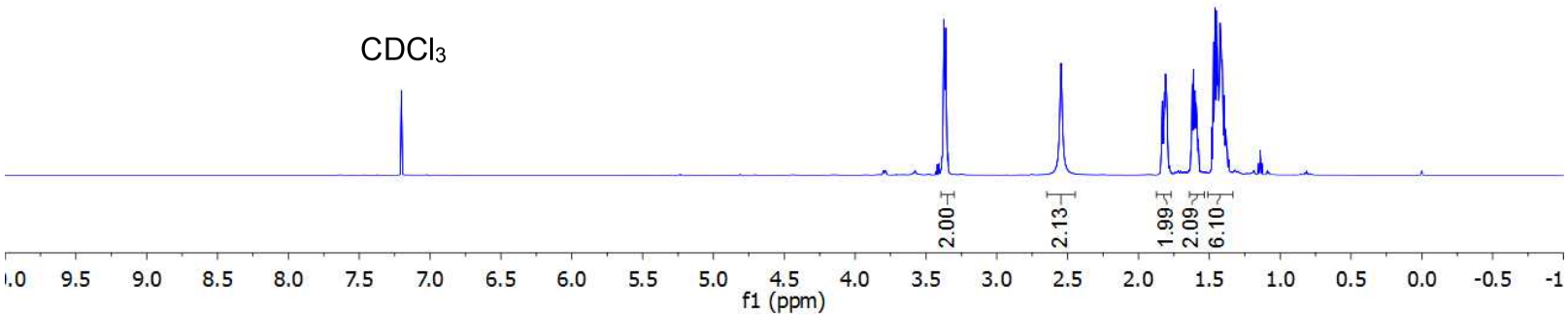

^{13}C NMR (100 MHz, $CDCl_3$)

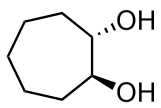

1-10

^{1}H NMR (400 MHz, $CDCl_3$)

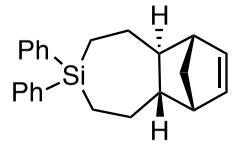

1-13

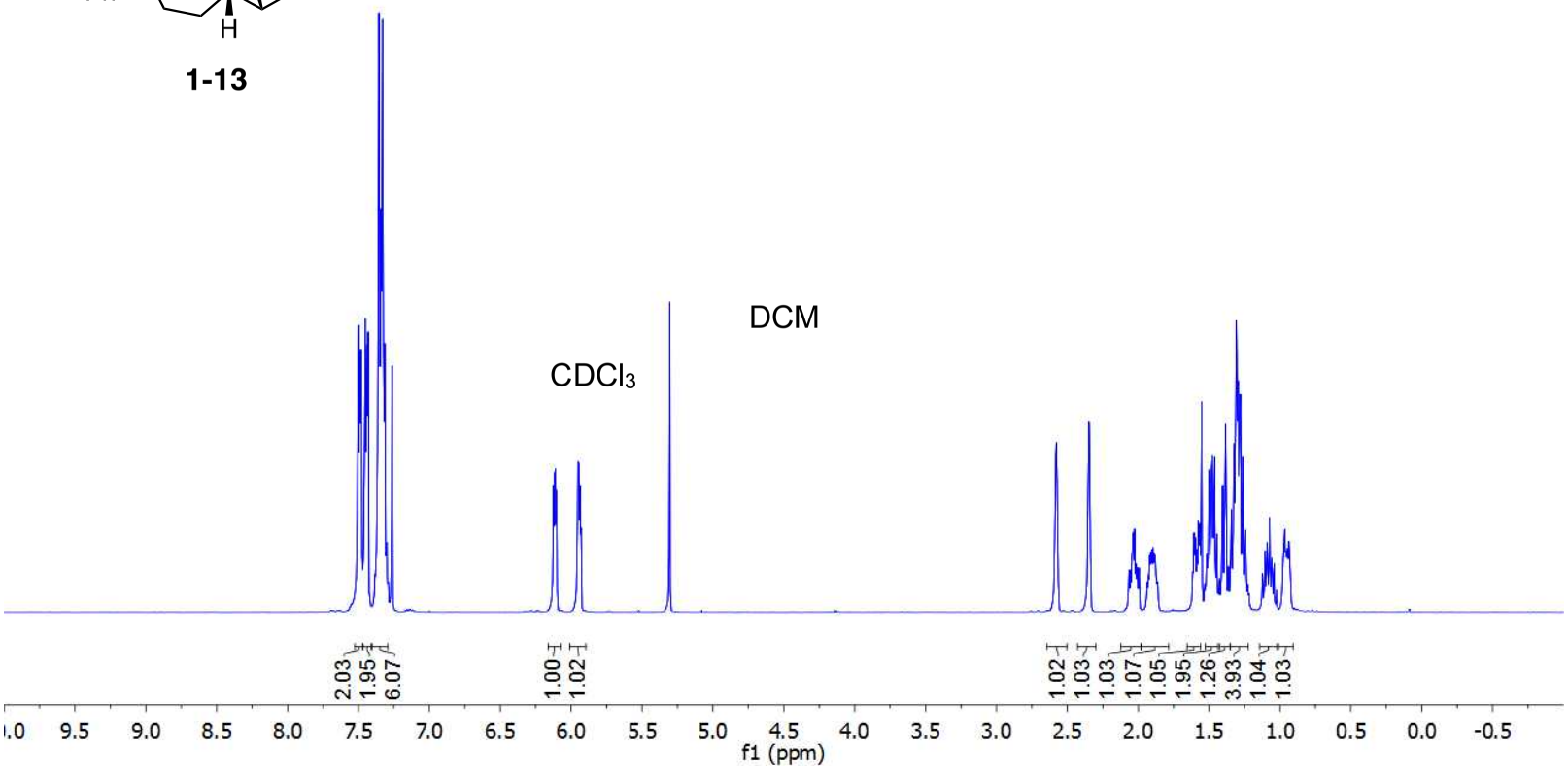

^{13}C NMR (150 MHz, C_6D_6)

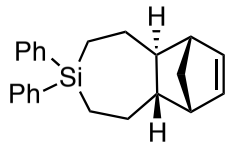

1-13

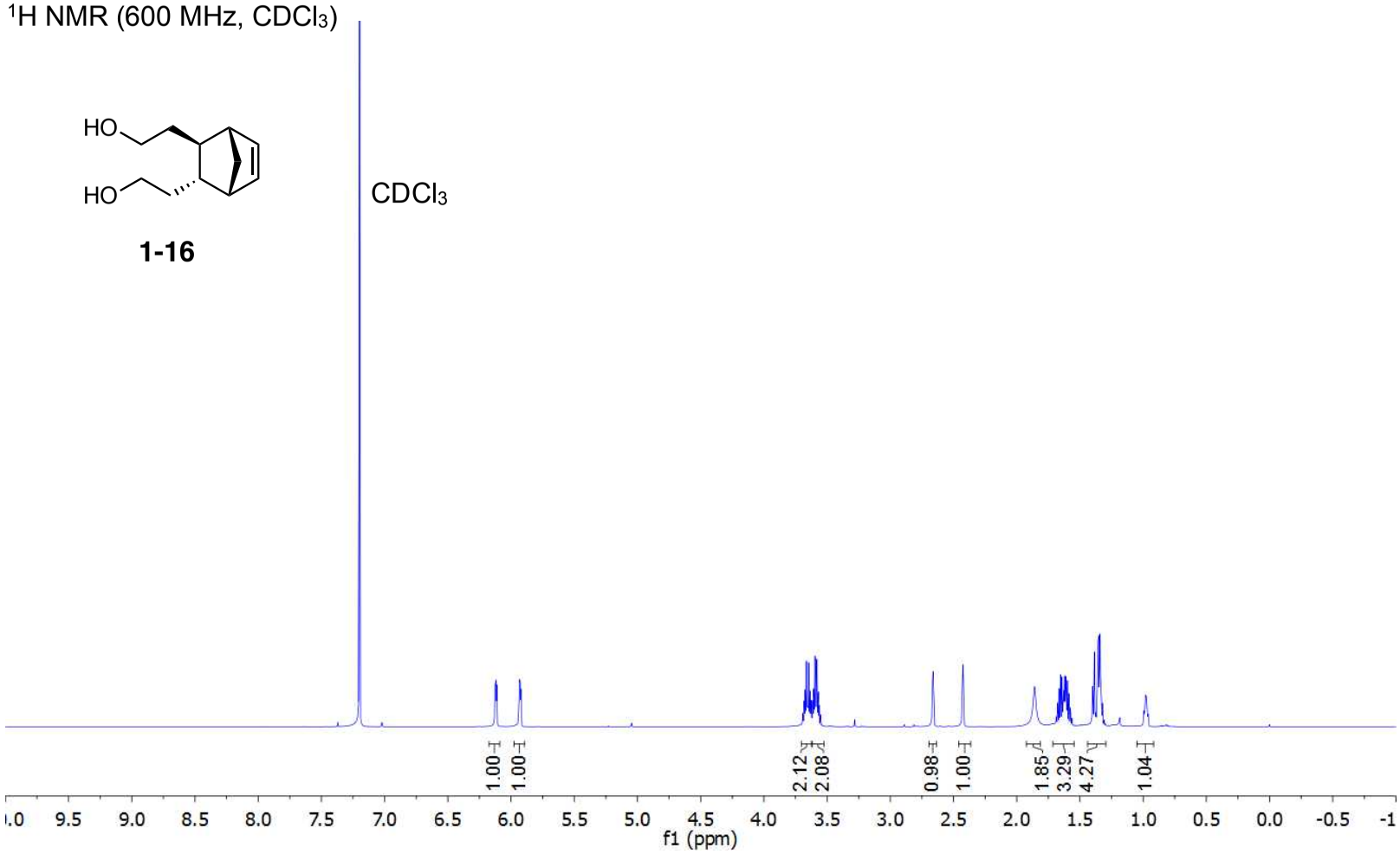
^{1}H NMR (600 MHz, $CDCl_3$)
HO
HO
1-16
$CDCl_3$
1.00
1.00
2.12
2.08
0.98
1.00
1.85
3.29
4.27
1.04
f1 (ppm)

^{13}C NMR (100 MHz, $CDCl_3$)

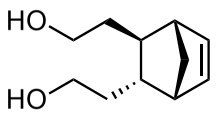

1-16

Appendix B

SPECTRAL DATA FOR CHAPTER 2

^{1}H NMR (600 MHz, D_2O)

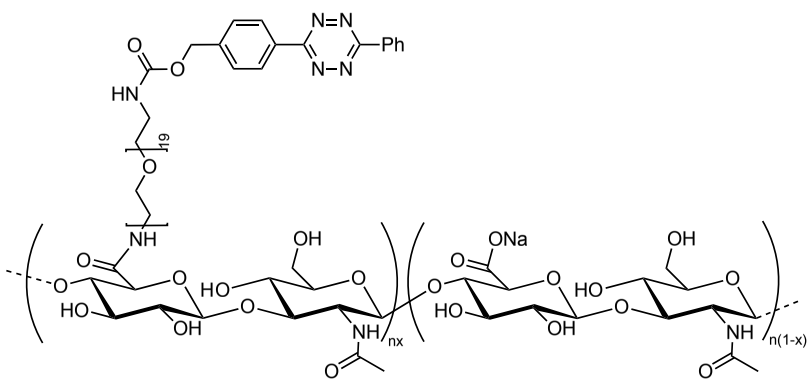

2-4 (x = Tz%)

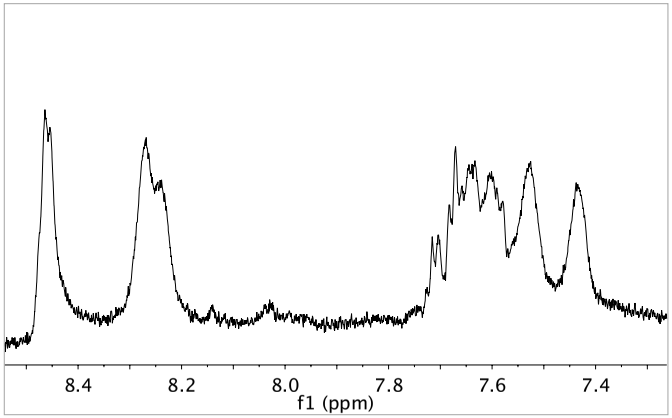

^{1}H NMR (400 MHz, $CDCl_3$)

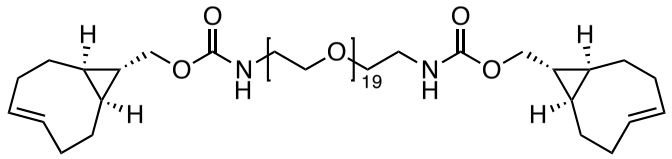

2-6

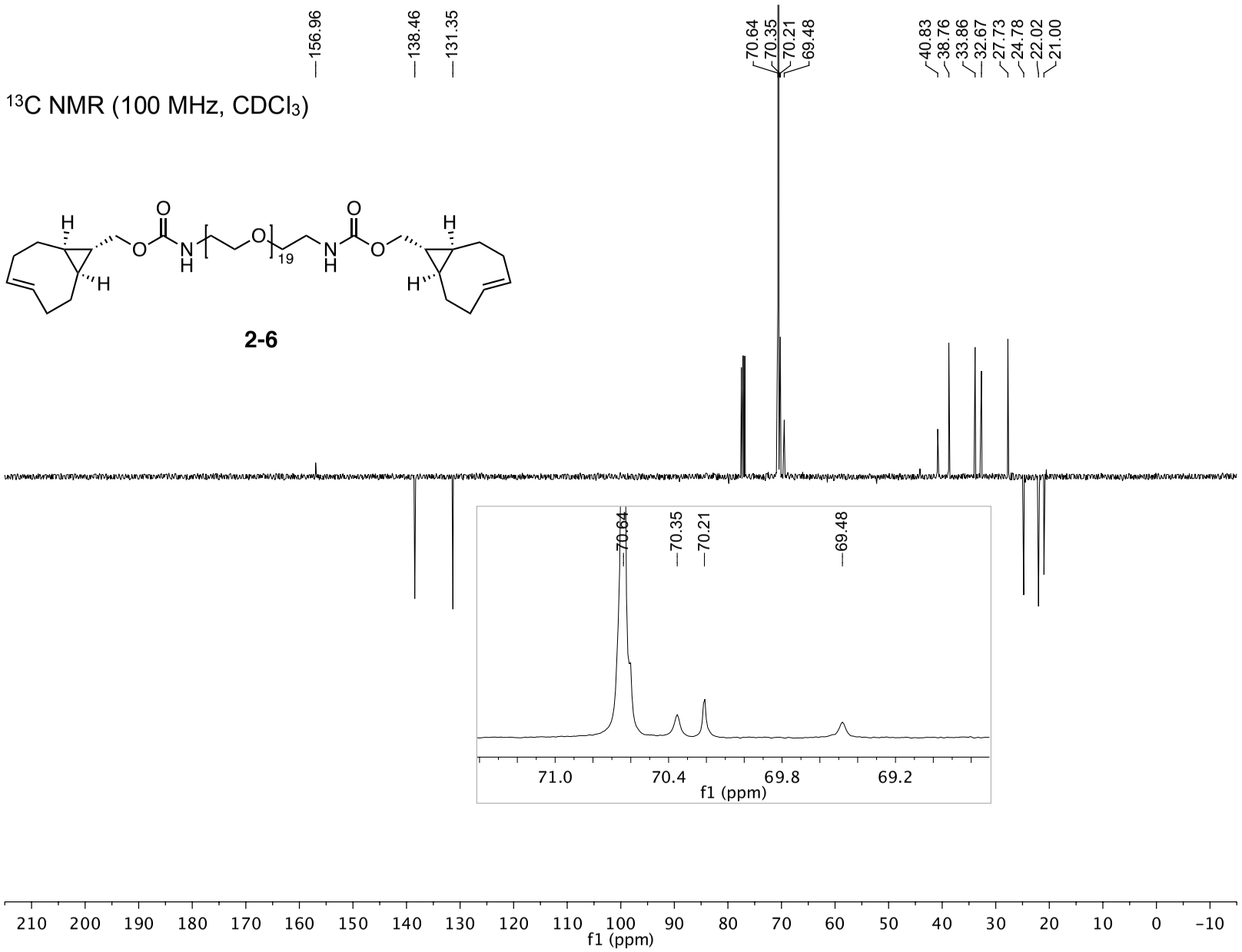
156.96
138.46
131.35
70.64
70.35
70.21
69.48
40.83
38.76
33.86
32.67
27.73
24.78
22.02
21.00
13C NMR (100 MHz, CDCl3)
2-6
71.0
70.4
69.8
69.2
f1 (ppm)
210 200 190 180 170 160 150 140 130 120 110 100 90 80 70 60 50 40 30 20 10 0 -10
f1 (ppm)

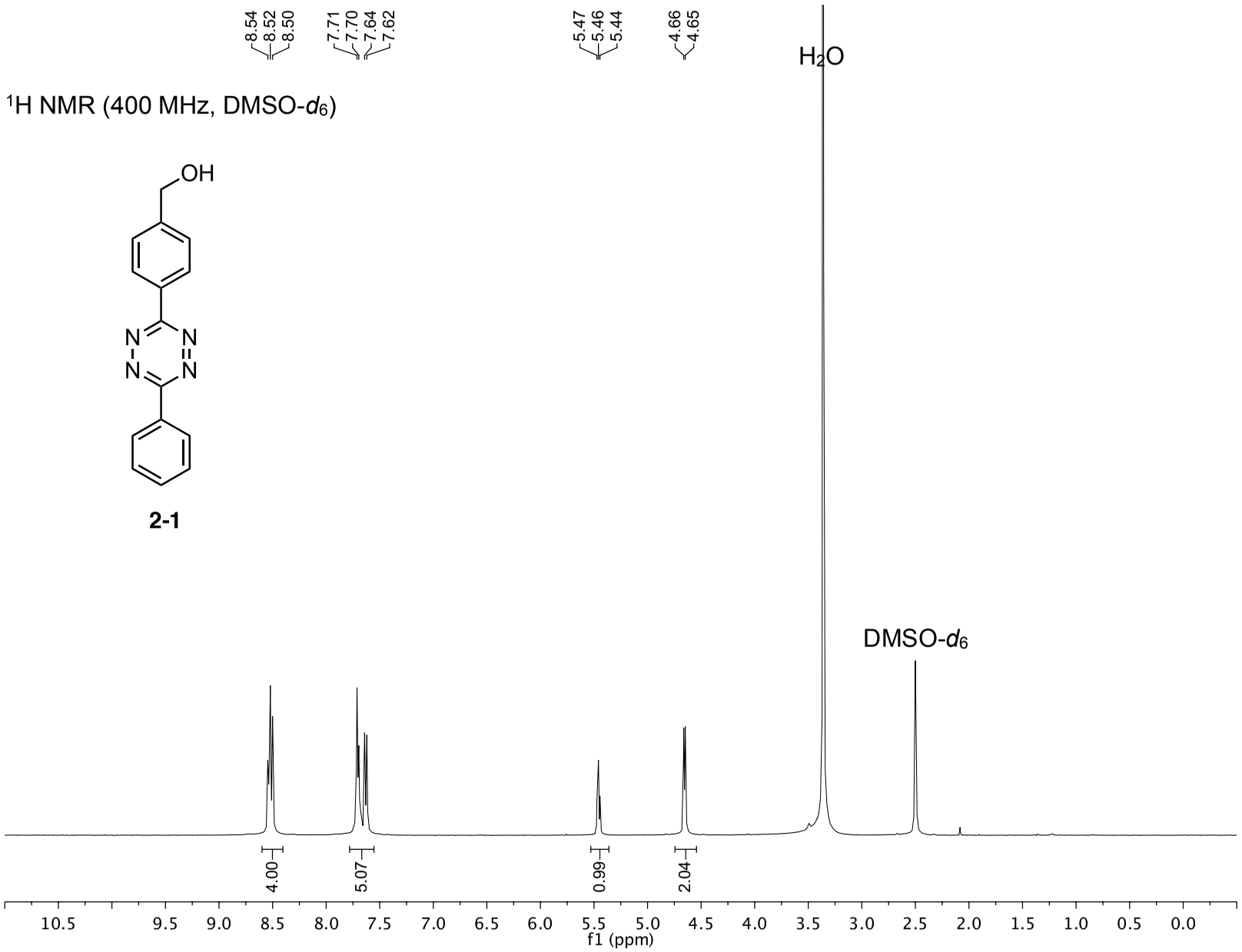

^{1}H NMR (400 MHz, DMSO-d_6)

2-1

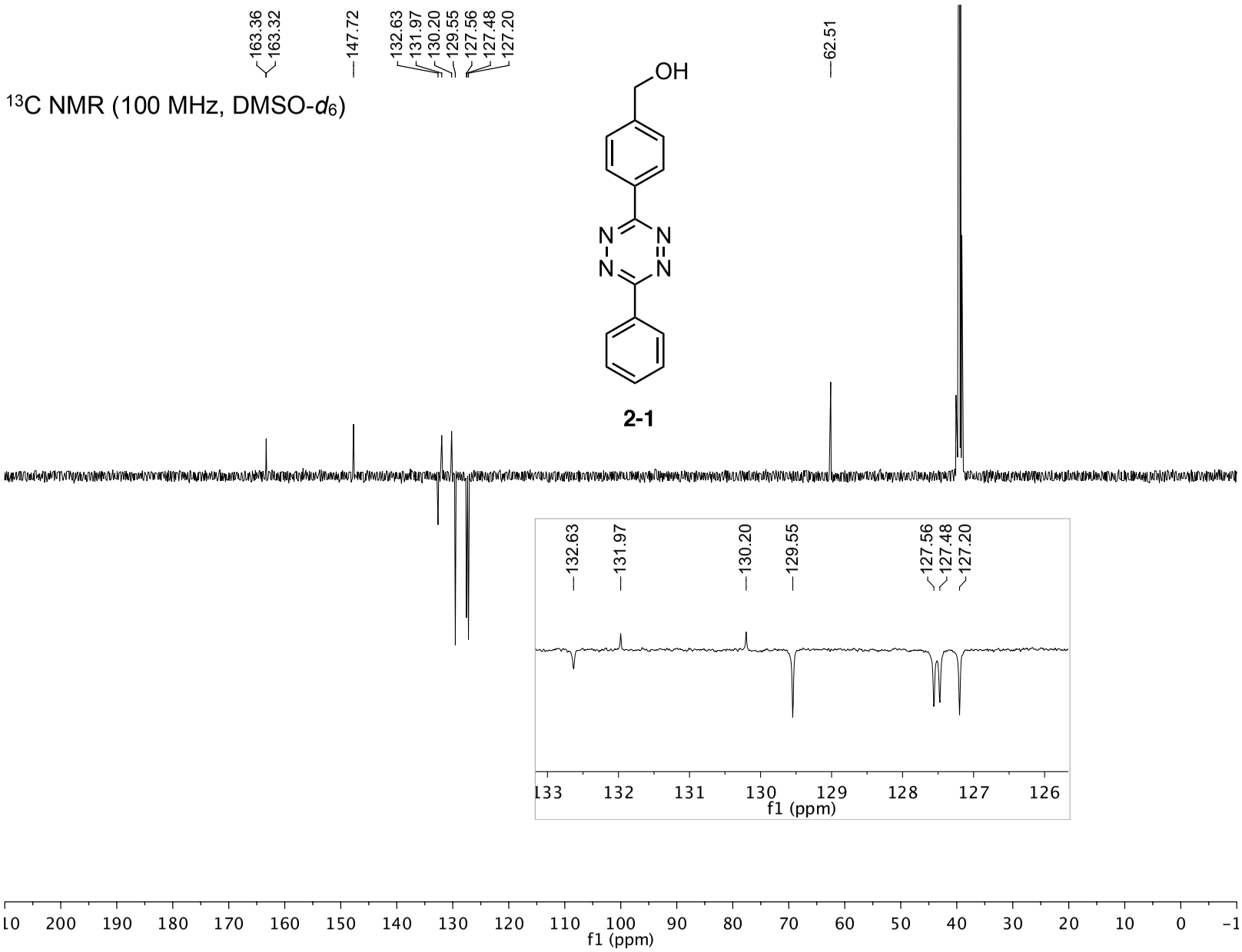
163.36
163.32
147.72
132.63
131.97
130.20
129.55
127.56
127.48
127.20
62.51
^{13}C NMR (100 MHz, DMSO-d_6)
OH
N
N
N
N
2-1
220
132.63
131.97
130.20
129.55
127.56
127.48
127.20
133
132
131
130
129
128
127
126
f1 (ppm)
10
200
190
180
170
160
150
140
130
120
110
100
90
80
70
60
50
40
30
20
10
0
−1
f1 (ppm)

8.73
8.71
8.31
8.29
7.71
7.69
7.65
7.63
7.43
7.41
5.43

^{1}H NMR (400 MHz, $CDCl_3$)

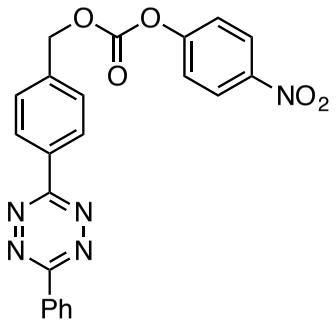

2-2

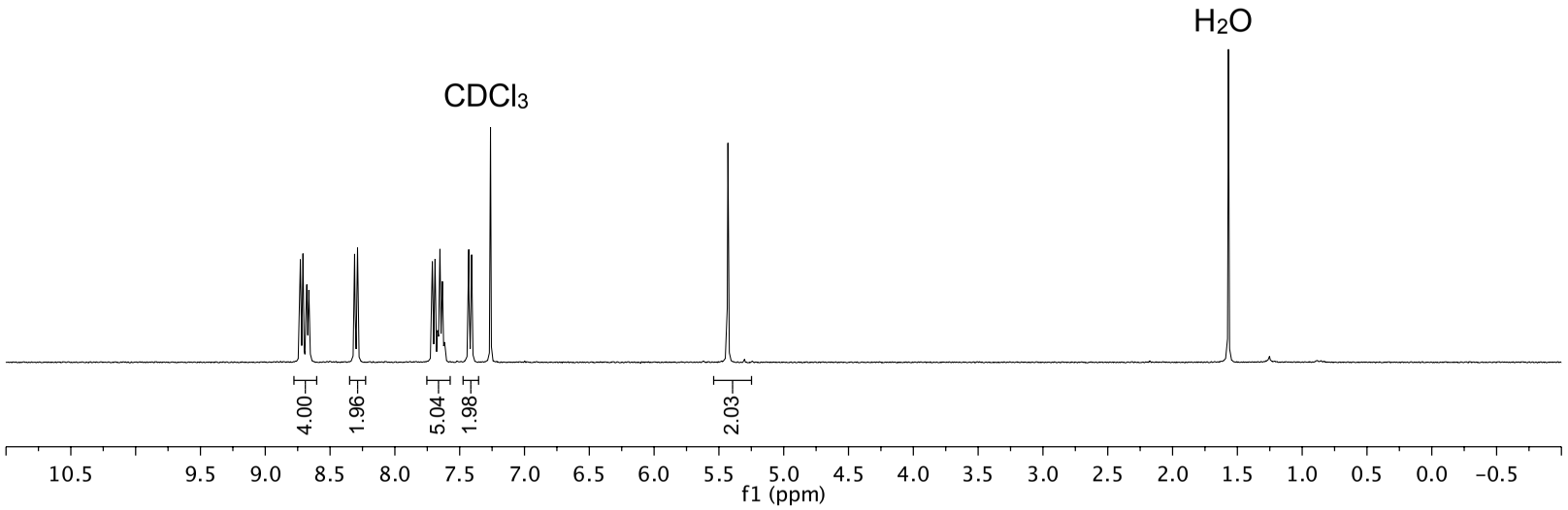

^{13}C NMR (100 MHz, $CDCl_3$)

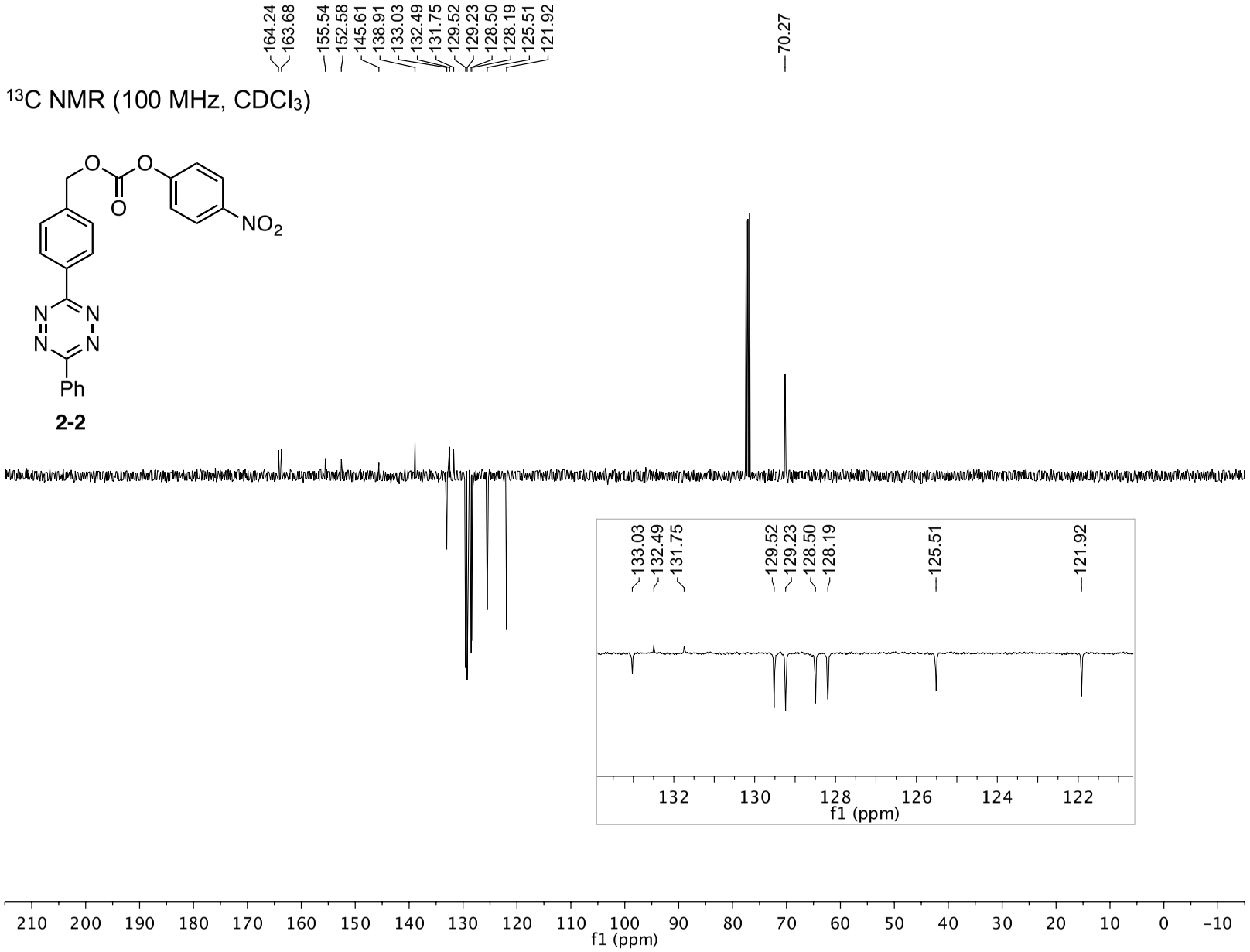

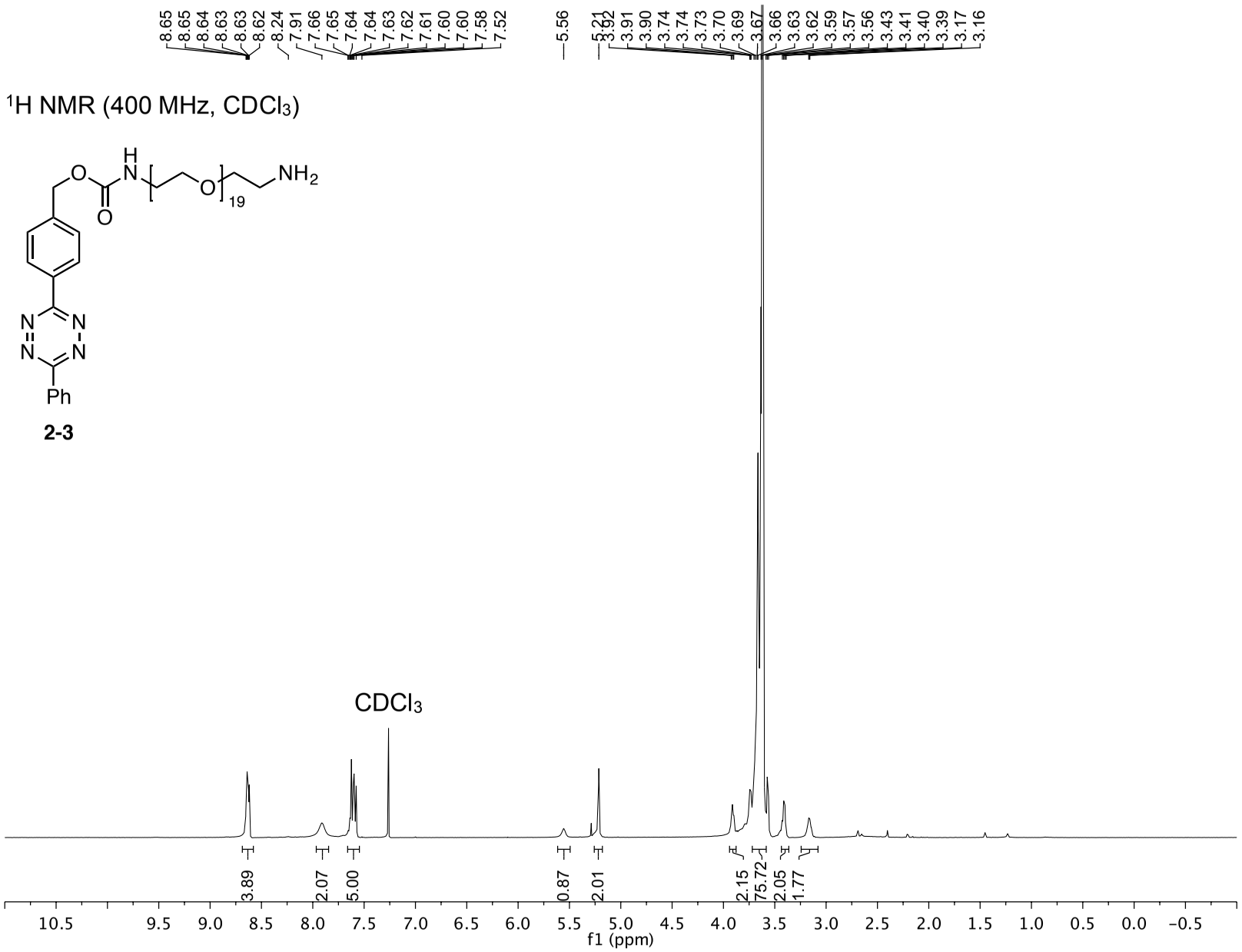
8.65
8.65
8.64
8.63
8.63
8.62
8.24
7.91
7.66
7.65
7.64
7.64
7.63
7.62
7.61
7.60
7.60
7.58
7.52
5.56
5.21
3.92
3.91
3.90
3.74
3.74
3.73
3.70
3.69
3.67
3.66
3.63
3.62
3.59
3.57
3.56
3.43
3.41
3.40
3.39
3.17
3.16
1H NMR (400 MHz, CDCl3)
O
H
N
O
O
19
NH2
N
N
N
N
Ph
2-3
CDCl3
3.89
2.07
5.00
0.87
2.01
2.15
75.72
2.05
1.77
10.5
9.5
9.0
8.5
8.0
7.5
7.0
6.5
6.0
5.5
5.0
4.5
4.0
3.5
3.0
2.5
2.0
1.5
1.0
0.5
0.0
-0.5
f1 (ppm)

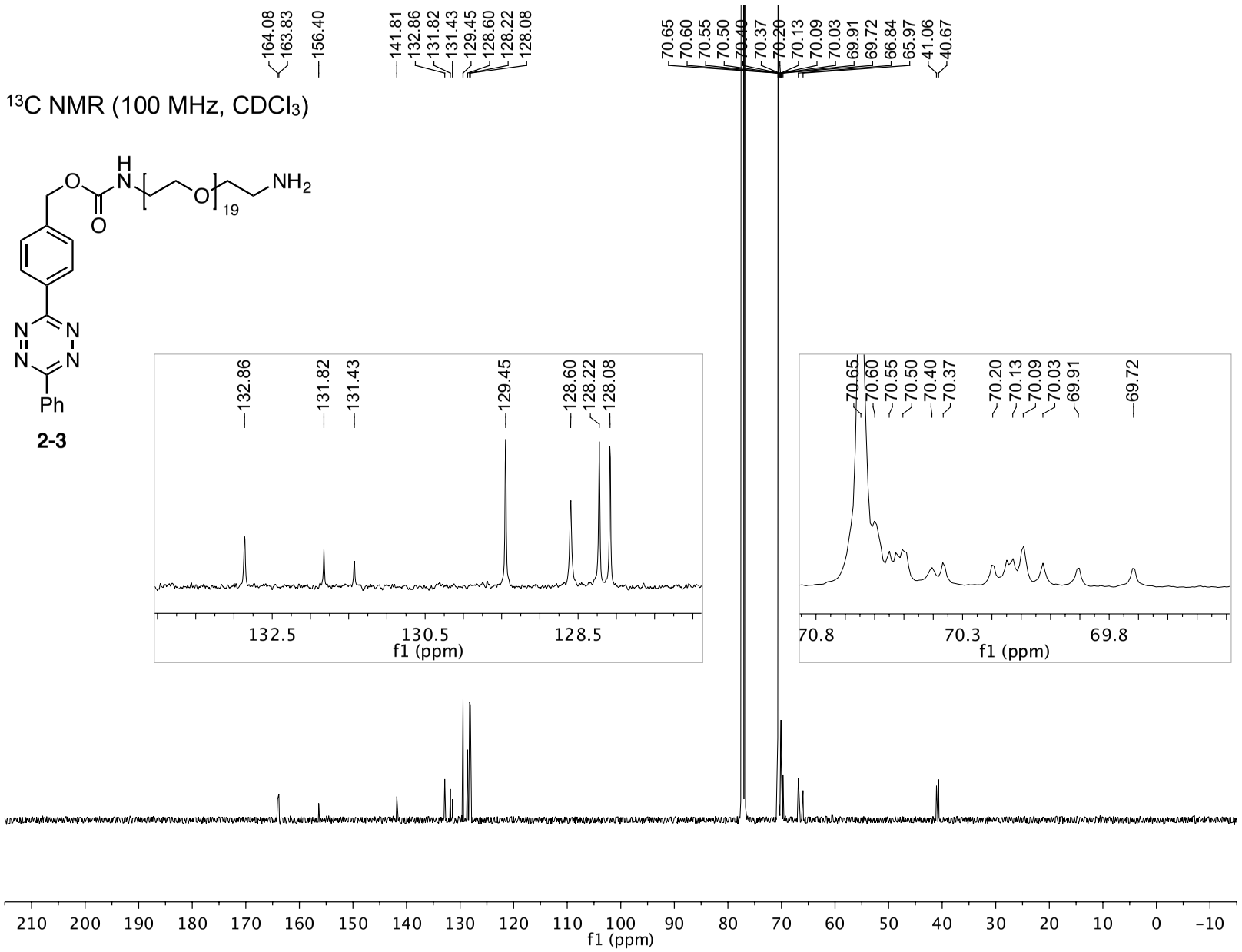
164.08
163.83
156.40
141.81
132.86
131.82
131.43
129.45
128.60
128.22
128.08
70.65
70.60
70.55
70.50
70.40
70.37
70.20
70.13
70.09
70.03
69.91
69.72
66.84
65.97
41.06
40.67
13C NMR (100 MHz, CDCl3)
2-3
f1 (ppm)
f1 (ppm)

LC-MS analysis of Alexa Fluor® 647-sTCO **2-7** with Shimadzu LCMS-2020.
(ESI negative mode, direct injection, 60% ACN/H_2O).

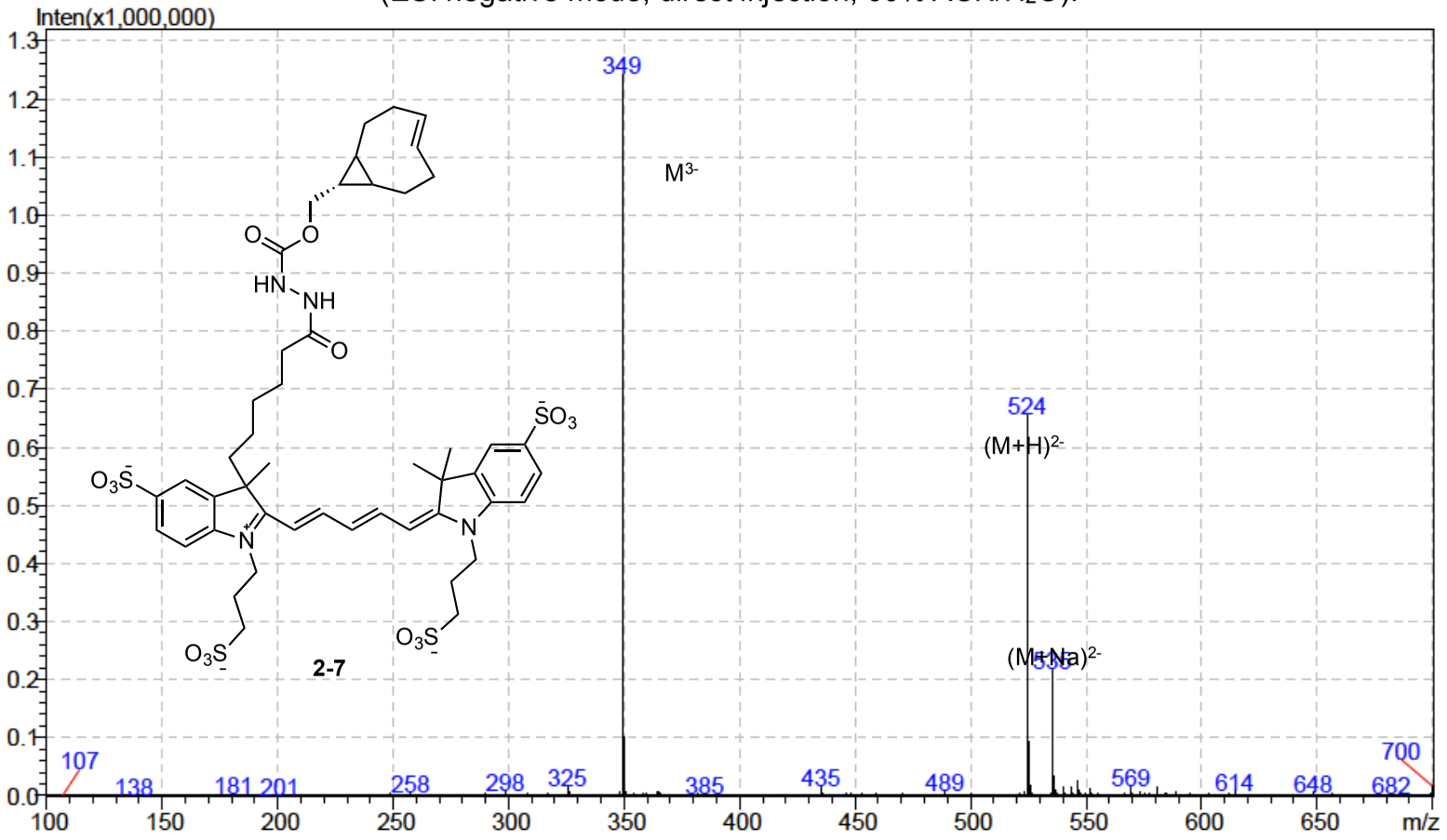

HPLC analysis of Alexa Fluor® 647-sTCO **2-7** with Shimadzu prominence HPLC with SPD-M20A diode array detector.

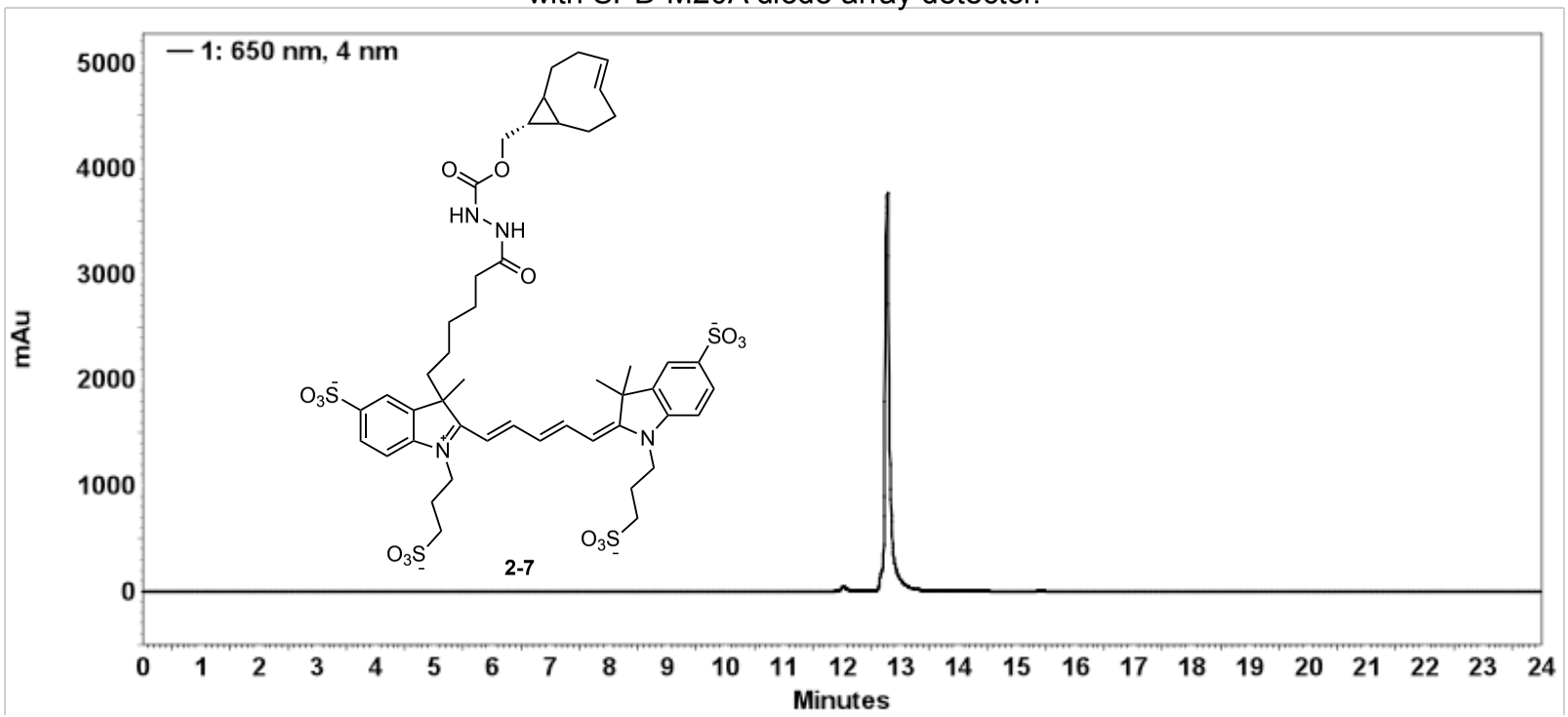

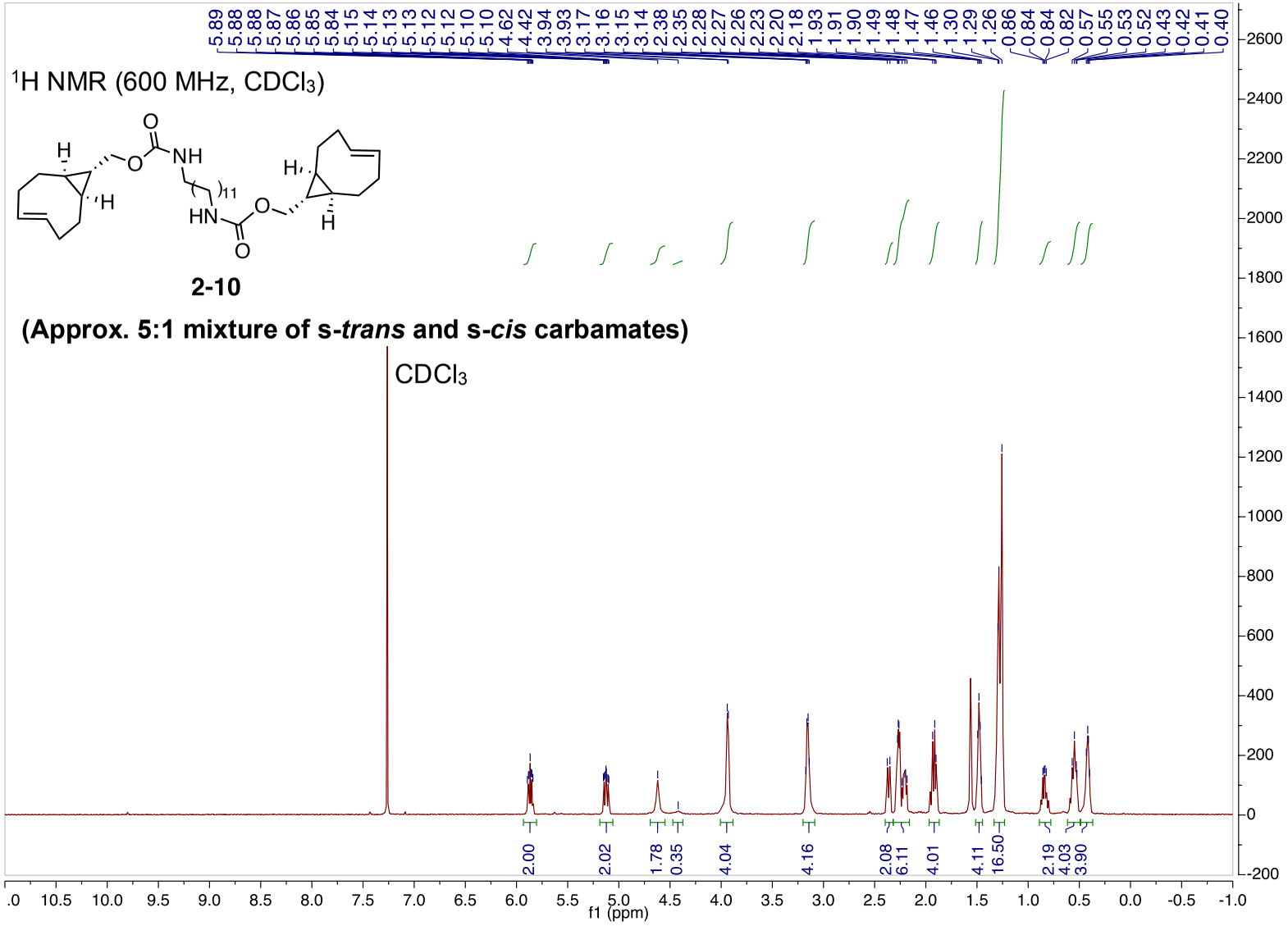
5.89 5.88 5.88 5.87 5.86 5.85 5.84 5.15 5.14 5.13 5.13 5.12 5.12 5.10 5.10 4.62 4.42 3.94 3.93 3.17 3.16 3.15 3.14 2.38 2.35 2.28 2.27 2.26 2.23 2.20 2.18 1.93 1.91 1.90 1.49 1.48 1.47 1.46 1.30 1.29 1.26 0.86 0.84 0.84 0.82 0.57 0.55 0.53 0.52 0.43 0.42 0.41 0.40
^{1}H NMR (600 MHz, $CDCl_3$)
2-10
(Approx. 5:1 mixture of s-*trans* and s-*cis* carbamates)
$CDCl_3$
2.00 2.02 1.78 0.35 4.04 4.16 2.08 6.11 4.01 4.11 16.50 2.19 4.03 3.90
f1 (ppm)

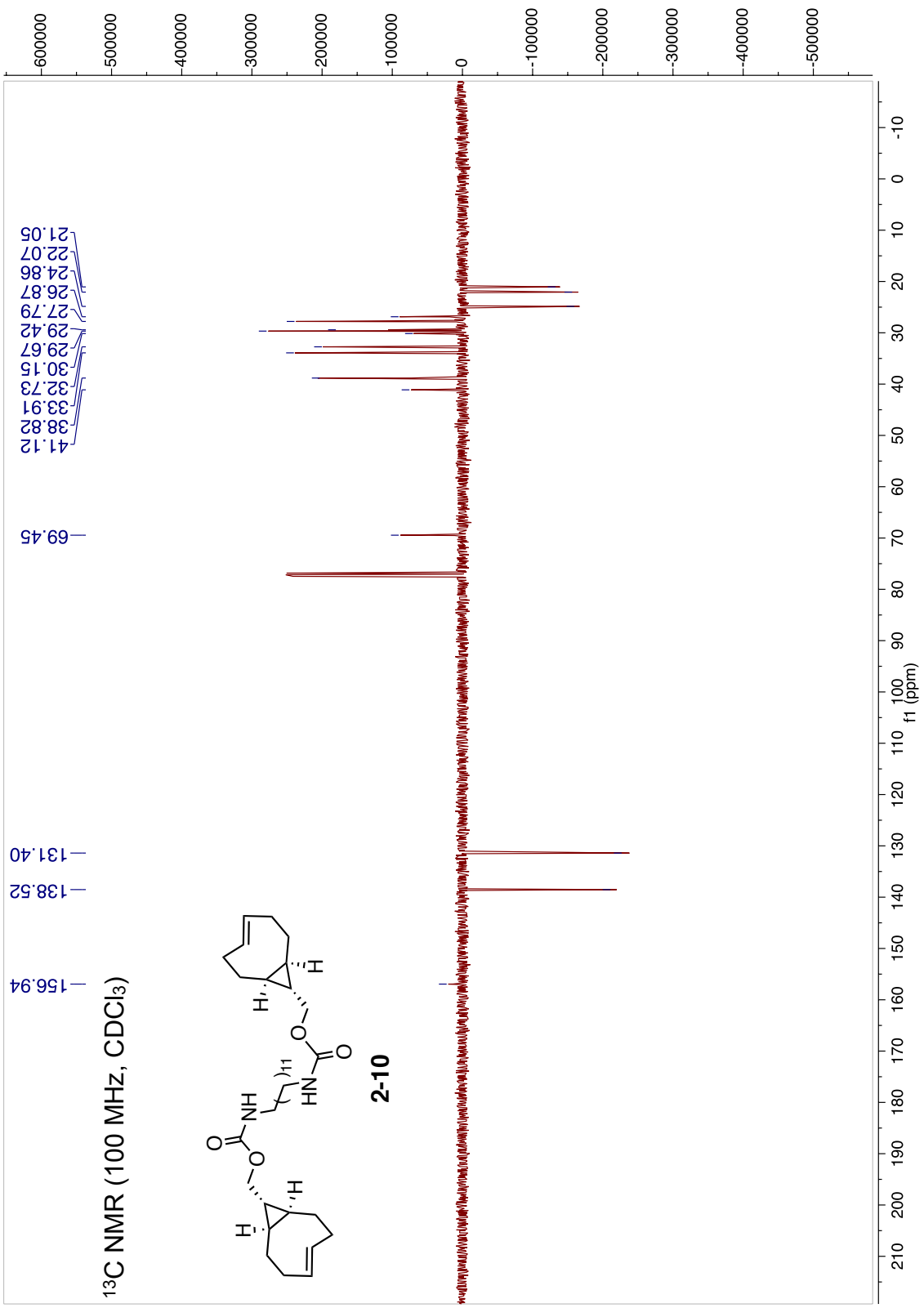
^{13}C NMR (100 MHz, $CDCl_3$)
156.94
138.52
131.40
69.45
41.12
38.82
33.91
32.73
30.15
29.67
29.42
27.79
26.87
24.86
22.07
21.05
2-10
f1 (ppm)

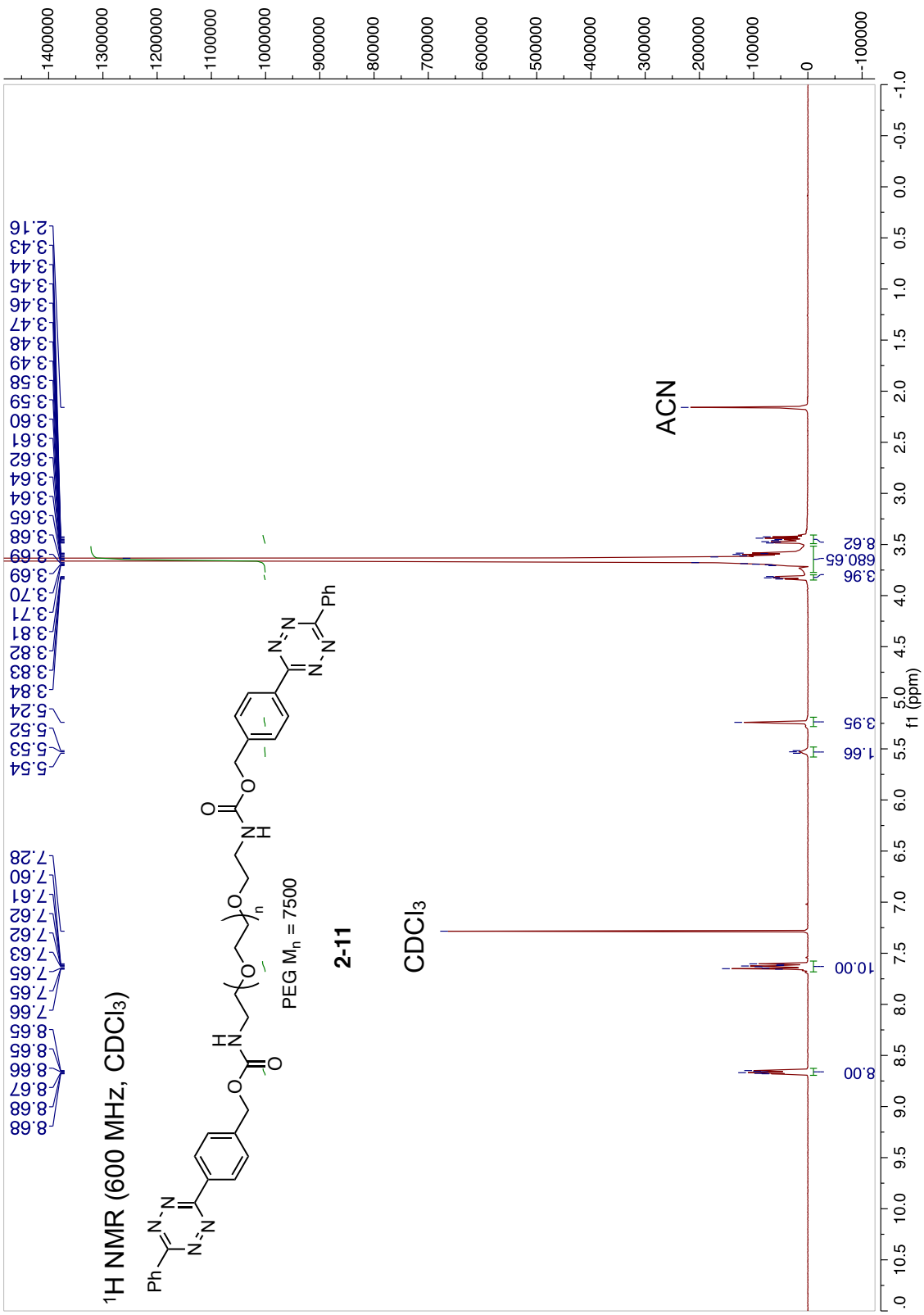
^{1}H NMR (600 MHz, CDCl$_3$)
2-11
PEG M_n = 7500
CDCl$_3$
ACN
f1 (ppm)

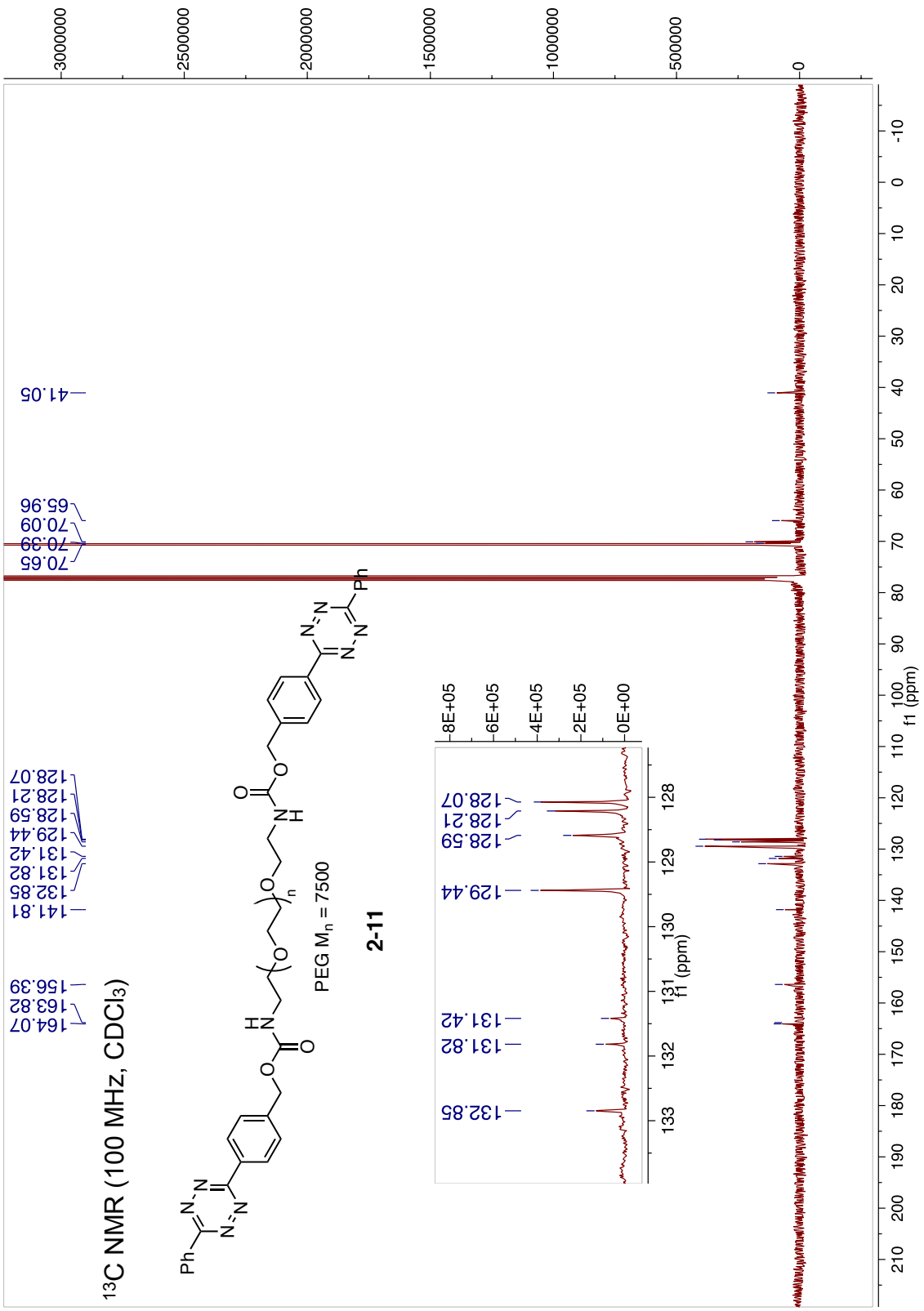
^{13}C NMR (100 MHz, CDCl$_3$)
PEG M_n = 7500
2-11
164.07
163.82
156.39
141.81
132.85
131.82
131.42
129.44
128.59
128.21
128.07
70.65
70.39
70.09
65.96
41.05
f1 (ppm)

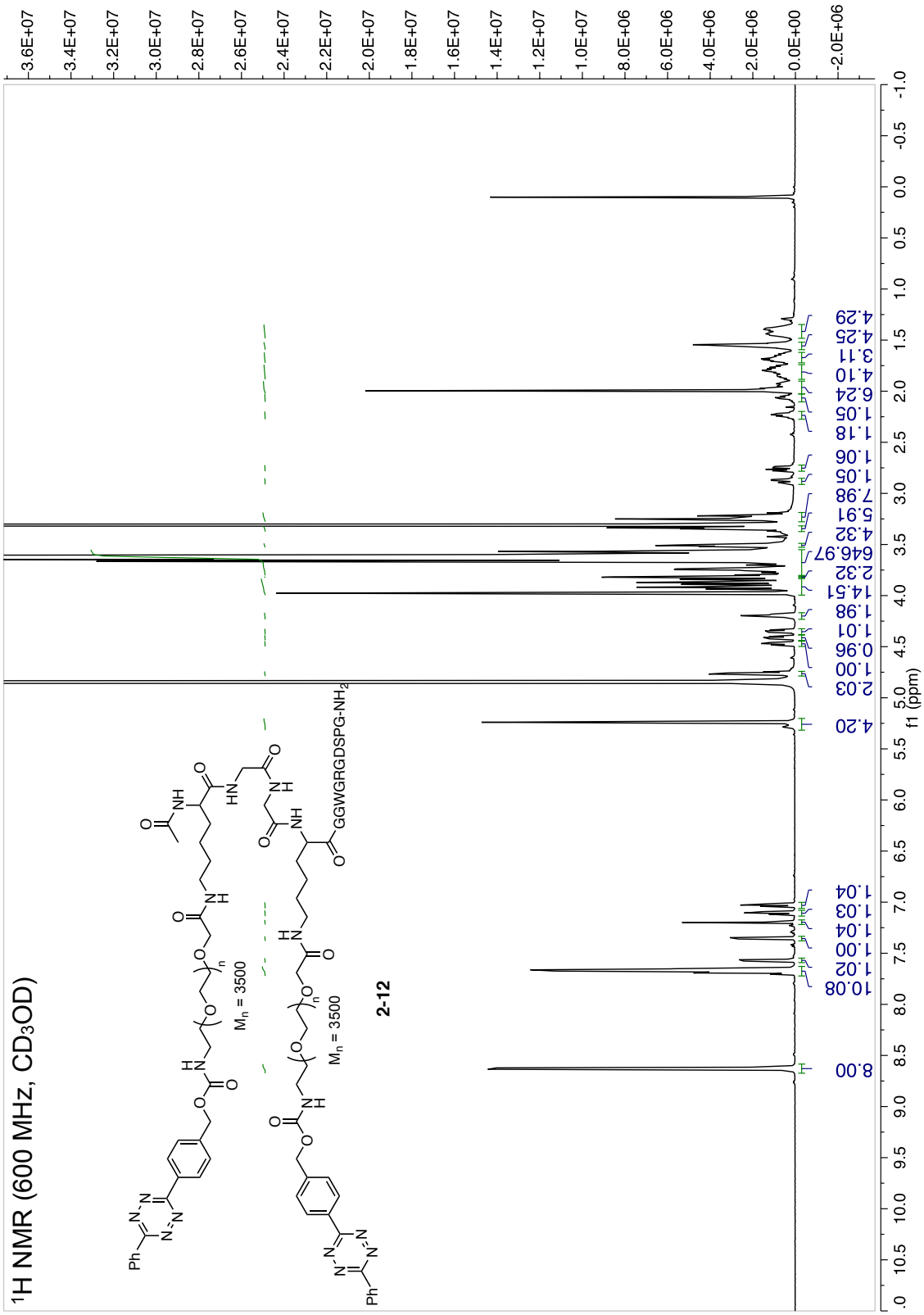
^{1}H NMR (600 MHz, CD_3OD)
2-12
M_n = 3500
M_n = 3500
GGWGRGDSPG-NH_2
f1 (ppm)
8.00
10.08
1.02
1.00
1.04
1.03
1.04
4.20
2.03
1.00
0.96
1.01
1.98
14.51
2.32
646.97
4.32
5.91
7.98
1.05
1.06
1.18
1.05
6.24
4.10
3.11
4.25
4.29

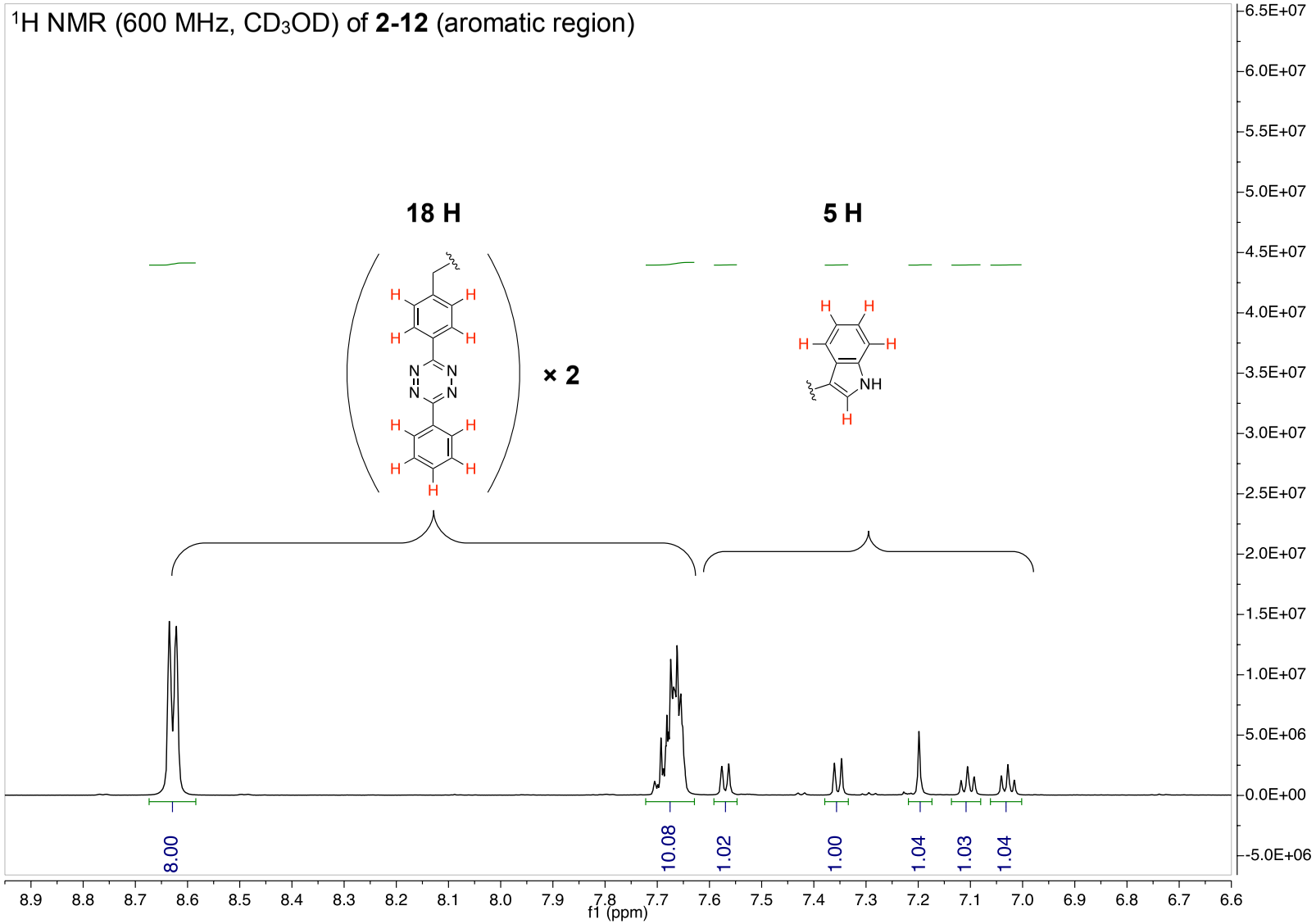
1H NMR (600 MHz, CD3OD) of 2-12 (aromatic region)
18 H
5 H
× 2
NH
8.00
10.08
1.02
1.00
1.04
1.03
1.04
f1 (ppm)

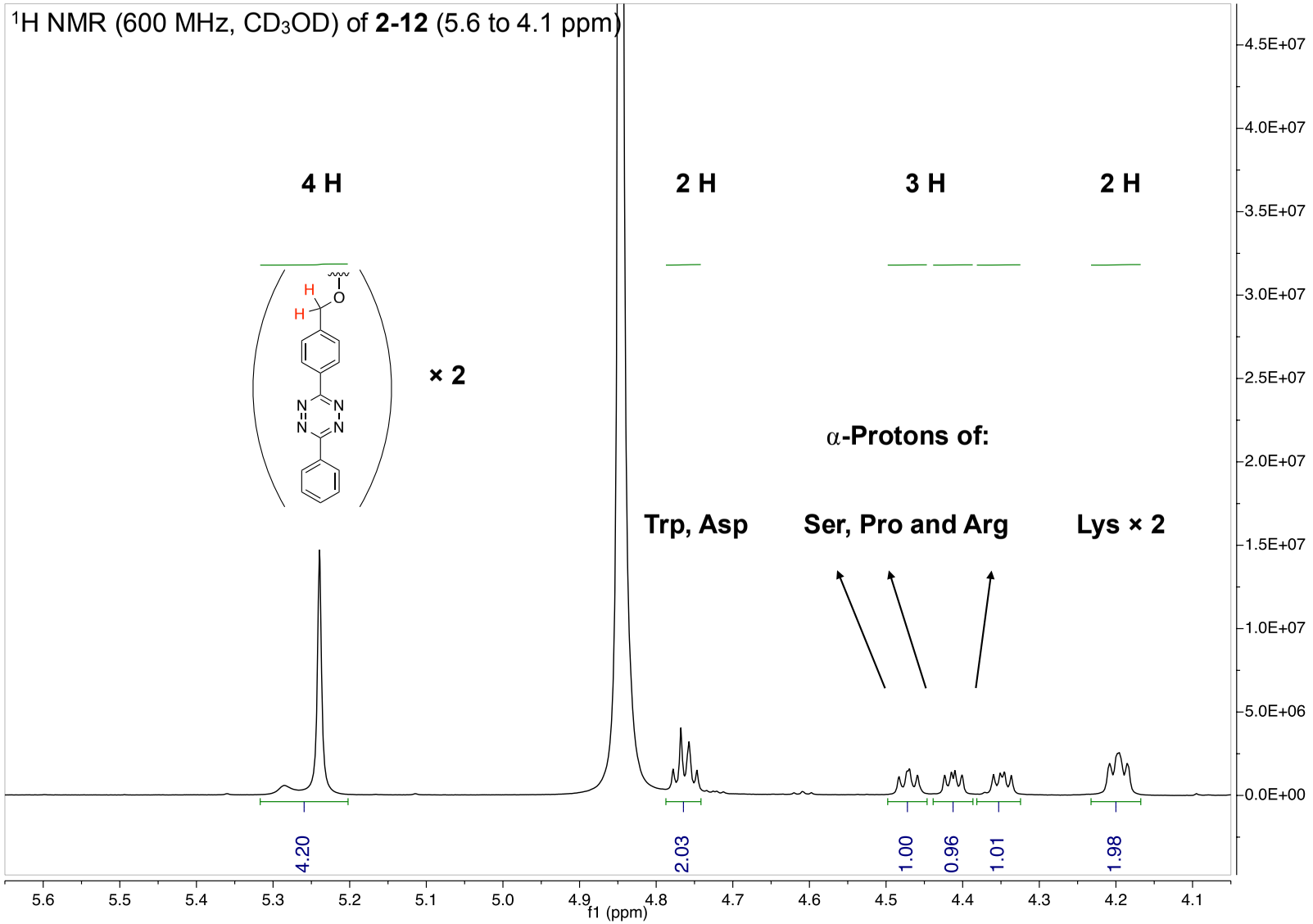
¹H NMR (600 MHz, CD3OD) of 2-12 (5.6 to 4.1 ppm)
4 H
2 H
3 H
2 H
× 2
α-Protons of:
Trp, Asp
Ser, Pro and Arg
Lys × 2
4.20
2.03
1.00
0.96
1.01
1.98
f1 (ppm)

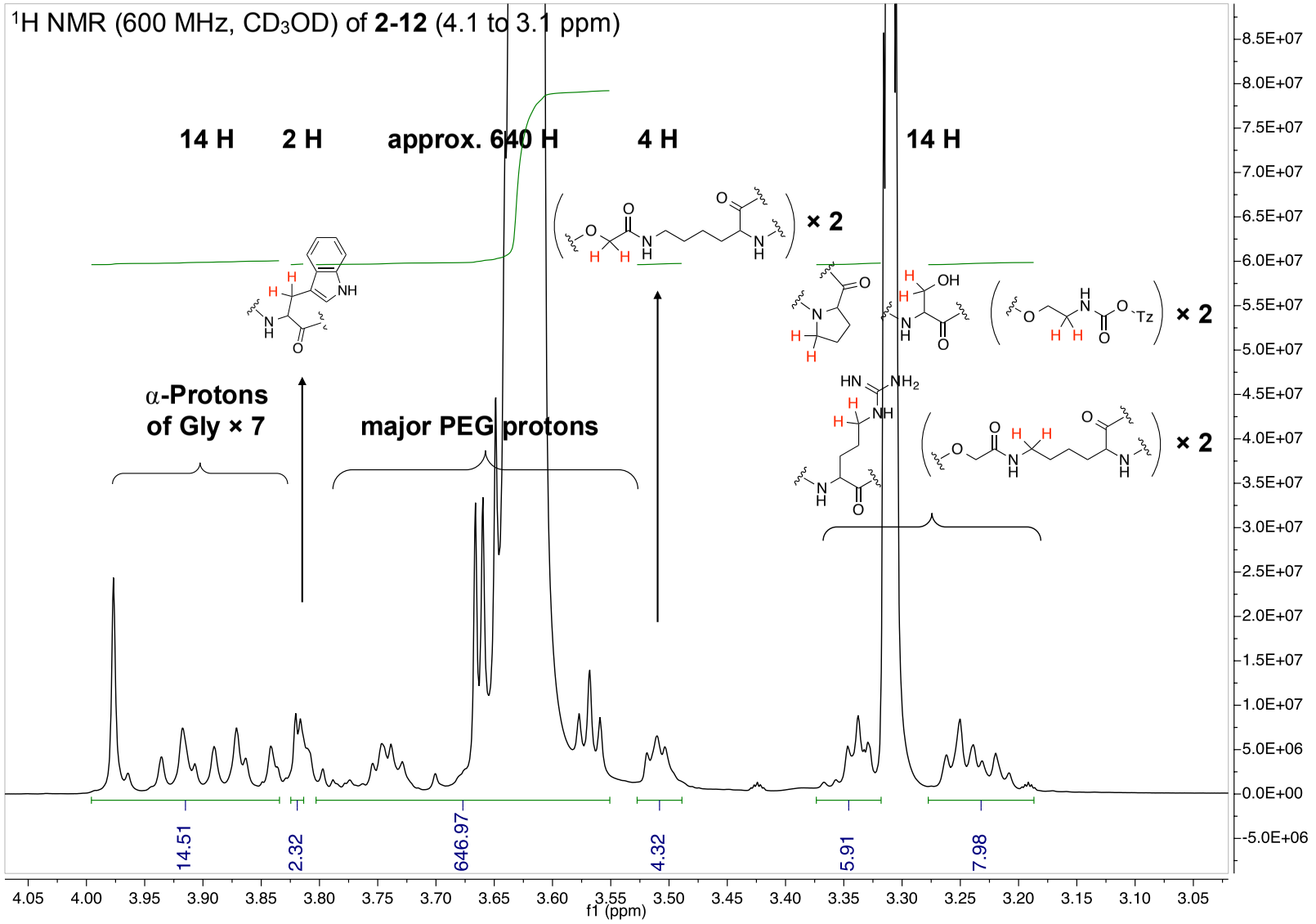
^{1}H NMR (600 MHz, CD_3OD) of **2-12** (4.1 to 3.1 ppm)
14 H
2 H
approx. 640 H
4 H
14 H
× 2
× 2
× 2
α-Protons of Gly × 7
major PEG protons
14.51
2.32
646.97
4.32
5.91
7.98
f1 (ppm)

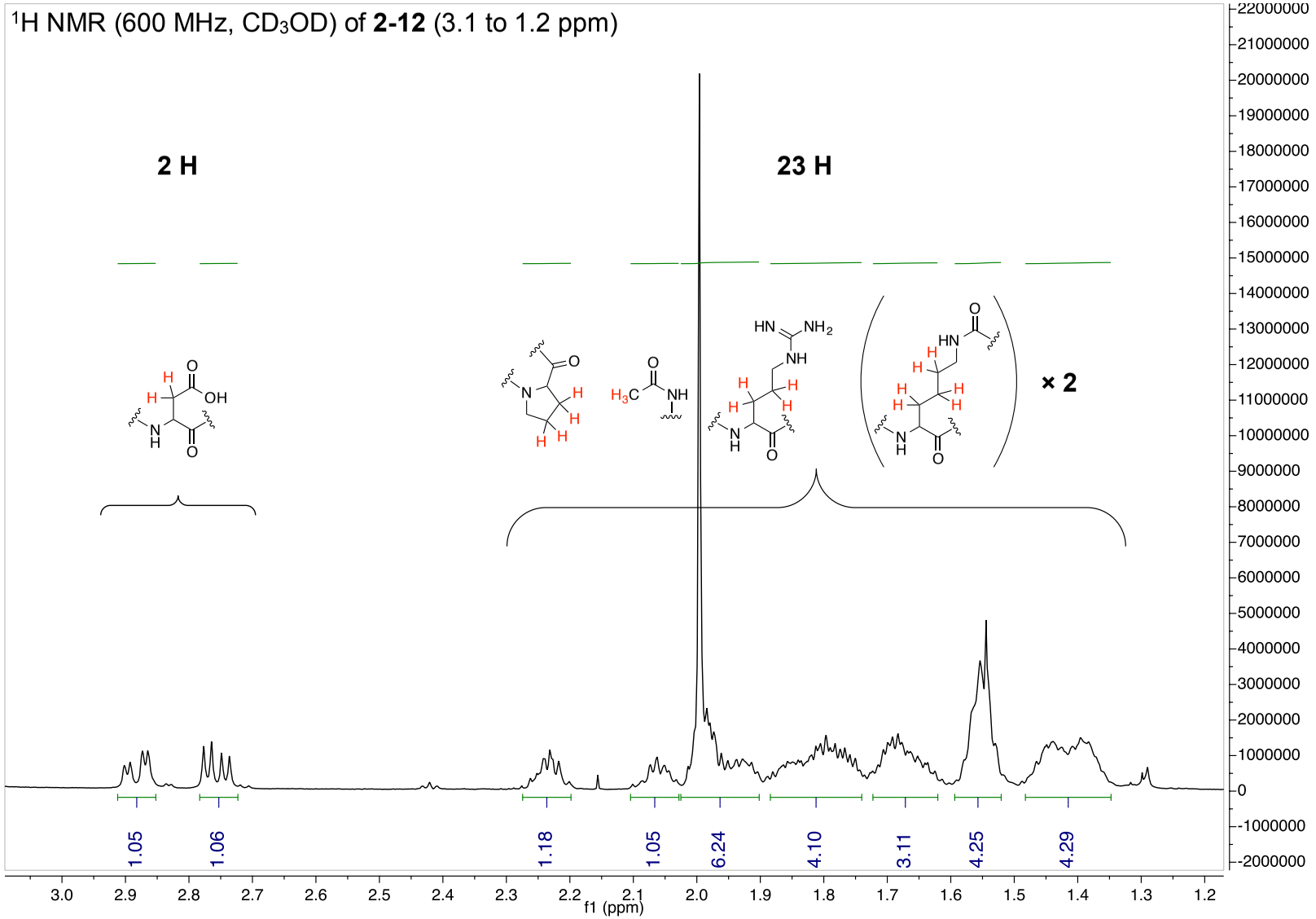
1H NMR (600 MHz, CD3OD) of 2-12 (3.1 to 1.2 ppm)
2 H
23 H
× 2
1.05
1.06
1.18
1.05
6.24
4.10
3.11
4.25
4.29
f1 (ppm)

Analytical HPLC chromatograms of *bis*-tetrazine **2-11**

UV absorbance at 300 and 254 nm was monitored.

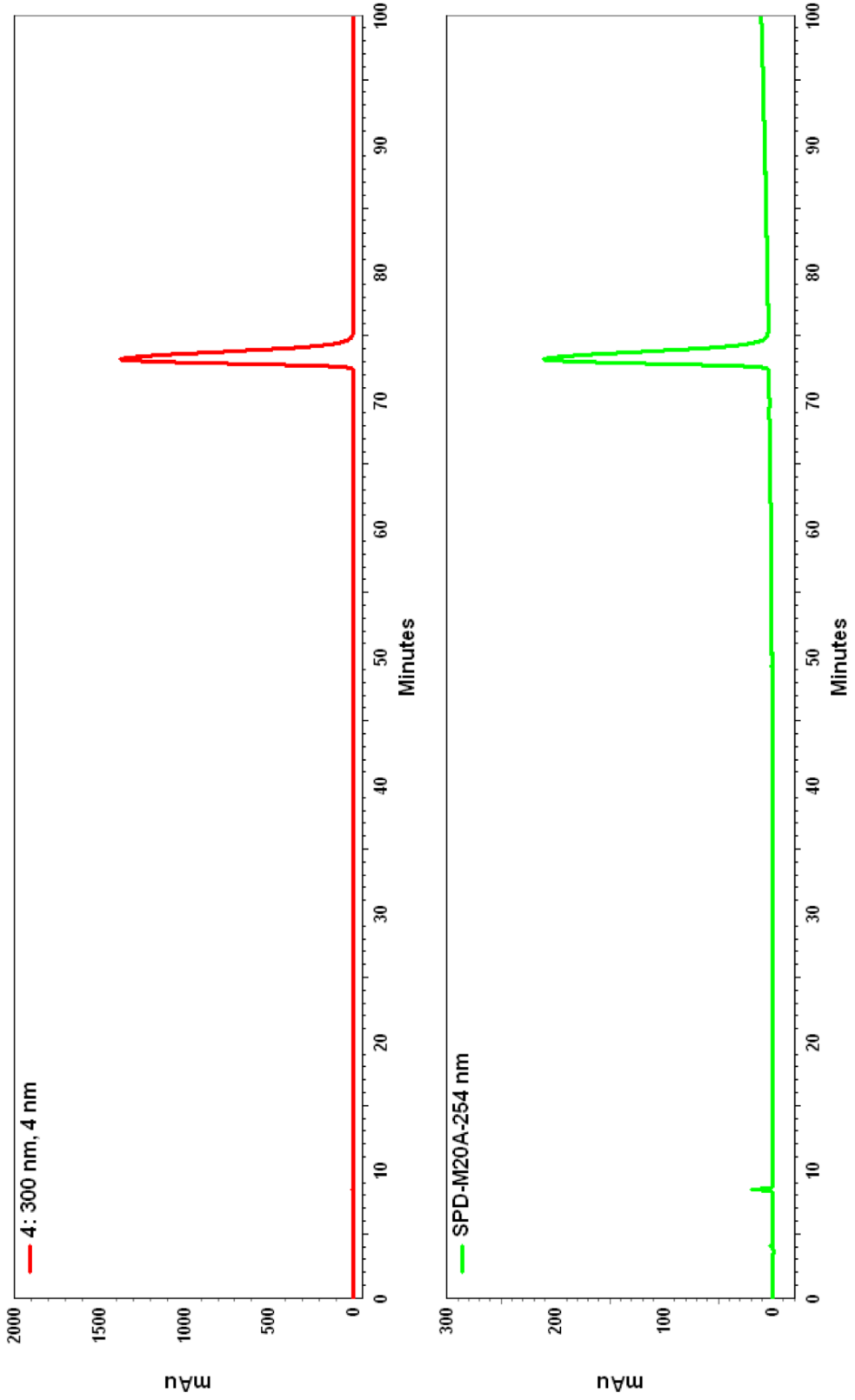

Analytical HPLC chromatograms of peptide KGGKGGWGRGDSPG.

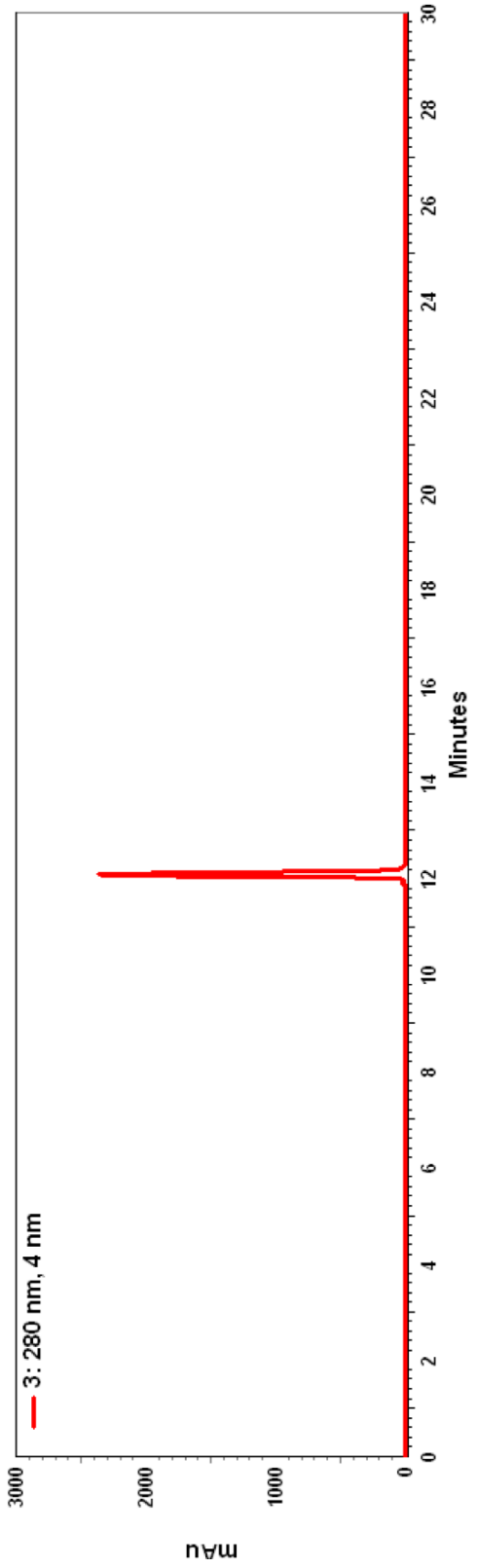

Analytical HPLC chromatograms of *bis*-tetrazine **2-12**

UV absorbance at 300 and 254 nm was monitored.

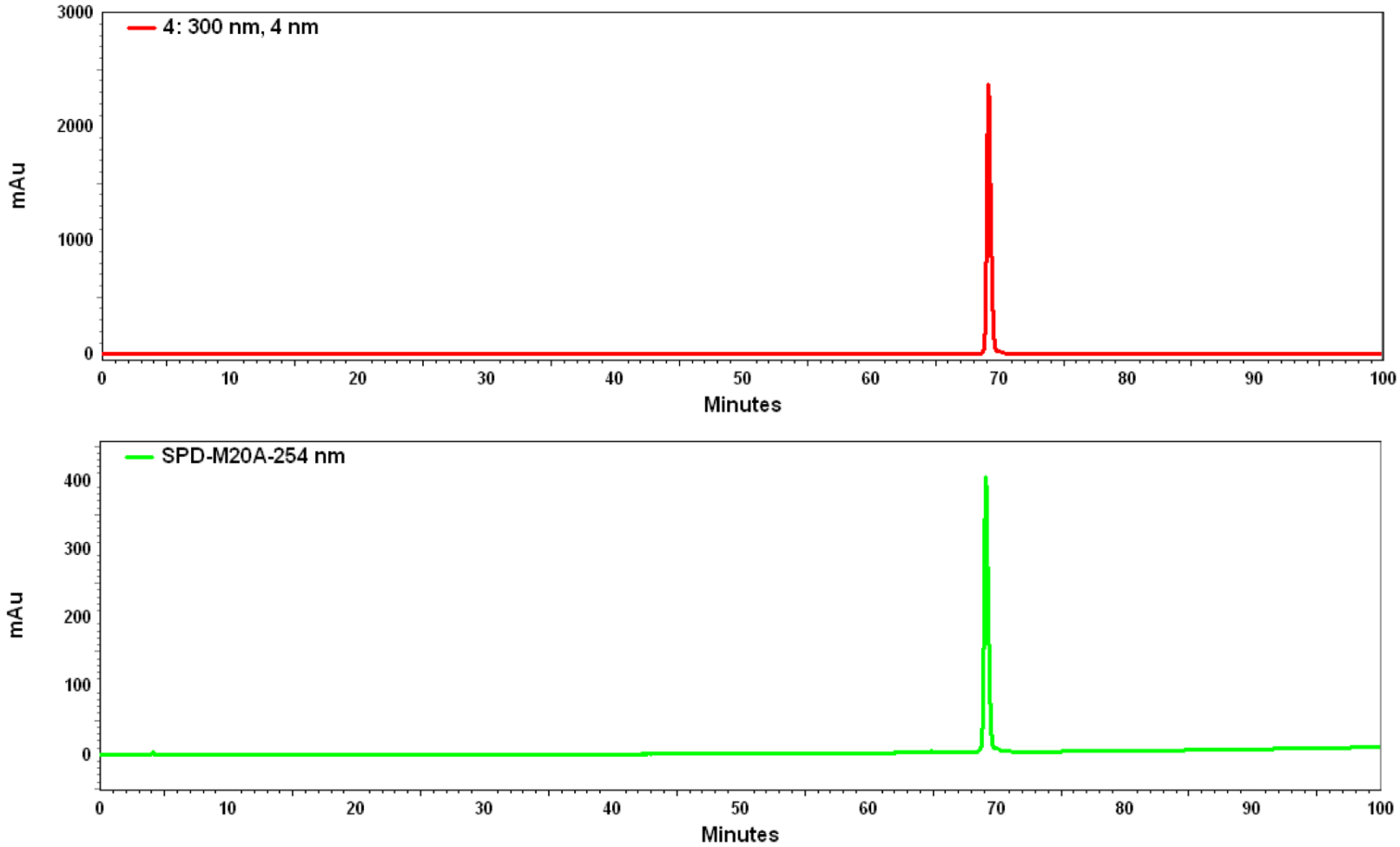

Appendix C

SPECTRAL DATA FOR CHAPTER 3

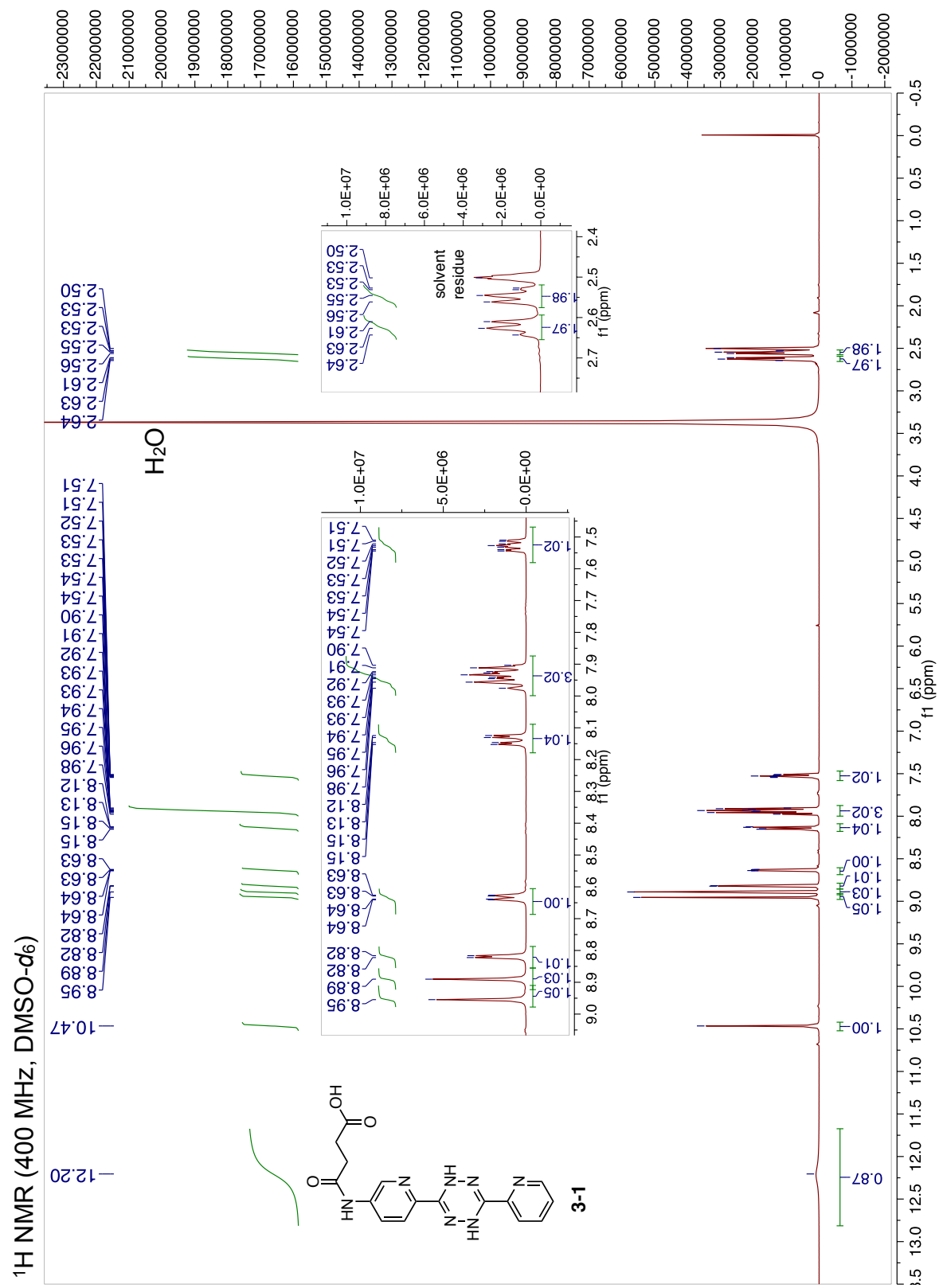
^{1}H NMR (400 MHz, DMSO-d_6)
H$_2$O
solvent residue
3-1
f1 (ppm)

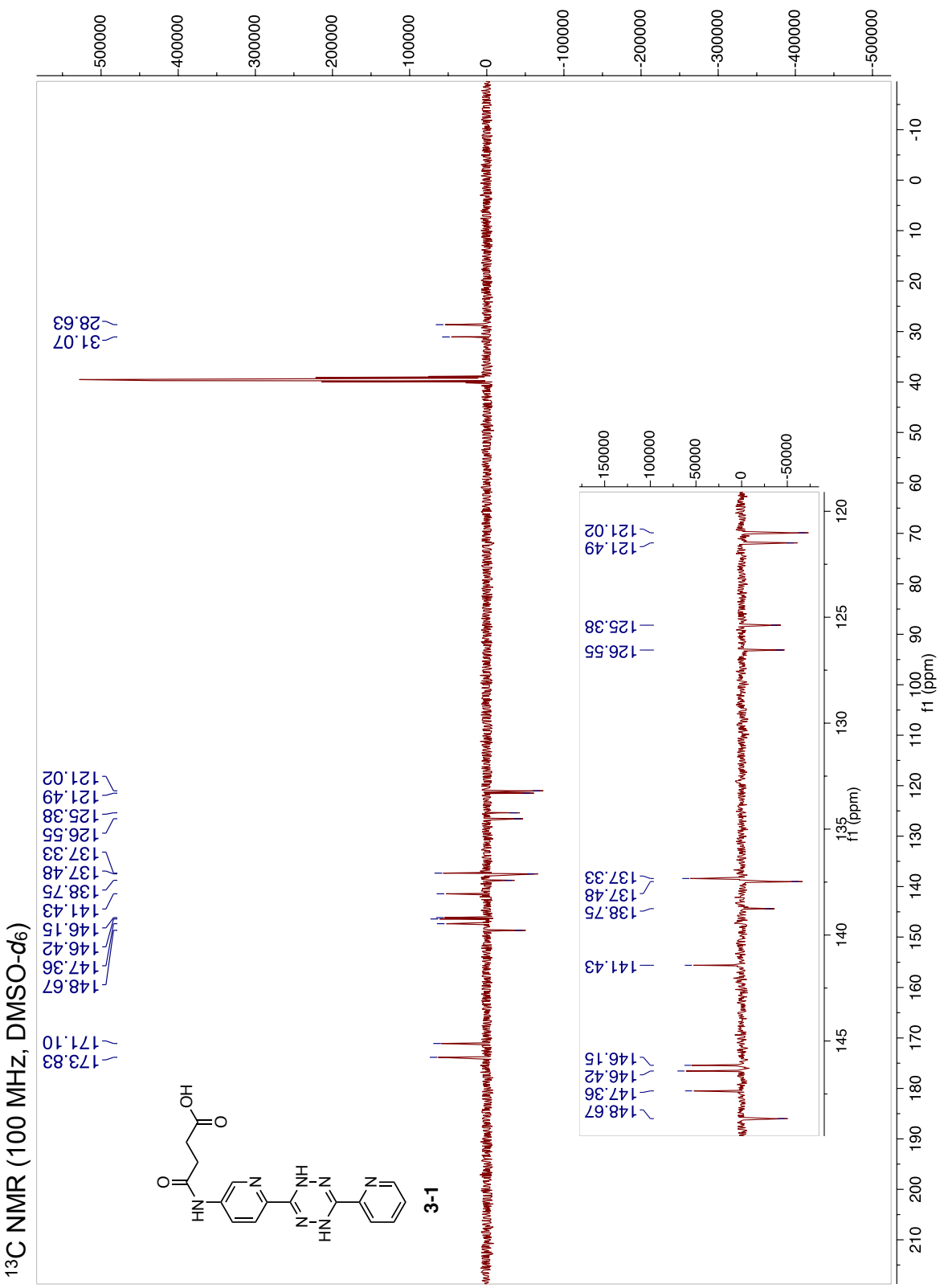
13C NMR (100 MHz, DMSO-d6)
3-1
173.83
171.10
148.67
147.36
146.42
146.15
141.43
138.75
137.48
137.33
126.55
125.38
121.49
121.02
31.07
28.63
f1 (ppm)

^{1}H NMR (600 MHz, DMSO-d_6)

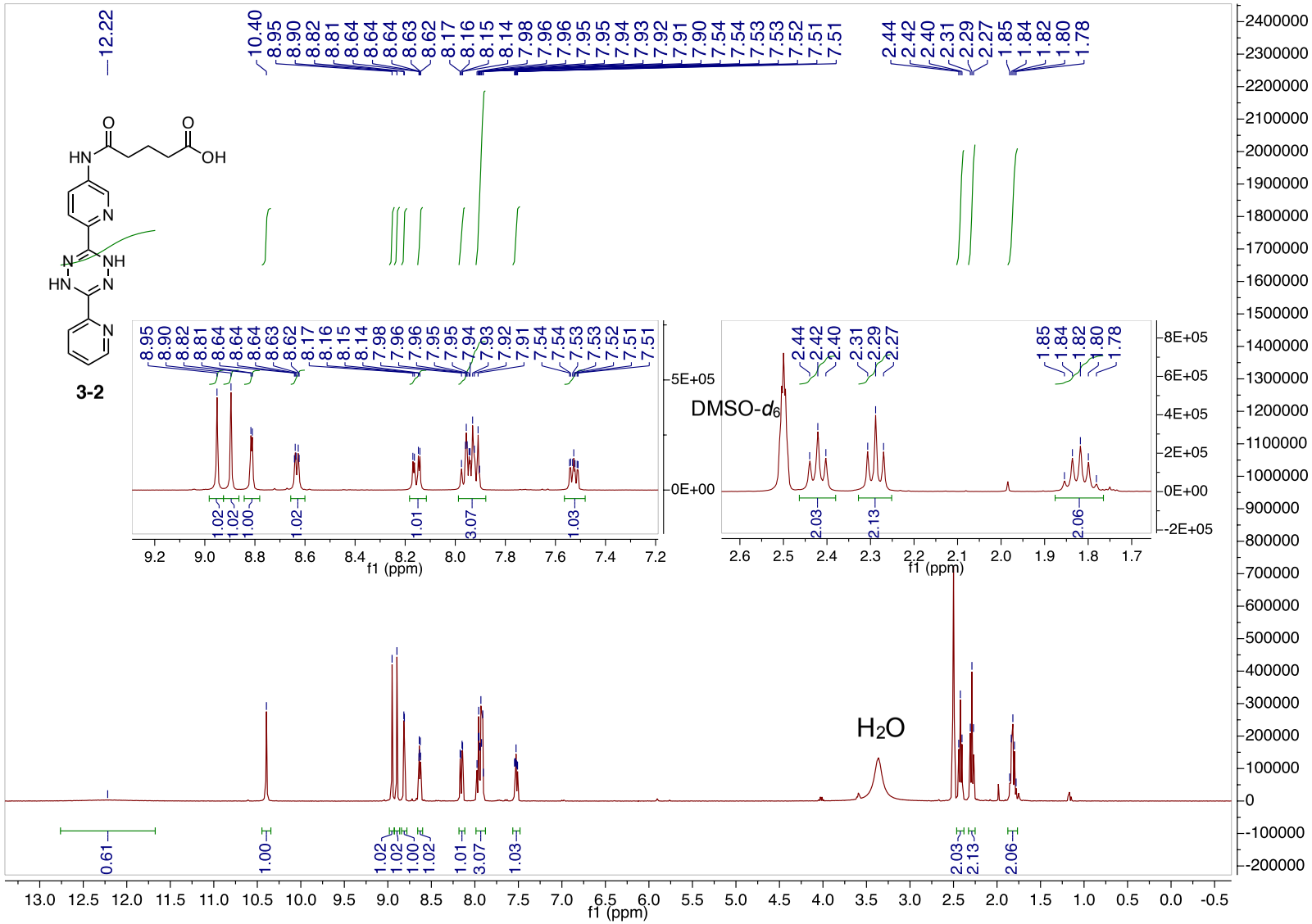

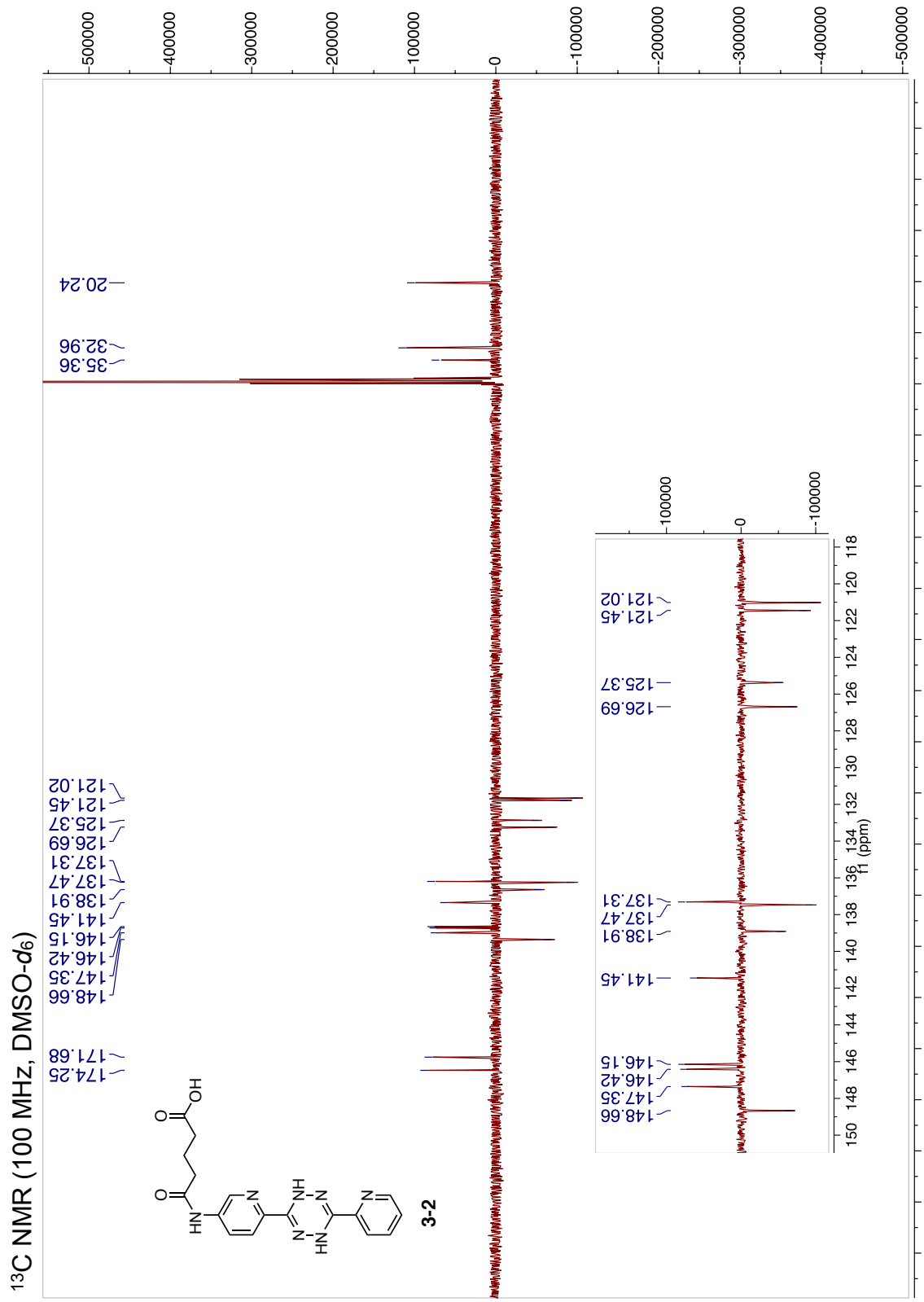
^{13}C NMR (100 MHz, DMSO-d_6)
3-2
174.25
171.68
148.66
147.35
146.42
146.15
141.45
138.91
137.47
137.31
126.69
125.37
121.45
121.02
35.36
32.96
20.24
f1 (ppm)

^{1}H NMR (600 MHz, $CDCl_3$)

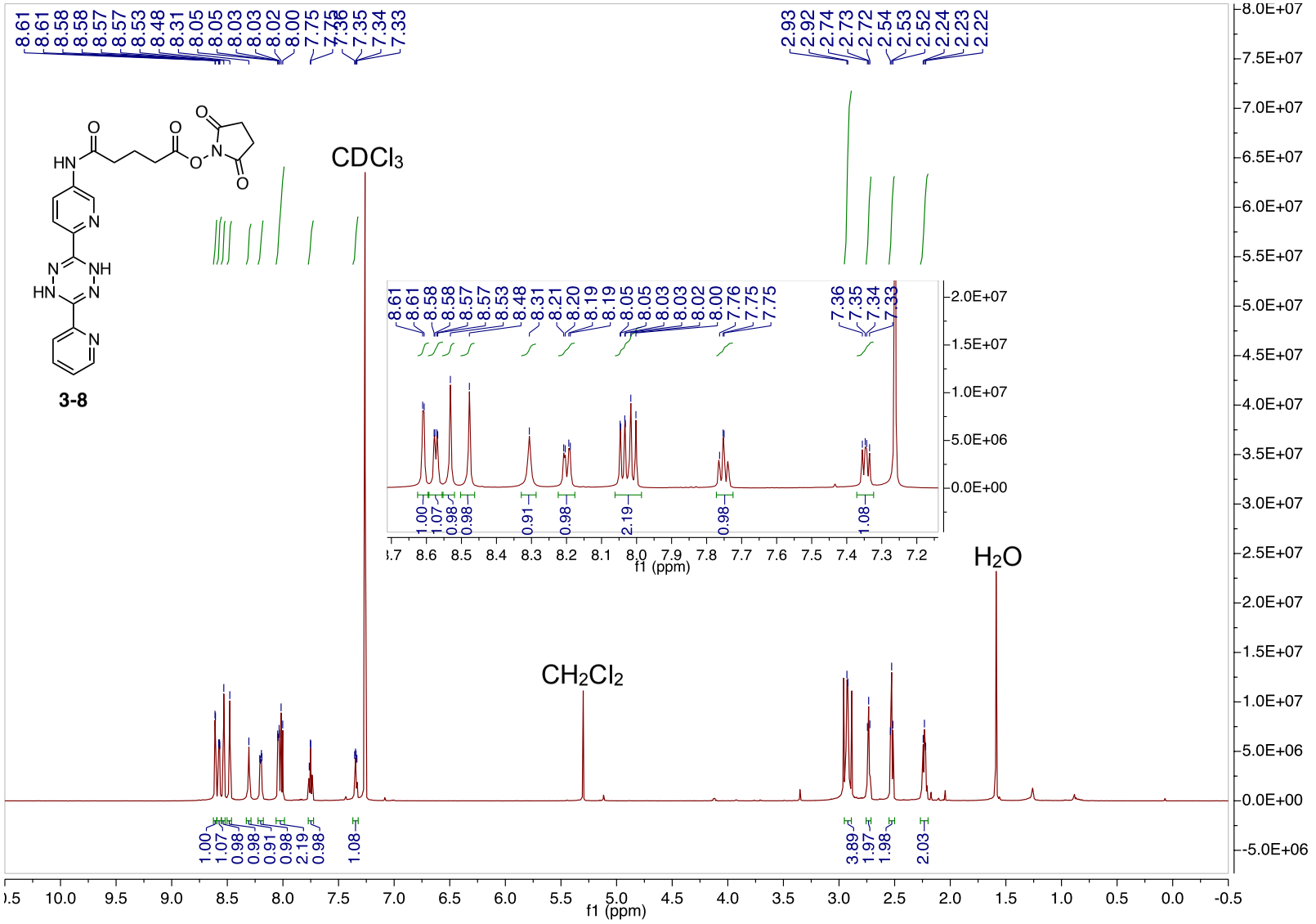

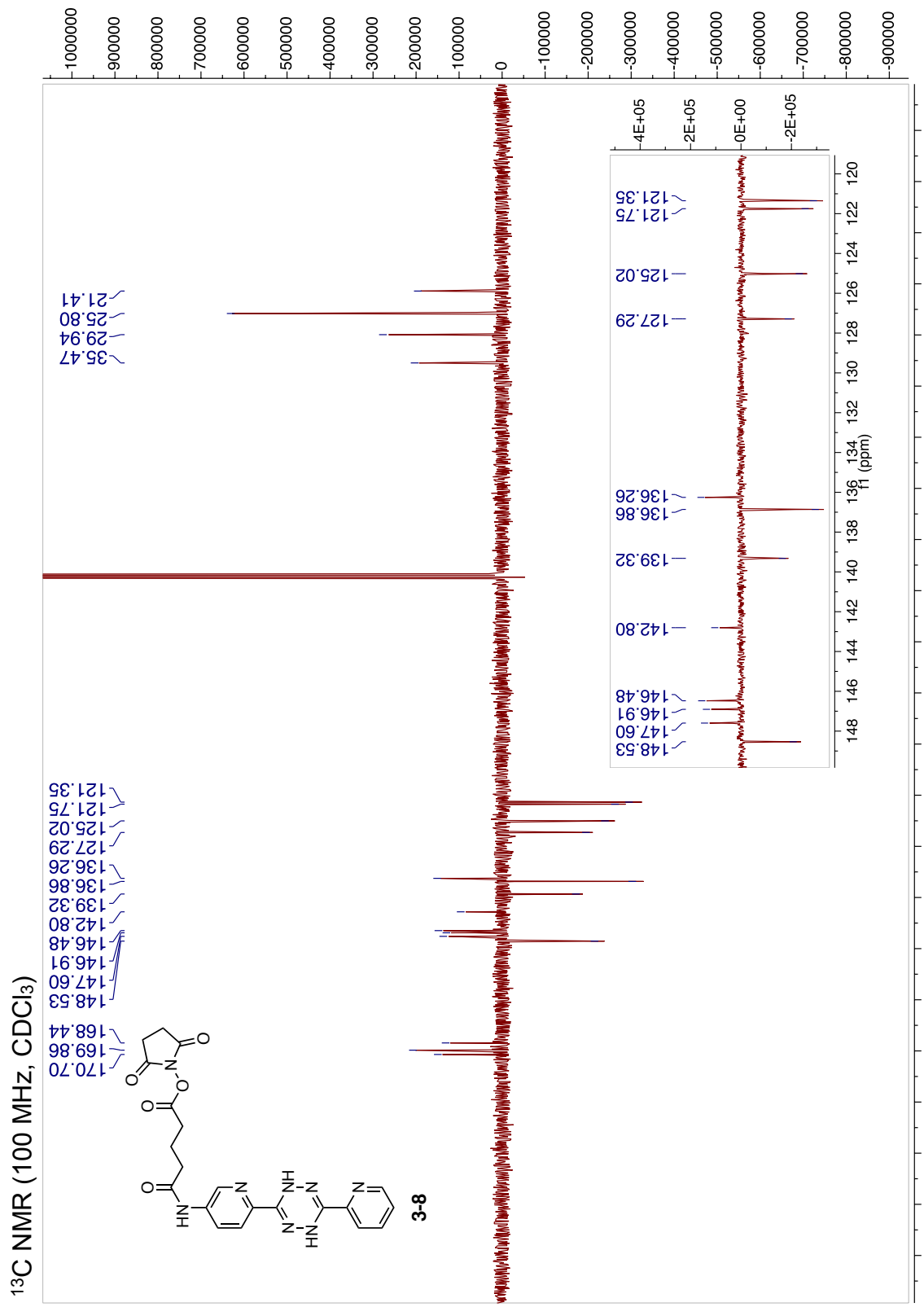
^{13}C NMR (100 MHz, CDCl$_3$)
3-8
170.70
169.86
168.44
148.53
147.60
146.91
146.48
142.80
139.32
136.86
136.26
127.29
125.02
121.75
121.35
35.47
29.94
25.80
21.41
f1 (ppm)

^{1}H NMR (600 MHz, $CDCl_3$)

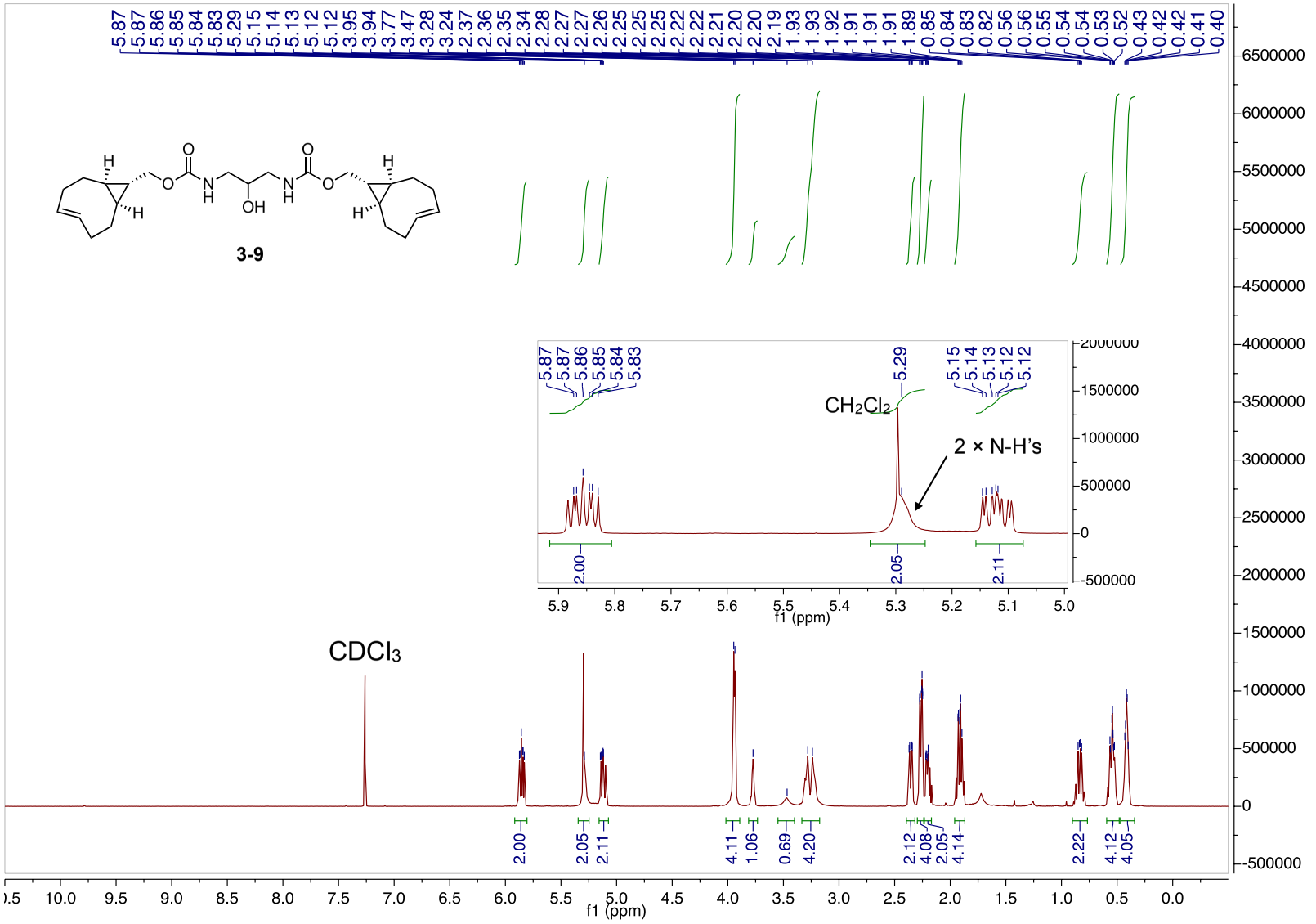

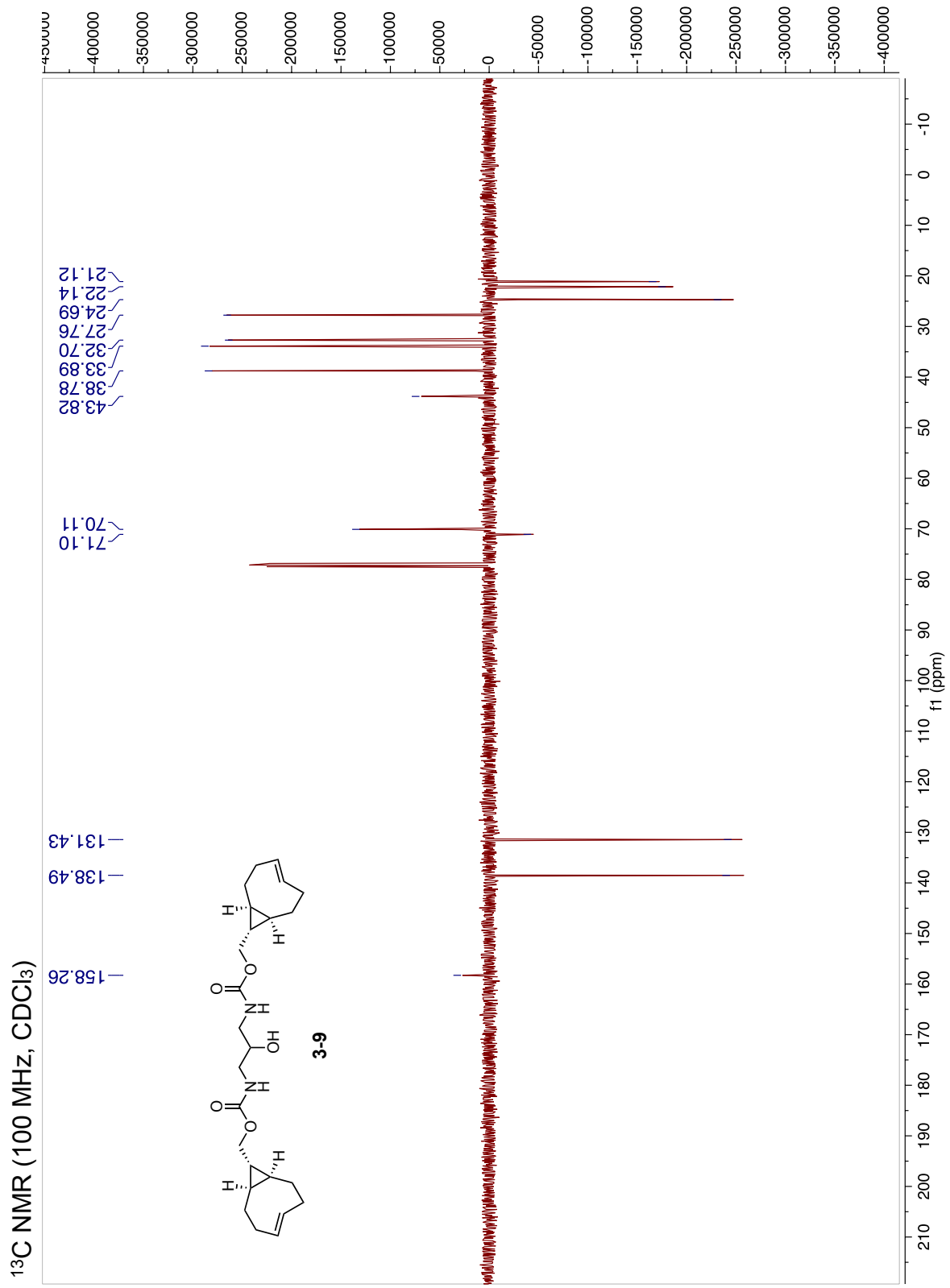
^{13}C NMR (100 MHz, CDCl$_3$)
158.26
138.49
131.43
71.10
70.11
43.82
38.78
33.89
32.70
27.76
24.69
22.14
21.12
3-9
f1 (ppm)

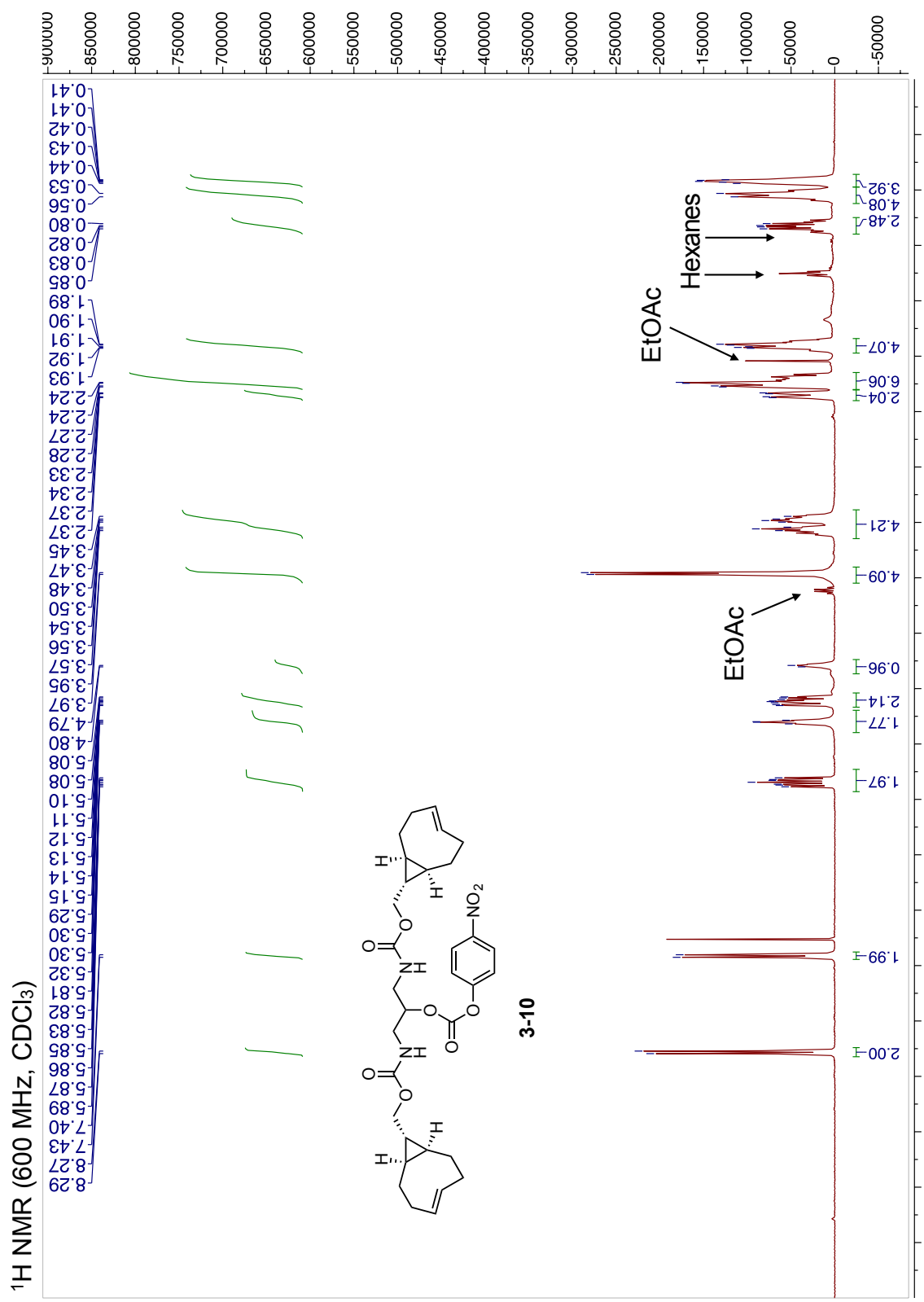
^{1}H NMR (600 MHz, CDCl$_3$)
EtOAc
Hexanes
EtOAc
3-10
f1 (ppm)

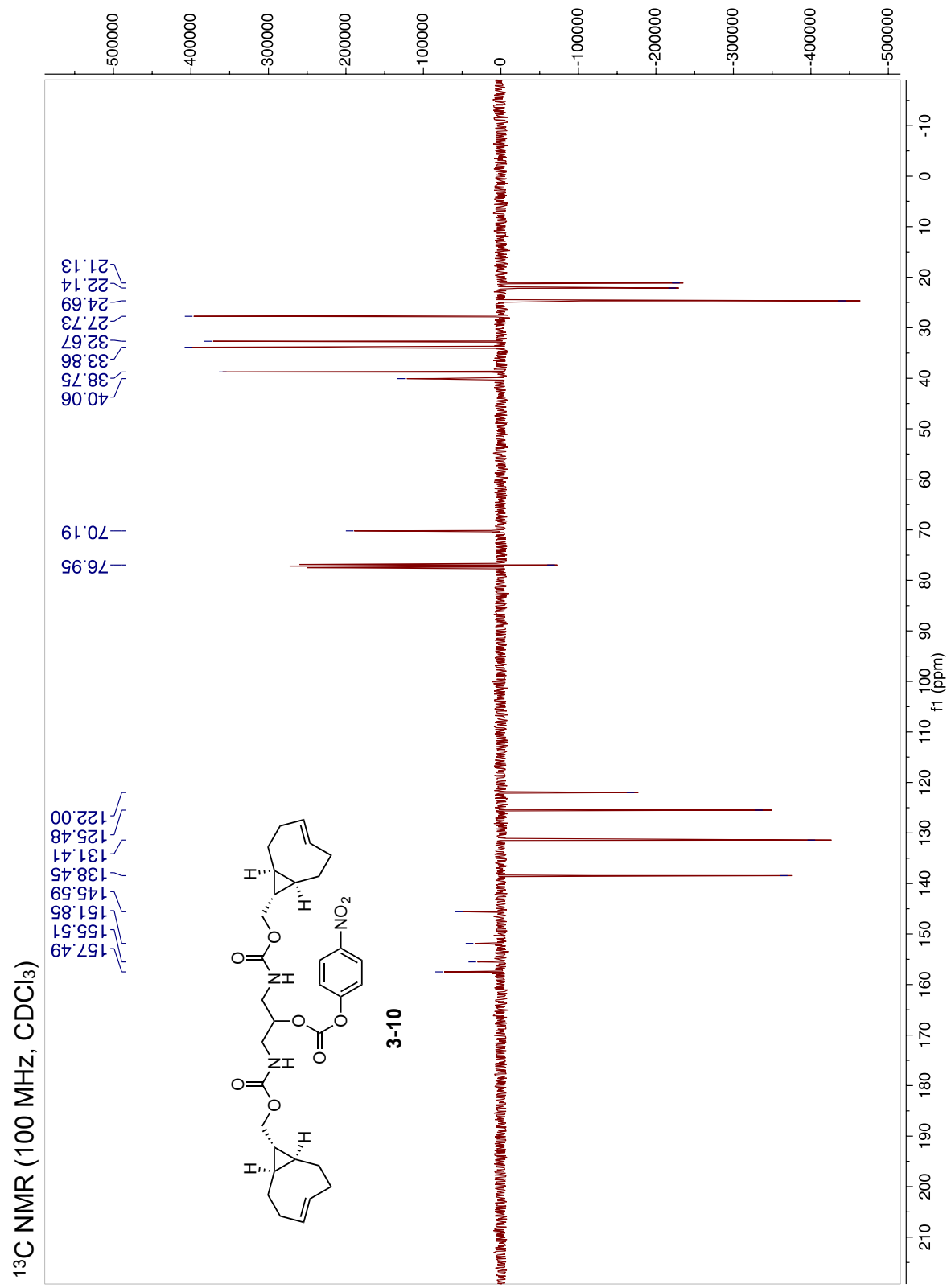
^{13}C NMR (100 MHz, CDCl$_3$)
21.13
22.14
24.69
27.73
32.67
33.86
38.75
40.06
70.19
76.95
122.00
125.48
131.41
138.45
145.59
151.85
155.51
157.49
3-10
f1 (ppm)

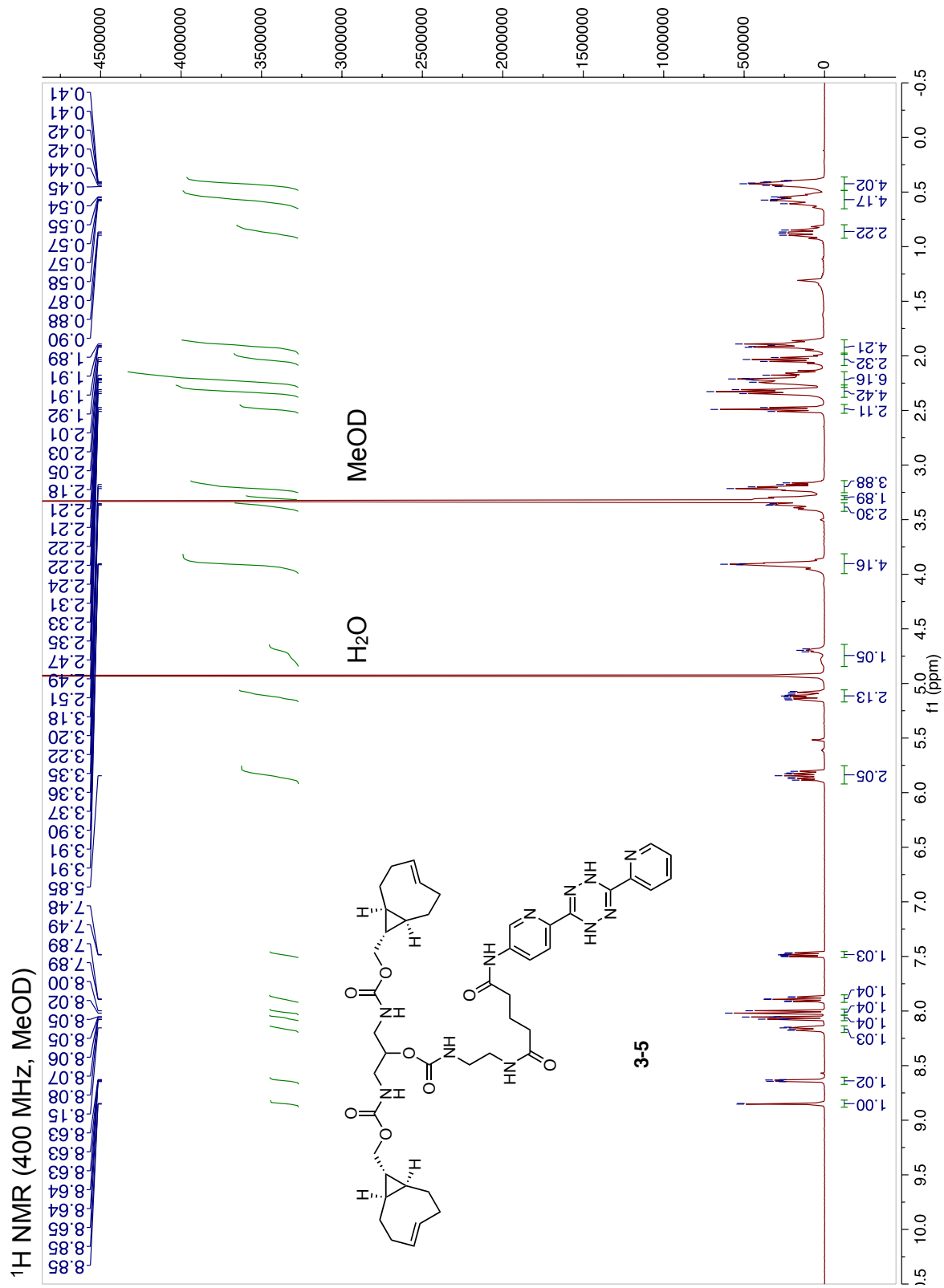
^{1}H NMR (400 MHz, MeOD)
MeOD
H_2O
3-5
f1 (ppm)

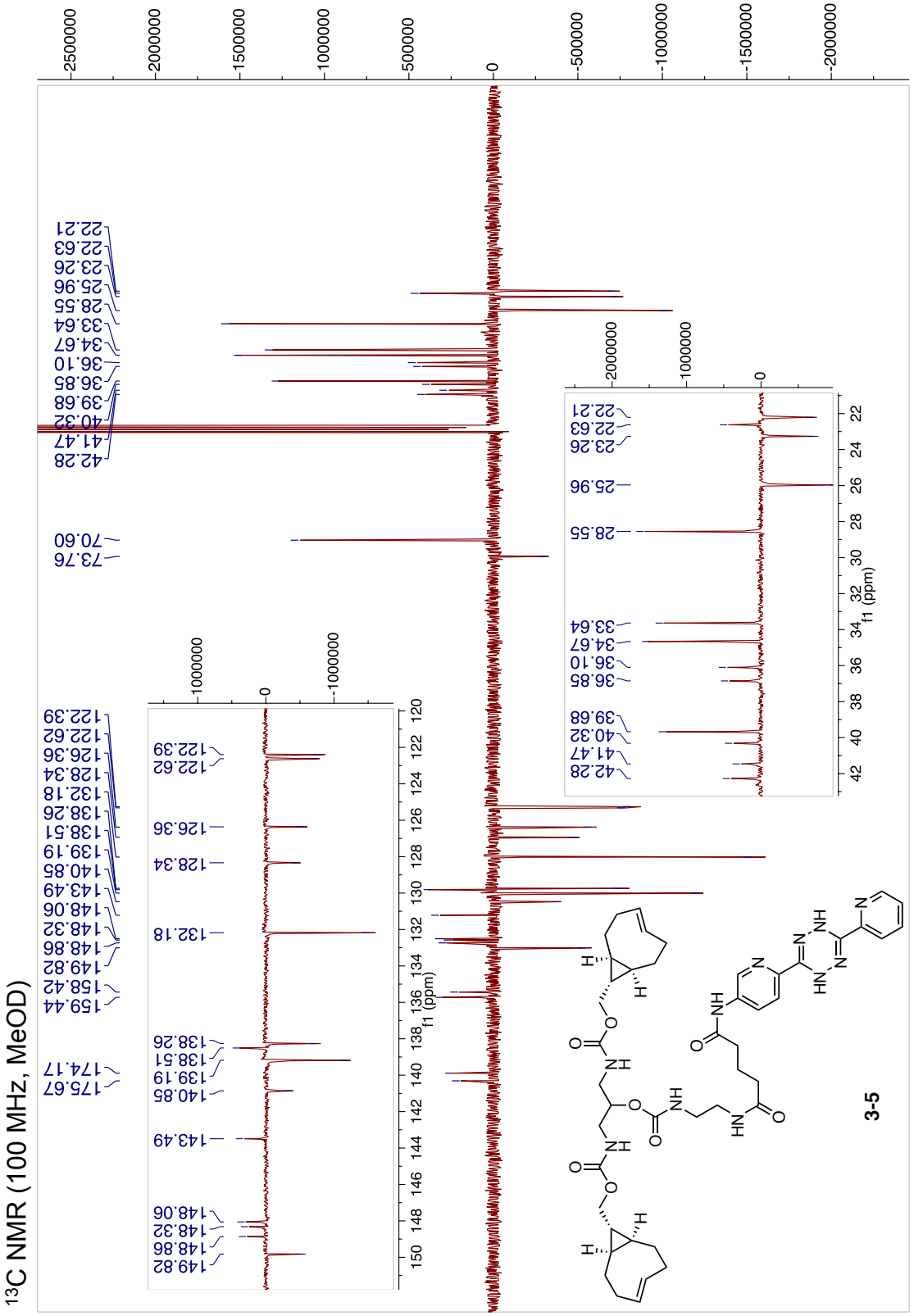
13C NMR (100 MHz, MeOD)
3-5

Appendix D

PERMISSION LETTERS

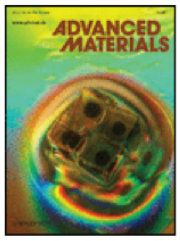

Title: Meter-Long Multiblock Copolymer Microfibers Via Interfacial Bioorthogonal Polymerization

Author: Shuang Liu,Han Zhang,Roddel A. Remy,Fei Deng,Michael E. Mackay,Joseph M. Fox,Xinqiao Jia

Publication: Advanced Materials

Publisher: John Wiley and Sons

Date: Mar 30, 2015

Order Completed

Thank you for your order.

This Agreement between Han Zhang ("You") and John Wiley and Sons ("John Wiley and Sons") consists of your license details and the terms and conditions provided by John Wiley and Sons and Copyright Clearance Center.

Your confirmation email will contain your order number for future reference.

Printable details.

License Number	4043830965651
License date	Feb 07, 2017
Licensed Content Publisher	John Wiley and Sons
Licensed Content Publication	Advanced Materials
Licensed Content Title	Meter-Long Multiblock Copolymer Microfibers Via Interfacial Bioorthogonal Polymerization
Licensed Content Author	Shuang Liu,Han Zhang,Roddel A. Remy,Fei Deng,Michael E. Mackay,Joseph M. Fox,Xinqiao Jia
Licensed Content Date	Mar 30, 2015
Licensed Content Pages	8
Type of use	Dissertation/Thesis
Requestor type	Author of this Wiley article
Format	Print and electronic
Portion	Full article
Will you be translating?	No
Title of your thesis / dissertation	Interfacial Bioorthogonal Chemistry For Biomaterials Synthesis And Patterning And Development Of Catalytic Method For "Turning-on" The Tetrazine Ligation
Expected completion date	Mar 2017
Expected size (number of pages)	300
Requestor Location	Han Zhang 5366 Tarkington Place COLUMBIA, MD 21044 United States Attn: Han Zhang
Publisher Tax ID	EU826007151
Billing Type	Invoice
Billing address	Han Zhang 5366 Tarkington Place

COLUMBIA, MD 21044
United States
Attn: Han Zhang

Total 0.00 USD

Would you like to purchase the full text of this article? If so, please continue on to the content ordering system located here: Purchase PDF

If you click on the buttons below or close this window, you will not be able to return to the content ordering system.

ORDER MORE CLOSE WINDOW

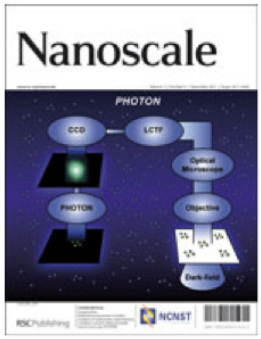

Title: Exploiting the tetrazine–norbornene reaction for single polymer chain collapse

Author: Claire F. Hansell,Annhelen Lu,Joseph P. Patterson,Rachel K. O'Reilly

Publication: Nanoscale

Publisher: Royal Society of Chemistry

Date: Mar 6, 2014

Order Completed

Thank you for your order.

This Agreement between Han Zhang ("You") and Royal Society of Chemistry ("Royal Society of Chemistry") consists of your license details and the terms and conditions provided by Royal Society of Chemistry and Copyright Clearance Center.

Your confirmation email will contain your order number for future reference.

Printable details.

License Number	4050601046156
License date	Feb 16, 2017
Licensed Content Publisher	Royal Society of Chemistry
Licensed Content Publication	Nanoscale
Licensed Content Title	Exploiting the tetrazine–norbornene reaction for single polymer chain collapse
Licensed Content Author	Claire F. Hansell,Annhelen Lu,Joseph P. Patterson,Rachel K. O'Reilly
Licensed Content Date	Mar 6, 2014
Licensed Content Volume	6
Licensed Content Issue	8
Type of Use	Thesis/Dissertation
Requestor type	academic/educational
Portion	figures/tables/images
Number of figures/tables/images	1
Distribution quantity	3
Format	print and electronic
Will you be translating?	no
Order reference number	
Title of the thesis/dissertation	Interfacial Bioorthogonal Chemistry For Biomaterials Synthesis And Patterning And Development Of Catalytic Method For "Turning-on" The Tetrazine Ligation
Expected completion date	Mar 2017
Estimated size	300
Requestor Location	Han Zhang 5366 Tarkington Place COLUMBIA, MD 21044 United States Attn: Han Zhang
Billing Type	Invoice

Billing address	Han Zhang 5366 Tarkington Place COLUMBIA, MD 21044 United States Attn: Han Zhang
Total	0.00 USD

ORDER MORE CLOSE WINDOW

Title:	Simultaneous Orthogonal Dual-Click Approach to Tough, in-Situ-Forming Hydrogels for Cell Encapsulation
Author:	Vinh X. Truong, Matthew P. Ablett, Stephen M. Richardson, et al
Publication:	Journal of the American Chemical Society
Publisher:	American Chemical Society
Date:	Feb 1, 2015

PERMISSION/LICENSE IS GRANTED FOR YOUR ORDER AT NO CHARGE

This type of permission/license, instead of the standard Terms & Conditions, is sent to you because no fee is being charged for your order. Please note the following:

- Permission is granted for your request in both print and electronic formats, and translations.
- If figures and/or tables were requested, they may be adapted or used in part.
- Please print this page for your records and send a copy of it to your publisher/graduate school.
- Appropriate credit for the requested material should be given as follows: "Reprinted (adapted) with permission from (COMPLETE REFERENCE CITATION). Copyright (YEAR) American Chemical Society." Insert appropriate information in place of the capitalized words.
- One-time permission is granted only for the use specified in your request. No additional uses are granted (such as derivative works or other editions). For any other uses, please submit a new request.

If credit is given to another source for the material you requested, permission must be obtained from that source.

Title:	Versatile click alginate hydrogels crosslinked via tetrazine–norbornene chemistry
Author:	Rajiv M. Desai,Sandeep T. Koshy,Scott A. Hilderbrand,David J. Mooney,Neel S. Joshi
Publication:	Biomaterials
Publisher:	Elsevier
Date:	May 2015

Order Completed

Thank you for your order.

This Agreement between Han Zhang ("You") and Elsevier ("Elsevier") consists of your license details and the terms and conditions provided by Elsevier and Copyright Clearance Center.

Your confirmation email will contain your order number for future reference.

Printable details.

License Number	4050601363173
License date	Feb 16, 2017
Licensed Content Publisher	Elsevier
Licensed Content Publication	Biomaterials
Licensed Content Title	Versatile click alginate hydrogels crosslinked via tetrazine–norbornene chemistry
Licensed Content Author	Rajiv M. Desai,Sandeep T. Koshy,Scott A. Hilderbrand,David J. Mooney,Neel S. Joshi
Licensed Content Date	May 2015
Licensed Content Volume	50
Licensed Content Issue	n/a
Licensed Content Pages	8
Type of Use	reuse in a thesis/dissertation
Portion	figures/tables/illustrations
Number of figures/tables/illustrations	1
Format	both print and electronic
Are you the author of this Elsevier article?	No
Will you be translating?	No
Order reference number	
Original figure numbers	Figure 1
Title of your thesis/dissertation	Interfacial Bioorthogonal Chemistry For Biomaterials Synthesis And Patterning And Development Of Catalytic Method For "Turning-on" The Tetrazine Ligation
Expected completion date	Mar 2017
Estimated size (number of pages)	300
Elsevier VAT number	GB 494 6272 12
Requestor Location	Han Zhang 5366 Tarkington Place COLUMBIA, MD 21044 United States Attn: Han Zhang
Publisher Tax ID	98-0397604

Total	0.00 USD

ORDER MORE CLOSE WINDOW

Title: Cooperative, Reversible Self-Assembly of Covalently Pre-Linked Proteins into Giant Fibrous Structures

Author: Saadyah Averick,Orsolya Karácsony,Jacob Mohin,Xin Yong,Nicholas M. Moellers,Bradley F. Woodman,Weipu Zhu,Ryan A. Mehl,Anna C. Balazs,Tomasz Kowalewski,Krzysztof Matyjaszewski

Publication: Angewandte Chemie International Edition

Publisher: John Wiley and Sons

Date: Jul 9, 2014

Order Completed

Thank you for your order.

This Agreement between Han Zhang ("You") and John Wiley and Sons ("John Wiley and Sons") consists of your license details and the terms and conditions provided by John Wiley and Sons and Copyright Clearance Center.

Your confirmation email will contain your order number for future reference.

Printable details.

License Number	4050610129094
License date	Feb 16, 2017
Licensed Content Publisher	John Wiley and Sons
Licensed Content Publication	Angewandte Chemie International Edition
Licensed Content Title	Cooperative, Reversible Self-Assembly of Covalently Pre-Linked Proteins into Giant Fibrous Structures
Licensed Content Author	Saadyah Averick,Orsolya Karácsony,Jacob Mohin,Xin Yong,Nicholas M. Moellers,Bradley F. Woodman,Weipu Zhu,Ryan A. Mehl,Anna C. Balazs,Tomasz Kowalewski,Krzysztof Matyjaszewski
Licensed Content Date	Jul 9, 2014
Licensed Content Pages	6
Type of use	Dissertation/Thesis
Requestor type	University/Academic
Format	Print and electronic
Portion	Figure/table
Number of figures/tables	1
Original Wiley figure/table number(s)	Scheme 1
Will you be translating?	No
Title of your thesis / dissertation	Interfacial Bioorthogonal Chemistry For Biomaterials Synthesis And Patterning And Development Of Catalytic Method For "Turning-on" The Tetrazine Ligation
Expected completion date	Mar 2017
Expected size (number of pages)	300
Requestor Location	Han Zhang

	5366 Tarkington Place COLUMBIA, MD 21044 United States Attn: Han Zhang
Publisher Tax ID	EU826007151
Billing Type	Invoice
Billing address	Han Zhang 5366 Tarkington Place COLUMBIA, MD 21044 United States Attn: Han Zhang
Total	0.00 USD

Would you like to purchase the full text of this article? If so, please continue on to the content ordering system located here: Purchase PDF

If you click on the buttons below or close this window, you will not be able to return to the content ordering system.

ORDER MORE CLOSE WINDOW

Title: Synthesis and Characterization of Elastin−Mimetic Hybrid Polymers with Multiblock, Alternating Molecular Architecture and Elastomeric Properties

Author: Sarah E. Grieshaber, Alexandra J. E. Farran, Sheng Lin-Gibson, et al

Publication: Macromolecules

Publisher: American Chemical Society

Date: Apr 1, 2009

PERMISSION/LICENSE IS GRANTED FOR YOUR ORDER AT NO CHARGE

This type of permission/license, instead of the standard Terms & Conditions, is sent to you because no fee is being charged for your order. Please note the following:

- Permission is granted for your request in both print and electronic formats, and translations.
- If figures and/or tables were requested, they may be adapted or used in part.
- Please print this page for your records and send a copy of it to your publisher/graduate school.
- Appropriate credit for the requested material should be given as follows: "Reprinted (adapted) with permission from (COMPLETE REFERENCE CITATION). Copyright (YEAR) American Chemical Society." Insert appropriate information in place of the capitalized words.
- One-time permission is granted only for the use specified in your request. No additional uses are granted (such as derivative works or other editions). For any other uses, please submit a new request.

If credit is given to another source for the material you requested, permission must be obtained from that source.